BREAKING OF DISCRETE SYMMETRIES AND GLOBAL LEPTON NUMBER IN NEUTRINO PHYSICS

PhD dissertation by

ALEJANDRO SEGARRA TAMARIT

under the supervision of

JOSÉ BERNABÉU ALBEROLA

JOSÉ A. PEÑARROCHA GANTES

Programa de Doctorat en Física
Falcultat de Física, Universitat de València

September 2019

VNIVERSITAT DE VALÈNCIA Facultat de Física
Departament de Física Teòrica

c/ Dr. Moliner, 50
46100 Burjassot – Valencia
Telf. 34 96 35 44349
Fax. 34 96 35 43381

José Bernabéu Alberola, profesor emérito del Departamento de Física Teórica de la Universidad de Valencia, y

José Antonio Peñarrocha Gantes, catedrático del Departamento de Física Teórica de la Universidad de Valencia

Certifican:

Que la presente memoria **"Breaking of Discrete Symmetries and Global Lepton Number in Neutrino Physics"** ha sido realizada bajo su dirección en el Departamento de Física Teórica de la Universidad de Valencia por **Alejandro Segarra Tamarit**, y constituye su Tesis para optar al grado de Doctor en Ciencias Físicas.

Y para que así conste, en cumplimiento de la legislación vigente, presentan en el Departamento de Física Teórica de la Universidad de Valencia la referida Tesis Doctoral, y firman el presente certificado.

Valencia, a 2 de septiembre de 2019,

José Bernabéu

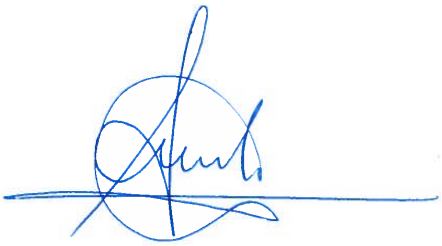

José A. Peñarrocha

A mi familia

This work is based on the following

PUBLICATIONS

J. Bernabéu and A. Segarra, «Stimulated transitions in resonant atom Majorana mixing,» *JHEP* **02** (2018) 017.

DOI: 10.1007/JHEP02(2018)017.

arXiv: 1706.08328 [hep-ph].

J. Bernabéu and A. Segarra, «Disentangling genuine from matter-induced CP violation in neutrino oscillations,» *Phys. Rev. Lett.* **121**, no. 21 (2018) 211802.

DOI: 10.1103/PhysRevLett.121.211802.

arXiv: 1806.07694 [hep-ph].

J. Bernabéu and A. Segarra, «Signatures of the genuine and matter-induced components of the CP violation asymmetry in neutrino oscillations,» *JHEP* **11** (2018) 063.

DOI: 10.1007/JHEP11(2018)063.

arXiv: 1807.11879 [hep-ph].

J. Bernabéu and A. Segarra, «Do T asymmetries for neutrino oscillations in uniform matter have a CP-even component?» *JHEP* **03** (2019) 103.

DOI: 10.1007/JHEP03(2019)103.

arXiv: 1901.02761 [hep-ph].

PROCEEDINGS

A. Segarra, «The coherent weak flavour charge of ordinary matter for neutrino-exchange forces,» *J. Phys. Conf. Ser.* **888**, no. 1 (2017) 012199.

DOI: 10.1088/1742-6596/888/1/012199.

A. Segarra and J. Bernabéu, «Stimulated X-rays in resonant atom Majorana mixing,» in *15th International Conference on Topics in Astroparticle and Underground Physics (TAUP 2017) Sudbury, Ontario, Canada, July 24-28*.

arXiv: 1711.04251 [hep-ph].

A. Segarra, «The coherent weak charge of matter,» in *18th Lomonosov Conference on Elementary Particle Physics Moscow, Russia, August 24-30*.

arXiv: 1712.01049 [hep-ph].

J. Bernabéu and A. Segarra, «Resonant atom Majorana mixing,» *PoS* **CORFU2017** (2018) 063.

DOI: 10.22323/1.318.0063.

A. Segarra and J. Bernabeu, «Disentangling genuine from matter-induced CP violation in neutrino oscillations,» in *6th Symposium on Prospects in the Physics of Discrete Symmetries (DISCRETE 2018) Vienna, Austria, November 26-30, 2018*.

arXiv: 1903.06099 [hep-ph].

CONTENTS

Global Lepton Number Violation by Majorana Neutrinos

RESUMEN

La Física de Neutrinos cambió el curso de su historia en 1998 con el descubrimiento de las oscilaciones de neutrinos en neutrinos atmosféricos, después corroborado en experimentos con neutrinos solares, de reactor y de acelerador. Así pues, los neutrinos tienen masa no nula y hay mezcla de sabor entre las tres familias de neutrinos ligeros levógiros activos. A pesar de los grandes avances que ha habido, todavía queda cierto número de preguntas abiertas en este campo. A partir de principios de simetría, esta Tesis ha estudiado:

1. Violación genuina de CP en el sector leptónico, un problema histórico debido a la falsa violación de CP que la propagación de neutrinos en materia induce en los observables, en cuyo estudio también han surgido nuevos observables para la determinación de la jerarquía de masas de los neutrinos. Hay dos ideas fundamentales con las que afrontar este problema, para las cuales esta Tesis ha proporcionado respuestas afirmativas:
   i) ¿Es teóricamente posible separar la asimetría CP observable en dos componentes, genuina y falsa, bien definidas?
   ii) ¿Son estas dos componentes observables por separado en los experimentos terrestres con neutrinos de acelerador planificados?
2. Violación de número leptónico global, a partir de conceptos alternativos a la profundamente estudiada desintegración doble beta sin neutrinos. La respuesta a la naturaleza de los neutrinos como partículas de Dirac o de Majorana es de crucial importancia, con sus implicaciones para la Física de más allá del Modelo Estándar y leptogénesis. Además de estas desintegraciones nucleares, hemos estudiado dos observables alternativos para comprobar la existencia de

términos de masas para los neutrinos violando número leptónico en dos unidades:

i) Doble captura electrónica sin neutrinos, que corresponde a una mezcla atómica con $\Delta L = 2$, a través de diferentes observables mediados por el átomo hija mezclado, aumentados por la condición de resonancia y con emisión estimulada por un haz de rayos X.

ii) Separar la dependencia en los términos de masa de los neutrinos, diferentes para Dirac o Majorana, en la interacción $\Delta L = 0$ de largo alcance entre materia agregada medida por el intercambio de un par de neutrinos, que serán especialmente relevantes a distancias del orden de una micra —la longitud de onda Compton del neutrino.

1. Violación genuina de CP

Hemos estudiado el problema del enmarañamiento de las distintas fuentes de violación de CP en la asimetría CP, junto con las asimetrías T y CPT, para oscilaciones de neutrinos en materia. Nuestros resultados culminan la solución de este problema histórico de la contaminación por efectos de materia en las asimetrías para las tres simetrías discretas CP, T y CPT en la propagación de neutrinos. Teniendo en cuenta que el Lagrangiano en vacío es simétrico bajo CPT y que los efectos de materia son invariantes bajo T, la separación de los distintos efectos queda realizada en términos de una base de tres componentes independientes: la genuina (invariante CPT), la inducida por materia (invariante T), la de interferencia (invariante CP).

De forma independiente del marco teórico para la dinámica de los tres sabores de neutrinos activos, hemos demostrado el Teorema de Desenmarañamiento

$$\mathcal{A}^{\mathrm{CP}}_{\alpha\beta} = A^{\mathrm{CP;T}}_{\alpha\beta} + A^{\mathrm{CP;CPT}}_{\alpha\beta}\,, \tag{2.13a}$$

$$\mathcal{A}^{\mathrm{T}}_{\alpha\beta} = A^{\mathrm{T;CPT}}_{\alpha\beta} + A^{\mathrm{T;CP}}_{\alpha\beta}\,, \qquad \bar{\mathcal{A}}^{\mathrm{T}}_{\alpha\beta} = A^{\mathrm{T;CPT}}_{\alpha\beta} - A^{\mathrm{T;CP}}_{\alpha\beta}\,, \tag{2.13b}$$

$$\mathcal{A}^{\mathrm{CPT}}_{\alpha\beta} = A^{\mathrm{CPT;T}}_{\alpha\beta} + A^{\mathrm{CPT;CP}}_{\alpha\beta}\,, \quad \bar{\mathcal{A}}^{\mathrm{CPT}}_{\alpha\beta} = A^{\mathrm{CPT;T}}_{\alpha\beta} - A^{\mathrm{CPT;CP}}_{\alpha\beta}\,, \tag{2.13c}$$

para las tres asimetrías experimentales independientes, en términos de nuestras tres componentes. Incluso para materia invarian-

te T, $\mathcal{A}^{\mathrm{T}}_{\alpha\beta}$ tiene una componente falsa debido a la interferencia cuántica.

Al escribir la regla de suma de las asimetrías para cualquier canal de sabor, $\mathcal{A}^{\mathrm{CPT}}_{\alpha\beta} = \mathcal{A}^{\mathrm{CP}}_{\alpha\beta} + \mathcal{A}^{\mathrm{T}}_{\alpha\beta}$ (2.10), en términos de las componentes separadas, el comportamiento bajo cada una de las tres simetrías discretas implica que $A^{\mathrm{S}_1;\mathrm{S}_2}_{\alpha\beta} = A^{\mathrm{S}_2;\mathrm{S}_1}_{\alpha\beta}$.

Para el Hamiltoniano efectivo escrito como la suma de propagación libre más el potencial de materia para neutrinos electrónicos, las tres componentes tienen paridades definidas bajo la distancia L recorrida por el neutrino, el potencial de materia a, la parte imaginaria $\sin\delta$ de la matriz de mezcla PMNS, y la jerarquía de masas de los neutrinos $h = \pm 1$: $A^{\mathrm{CP;T}}_{\alpha\beta}$ es impar en L y $\sin\delta$, par en a y h; $A^{\mathrm{CP;CPT}}_{\alpha\beta}$ es par en L y $\sin\delta$, impar en a y h; $A^{\mathrm{T;CPT}}_{\alpha\beta}$ es impar en L, $\sin\delta$, a y h.

A distancia L y energía E fijadas, hemos comprobado el Teorema de Desenmarañamiento estudiando las componentes en función del potencial de materia V en $a = 2EV$ y del parámetro de violación de CP $\sin\delta$. Las componentes genuina y de interferencia se anulan si $\sin\delta = 0\ \forall a$, mientras que las dos componentes falsas se anulan si $a = 0\ \forall \sin\delta$.

Con el potencial V fijado para el valor de propagación a través de la corteza terrestre, hemos estudiado la región de energías $\Delta m^2_{21} \ll |a| \ll |\Delta m^2_{31}|$ entre las dos resonancias MSW, relevante para los experimentos de acelerador actuales y de la siguiente generación. Hemos podido resolver el problema de autovalores y autoestados del Hamiltoniano H en materia, así como expresar todas las componentes de las asimetrías a primer orden en Δm^2_{21} y a. Vienen dadas por:

Componente Genuina

$$A^{\mathrm{CP;T}}_{\mu e} \approx -16\, J_r \sin\delta\, \Delta_{21} \sin^2\Delta_{31}\,, \tag{3.35a}$$

Componente Inducida por Materia

$$A^{\mathrm{CP;CPT}}_{\mu e} \approx 16\Delta_a \left[\frac{\sin\Delta_{31}}{\Delta_{31}} - \cos\Delta_{31}\right](S\sin\Delta_{31} + J_r\cos\delta\,\Delta_{21}\cos\Delta_{31})\,, \tag{3.35b}$$

Componente de Interferencia

$$A^{\mathrm{T;CPT}}_{\mu e} \approx -16\Delta_a J_r \sin\delta\,\Delta_{21}\sin\Delta_{31}\left[\frac{\sin\Delta_{31}}{\Delta_{31}} - \cos\Delta_{31}\right]. \tag{3.35c}$$

Estas expresiones analíticas, aun siendo sencillas, dan resultados precisos, en comparación a la resolución numérica del problema. Este hecho se entiende gracias a la paridad definida de cada componente bajo a.

Los resultados analíticos demuestran que la componente genuina $A_{\mu e}^{\mathrm{CP;T}}$ es ciega a efectos de jerarquía de masas, mientras que el signo de las componentes falsas $A_{\mu e}^{\mathrm{CP;CPT}}$ y $A_{\mu e}^{\mathrm{T;CPT}}$ es suficiente para discriminar entre Jerarquía Normal e Invertida.

La medida separada de todas las componentes solo se puede conseguir en factorías de neutrinos o con neutrinos atmosféricos. En estos casos, las tres componentes se pueden extraer bien de $\mathcal{A}_{\mu e}^{\mathrm{T}}$, $\bar{\mathcal{A}}_{\mu e}^{\mathrm{T}}$, $\mathcal{A}_{\mu e}^{\mathrm{CP}}$ o de $\mathcal{A}_{\mu e}^{\mathrm{CP}}$, $\mathcal{A}_{\mu e}^{\mathrm{T}}$, $\mathcal{A}_{\mu e}^{\mathrm{CPT}}$.

Para las fuentes de neutrinos y antineutrinos muónicos de los experimentos de acelerador actuales, las dos componentes de la asimetría CP de aparición $\mathcal{A}_{\mu e}^{\mathrm{CP}}$ se pueden separar mediante su dependencia en la distancia (T2HKK) o su dependencia en la energía (DUNE). Con un único detector en el primer máximo de oscilación, la medida en T2HK está dominada por el efecto genuino, mientras que la componente falsa se puede sustraer una vez se conozca la jerarquía de masas.

A la distancia de DUNE, la componente inducida por materia $A_{\mu e}^{\mathrm{CP;CPT}}$ domina en la región de alta energía por encima del primer nodo de oscilación, de forma que el signo de la asimetría CP experimental $\mathcal{A}_{\mu e}^{\mathrm{CP}}$ determina la jerarquía de masas.

Complementariamente, se puede explotar un configuración mágica de energía con $L/E = 1420$ km/GeV, alrededor del segundo máximo de oscilación, en la que la componente inducida por materia $A_{\mu e}^{\mathrm{CP;CPT}}$ tiene un cero de primer rango mientras que la componente genuina $A_{\mu e}^{\mathrm{CP;T}}$ tiene un extremo (proporcional a $\sin\delta$).

Ese valor mágico de L/E viene dado por

$$E = 0{,}92\ \mathrm{GeV}\ \frac{L}{1300\ \mathrm{km}}\ \frac{\left|\Delta m_{31}^2\right|}{2{,}5\times 10^{-3}\ \mathrm{eV}^2}\,, \tag{4.21}$$

que corresponde a $E = 0{,}92$ GeV para la distancia experimental de DUNE. Con una resolución energética modesta de $\Delta E \sim 200$ MeV, se mantiene un cero efectivo para la componente inducida por materia.

2.i. Doble captura electrónica sin neutrinos

A diferencia de la desintegración doble beta sin neutrinos, la doble captura electrónica sin neutrinos no es un proceso, sino una mezcla virtual entre un átomo padre ${}^{A}\mathrm{Z}$ y un átomo hijo ${}^{A}(\mathrm{Z}-2)^{*}$ excitado con dos huecos. La señal observable es la emisión de 2 rayos X debidos a los huecos. Además de esta diferente señal, la estrategia para su detección y los eventos de fondo del experimento son diferentes respecto a los encontrados en la desintegración doble beta sin neutrinos.

La mezcla es resonante para la cuasi-degeneración de los niveles energéticos padre e hijo y, bajo estas circunstancias, no hay fondo irreducible debido al canal con emisión de dos neutrinos.

Hemos reconstruido la historia natural de un átomo padre nominalmente estable desde su producción, ya sea en la naturaleza o en el laboratorio. Después de los períodos de oscilaciones de átomos y de la desintegración de estado excitado de vida media corta del átomo hijo, los estados "estacionarios" relevantes a tiempos observables son el estado mezclado metaestable de vida media larga y el estado excitado no ortogonal de vida media corta, así como el estado fundamental del átomo hijo. Hemos descubierto que este sistema se encuentra de forma natural en inversión de población, hecho que se puede aprovechar para explotar la naturaleza bosónica de la radiación emitida por las transiciones atómicas observadas.

De entre diferentes observables para este fenómeno de mezcla atómica de Majorana, destacamos la emisión estimulada de rayos X del estado metaestable de vida media larga mediante un haz de alta intensidad de rayos X: se pueden esperar ganancias de hasta $G \sim 100$ en las presentes instalaciones de láseres de rayos X (XFEL).

Por otro lado, la población histórica en el estado fundamental del átomo hijo se puede muestrear excitando la muestra con un láser pulsado actual, que mostraría el espectro de absorción característico del átomo hijo.

Los valores numéricos en estos resultados quedan supeditados a que se encuentre un isótopo que cumpla mejor la condición de resonancia $\Delta \sim \Gamma$, con una posible mejora de hasta un factor ~ 1000 en la vida media de los observables.

2.ii. Fuerzas de largo alcance mediadas por un par de neutrinos

Por primera vez, presentamos un cálculo realista de la interacción de largo alcance entre materia agregada, mediada por un par de neutrinos, para distancias cercanas a su alcance, cuyo acoplamiento es coherente. Hemos incluido todos los ingredientes conocidos a día de hoy en física de neutrinos relevantes para la interacción coherente con materia, incluyendo las cargas vectoriales para electrones, protones y neutrones, los términos de masa de neutrinos relevantes a distancias del orden de su longitud de onda Compton y la matriz de mezcla PMNS, que distingue los neutrinos de sabor en el vértice $\nu_e\, e$ de corrientes cargadas de los neutrinos de masa definida que aparecen en el estado intermedio que determina la parte absortiva de la amplitud. De nuestro tratamiento surge un resultado clave: la medida de esta interacción a distancias del orden de la micra supondría un metodología completamente nueva para la distinción de la naturaleza Dirac o Majorana del neutrino. En lugar de buscar un observable $\Delta L = 2$ que solo está permitido para neutrinos de Majorana, esta interacción permite distinguir si los neutrinos son de Dirac o Majorana a partir de los efectos de masa en un observable permitido en ambos casos.

La longitud de onda Compton de los neutrinos masivos es del orden de una micra. Aunque todavía se desconoce la escala absoluta de masas de los neutrinos, los límites experimentales y los valores conocidos de $\left|\Delta m^2_{31}\right|$ y Δm^2_{21} hacen que $m_\nu \sim 0{,}1$ eV sea de esperar. Nuestro cálculo en teoría dispersiva para la fuerza mediada por dos neutrinos incluye precisamente esta región de distancias. De hecho, nuestro resultados muestran la fuerte dependencia del potencial de interacción a la masa del neutrino más ligero, y por tanto a la escala absoluta de masas de los neutrinos, para distancias entre 1 y 10 micras.

El alcance de esta interacción mediada por dos neutrinos está muy por encima de la escala atómica, garantizando que será operativa para átomos y agregados de materia neutros de carga eléctrica, siempre y cuando sí tengan una carga débil no nula. Efectivamente, hemos construido dicha carga débil a partir de las interacciones por corrientes neutras con electrones, protones y neutrones, así como la interacción de neutrinos electrónicos por

corrientes cargadas con electrones. Estas cargas débiles para la interacción de materia con ν_e y $\nu_{\mu\,\tau}$ son proporcionales al operador número, por lo que violan el principio débil de equivalencia. No se han encontrado desviaciones del principio de equivalencia en medidas con precisiones que alcanzan los 10^{-14}, por lo que un estudio más detallado sobre las implicaciones de nuestro potencial será conveniente.

En las interacciones por corrientes neutras, la mezcla de sabor en la matriz PMNS es irrelevante, por lo que el estado intermedio de propagación con neutrinos de masa definida aparece de forma directa. En las interacciones por corrientes cargadas, en cambio, las mezclas U_{ei} de neutrinos electrónicos con todos los estados de masa definida son necesarias. Estas cantidades son bien conocidas por las medidas de oscilaciones de neutrinos.

La teoría dispersiva para las fuerzas de largo alcance nos ha conducido a la determinación del potencial efectivo en términos de la parte absortiva de la amplitud a bajos t, es decir, a baja energía del par de neutrinos en la amplitud del canal t. Por tanto, unitariedad indica que la física que domina el potencial es la de un par de neutrinos no relativistas con masa definida.

Para neutrinos de Dirac con número leptónico definido, el vértice de interacción es la carga quiral que distingue neutrinos de antineutrinos. Para neutrinos de Majorana sin ninguna carga conservada, el vértice de interacción es la carga axial, por lo que, a diferencia del caso Dirac, el par de neutrinos se encuentra en onda P. Las partes absortivas para neutrinos de Dirac y Majorana difieren en los términos que dependen de sus masas.

Para neutrinos con masa, independientemente de su carácter de Dirac o Majorana, las tres cargas de sabor Q_W^α encontradas en el potencial de neutrinos sin masa aparecen mezcladas, hecho que da lugar a un tensor 3×3 simétrico Q_W^{ij}. Este tensor depende de los elementos U_{ei} de la matriz de mezcla, y cada uno de sus elementos se corresponde con el vértice de intercambio del par $\nu_i \bar{\nu}_j$. La unitariedad de la matriz PMNS garantiza la consistencia de las dos descripciones en la región con neutrinos efectivamente sin masa, $m_\nu r \ll 1$.

A distancias por debajo de una micra, los potenciales que hemos obtenido para neutrinos de Dirac y Majorana reproducen

la dependencia r^{-5} conocida para neutrinos sin masa. Por encima de la escala de la micra, donde los efectos de masa son relevantes, los potenciales presentan una supresión tipo Yukawa, con un comportamiento prácticamente independiente de la jerarquía de masas de los neutrinos. La región en torno a la micra donde los efectos de masa ya son relevantes pero los potenciales todavía no están demasiado suprimidos es la escala óptima para la distinción del carácter Dirac o Majorana de los neutrinos a partir de este observable.

1 INTRODUCTION

The last two decades have seen a revolution in neutrino physics with the discovery of, and precision studies on, flavor oscillations in atmospheric [1], solar [2], reactor [3] and accelerator [4] neutrinos. These phenomena are interpreted in terms of non-vanishing masses and flavor mixing, the unitary PMNS matrix [5, 6] describing the mismatch between flavor and mass eigenstates. Global fits to all observable quantities provide better and better determination of the two mass differences Δm^2_{21} and $\left|\Delta m^2_{31}\right|$, as well as the three mixing angles [7–9].

The most fundamental pending questions are the Dirac-Majorana confusion on the nature of neutrinos and their absolute mass scale, properties studied by means of non-accelerator methods, as well as the novel challenges for the next-generation neutrino flavor oscillation experiments like T2HK [10] and DUNE [11] using terrestrial accelerators. Above all, once known that the three mixing angles are non-vanishing [12–14], they should answer whether the lepton sector of elementary particles also incorporates CP violation, opening the door to concepts able to explain the matter-antimatter asymmetry of the Universe through leptogenesis [15] at higher energy scales. An additional open problem is the ordering of the neutrino mass spectrum, with the so-called either Normal or Inverted Hierarchies.

This work addresses the problems in neutrino physics just mentioned, providing novel concepts and methodologies relevant to their experimental attack at present and near future facilities.

Chapters 2, 3 and 4 represent the culmination of the understanding of the physics involved in the discrete CP, T and CPT asymmetries for neutrinos propagating in matter. Contrary to an attitude of considering as irremediable the contamination of matter-effects [16, 17] in the search of the genuine asymmetry, we prove Asymmetry Disentanglement Theorems using as guid-

ing principle the different symmetry properties of the free and interaction Hamiltonian terms under T and CPT. In addition, the disentangled genuine and matter-induced components offer peculiar experimental signatures in their baseline and energy distributions which allow their separation.

Chapter 5 presents a discussion of neutrinoless double electron capture, as alternative to neutrinoless double beta decay, in terms of a virtual $\Delta L = 2$ atom mixing generated by Majorana neutrino exchange. We put forward the idea, quantified in this Thesis, of the possibility of stimulating the X-ray decay induced by the atom mixing by means of XLaser facilities such as the new ones operating at DESY [18] and Stanford [19, 20].

Chapter 6 gives the reader the first consistent calculation of the long-range coherent interaction between ordinary matter mediated by two-neutrino exchange, including both the flavor mixing and the Dirac-Majorana neutrino mass distinction relevant at distances of the order of the neutrino Compton wavelength —the micron.

Chapter 7 presents our main conclusions and prospects.

1.1 THE BIRTH OF THE NEUTRINO

Before 1930, the only subatomic particles known were the electron [21] and the proton [22]. Together with a still-developing quantum theory, these two elementary particles were enough to describe the atomic spectrum of hydrogen. The structure of atomic nuclei [23] was initially thought of in terms of bounded protons and electrons, especially motivated by the identification of β radioactivity [24] with electron emission [25]

$$ {}^{A}_{Z}\mathrm{X} \to {}^{A}_{Z+1}\mathrm{Y} + e^{-} \,, \tag{1.1} $$

as is the case of ${}^{14}_{6}\mathrm{C}$ decaying into ${}^{14}_{7}\mathrm{N}$ with a half-life of about 5730 years. Conservation of energy and momentum in this two-body decay predicts a definite value for the emitted electron energy,

$$ E_e = \frac{m_X^2 - m_Y^2 + m_e^2}{2m_X} \,. \tag{1.2} $$

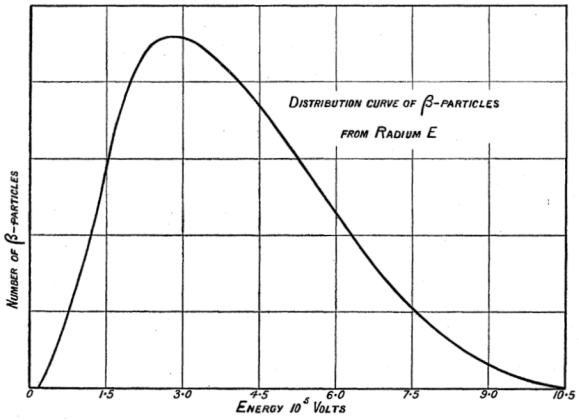

Figure 1.1: β-decay electron energy spectrum [31].

Lise Meitner and Otto Hahn in 1911 [26] and Jean Danysz in 1912 [27] obtained the first hint that β particles have a continuous spectrum, against the energy conservation rule leading to Eq. (1.2). Further evidence of the violation of energy conservation was given by James Chadwick in 1914 [28], measuring that the spectrum was continuous. In addition, molecular band spectra established [29] that the nuclear spin of Nitrogen-14 is 1, implying the violation of angular momentum conservation too in the process (1.1), which would thus involve the spins $0 \to 1 + \frac{1}{2}$. Dedicated studies in 1920–1927 by Charles Drummond Ellis and others [30–32] finally demonstrated beyond any doubt that the spectrum is continuous, as shown in Figure 1.1.

In a desperate reaction to these experimental facts, Niels Bohr postulated that conservation of energy was true in a statistical sense only [33]. These *β decay puzzles* of non-conservation of energy and angular momentum were on the forefront of the open problems in the fundamental physics endeavor.

Indeed, the fact that the measured energy ranged from zero to a maximum given by its nominal value in Eq. (1.2), cannot be explained in this framework. Furthermore, the nuclear models with A protons and $Z - A$ electrons were not able to explain the spin of the nuclei, which for e.g. ${}^{14}_{7}\mathrm{N}$ should have been half-odd instead of the measured integer value. In this context, both

conservation of energy and angular momentum seemed to be failing.

In 1930, Wolfgang Pauli wrote the famous letter in Figure 1.2 of the 4th of December, addressed to the "Dear Radioactive Ladies and Gentlemen" participating in the Tübingen Conference: he proposed the existence of a hitherto unobserved spin-1/2 neutral particle with a small mass, no greater than 1% the mass of a proton, which he called a "neutron". In his words, this was a desperate remedy to save the exchange theorem of statistics and the law of conservation of energy. Assuming that this particle was emitted together with the electron in β processes,

$$^{14}_{6}\mathrm{C} \rightarrow {}^{14}_{7}\mathrm{N} + e^{-} + \nu\,, \tag{1.3}$$

the law of conservation of energy could successfully explain the spectrum in Figure 1.1, and angular momentum conservation could describe the $0 \rightarrow 1 + \frac{1}{2} + \frac{1}{2}$ transition too. Moreover, the presence of this hypothetical neutral particle in the nucleus in the same number as electrons could also solve the problem of nuclear spin.

Pauli excused his participation in the conference: « I cannot appear in Tübingen personally since I am indispensable here in Zurich because of a ball on the night of the 6th to 7th of December ». The fact that this hypothetical particle had not been observed in β decay forced it to be very weakly interacting, to the point that Pauli himself believed that it would never be observed. Unlike nowadays, when theoreticians have no problem in proposing particles whose observation is unfeasible, Pauli avoided claiming his solution in a scientific journal.

The nuclear spin problem was soon solved: James Chadwick discovered the neutron in 1932 [34]. Its spin 1/2 and mass similar to the proton mass opened the door to the understanding of the atomic nucleus in terms of protons and nucleons. Its heavy mass, however, made it clear that this particle could not be identified as Pauli's "neutron", and indeed the problems with conservation of energy and angular momentum in β decays were still present.

The description of the subatomic world in terms of protons, electrons and neutrons lived a short life. A few months after Chadwick's discovery of the neutron, Carl D. Anderson took

Abschrift/15.12.30

Offener Brief an die Gruppe der Radioaktiven bei der Gauvereins-Tagung zu Tübingen.

Abschrift

Physikalisches Institut
der Eidg. Technischen Hochschule
Zürich

Zürich, 4. Dez. 1930
Gloriastrasse

Liebe Radioaktive Damen und Herren,

Wie der Ueberbringer dieser Zeilen, den ich huldvollst anzuhören bitte, Ihnen des näheren auseinandersetzen wird, bin ich angesichts der "falschen" Statistik der N- und Li-6 Kerne, sowie des kontinuierlichen beta-Spektrums auf einen verzweifelten Ausweg verfallen um den "Wechselsatz" (1) der Statistik und den Energiesatz zu retten. Nämlich die Möglichkeit, es könnten elektrisch neutrale Teilchen, die ich Neutronen nennen will, in den Kernen existieren, welche den Spin 1/2 haben und das Ausschliessungsprinzip befolgen und sich von Lichtquanten ausserdem noch dadurch unterscheiden, dass sie nicht mit Lichtgeschwindigkeit laufen. Die Masse der Neutronen müsste von derselben Grössenordnung wie die Elektronenmasse sein und jedenfalls nicht grösser als 0,01 Protonenmasse.- Das kontinuierliche beta- Spektrum wäre dann verständlich unter der Annahme, dass beim beta-Zerfall mit dem Elektron jeweils noch ein Neutron emittiert wird, derart, dass die Summe der Energien von Neutron und Elektron konstant ist.

Nun handelt es sich weiter darum, welche Kräfte auf die Neutronen wirken. Das wahrscheinlichste Modell für das Neutron scheint mir aus wellenmechanischen Gründen (näheres weiss der Ueberbringer dieser Zeilen) dieses zu sein, dass das ruhende Neutron ein magnetischer Dipol von einem gewissen Moment μ ist. Die Experimente verlangen wohl, dass die ionisierende Wirkung eines solchen Neutrons nicht grösser sein kann, als die eines gamma-Strahls und darf dann μ wohl nicht grösser sein als $e \cdot (10^{-13}$ cm).

Ich traue mich vorläufig aber nicht, etwas über diese Idee zu publizieren und wende mich erst vertrauensvoll an Euch, liebe Radioaktive, mit der Frage, wie es um den experimentellen Nachweis eines solchen Neutrons stände, wenn dieses ein ebensolches oder etwa 10mal grösseres Durchdringungsvermögen besitzen würde, wie ein gamma-Strahl.

Ich gebe zu, dass mein Ausweg vielleicht von vornherein wenig wahrscheinlich erscheinen wird, weil man die Neutronen, wenn sie existieren, wohl schon längst gesehen hätte. Aber nur wer wagt, gewinnt und der Ernst der Situation beim kontinuierliche beta-Spektrum wird durch einen Ausspruch meines verehrten Vorgängers im Amte, Herrn Debye, beleuchtet, der mir kürzlich in Brüssel gesagt hat: "O, daran soll man am besten gar nicht denken, sowie an die neuen Steuern." Darum soll man jeden Weg zur Rettung ernstlich diskutieren.- Also, liebe Radioaktive, prüfet, und richtet.- Leider kann ich nicht persönlich in Tübingen erscheinen, da ich infolge eines in der Nacht vom 6. zum 7 Dez. in Zürich stattfindenden Balles hier unabkömmlich bin.- Mit vielen Grüssen an Euch, sowie an Herrn Back, Euer untertänigster Diener

gez. W. Pauli

Figure 1.2: Pauli and his famous letter to the Tübingen Conference proposing the neutrino.

the photograph of a positron [35] shown in Figure 1.3, finding the first evidence on the existence of antimatter. In 1934, Enrico Fermi incorporated Pauli's neutral particle, which he named "neutrino", together with all of these particles into his theory of $\beta^{\pm}$ decays [36], described as the subatomic processes

$$n \to p + e^- + \bar{\nu}\,, \tag{1.4a}$$

$$p \to n + e^+ + \nu\,. \tag{1.4b}$$

His theory successfully predicted the spectrum shapes, and provided a framework to calculate their lifetimes, supporting Pauli's proposed particle.

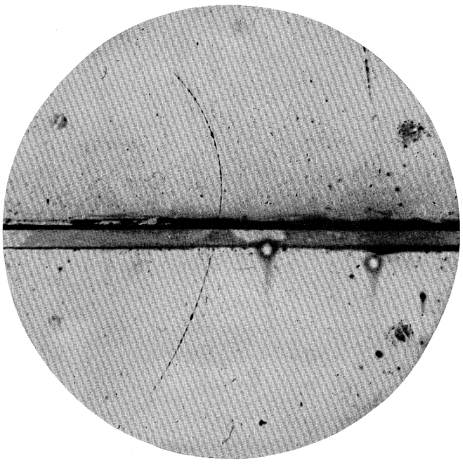

Figure 1.3: Positron track in a cloud chamber [35]. The particle track is curved due to the effect of an orthogonal magnetic field, and the curvature gets tighter after the particle is slowed down by the lead plate across the center of the chamber —so the particle is moving upwards. The direction of the curvature shows that the charge is positive, the radius that its charge-to-mass ratio is that of an electron.

Using Fermi's theory, Hans Bethe and Rudolf Peierls estimated in 1934 [37] the mean absorption length of neutrinos in solid matter, a value larger than 10^{14} km: the expected cross section of neutrinos with matter was so low that they could traverse the Earth without any interaction. They concluded that « it is absolutely impossible to observe processes of this kind ».

Due to this low interaction rate, it was not unitl 1956 that the Cowan–Reines experiment [38] at the Savannah River Nuclear Reactor proved the existence of the neutrino. Antineutrinos created in the nuclear reactor by the β decay (1.4a) were subsequently detected by the process

$$\bar{\nu} + p \to n + e^+ \tag{1.5}$$

in a large water tank. The signature of the process are the two 511 keV gammas from the positron annihilation, in coincidence with the nuclear gamma

$$n + {}^{108}\mathrm{Cd} \to {}^{109}\mathrm{Cd} + \gamma \tag{1.6}$$

due to the de-excitation of the ^{109}Cd nucleus after the neutron was captured by cadmium chloride molecules ($CdCl_2$) dissolved in the water.

Beyond the theoretical motivation for such a neutral particle proposed by Pauli and bolstered by Fermi, unquestionable evidence for its existence had been provided by Reines and Cowan. And so the neutrino was born.

1.2 THE FAMILY PROBLEM: LEPTON FLAVOR

With the discovery of the muon [39, 40], a first problem appeared with its insertion in the Fermi theory of charged current weak interactions. Indeed, the muon was so unexpected that, regarding its discovery, Isidor Isaac Rabi famously quipped «Who ordered that?». A decade before the V-A theory [41], Bruno Pontecorvo discussed [42] the "universality" of Weak Interactions for nuclear β-decay processes together with those with muons and neutrinos. He introduced muon capture by nuclei and compared it with the probability for electron capture.

The idea of $\mu - e$ universality was also followed by Giampietro Puppi [43] with the famous "Puppi triangle" in Figure 1.4, involving β decay, muon decay and muon capture. However, a question remained: was it the same neutrino in all vertices?

The idea of different neutrinos $\nu_\mu \neq \nu_e$ appeared published in 1959 by Pontecorvo [44] and, ever more important, in the

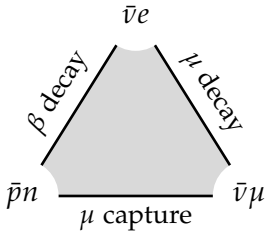

Figure 1.4: Puppi and his triangle, relating the processes on its sides.

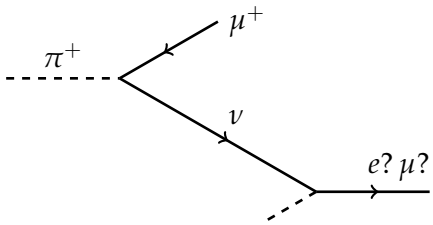

Figure 1.5: Pontecorvo and a diagram of the process he proposed to test whether $\nu_e = \nu_\mu$.

proposal he made for the generation of a neutrino beam from pion decay [45], as schematically represented in Figure 1.5.

In 1962, there was already a hint towards the different nature of the electron and muon neutrinos, coming from the $\mu \to e\gamma$ decay. An estimation of its branching ratio in the V-A theory with the W boson had yielded, if $\nu_\mu = \nu_e$, the value [46] $R_{\text{th}} \sim 10^{-4}$, whereas a limit $R_{\text{exp}} < 10^{-8}$ was found [47].

The Brookhaven experiment [48] was the first one involving high-energy neutrinos from pion decay. Using about 10^{14} muon antineutrinos from π^-, the experiment detected 29 events of the expected

$$\bar{\nu}_\mu + p \to \mu^+ + n \tag{1.7}$$

and no events of the forbidden

$$\bar{\nu}_\mu + p \to e^+ + n\,. \tag{1.8}$$

The demonstration that $\nu_\mu \neq \nu_e$ was a great event in physics and thus two lepton families were completed:

1. $(\nu_e,\, e)$ **2.** $(\nu_\mu,\, \mu)$

After the discovery of the third charged lepton τ [49], the existence of (at least) a third neutrino was to be expected. The third neutrino ν_τ was directly observed in 2000 in an experiment at Fermilab performed by the DONUT collaboration [50]. Using the Tevatron beam, a ν_τ beam was mainly produced from τ decay, with the τ produced in the leptonic decay of a D_S meson. These ν_τ were detected by means of the reaction

$$\nu_\tau + n \to p + \tau^-\,, \tag{1.9}$$

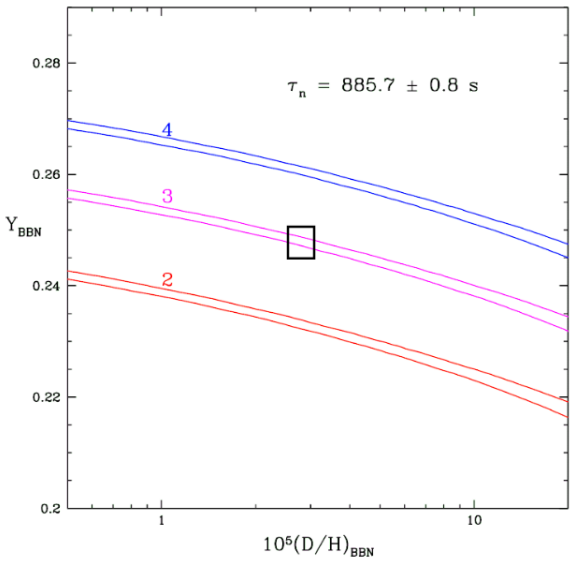

Figure 1.6: The Big Bang Nucleosynthesis (BBN) prediction for the primordial helium mass fraction Y and the deuterium abundance D/H, for $N_\nu = 2, 3, 4$. The width of the bands represents the theoretical uncertainty, largely due to that of the neutron lifetime τ_n in the Figure. The black square shows the measured values. [52]

by identifying the τ lepton as the only lepton created in the interaction vertex. Even before this direct observation of the ν_τ, the number of neutrino species has been fixed following different methods.

A first method was the determination of the primordial helium abundance in the Universe. Since nucleosynthesis is affected by the energy density of all relativistic particles, it depends on the number of neutrino species, changing the helium abundance Y_P if the number of neutrinos differs from three by ΔN_ν as [51]

$$\Delta Y_P = 0.056 Y_P \, \Delta N_\nu \, . \tag{1.10}$$

As shown in Figure 1.6, these measurements of primordial abundances clearly show the existence of three neutrino species.

Two complementary methods led to a highlighted LEP e^+e^- Collider legacy at CERN [53]. The invisible width of the Z boson

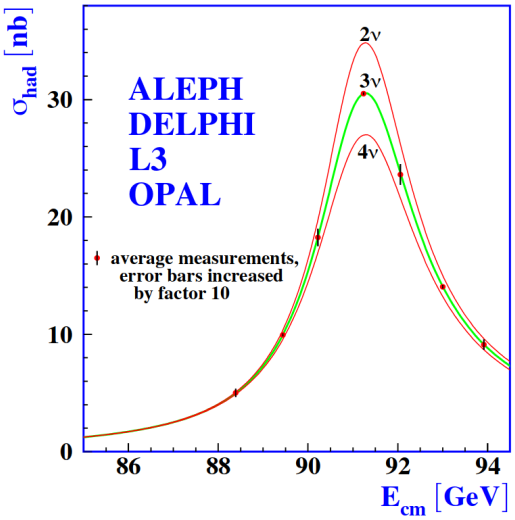

Figure 1.7: Measurements of the hadron production cross-section around the Z resonance. The curves indicate the predicted cross-section for two, three and four neutrino species with SM couplings and negligible mass. [53]

$\Gamma_{\text{inv}} = N_\nu \Gamma_\nu$ is not measurable directly, but the visible cross section depends on the number of neutrino species N_ν as

$$\sigma = \frac{4\pi s}{M_Z^2}\Gamma_{ee}\frac{\Gamma_Z - N_\nu\Gamma_\nu}{(s - M_Z^2)^2 + \Gamma_Z^2 M_Z^2}\,, \tag{1.11}$$

as shown in Figure 1.7, from which LEP could determine the existence of three (and only three) light active neutrinos.

An alternative at LEP was the measurement of the cross section for $e^+e^- \to \gamma Z \to \gamma\nu\bar{\nu}$, detecting the photon plus nothing else. This cross section in Figure 1.8, normalized to $\gamma\mu\mu$, is a known function of N_ν, and consistently reproduced the previous answers: there are three light active neutrinos.

1.3 NEUTRINO MASS: UPS AND DOWNS

Parity violation in processes involving neutrinos, like β decay, is automatic if neutrinos have a definite helicity. This fact led

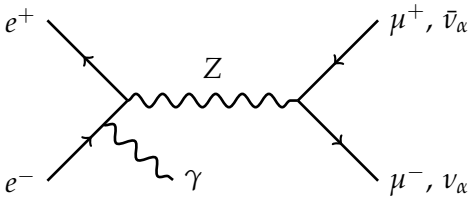

Figure 1.8: Tree-level Feynman diagram for the $Z \to \gamma + \text{MET}$ decay at LEP, probing the number of neutrino species ν_α, together with the normalization channel to muons.

to the advent of the two-component theory —introduced by Hermann Weyl in 1929 [54]— if neutrinos are exactly massless, for which the Dirac equation

$$i\gamma^\mu \partial_\mu \nu_L(x) - m_\nu \, \nu_R(x) = 0 \tag{1.12}$$

decouples. Non-conservation of parity was first observed in 1957 with Wu's experiment [55], measuring an asymmetry in the electron angular distribution emitted from the β decay of polarized ${}^{60}_{27}\text{Co}$. In 1958, the celebrated Goldhaber experiment [56] proved that the neutrino helicity is -1, using conservation of angular momentum in a selected electron capture transition in ${}^{152\text{m}1}_{63}\text{Eu}$ leading to an excited nuclear state of ${}^{152}_{62}\text{Sm}$ —the measurement of the circular polarization of the de-exciting γ ray fixed the neutrino helicity.

Even though this picture was consistent for massless neutrinos with definite helicity, the universal V-A theory of charged-current weak interactions was also formulated in 1958 [41], extending Fermi's theory of β decay into a high-energy picture where left-handed chiral fields enter for *all* fermions, either neutrinos or not. Thus there is no rationale why neutrinos should be special and massless. Still, contrary to other fermions, neutrinos have no electric charge, so they present unique possibilities in the explanation of the origin of their masses. Whether these possibilities can be realized depends on the existence of a lepton charge that distinguishes ν and $\bar{\nu}$. This is the most important open question even today!

Already in 1946 (!!), Pontecorvo asked the question whether antineutrinos produced from β decay in reactors could produce

electrons [57]. The negative result in 1959 of the Davis experiment [58] for

$$\bar{\nu} + {}^{37}_{17}\mathrm{Cl} \to e^- + {}^{37}_{18}\mathrm{Ar} \tag{1.13}$$

suggested the existence of definite lepton numbers with values $L_{e^-} = L_\nu = 1$ and $L_{e^+} = L_{\bar{\nu}} = -1$. Such a flavor charge would imply that neutrinos are not neutral particles, and so their mass could only be described with the same theories as all other fermions. The genius of Pontecorvo was the first to realize that this conclusion was referring to interacting neutrinos, and that there was still a possibility for neutrinos to acquire a Majorana mass.

The theory of Majorana particles had been introduced in 1937 by Ettore Majorana [59], who noticed that there are solutions of the Dirac equation for neutral particles with only two degrees of freedom: « the meaning of the Dirac equations is somewhat modified and there is no longer any reason to speak of negative-energy states nor to assume, for any other types of particles, especially neutral ones, the existence of antiparticles, corresponding to the "holes" of negative energy ».

Forbidden for the other elementary fermions due to exact electric charge conservation, a Majorana mass for neutrinos is a priori allowed if the mass terms violate global lepton number by two units. In this case, the states of neutrinos with definite Majorana mass would be a linear superposition of weak interacting neutrinos with opposite lepton charge. Global lepton number would then be undefined for neutrinos with definite Majorana mass. Even more: one can have massive neutrinos with the active (left-handed) chiral component ν_L only and the sterile (right-handed) component ν_R is not needed. Contrary to Dirac fermions, Majorana fermions have only two degrees of freedom, the neutrino of left-handed chirality and its conjugate ν_L^c. The states of definite mass and helicity, which are compatible observables, are the left-handed with a relative m/E component of the conjugate, and its orthogonal.

It is astonishing that the early ideas on neutrino mixing came through these reasonings. In 1957, Pontecorvo writes [5]: «If the theory of two-component neutrinos were not valid, and if the

conservation law for "neutrino charge" took not place, neutrino-antineutrino transitions would be possible». In this statement one finds the two essential ingredients for oscillations: neutrino mass and mixing. He calculated [60] the survival probability of active neutrinos in a model of two Majorana neutrinos, one active, the other sterile, and suggested that the Cowan-Reines experiment should be repeated as function of the baseline for the detector. This kind of measurement in reactors was only performed for the first time in 2003 in the KAMLAND experiment [61].

In 1962, in the context of the Nagoya model of Baryons as bound states of neutrinos and "a new sort of matter" vector boson, Ziro Maki, Masami Nakagawa and Shoichi Sakata [6] introduced a mixing between two neutrinos to form the "true neutrinos" in these baryons. The objective was the explanation of the smallness of the leptonic decay rate of the hyperons, later explained by the Cabibbo mixing [62]. Although these ideas were not connected to neutrino oscillation phenomena, the concept of quantum mixings between neutrino states was there.

In 1967, after the discovery of the muon neutrino, Pontecorvo discussed [63] the phenomenology of neutrino oscillations in modern views, including the flavor transitions $\nu_e \to \nu_\mu$ and the Majorana transitions $\nu_e \to (\nu_e^c)_L$ and $\nu_\mu \to (\nu_\mu^c)_L$. Among other subjects, he applied this study to solar neutrino oscillations. At that time, Raymond Davis started his famous experiment on the detection of solar neutrinos [64]. They were detected via the observation of the reaction

$$\nu_e + {}^{37}_{17}\mathrm{Cl} \to e^- + {}^{37}_{18}\mathrm{Ar}\,. \tag{1.14}$$

The results, measuring a ν_e flux significantly smaller than expected from solar models, created the *solar neutrino problem*.

The other grand historical problem in the neutrino field, the *atmospheric neutrino problem*, appeared in 1988 with the measurement of an anomalously small ν_μ flux at Kamiokande [65]. The understood origin of atmospheric neutrinos from cosmic rays,

$$\pi \to \mu\,\nu_\mu\,, \qquad \mu \to e\,\nu_e\,\nu_\mu\,, \tag{1.15}$$

predicted a precise ratio of muon to electron neutrinos of 2:1, whereas the smaller muon neutrino flux observed lead to a ratio of 1.2.

These two problems were eventually solved with the consolidation of the oscillation paradigm. The discovery of neutrino oscillations in 1998 by Super Kamiokande [1], solving the atmospheric neutrino problem, together the later corroboration with solar neutrinos by SNO [2], solving the solar neutrino problem, marked the birth of the modern era in neutrino physics.

Historically, it is spectacular that the fundamental concepts of $e-\mu$ universality, flavor families, neutrino mixing and oscillations were understood in a period in which the prevailing idea was that of massless neutrinos. In the centenary of the birth of Pontecorvo, José Bernabeu [66] concluded that it is fair to name the neutrino mismatch of flavor states with mass eigenstates as the PMNS Mixing Matrix.

1.4 PENDING QUESTIONS IN NEUTRINO OSCILLATIONS

The framework of neutrino oscillations is now established, and many of its parameters have reached the precision era thanks to the effort of countless experiments [1–4, 12–14, 67–88]. The standard parametrization of the PMNS matrix in terms of three mixing angles θ_{12}, θ_{23}, θ_{13} and a CP phase δ reads

$$U = \begin{bmatrix} 1 & 0 & 0 \\ 0 & c_{23} & s_{23} \\ 0 & -s_{23} & c_{23} \end{bmatrix} \begin{bmatrix} c_{13} & 0 & s_{13}\, e^{-i\delta} \\ 0 & 1 & 0 \\ -s_{13}\, e^{i\delta} & 0 & c_{13} \end{bmatrix} \begin{bmatrix} c_{12} & s_{12} & 0 \\ -s_{12} & c_{12} & 0 \\ 0 & 0 & 1 \end{bmatrix}, \tag{1.16}$$

where $c_{ij} \equiv \cos\theta_{ij}$ and $s_{ij} \equiv \sin\theta_{ij}$.

These $U_{\alpha k}$ matrix elements describe the mismatch between the flavor eigenstates $|\nu_\alpha\rangle$, produced and detected in weak interactions, and the time evolution eigenstates $|\nu_k\rangle$ with definite

mass m_k. If (relativistic) neutrinos travel a certain distance L in vacuum, their state evolves with time as

$$|\nu_\alpha(t)\rangle = \sum_k U_{\alpha k}\, e^{-iHt}\, |\nu_k\rangle \approx e^{-iEt} \sum_k U_{\alpha k}\, e^{-im_k^2 t/2E}\, |\nu_k\rangle \ . \quad (1.17)$$

Therefore, the probability of measuring flavor β after a certain time $t \approx L$ is given by $\left|\langle \nu_\beta | \nu_\alpha(t)\rangle\right|^2$ as

$$P_{\alpha\beta}(t) = \delta_{\alpha\beta} - 4\sum_{j<i} \mathrm{Re}\, J^{ij}_{\alpha\beta}\, \sin^2\Delta_{ij} - 2\sum_{j<i} \mathrm{Im}\, J^{ij}_{\alpha\beta}\, \sin 2\Delta_{ij}\,, \quad (1.18)$$

where $J^{ij}_{\alpha\beta} \equiv U_{\alpha i} U^*_{\alpha j} U^*_{\beta i} U_{\beta j}$ are rephasing-invariant combinations of the mixing matrix elements, and $\Delta_{ij} \equiv \frac{\Delta m^2_{ij} L}{4E}$ are the oscillation phases. This expression shows that neutrino oscillation experiments are sensible, besides the elements of the PMNS matrix, to the differences of squared neutrino masses $\Delta m^2_{ij} \equiv m^2_i - m^2_j$, but not to the absolute scale of neutrino masses.

In this parametrization, all the experimental measurements of neutrino oscillations converge to a standard picture whose key parameters are [9]

$$\begin{aligned} \Delta m^2_{21} &= 7.55(20) \times 10^{-5}\ \mathrm{eV}^2\,, & s^2_{12} &= 3.20(20) \times 10^{-1}\,, \\ \left|\Delta m^2_{31}\right| &= 2.50(3) \times 10^{-3}\ \mathrm{eV}^2\,, & s^2_{23} &= 5.51(30) \times 10^{-1}\,, \\ & & s^2_{13} &= 2.160(83) \times 10^{-2}\,. \end{aligned} \quad (1.19)$$

As seen, the small uncertainties in these quantities ensure that the oscillation paradigm is consistent, with the unitarity of the PMNS matrix granted up to possible deviations of a few percent. Consistent with these best-fit values, we perform all the computations in this work using the benchmark configuration

$$\begin{aligned} \theta_{12} &= 34.5^\mathrm{o}\,, \qquad \theta_{13} = 8.45^\mathrm{o}\,, \qquad \theta_{23} = 47.7^\mathrm{o}\,, \\ \Delta m^2_{21} &= 7.5 \times 10^{-5}\ \mathrm{eV}^2\,, \quad \left|\Delta m^2_{31}\right| = 2.5 \times 10^{-3}\ \mathrm{eV}^2\,. \end{aligned} \quad (1.20)$$

Despite the increasing precision in these parameters, some very crucial neutrino properties are still unknown. Regarding the oscillation picture, only the absolute value $\left|\Delta m^2_{31}\right|$ has been measured, but not its sign —unlike Δm^2_{21}, whose sign is known

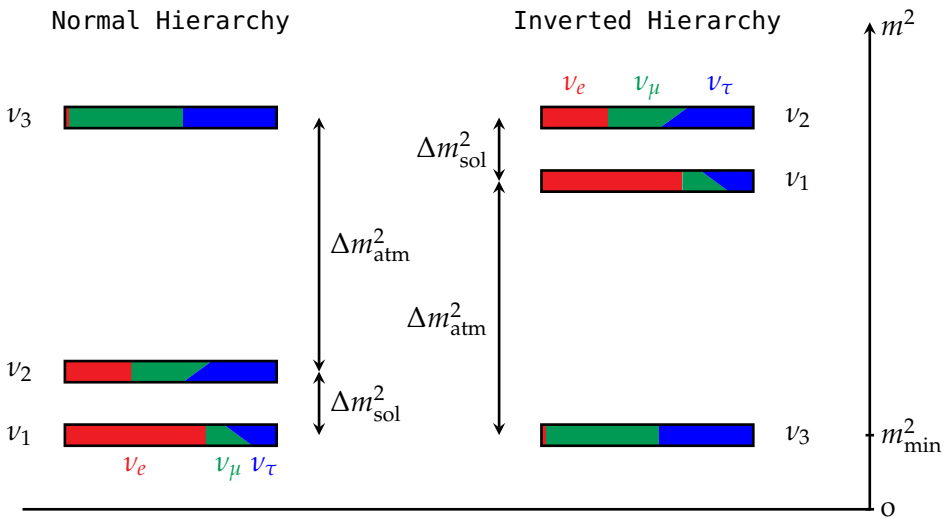

Figure 1.9: Possible neutrino mass orderings, with the mass eigenstates ν_k separated by the known atmospheric and solar mass splittings; the unknown absolute mass scale m_{min} is also shown. The colored areas show the flavor fraction $|U_{\alpha k}|^2$ of each ν_k for $\alpha = e$ (red), μ (green), τ (blue). The change in $|U_{\alpha k}|^2$ from the bottom to the top of the boxes corresponds to changing $\cos\delta$ from 1 to -1.

through the matter effects in the Sun for solar neutrinos. This sign choice opens the door to two possible mass orderings, the so-called Normal Hierarchy with $m_1 < m_2 < m_3$, and the Inverted Hierarchy with $m_3 < m_1 < m_2$, as illustrated in Figure 1.9. Fixing the Hierarchy is one of the main goals of the next-generation experiments, as is the case of the long-baseline accelerator experiment DUNE [11] or the neutrino telescopes ORCA [89] and PINGU [90].

Another most important open question is whether there is CP violation in the lepton sector. Unlike the quark sector, where CP-violating measurements have been long established [91], there is still no evidence of CP violation in the lepton sector, as could be tested in neutrino oscillations. That is a crucial property to be determined, because the quark sector by itself cannot provide the CP violation needed to explain the observed matter-antimatter

asymmetry in the universe, and CP violation in the lepton sector could compensate this deficit via leptogenesis [15]. Therefore, a measurement of CP violation in neutrino oscillations can tell us whether a Beyond the Standard Model mechanism for CP violation is needed. This is a main goal of next-generation neutrino oscillation experiments such as T2HK [10] and DUNE [11].

We analyzed the possibility to extract the answer to these two questions from the measurement of the CP, T and CPT asymmetries in neutrino oscillation transitions, as presented in Chapters 2, 3 and 4.

1.5 MAJORANA NEUTRINOS

The experimental evidence of neutrino oscillations is one of the most important discoveries in particle physics, confirming that neutrinos are massive particles and that the three left-handed flavor neutrinos ν_α are mixtures of the neutrinos with definite masses ν_k.

Knowing that neutrinos are massive, the most fundamental open problem is the determination of the nature of neutrinos with definite mass: are they four-component Dirac particles with a conserved total lepton number L, distinguishing neutrinos from antineutrinos, or two-component truly neutral (no electric charge and no total lepton number) self-conjugate Majorana particles? The fields required to realize each of these cases are schematically shown in Figure 1.10.

For Dirac neutrinos, like quarks and charged leptons, their masses can be generated in the Standard Model of particle physics by spontaneous breaking of the gauge symmetry with the Higgs scalar as

$$\mathscr{L} \supset \bar{\nu}_R \, m_D \, \nu_L \,, \tag{1.21}$$

if there were additional right-handed sterile neutrinos. In doing so, one must be willing to accept Yukawa couplings many orders of magnitude smaller than those of the other fermions, but this fact in itself is not forbidden by the gauge principle.

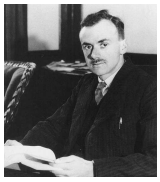

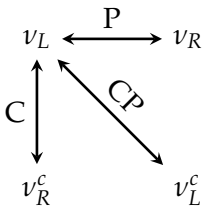

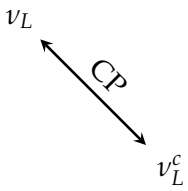

Figure 1.10: Dirac (left) and Majorana (right), with a schematic representation of the fields required to write the mass terms in Eqs. (1.21) and (1.23), as well as the C, P and CP relations between them. Notice that $\nu^c_{L(R)}$ is right (left) handed.

The crucial point comes from the fact that, once right-handed neutrinos are included in the model, the gauge-group invariance allows Majorana mass terms for them by hand. The mass terms in the Lagrangian become

$$\mathscr{L} \supset \begin{bmatrix} \bar{\nu}_L^c & \bar{\nu}_R \end{bmatrix} \begin{bmatrix} 0 & m_D \\ m_D & m_M \end{bmatrix} \begin{bmatrix} \nu_L \\ \nu_R^c \end{bmatrix}, \tag{1.22}$$

which give rise to Majorana masses for both mass eigenstates. The unavoidable conclusion is thus that there is New Physics in the neutrino sector: either one needs to add a new mechanism to forbid the gauge-allowed Majorana mass terms for ν_R, or neutrinos are the first (and only) fundamental Majorana fields.

A Majorana $\Delta L = 2$ mass term, with the active left-handed neutrinos only,

$$\mathscr{L} \supset \bar{\nu}_L^c \, m_M \, \nu_L \,, \tag{1.23}$$

leads to definite mass neutrinos with no definite charge, being a coherent superposition of the chiral left-handed neutrino and its CP-conjugate chiral right-handed antineutrino.

$$\nu_M = \nu_L + \eta \, \nu_L^c \,, \tag{1.24}$$

where η is a phase factor.

Is this superposition observable? Due to the Majorana condition of neutrinos with definite mass being their own antiparticles, Majorana neutrinos have additional CP violating phases [92–94]

beyond the Dirac case, which can be included in the PMNS mixing matrix adding the diagonal phases

$$U_{\rm PMNS} \mapsto U_{\rm PMNS} \times \begin{bmatrix} 1 & 0 & 0 \\ 0 & e^{i\alpha/2} & 0 \\ 0 & 0 & e^{i\beta/2} \end{bmatrix} . \tag{1.25}$$

Neutrino flavor oscillation experiments cannot answer the fundamental question of the nature of massive neutrinos, because in these flavor transitions the total lepton number L is conserved. Indeed, all oscillation observables are blind to the value of the Majorana phases in the PMNS matrix —they cancel out from the rephasing-invariant $J^{ij}_{\alpha\beta}$ in the transition probabilities (1.18).

In order to probe whether neutrinos are Dirac or Majorana particles, we need to study observables violating the total lepton number L. The difficulty encountered in these studies is well illustrated by the so-called "confusion theorem" [95, 96], stating that in the limit of zero mass there is no difference between Dirac and Majorana neutrinos. As all known neutrino sources produce highly relativistic neutrinos (except for the cosmic neutrino background in the universe), the $\Delta L = 2$ observables induced by the mass term (1.23) are highly suppressed by powers of m/E.

Two alternative approaches can be taken in order to probe these observables. The first one is to probe a $\Delta L = 2$ process, such as the well known neutrinoless double beta decay or the alternative neutrinoless double electron capture discussed in Chapter 5. We suggest a second novel method, looking for virtual effects of non-relativistic neutrino exchange for $\Delta L = 0$ observables when the mass terms are relevant. This situation appears for the long-range force between ordinary matter, mediated by two neutrinos, at distances of the order of the micron, studied in Chapter 6.

CP VIOLATION FOR NEUTRINO OSCILLATIONS IN MATTER

2 DISENTANGLEMENT THEOREMS

The straightforward observable to directly test whether CP is broken is a CP-violating asymmetry

$$\mathcal{A}^{\mathrm{CP}}_{\alpha\beta} \equiv P(\nu_\alpha \to \nu_\beta) - P(\bar{\nu}_\alpha \to \bar{\nu}_\beta)\,, \tag{2.1}$$

whose non-vanishing value is a proof of the violation of the symmetry. In the case of vacuum oscillations, CP-violating contributions are forbidden in the oscillation probabilities of the flavor-conserving T-invariant channels $\overset{(-)}{\nu}_\alpha \to \overset{(-)}{\nu}_\alpha$, so an appearance experiment with $\alpha \neq \beta$ is needed. This T-odd and CP-odd $\mathcal{A}^{\mathrm{CP}}_{\alpha\beta}$, which is an odd function of L/E, is a bona fide observable to test CP in the lepton sector.

The observation of CP violation, however, is very demanding. In actual experiments, neutrinos travel through the Earth matter in their path from production to detection. Due to the fact that matter is CP asymmetric —composed of protons, neutrons and electrons, but no antiparticles— this background induces extra CP-violating contributions [16, 17] in the oscillation probabilities.

Even though this fact gives the impression that a CP asymmetry is no longer a trustworthy observable to test CP in the lepton sector, we point out that these two sources of CP violation come from different principles: the genuine one, present in vacuum oscillations, behaves as a T-violating and CPT-invariant effect, whereas matter effects are CPT violating and T invariant in terrestrial experiments. In this Chapter, we will exploit these different origins to separate their effects in the observable CP asymmetry $\mathcal{A}^{\mathrm{CP}}_{\alpha\beta}$.

2.1 CP ASYMMETRY DISENTANGLEMENT THEOREM

Neutrino oscillations in matter are described through the effective Hamiltonian in the flavor basis [16, 97–101]

$$H = \frac{1}{2E}\left\{ U \begin{bmatrix} m_1^2 & 0 & 0 \\ 0 & m_2^2 & 0 \\ 0 & 0 & m_3^2 \end{bmatrix} U^\dagger + \begin{bmatrix} a & 0 & 0 \\ 0 & 0 & 0 \\ 0 & 0 & 0 \end{bmatrix} \right\} = \frac{1}{2E}\, \tilde{U}\tilde{M}^2\tilde{U}^\dagger\,, \tag{2.2}$$

where the first term describes neutrino oscillations in vacuum, leading to the transition probabilities in Eq. (1.18), and the second one accounts for matter effects. The a parameter is given by $a = 2EV$, with V the interaction potential with matter and E the relativistic neutrino energy. The reason why matter effects only enter the H_{ee} matrix element is that the only non-diagonal neutrino-matter interaction is $V_{ee} = \pm\sqrt{2}G_F N_e$, generated by charged current $\nu_e e$ coherent forward scattering, where the $+(-)$ sign is for (anti)neutrinos, G_F is the Fermi constant and N_e is the electron fraction density.

For antineutrinos, $U \to U^*$, originating a genuine CP violation effect through the CP phase δ in the mixing matrix (1.16), as well as $a \to -a$, originating matter-induced CP violation. All neutrino masses $(\tilde{M}^2)$ and mixings $(\tilde{U})$ in matter, i.e. eigenvalues and eigenstates of H, can be calculated in terms of the parameters in the vacuum Hamiltonian (M^2, U) and a, as studied in Chapter 3.

For any number of mass eigenstates, the exact Hamiltonian leads to the flavor oscillation probabilities $P_{\alpha\beta}$ for any $\nu_\alpha \to \nu_\beta$ transition

$$P_{\alpha\beta} = \delta_{\alpha\beta} - 4\sum_{j<i} \mathrm{Re}\ \tilde{J}^{ij}_{\alpha\beta}\, \sin^2\tilde{\Delta}_{ij} - 2\sum_{j<i} \mathrm{Im}\ \tilde{J}^{ij}_{\alpha\beta}\, \sin 2\tilde{\Delta}_{ij}\,, \tag{2.3}$$

which are formally equivalent to the oscillation probabilities in Eq. (1.18) after replacing for the effective values in matter of the rephasing-invariant mixings $\tilde{J}^{ij}_{\alpha\beta} \equiv \tilde{U}_{\alpha i}\tilde{U}^*_{\alpha j}\tilde{U}^*_{\beta i}\tilde{U}_{\beta j}$, and the oscillation phases $\tilde{\Delta}_{ij} \equiv \frac{\Delta\tilde{m}^2_{ij}L}{4E}$. Notice that both $\tilde{J}^{ij}_{\alpha\beta}$ and $\Delta\tilde{m}^2_{ij}$ are energy

dependent in matter via the matter parameter a. Antineutrino oscillations are given in general by the same expression with different masses ($\Delta\tilde{\bar{m}}^2_{ij}$) and mixings ($\tilde{\bar{J}}^{ij}_{\alpha\beta}$), so one can explicitly write the CP asymmetry $\mathcal{A}^{\rm CP}_{\alpha\beta}$ defined in Eq. (2.1) as

$$\begin{aligned}\mathcal{A}^{\rm CP}_{\alpha\beta} = &-4\sum_{j<i}\left[\text{Re}\,\tilde{J}^{ij}_{\alpha\beta}\,\sin^2\tilde{\Delta}_{ij} - \text{Re}\,\tilde{\bar{J}}^{ij}_{\alpha\beta}\,\sin^2\tilde{\bar{\Delta}}_{ij}\right]\\ &-2\sum_{j<i}\left[\text{Im}\,\tilde{J}^{ij}_{\alpha\beta}\,\sin 2\tilde{\Delta}_{ij} - \text{Im}\,\tilde{\bar{J}}^{ij}_{\alpha\beta}\,\sin 2\tilde{\bar{\Delta}}_{ij}\right]\,. \qquad (2.4)\end{aligned}$$

With the objective to check which terms are either genuine (CP&T-violating) or matter induced (CP&CPT-violating), we first explore the CPT- and T-invariant limits.

If CPT holds, as assumed in vacuum, necessarily $\Delta\bar{m}^2_{ij} = \Delta m^2_{ij}$ and $\bar{J}^{ij}_{\alpha\beta} = (J^{ij}_{\alpha\beta})^*$. The two terms in the first line of Eq. (2.4) would thus cancel each other out, which shows that all L-even terms in $\mathcal{A}^{\rm CP}_{\alpha\beta}$ are CPT violating.

In the absence of genuine CP violation, on the other hand, T invariance leads to real $\tilde{J}^{ij}_{\alpha\beta}$ and $\tilde{\bar{J}}^{ij}_{\alpha\beta}$, so all imaginary parts vanish and the transition probabilities are L-even functions. This result shows that L-odd terms in both $P_{\alpha\beta}$ and $\mathcal{A}^{\rm CP}_{\alpha\beta}$ are T violating.

From the different character of each of these terms under the discrete T and CPT symmetries, one derives the **Asymmetry Disentanglement Theorem** by separating the observable CP asymmetry in any flavor transition into L-even (matter-induced CP&CPT violating) and L-odd (genuine CP&T violating) functions, $\mathcal{A}^{\rm CP}_{\alpha\beta} = A^{\rm CP;T}_{\alpha\beta} + A^{\rm CP;CPT}_{\alpha\beta}$, given by

$$A^{\rm CP;T}_{\alpha\beta} = -2\sum_{j<i}\left[\text{Im}\,\tilde{J}^{ij}_{\alpha\beta}\,\sin 2\tilde{\Delta}_{ij} - \text{Im}\,\tilde{\bar{J}}^{ij}_{\alpha\beta}\,\sin 2\tilde{\bar{\Delta}}_{ij}\right]\,, \quad (2.5a)$$

$$A^{\rm CP;CPT}_{\alpha\beta} = -4\sum_{j<i}\left[\text{Re}\,\tilde{J}^{ij}_{\alpha\beta}\,\sin^2\tilde{\Delta}_{ij} - \text{Re}\,\tilde{\bar{J}}^{ij}_{\alpha\beta}\,\sin^2\tilde{\bar{\Delta}}_{ij}\right]\,. \quad (2.5b)$$

Let us emphasize that not only $A^{\rm CP;CPT}_{\alpha\beta}$ is CPT violating and $A^{\rm CP;T}_{\alpha\beta}$ is T violating, we also find that $A^{\rm CP;CPT}_{\alpha\beta}$ is T invariant and $A^{\rm CP;T}_{\alpha\beta}$ is CPT invariant. In this sense the two terms are truly

disentangled. To prove these properties, we analyze the effects of both CPT and T transformations,

$$\text{CPT}: \begin{cases} \Delta\tilde{m}^2_{ij} \leftrightarrow \Delta\tilde{\bar{m}}^2_{ij} \\ \tilde{J}^{ij}_{\alpha\beta} \leftrightarrow (\tilde{\bar{J}}^{ij}_{\alpha\beta})^* \end{cases}, \qquad \text{T}: \begin{cases} \tilde{J}^{ij}_{\alpha\beta} \to (\tilde{J}^{ij}_{\alpha\beta})^* \\ \tilde{\bar{J}}^{ij}_{\alpha\beta} \to (\tilde{\bar{J}}^{ij}_{\alpha\beta})^* \end{cases}. \tag{2.6}$$

Under CPT, neutrino and antineutrino terms in $A^{\text{CP;CPT}}_{\alpha\beta}$ are interchanged, so $A^{\text{CP;CPT}}_{\alpha\beta}$ changes its sign. This sign in $A^{\text{CP;T}}_{\alpha\beta}$ is compensated by the change of sign in both $\text{Im}\,\tilde{J}^{ij}_{\alpha\beta}$ and $\text{Im}\,\tilde{\bar{J}}^{ij}_{\alpha\beta}$, leaving $A^{\text{CP;T}}_{\alpha\beta}$ invariant. Under T, on the other hand, the only change in the asymmetries is a change of sign in all imaginary parts, changing the sign of $A^{\text{CP;T}}_{\alpha\beta}$ and leaving $A^{\text{CP;CPT}}_{\alpha\beta}$ invariant.

These properties lead cleanly to the disentanglement of the CP asymmetry $\mathcal{A}^{\text{CP}}_{\alpha\beta} = A^{\text{CP;T}}_{\alpha\beta} + A^{\text{CP;CPT}}_{\alpha\beta}$, where $A^{\text{CP;T}}_{\alpha\beta}$ is CPT invariant and T-odd in L, whereas $A^{\text{CP;CPT}}_{\alpha\beta}$ is T invariant (even in L) and CPT odd. These complementary behaviors of the two components of the experimental CP asymmetry identify the component $A^{\text{CP;T}}_{\alpha\beta}$ as CPT invariant and thus a fully genuine CPV observable, whereas the component $A^{\text{T;CPT}}_{\alpha\beta}$ is T invariant and thus a fully fake matter-induced CPV observable.

2.2 DEFINITE PARITIES IN THE STANDARD PARAMETERS

The disentanglement (2.5) provides a conceptually clean criterion to separate genuine from matter-induced terms in the CP asymmetry. However, the measurement of $\mathcal{A}^{\text{CP}}_{\alpha\beta}$ as a function of the baseline is not always feasible, due to the large requirements of a neutrino detector. In order to connect with actual experiments, we analyze the consequences of the disentanglement in terms of the parameters in the Hamiltonian (2.2).

The only difference between neutrinos and antineutrinos in the Hamiltonian is the sign change in a and δ, that corresponds to a CP transformation. As in vacuum, the only effect of the anti-unitary T transformation in the matter Hamiltonian comes from

Table 2.1: Definite parities of the mixing parameters under all discrete symmetries: CP (diagonals), T (rows) and CPT (columns).

	CPT-even	CPT-odd	
T-even	$\cos\delta$	a, $a\cos\delta$	CP-odd
T-odd	$\sin\delta$	$a\sin\delta$	CP-even

changing $e^{i\delta} \mapsto e^{-i\delta}$, all other parameters remaining invariant. The effects of CPT are thus only changing the sign of a. This behavior of the key parameters a, δ under the three discrete symmetries is summarized in Table 2.1.

In the disentangled components (2.5) with definite L parities, one expects the definite parities under T and CPT to translate into definite parities in the CP phase δ and the matter parameter a, respectively. In order to check whether this happens, we study the functional dependence of the components on these two parameters.

The CPT-invariant T-odd component (2.5a) depends on the mixings only via their imaginary parts, so the functional form of this $\nu - \bar{\nu}$ difference must be $f(a)\sin\delta - f(-a)\sin(-\delta)$. Indeed, this expression shows that $A_{\alpha\beta}^{\mathrm{CP;T}}$ must be an odd function in $\sin\delta$, consistent with its T-odd character, and an even function in a. As expected, this even parity in a is consistent with its non-vanishing value in vacuum, whereas the odd parity in $\sin\delta$ forces this component to vanish in the absence of T violation, i.e. for a real mixing matrix, even in matter.

The CPT-odd T-invariant component (2.5b), on the other hand, depends on the mixings only via their real parts, so its functional form must be $f(a,\cos\delta) - f(-a,\cos(-\delta))$. Indeed, this expression shows that $A_{\alpha\beta}^{\mathrm{CP;CPT}}$ must be an even function in δ, consistent with its T-invariant character, and an odd function in a. Since CPT violation only comes into the Hamiltonian (2.2) from matter effects, this odd parity in a ensures that the CPT-violating component vanishes in the vacuum limit $a \to 0$, as it must. On

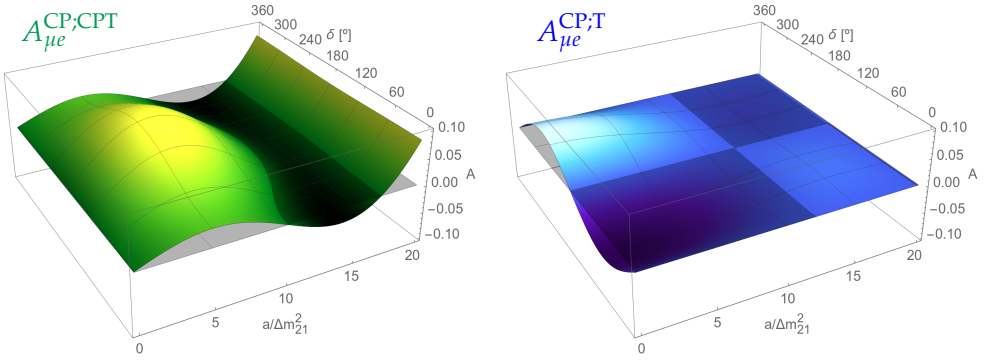

Figure 2.1: CPT-odd (left) and T-odd (right) components of the CP asymmetry $\mathcal{A}_{\mu e}^{CP}$ at $L = 1300$ km and $E = 0.75$ GeV, as function of the matter parameter a (in units of Δm_{21}^2) and the CP phase δ.

the contrary, nothing can be imposed in the T-invariant limit, since an even function of δ can have any value even if δ is zero —one thus expects a non-vanishing CP asymmetry in matter even in T-invariant disappearing channels $\mathcal{A}_{\alpha\alpha}^{CP}$, unlike the vacuum case.

We illustrate in Figure 2.1 the power and expected behavior of the Disentanglement Theorem by a separate representation of $A_{\mu e}^{CP;CPT}$ and $A_{\mu e}^{CP;T}$ as function of the matter potential a and the CP phase δ. The chosen (E, L) point gives comparable values of the two components, showing their appropriate parities under these two parameters.

2.3 FULL DISENTANGLEMENT OF ALL ASYMMETRIES

In the previous Sections of this Chapter we analyzed the disentanglement of the CP asymmetry into two separate components, one of them also CPT violating and T invariant, the other one T violating and CPT invariant. The same reasoning can be applied to both T and CPT asymmetries, separating them into components with definite behavior under the other two discrete symmetries.

Let us focus first on the T-violating asymmetries. According to the definition of the rephasing-invariant mixings below Eq. (2.3), the identity $\tilde{J}^{ij}_{\beta\alpha} = (\tilde{J}^{ij}_{\alpha\beta})^*$ holds, so the $\alpha \leftrightarrow \beta$ exchange in the T asymmetry leads to

$$\mathcal{A}^{\rm T}_{\alpha\beta} \equiv P_{\alpha\beta} - P_{\beta\alpha} = -4 \sum_{j<i} {\rm Im}\ \tilde{J}^{ij}_{\alpha\beta}\, \sin 2\tilde{\Delta}_{ij}\,, \tag{2.7}$$

which is an odd function of the baseline L, as imposed by its T-odd character. Notice that, even though matter may affect the T asymmetry, it cannot generate a non-vanishing T asymmetry in the absence of genuine T violation —the real mixing matrix would ensure a vanishing $\mathcal{A}^{\rm T}_{\alpha\beta}$. Therefore, contrary to the CP asymmetry case, a non-vanishing T asymmetry in matter is a direct proof of the existence of genuine CP violation in the lepton sector. Strangely enough, this reasoning does not prove that CP violation has actually been seen in the T asymmetry, unless one is able to separate a genuine T&CP-odd component.

To check whether the asymmetry (2.7) violates CP or CPT, as well as T, one should compare it with its $\bar{\nu}$ equivalent,

$$\bar{\mathcal{A}}^{\rm T}_{\alpha\beta} \equiv \bar{P}_{\alpha\beta} - \bar{P}_{\beta\alpha} = -4 \sum_{j<i} {\rm Im}\ \tilde{\bar{J}}^{ij}_{\alpha\beta}\, \sin 2\tilde{\bar{\Delta}}_{ij}\,, \tag{2.8}$$

and separately check their behavior in the CP- and CPT-invariant limits. Imposing CP: $\{\Delta\tilde{m}^2_{ij} = \Delta\tilde{\bar{m}}^2_{ij},\ \tilde{J}^{ij}_{\alpha\beta} = \tilde{\bar{J}}^{ij}_{\alpha\beta}\}$ leads to the identity $\bar{\mathcal{A}}^{\rm T}_{\alpha\beta} = \mathcal{A}^{\rm T}_{\alpha\beta}$. Conversely, CPT: $\{\Delta\tilde{m}^2_{ij} = \Delta\tilde{\bar{m}}^2_{ij},\ \tilde{J}^{ij}_{\alpha\beta} = (\tilde{\bar{J}}^{ij}_{\alpha\beta})^*\}$ imposes $\bar{\mathcal{A}}^{\rm T}_{\alpha\beta} = -\mathcal{A}^{\rm T}_{\alpha\beta}$. Therefore, we expect from symmetry principles that all terms in $\mathcal{A}^{\rm T}_{\alpha\beta}$ will also appear in $\bar{\mathcal{A}}^{\rm T}_{\alpha\beta}$, either with the same sign —and so conserving CP and violating CPT— or with opposite sign —violating CP, and CPT invariant.

These symmetry principles imply that a consistent separation of the T asymmetry into two disentangled components, $\mathcal{A}^{\rm T}_{\alpha\beta} = A^{\rm T;CP}_{\alpha\beta} + A^{\rm T;CPT}_{\alpha\beta}$, needs the decomposition of the antineutrino asymmetry, in terms of the *same* components as $\mathcal{A}^{\rm T}_{\alpha\beta}$, into $\bar{\mathcal{A}}^{\rm T}_{\alpha\beta} = -A^{\rm T;CP}_{\alpha\beta} + A^{\rm T;CPT}_{\alpha\beta}$. These two disentangled components with definite parities under all CP, T and CPT can thus be understood as a symmetry-inspired basis of functions to describe the experimental T asymmetries.

Explicit expressions for these two components can be obtained from linear combinations of Eqs. (2.7, 2.8) as

$$A^{\mathrm{T;CP}}_{\alpha\beta} = -2\sum_{j<i}\left[\mathrm{Im}\ \tilde{J}^{ij}_{\alpha\beta}\,\sin 2\tilde{\Delta}_{ij} - \mathrm{Im}\ \tilde{\bar{J}}^{ij}_{\alpha\beta}\,\sin 2\tilde{\bar{\Delta}}_{ij}\right], \quad (2.9a)$$

$$A^{\mathrm{T;CPT}}_{\alpha\beta} = -2\sum_{j<i}\left[\mathrm{Im}\ \tilde{J}^{ij}_{\alpha\beta}\,\sin 2\tilde{\Delta}_{ij} + \mathrm{Im}\ \tilde{\bar{J}}^{ij}_{\alpha\beta}\,\sin 2\tilde{\bar{\Delta}}_{ij}\right]. \quad (2.9b)$$

Notice that the expression (2.9a) for the CP-odd CPT-invariant component of the T asymmetry is the same as the genuine T-odd CPT-invariant component of the CP asymmetry in Eq. (2.5a). This fact can be understood from the *asymmetry sum rule*[1]

$$\mathcal{A}^{\mathrm{CPT}}_{\alpha\beta} = \mathcal{A}^{\mathrm{CP}}_{\alpha\beta} + \bar{\mathcal{A}}^{\mathrm{T}}_{\alpha\beta}\,. \quad (2.10)$$

In the CPT-invariant limit, this relation reduces to $A^{\mathrm{T;CP}}_{\alpha\beta} = A^{\mathrm{CP;T}}_{\alpha\beta}$. The fact that these two components are always CPT invariant ensures that this identity is valid even if there is CPT violation, thus explaining the obtained result.

On the other hand, a new component $A^{\mathrm{T;CPT}}_{\alpha\beta}$ (2.9b) appears in the T asymmetry not seen in the CP asymmetry. Contrary to the matter-induced $A^{\mathrm{CP;CPT}}_{\alpha\beta}$ (2.5b), a non-vanishing value of this component requires the combined effect of both genuine CP violation *and* the matter-induced CPT violation. Hence it is clear that, in general, a non-vanishing T asymmetry in matter will present contributions from this CP-even component.

One can further exploit the sum rule in Eq. (2.10) to constraint a consistent separation of the CPT asymmetry, following the same guiding principles as with the CP and T asymmetries, into T-odd CP-invariant and CP-odd T-invariant components, $\mathcal{A}^{\mathrm{CPT}}_{\alpha\beta} \equiv P_{\alpha\beta} - \bar{P}_{\beta\alpha} = A^{\mathrm{CPT;CP}}_{\alpha\beta} + A^{\mathrm{CPT;T}}_{\alpha\beta}$. The expression of the sum rule fully expanded into components,

$$A^{\mathrm{CPT;CP}}_{\alpha\beta} + A^{\mathrm{CPT;T}}_{\alpha\beta} = A^{\mathrm{CP;CPT}}_{\alpha\beta} + A^{\mathrm{CP;T}}_{\alpha\beta} + A^{\mathrm{T;CPT}}_{\alpha\beta} - A^{\mathrm{T;CP}}_{\alpha\beta}\,, \quad (2.11)$$

1 This identity is trivially proved from the definition of the three asymmetries as differences of oscillation probabilities, $P_{\alpha\beta} - \bar{P}_{\beta\alpha} = P_{\alpha\beta} - \bar{P}_{\alpha\beta} + \bar{P}_{\alpha\beta} - \bar{P}_{\beta\alpha}$.

implies that, due to the separate invariance under the three discrete symmetries, the following three equalities must be independently satisfied:

$$\text{the CP-invariant} \qquad A^{\text{CPT;T}}_{\alpha\beta} = A^{\text{T;CPT}}_{\alpha\beta}\,, \tag{2.12a}$$

$$\text{the T-invariant} \qquad A^{\text{CPT;CP}}_{\alpha\beta} = A^{\text{CP;CPT}}_{\alpha\beta}\,, \tag{2.12b}$$

$$\text{the CPT-invariant} \qquad A^{\text{CP;T}}_{\alpha\beta} = A^{\text{T;CP}}_{\alpha\beta}\,. \tag{2.12c}$$

Therefore, the decomposition of all asymmetries,

$$\mathcal{A}^{\text{CP}}_{\alpha\beta} = A^{\text{CP;T}}_{\alpha\beta} + A^{\text{CP;CPT}}_{\alpha\beta}\,, \tag{2.13a}$$

$$\mathcal{A}^{\text{T}}_{\alpha\beta} = A^{\text{T;CPT}}_{\alpha\beta} + A^{\text{T;CP}}_{\alpha\beta}\,, \qquad \bar{\mathcal{A}}^{\text{T}}_{\alpha\beta} = A^{\text{T;CPT}}_{\alpha\beta} - A^{\text{T;CP}}_{\alpha\beta}\,, \tag{2.13b}$$

$$\mathcal{A}^{\text{CPT}}_{\alpha\beta} = A^{\text{CPT;T}}_{\alpha\beta} + A^{\text{CPT;CP}}_{\alpha\beta}\,, \quad \bar{\mathcal{A}}^{\text{CPT}}_{\alpha\beta} = A^{\text{CPT;T}}_{\alpha\beta} - A^{\text{CPT;CP}}_{\alpha\beta}\,, \tag{2.13c}$$

is written in a basis of only three (per flavor channel) independent components, since the two superindices of all components commute. These indices state under which two symmetries the component is odd, being invariant under the third one.

Their peculiar behavior under the CP, T and CPT discrete symmetries shows that these three independent components correspond to:

- $A^{\text{CP;T}}_{\alpha\beta}$ (2.5a) the CPT-invariant CP&T-odd genuine component of the CP asymmetry
- $A^{\text{CP;CPT}}_{\alpha\beta}$ (2.5b) the T-invariant CP&CPT-odd matter-induced component of the CP asymmetry
- $A^{\text{T;CPT}}_{\alpha\beta}$ (2.9b) the CP-invariant T&CPT-odd interference component, induced by matter in presence of genuine CP violation, breaking the vacuum identity $\bar{\mathcal{A}}^{\text{T}}_{\alpha\beta} = -\mathcal{A}^{\text{T}}_{\alpha\beta}$.

Notice that the interchange of flavor indices corresponds to a T transformation, so all T-odd components will be odd under $\alpha \leftrightarrow \beta$, whereas T-invariant components will remain unchanged.

These components are a theoretically clean tool to study effects of the violation of the discrete symmetries in neutrino oscillations. We will exploit their properties in the next two Chapters in order

Table 2.2: Definite parities of the three independent components under the three CP, T and CPT discrete symmetries. These parities are associated to definite parities of the functions under the parameters in brackets.

	CP	T $(L, \sin\delta)$	CPT (a)
$A_{\alpha\beta}^{\mathrm{CP;T}}$	odd	odd	even
$A_{\alpha\beta}^{\mathrm{CP;CPT}}$	odd	even	odd
$A_{\alpha\beta}^{\mathrm{T;CPT}}$	even	odd	odd

to design clear, direct tests of the violation of CP in the lepton sector. For further reference, all the properties discussed in this Section are summarized in Table 2.2

3 METHODS TO EXPLORE THE THEOREMS IMPLICATIONS

In the picture described by the Hamiltonian (2.2), where no BSM effects are included in the vacuum limit, the mixing matrix $\tilde{U}$ is unitary and the only sources of CP violation are the CPT-even genuine phase δ, and the T-even matter parameter a. In the vacuum limit $a \to 0$, the two CPT-odd components defined in the previous Chapter vanish, as well as the whole CPT asymmetries $\mathcal{A}^{\text{CPT}}_{\alpha\beta}$, and the other two experimental asymmetries are fully genuine, $\mathcal{A}^{\text{CP}}_{\alpha\beta} = \mathcal{A}^{\text{T}}_{\alpha\beta} = A^{\text{CP;T}}_{\alpha\beta}$.

Three generations are needed so that there is room for a CP violating phase in the mixing matrix: the most general 2×2 unitary matrix is described by a single angle, whereas a 3×3 unitary matrix —such as the PMNS matrix in Eq. (1.16)— requires 3 angles and 1 phase. This effective erasing of all CP-violating effects in the 2-generation limit implies that the only experimental regimes where CP violation can be probed are those where all three generations play a relevant role.

In the case of neutrino oscillations in vacuum, this only happens at L/E values where the phases associated to Δm^2_{21} and Δm^2_{31} are both neither negligible nor averaged out. In order to lay in this region, the experimental relation $\Delta m^2_{31} \approx 33 \Delta m^2_{21}$ requires an L/E so that the phase Δ_{31} is not too large and the phase Δ_{21} not too small. At long-baseline accelerator experiments, even with the phase displacement due to matter effects in the neutrino propagation, one finds that energies $E \sim$ GeV and baselines $L \sim 10^3$ km provide a convenient setup to observe CP-violating effects in neutrino oscillations. Therefore, we will focus on the baselines and energy ranges of the T2HK [10] and DUNE [11] experiments.

Accelerator experiments favor the $\nu_\mu \to \nu_e$ transition, and are also sensitive to its CP counterpart $\bar{\nu}_\mu \to \bar{\nu}_e$. As discussed in the previous Chapter, the disentanglement of genuine and

matter-induced CP violation in these channels can be achieved separating the CP asymmetry $\mathcal{A}_{\mu e}^{\rm CP}$ into its T-odd CPT-even and CPT-odd T-even components, $A_{\mu e}^{\rm CP;T}$ and $A_{\mu e}^{\rm CP;CPT}$. As a complete study, we will also analyze the third independent component $A_{\mu e}^{\rm T;CPT}$, induced by matter effects in the T asymmetry $\mathcal{A}_{\mu e}^{\rm T}$. Its direct observability would require terrestrial sources of electron neutrinos with equal energies to those for muon neutrino sources, not accessible at present. However, these $\mathcal{A}_{\mu e}^{\rm T}$ and $\bar{\mathcal{A}}_{\mu e}^{\rm T}$ asymmetries would be natural for a neutrino factory [102] and they are ingredients for an analysis using atmospheric neutrinos.

With this objective of testing genuine CP violation in mind, we develop tools to explore whether, at fixed L through the Earth's crust, the energy distributions of the three disentangled components present signatures of their separation in the observable asymmetries.

3.1 FIRST APPROACH: A NUMERICAL SCAN

Starting from the 3×3 Hamiltonian (2.2) in matter

$$H = \frac{1}{2E}\left\{ U \begin{bmatrix} m_1^2 & 0 & 0 \\ 0 & m_2^2 & 0 \\ 0 & 0 & m_3^2 \end{bmatrix} U^\dagger + \begin{bmatrix} a & 0 & 0 \\ 0 & 0 & 0 \\ 0 & 0 & 0 \end{bmatrix} \right\} = \frac{1}{2E}\, \tilde{U}\tilde{M}^2\tilde{U}^\dagger$$

with the best-fit oscillation parameters in Eq. (1.20),

$$\begin{aligned} \theta_{12} = 34.5^\circ\,, \qquad \theta_{13} = 8.45^\circ\,, \qquad \theta_{23} = 47.7^\circ\,, \\ \Delta m_{21}^2 = 7.5 \times 10^{-5}\ \text{eV}^2\,, \qquad \left|\Delta m_{31}^2\right| = 2.5 \times 10^{-3}\ \text{eV}^2\,, \end{aligned}$$

computing the neutrino evolution numerically is straightforward. The eigenvalues of this matrix are the effective neutrino masses in matter, whereas its eigenstates (whose phase must be chosen so that $\lim_{a\to 0} |\tilde{\nu}_i\rangle = |\nu_i\rangle$) determine the elements of $\tilde{U}$. For any value of δ and a chosen Hierarchy, this diagonalization can be performed iteratively to compute these quantities as a function of the matter potential, as shown in Figure 3.1. Once this process is done, deriving the disentangled components is a matter of

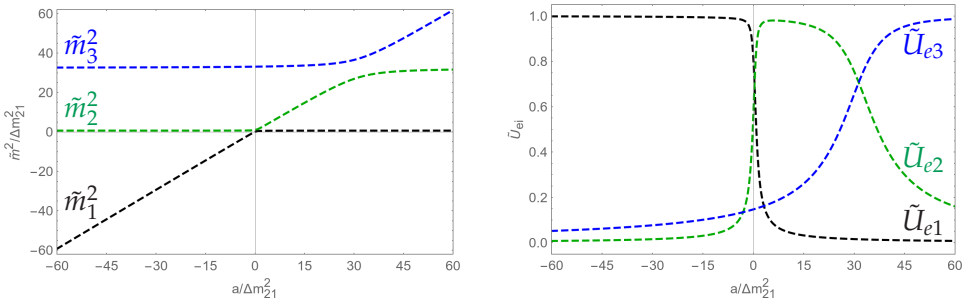

Figure 3.1: Effective masses (left) and mixings $\tilde{U}_{ei}$ (right) as a function of the matter parameter a in units of Δm^2_{21}, as an example of the results provided by the numerical diagonalization of the Hamiltonian (2.2). Normal Hierarchy and $\delta = 0$ assumed, as well as the best-fit values in Eq.(1.20).

computing them from their definitions in the previous Chapter's Eqs. (2.5) and (2.9).

Figure 3.2 gives the predictions for the energy distributions of $A_{\mu e}^{\mathrm{CP;T}}$, $A_{\mu e}^{\mathrm{CP;CPT}}$ and $A_{\mu e}^{\mathrm{T;CPT}}$ at an intermediate baseline $L = 295$ km, for both Normal and Inverted Hierarchies. In order to compare the two Hierarchies for the same physical configuration of masses, we always use the NH best-fit values in Eq. (1.20), and compute the Inverted Hierarchy case with the condition $\Delta m^2_{31}|_{\mathrm{IH}} = -\Delta m^2_{32}|_{\mathrm{NH}}$, keeping the same values for all other quantities. In this way, one is consistent in isolating the observable effects due to the change in the ordering of the same neutrino mass states.

It is worth to note the lack of oscillating structure in the neutrino energy for all three components, and hence for the asymmetries. The magnitude of the CPT-odd components $A_{\mu e}^{\mathrm{CP;CPT}}$ and $A_{\mu e}^{\mathrm{T;CPT}}$ is small, as expected, and slightly dependent on the CP phase δ through the small contributions of order Δm^2_{21}, more visible at low energies —the first component as a genuine CP-conserving $\cos\delta$, the second one as a genuine CP-odd $\sin\delta$. When these results for a Normal Hierarchy are re-calculated for an Inverted Hierarchy, the net effect is essentially a change of sign in the two components.

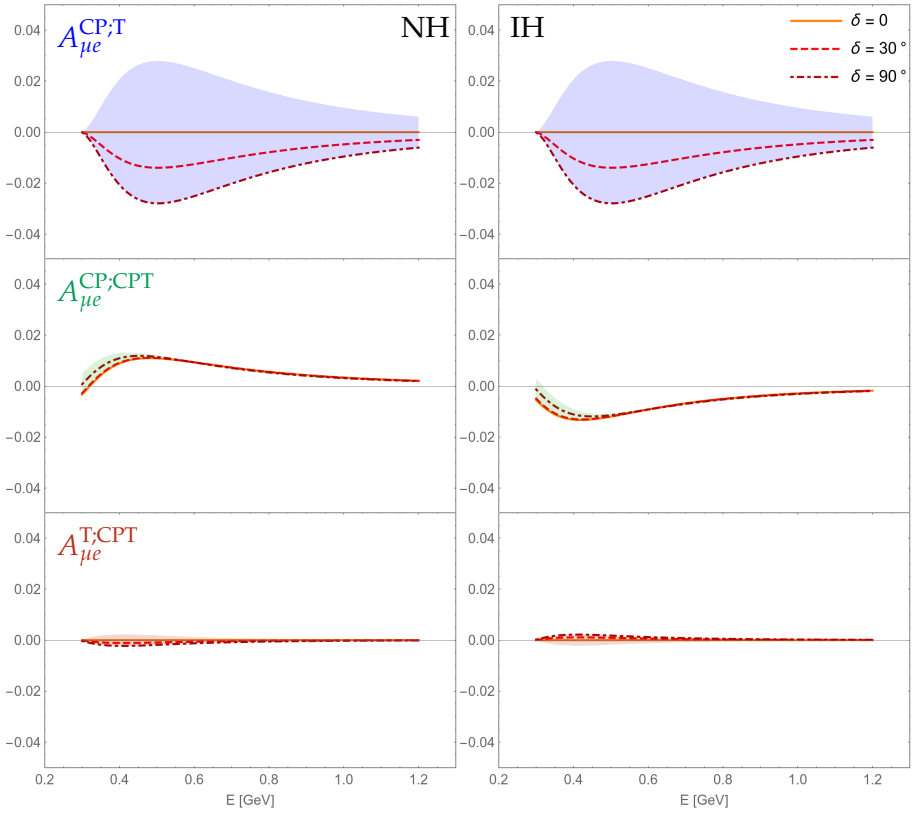

Figure 3.2: Energy distribution of the genuine $A_{\mu e}^{CP;T}$ (top), matter-induced $A_{\mu e}^{CP;CPT}$ (middle) and interference $A_{\mu e}^{T;CPT}$ (bottom) components for the T2HK baseline $L = 295$ km. Normal (Inverted) Hierarchy in the left (right). The bands show all possible values of each term changing δ in $(0, 2\pi)$.

Unlike the matter-induced component of the CP asymmetry, the magnitude of $A_{\mu e}^{CP;T}$ is proportional to $\sin\delta$ without any degeneracy when $\sin\delta$ is varied in the entire interval from -1 to 1. In this genuine term of $\mathcal{A}_{\mu e}^{CP}$, in addition, the Hierarchy in the neutrino mass spectrum plays no role: it remains invariant when the sign of the largest mass splitting is changed.

We thus conclude that a separate determination of the CP asymmetry components would (i) fix the Hierarchy, via the sign of the matter-induced component $A_{\mu e}^{CP;CPT}$, and (ii) fix $\sin\delta$ from

the magnitude and sign of the genuine component $A_{\mu e}^{\mathrm{CP;T}}$. Due to the fact that both genuine CP violation and Hierarchy effects are present in the interfere component $A_{\mu e}^{\mathrm{T;CPT}}$, the value of one of them can only be extracted once the other one is known.

For any flavor channel $\alpha \to \beta$, this beautiful different behavior of the genuine CPT-invariant component with respect to the two CPT-odd components for the discrimination of the Hierarchy is well understood to leading order in Δm_{21}^2: zeroth order for the T-even $A_{\alpha\beta}^{\mathrm{CP;CPT}}$, independent of δ, and first order for the T-odd $A_{\alpha\beta}^{\mathrm{CP;T}}$ and $A_{\alpha\beta}^{\mathrm{T;CPT}}$. The mass spectrum in matter changes from neutrinos to antineutrinos as

$$\Delta\tilde{m}_{21}^2 \leftrightarrow \Delta\bar{\tilde{m}}_{21}^2\,, \quad \Delta\tilde{m}_{31}^2 \leftrightarrow -\Delta\bar{\tilde{m}}_{32}^2\,, \quad \Delta\tilde{m}_{32}^2 \leftrightarrow -\Delta\bar{\tilde{m}}_{31}^2\,. \tag{3.1}$$

Under this exchange of neutrinos by antineutrinos, the imaginary part of $\tilde{J}_{\alpha\beta}^{ij}$, as that of $J_{\alpha\beta}^{ij}$, changes sign whereas the real parts do not. As the CP asymmetries (2.1) are a difference between neutrino and antineutrino oscillation probabilities, we discover that $A_{\alpha\beta}^{\mathrm{CP;CPT}}$ is changing its sign, whereas the sign of $A_{\alpha\beta}^{\mathrm{CP;T}}$ remains invariant under the change of Hierarchy, as seen in our numerical results. The interference component $A_{\alpha\beta}^{\mathrm{T;CPT}}$, on the other hand, is a sum of imaginary parts, so it changes its sign as the other CPT-odd component. The modifications to this argument due to a non-vanishing Δm_{21}^2 will be analyzed in detail in Section 4.2.

The increase in the baseline from $L = 295$ km to $L = 1300$ km has a very important implication: the appearance of oscillations in the low and medium neutrino energy regions of the distributions. There is a different pattern for the two components of the experimental CP asymmetry, with the zeros at different values and $A_{\mu e}^{\mathrm{CP;CPT}}$ changing its sign around the zeros, whereas $A_{\mu e}^{\mathrm{CP;T}}$ does not. This contrast is very well apparent in the results we show in Figure 3.3, where one also sees that the interference component $A_{\mu e}^{\mathrm{T;CPT}}$ presents the same oscillation pattern as the matter-induced $A_{\mu e}^{\mathrm{CP;CPT}}$.

Besides this additional effect of having in the different energy distributions a signature to separate the two components of the CP asymmetry, all the other properties discussed above remain the same, independent of the baseline. These are the slight

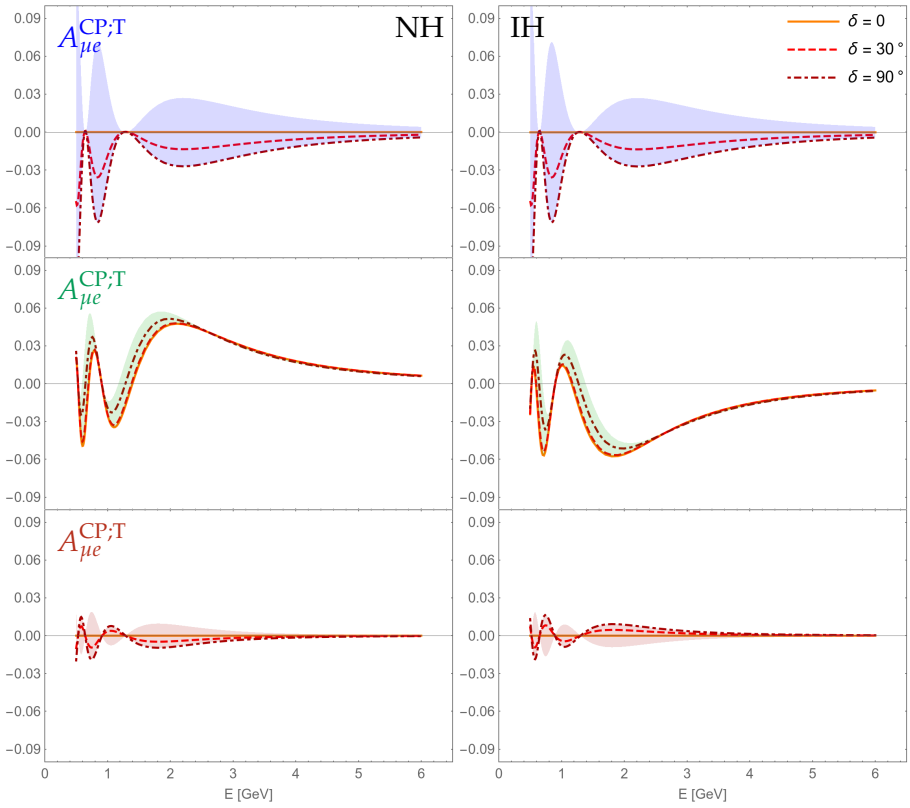

Figure 3.3: Energy distribution of the genuine $A_{\mu e}^{CP;T}$ (top), matter-induced $A_{\mu e}^{CP;CPT}$ (middle) and interference $A_{\mu e}^{T;CPT}$ (bottom) components for the DUNE baseline $L = 1300$ km. Normal (Inverted) Hierarchy in the left (right). The bands show all possible values of each term changing δ in $(0, 2\pi)$.

dependence of $A_{\mu e}^{CP;CPT}$ and $A_{\mu e}^{T;CPT}$ on δ due to effects of Δm_{21}^2 at low energies, and the Hierarchy discrimination with the sign of $A_{\mu e}^{CP;CPT}$, as well as the proportionality of $A_{\mu e}^{CP;T}$ with $\sin\delta$ independent of the neutrino Hierarchy.

Our scan of the different behavior in the energy distribution at $L = 1300$ km of the three disentangled components points towards a magic energy interval around $E \sim 0.9$ GeV with a zero for $A_{\mu e}^{CP;CPT}$ and $A_{\mu e}^{T;CPT}$, and a relative maximum for $\left|A_{\mu e}^{CP;T}\right|$. With our numerical simulation, we checked that this energy value

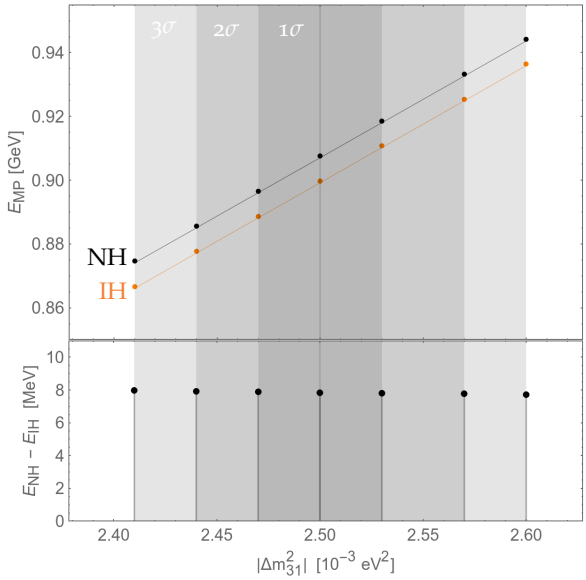

Figure 3.4: Energy value at which the matter-induced component $A_{\mu e}^{\mathrm{CP;CPT}}$ of the CP asymmetry vanishes, as a function of the measured $\left|\Delta m_{31}^2\right|$ in its 3σ range. Both Normal (black) and inverted (orange) Hierarchies , and the difference in E_{MP} between them is shown in the lower panel.

changes linearly with the vacuum $\left|\Delta m_{31}^2\right|$ and is blind to all other fit parameters, as well as nearly Hierarchy independent. These properties are shown in Figure 3.4, from which it is clear that Hierarchy effects in this energy value are below 1%.

This remarkable configuration is well seen in the results presented in Figure 3.5, with the three bands for $A_{\mu e}^{\mathrm{CP;CPT}}$ (green), $A_{\mu e}^{\mathrm{T;CPT}}$ (red) and $A_{\mu e}^{\mathrm{CP;T}}$ (blue) superposed. The zero in the two CPT-odd components is independent of δ, and both $A_{\mu e}^{\mathrm{CP;CPT}}$ and $A_{\mu e}^{\mathrm{T;CPT}}$ change sign around this first-order zero, whereas $A_{\mu e}^{\mathrm{CP;T}}$ has a maximal value proportional to $\sin\delta$. For a measurement of the CP asymmetry in future accelerators, this behavior ensures that, for a bin width up to the feasible [103] $0.15 - 0.20$ GeV, the mean value of $A_{\mu e}^{\mathrm{CP;CPT}}$ is below 10% $\left|A_{\mu e}^{\mathrm{CP;T}}\right|_{\mathrm{max}}$, whereas $A_{\mu e}^{\mathrm{CP;T}}$ is above 95% of its peak value, as shown in Figure 3.6

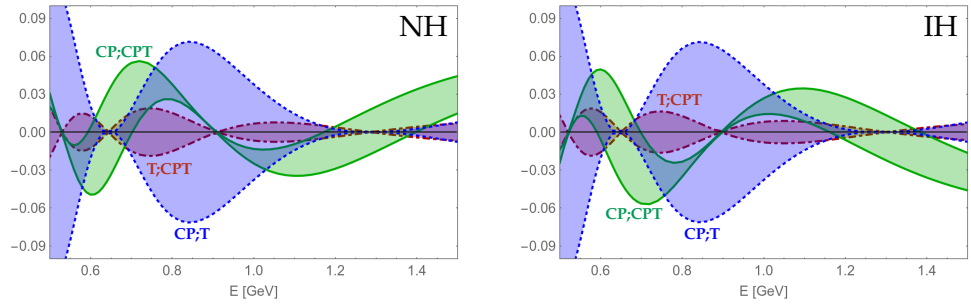

Figure 3.5: Zooming Figure 3.3 at low E, superposing the CPT-odd (green/solid) and T-odd (blue/dashed) components of the CP asymmetry $\mathcal{A}^{\rm CP}_{\mu e}$, together with the CPT-odd component (red/dot-dashed) of the T asymmetry $\mathcal{A}^{\rm T}_{\mu e}$. Normal (Inverted) Hierarchy in the left (right). The bands correspond to all possible values changing δ in $(0, 2\pi)$; the upper/lower lines for the T-even (T-odd) components correspond to $\cos\delta(\sin\delta) = \pm 1$.

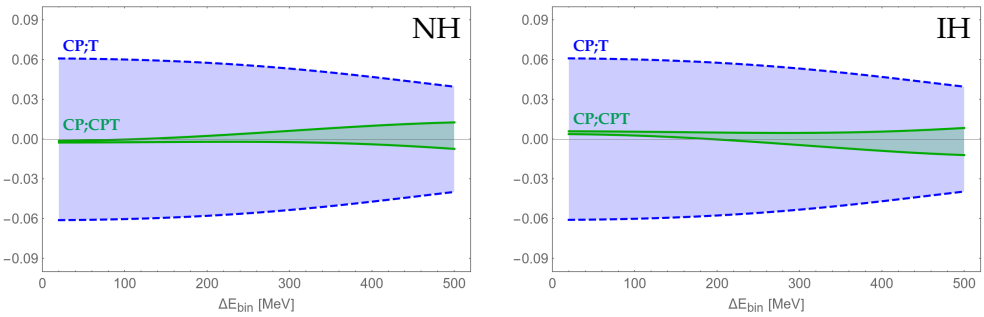

Figure 3.6: Average value of the CPT-odd (green/solid) and T-odd (blue/dashed) components of $\mathcal{A}^{\rm CP}_{\mu e}$, at DUNE $L = 1300$ km, in an energy bin width $\Delta E_{\rm bin}$ centered on the magic energy 0.9 GeV. Normal (Inverted) Hierarchy in the left (right) panel. The bands correspond to all possible values changing δ in $(0, 2\pi)$; the upper/lower lines for $A^{\rm CP;CPT}_{\mu e}(A^{\rm CP;T}_{\mu e})$ correspond to $\cos\delta(\sin\delta) = -1, 1$.

Since this $(E, L) \sim (0.9 \text{ GeV}, 1300 \text{ km})$ point is a promising configuration to genuinely test CP in the lepton sector, we focus in the remaining of this Chapter on obtaining precise-enough analytical expressions able to help understand its existence and dependence on the oscillation parameters. We aim to determine its precise dependence on Δm^2_{31}, as well as explain why maximal genuine and vanishing matter-induced happen simultaneously at those (E, L) values and whether other configurations like this one might exist. The tool we need in order to proceed is thus a set of simple analytical expressions that provide insight into the relevant physical mechanisms. We will check the accuracy of these expressions comparing them with the numerical exact results.

3.2 ANALYTIC PERTURBATION EXPANSIONS

To understand the behavior of the three disentangled components $A_{\mu e}^{\text{CP;CPT}}$, $A_{\mu e}^{\text{CP;T}}$ and $A_{\mu e}^{\text{T;CPT}}$ in Eqs. (2.5) and (2.9) required by the CP, T and CPT symmetries, as proved in the previous Chapter, we proceed to their analytic study for neutrino oscillations in matter of constant density. Notice that the formal description of the system is equivalent to neutrino oscillations in vacuum, if one parametrizes matter effects as a redefinition of neutrino masses and mixings as in the Hamiltonian (2.2). However, this redefinition is strongly dependent on the neutrino energy, so it does not provide a clear insight into the intrinsic properties of the system. A useful description should write all observables in matter, relevant to our two components of the experimentally accessible CP asymmetry, as well as the interference component of the T asymmetry, as functions of the vacuum parameters and the matter potential a. A similar methodology is being applied to calculations of the full CPT [104] and T [105] asymmetries.

The search of these formulae unavoidably finds the same issue: an exact description of the matter effects in neutrino oscillations leads to cumbersome expressions which do not provide a clear understanding [106]. The way to simplify the results is to

treat perturbatively the small parameters of the system, namely $\Delta m^2_{21} \ll |\Delta m^2_{31}|$ and $|U_{e3}|^2 \ll 1$. The most important drawback of this procedure is that, in perturbing in Δm^2_{21}, the implicit relation $\Delta m^2_{21} \ll |a|$ is also assumed, so one should not expect to reproduce the right vacuum limit $a \to 0$ for all matter ingredients. Even so, this perturbation theory leads to compact and percent-level precise expressions for neutrino oscillation probabilities written in terms of vacuum parameters only [107], as well as more precise relations mapping the mixings in matter to the quantities in vacuum [108, 109].

We develop a new perturbative expansion in Δm^2_{21}, $|a| \ll |\Delta m^2_{31}|$ without assumptions between Δm^2_{21} and a, similar to Ref. [110], oriented to the understanding of masses, mixings and the separate behavior of $A^{\text{CP;CPT}}_{\mu e}$, $A^{\text{CP;T}}_{\mu e}$ and $A^{\text{T;CPT}}_{\mu e}$ as functions of the different variables. In doing so, we can check from our analytic expressions both the vacuum limit $a \to 0$ and the T-invariant limit $\Delta m^2_{21} \to 0$. The expansion in $|a| \ll |\Delta m^2_{31}|$ holds for energies below a few GeV taking into account the definite a-parity of each component, so that corrections are quadratic. This way, we find the most simple expressions for $A^{\text{CP;CPT}}_{\mu e}$ and $A^{\text{CP;T}}_{\mu e}$ at the energies accessible by accelerator experiments, which are accurate enough to let the reader clearly understand their behavior. Even though it is unobservable at accelerator experiments, we will present also the results for the interference component $A^{\text{T;CPT}}_{\mu e}$ at these configurations, in order to compare its behavior with that of the other two components.

We emphasize that any desired precision can be achieved using a numerical computation of the neutrino propagation. Our aim is not finding very precise expansions, but precise enough to identify and understand the distinct characteristic patterns of the energy behavior of the three components with the objective of serving as a guide for experimental signatures.

3.2.1 The crucial role of the reference $\tilde{m}_0^2$ in matter

Since a diagonal $m_1^2\,\mathbf{1}$ in the Hamiltonian H in Eq. (2.2) leads to a global phase in time evolution, which is unobservable, the equivalent Hamiltonian

$$2E\,\Delta H \equiv \Delta H' = U\,\Delta M^2\,U^\dagger + a\,P_e\,, \tag{3.2}$$

is widely used, where $P_e = \mathrm{diag}(1,0,0)$ is the e-flavor projector and $\Delta M^2 = \mathrm{diag}(0,\,\Delta m^2_{21},\,\Delta m^2_{31})$.

Analogously, one could argue that $\tilde{m}_1^2$ is unobservable in neutrino oscillations in matter. Even though this is true, one must take into account that either m_1^2 or $\tilde{m}_1^2$ can be chosen as origin of phases, but not both of them at the same time when connecting the parameters in matter to those in vacuum. Indeed, one can easily check that the Hamiltonian $\Delta H'$ has three non-vanishing eigenvalues, so choosing $m_1^2 = 0$ automatically leads to all $\tilde{m}_i \neq 0$, despite one of them being unobservable.

On the following, we call $\tilde{m}_0^2$ the mass squared in matter leading to the relative phase shift between the unobservable global phases in vacuum and matter, writing the Hamiltonian as

$$\Delta H' = U\,\Delta M^2\,U^\dagger + a\,P_e = \tilde{m}_0^2\,\mathbf{1} + \tilde{U}\,\Delta\tilde{M}^2\,\tilde{U}^\dagger\,. \tag{3.3}$$

In this notation, the three eigenvalues of $\Delta H'$ will be the reference scale in matter $\tilde{m}_0^2$ and the two observable mass squared differences in matter $\Delta\tilde{m}^2_{ij}$.

As proposed in Ref. [106], we choose to diagonalize the Hamiltonian in the vacuum mass eigenbasis,

$$\Delta H'_{ij} = \Delta M^2 + a\,U^\dagger P_e U = \tilde{m}_0^2\mathbf{1} + V\Delta\tilde{M}^2 V^\dagger\,. \tag{3.4}$$

Since the eigenvalues are basis independent and real, this equation cleanly shows that $\tilde{m}_0^2$ and $\Delta\tilde{m}^2_{ij}$ can only depend on the parameters $(\Delta m^2_{ij},\,|U_{ei}|,\,a)$. Moreover, working in this basis factorizes the mixing matrix in matter into $\tilde{U} = UV$, where U is the (vacuum) PMNS matrix and V is the change of basis between vacuum and matter eigenstates, which must go to the identity when $a \to 0$.

The Hamiltonian being a 3×3 matrix leads to the characteristic equation

$$p(\lambda) \equiv -\lambda^3 + \lambda^2 \,\mathrm{tr}\big(\Delta H'\big) + \\ + \frac{1}{2}\lambda\left[\mathrm{tr}\big[(\Delta H')^2\big] - \mathrm{tr}^2(\Delta H')\right] + \det\big(\Delta H'\big) = 0\,, \quad (3.5)$$

where $p(\lambda)$ is the characteristic polynomial of $\Delta H'$ and its roots λ_i provide the three neutrino squared masses in matter, as well as the observable mass squared differences $\Delta\tilde{m}^2_{ij} = \lambda_i - \lambda_j$. The three invariants appearing in the characteristic equation (3.5) can be easily calculated,

$$\mathrm{tr}\big(\Delta H'\big) = \Delta m^2_{21} + \Delta m^2_{31} + a\,, \quad (3.6a)$$

$$\mathrm{tr}\big[(\Delta H')^2\big] = (\Delta m^2_{21})^2 + (\Delta m^2_{31})^2 + a^2 + \\ + 2a\left[\Delta m^2_{21}|U_{e2}|^2 + \Delta m^2_{31}|U_{e3}|^2\right]\,, \quad (3.6b)$$

$$\det\big(\Delta H'\big) = a|U_{e1}|^2\Delta m^2_{21}\Delta m^2_{31}\,. \quad (3.6c)$$

From this straightforward setup of the problem, even before trying to solve Eq. (3.5), we find a fundamental result. Since

$$p(0) = a|U_{e1}|^2\Delta m^2_{21}\Delta m^2_{31} \geq 0\,, \quad (3.7a)$$

$$p(\Delta m^2_{21}) = a|U_{e2}|^2\Delta m^2_{21}(\Delta m^2_{21} - \Delta m^2_{31}) \leq 0, \quad (3.7b)$$

at least one of the eigenvalues of $\Delta H'$ will always lie in the range $[0, \Delta m^2_{21}]$. All $\Delta\tilde{m}^2_{ij}$ are known to be nonbound by Δm^2_{21}, as can be read from the dependence on a of the effective masses in matter in Figure 3.1, so we find that $0 \leq \tilde{m}^2_0 \leq \Delta m^2_{21}$. Although the inequalities in (3.7a) and (3.7b) have been written for Normal Hierarchy neutrinos, the argument is also valid for the Inverted Hierarchy and antineutrinos, since the product $p(0)p(\Delta m^2_{21})$ is always negative regardless of the signs of Δm^2_{31} and a.

Given that physically $\Delta m^2_{21} \ll |\Delta m^2_{31}|$, this result shows that $\tilde{m}^2_0 \leq \Delta m^2_{21}$ is also a good perturbative parameter. Therefore, we focus in this Subsection on writing the two observable $\Delta\tilde{m}^2_{ij}$ exactly as functions of $(\Delta m^2_{ij}, \tilde{m}^2_0, |U_{ei}|, a)$, which gives enough information to calculate all observables of neutrino oscillations in matter.

A simple way to calculate the physical $\Delta\tilde{m}^2_{ij}$ is the diagonalization of the displaced Hamiltonian

$$\Delta H'_{ij} - \tilde{m}^2_0 \mathbf{1} = \Delta M^2 + a\, U^\dagger P_e U - \tilde{m}^2_0 \mathbf{1} = V \Delta\tilde{M}^2 V^\dagger . \qquad (3.8)$$

By construction, one of its eigenvalues is zero, so its determinant is zero and its characteristic equation reduces to a quadratic polynomial whose (non-vanishing) roots are

$$\Delta\tilde{m}^2_\pm = \frac{1}{2}\left(\Delta m^2_{21} + \Delta m^2_{31} + a - 3\tilde{m}^2_0\right) \pm \\ \pm \frac{1}{2}\sqrt{l^2 + 2\tilde{m}^2_0(\Delta m^2_{21} + \Delta m^2_{31} + a) - 3(\tilde{m}^2_0)^2}\,, \qquad (3.9)$$

where

$$l^2 \equiv \left(\Delta m^2_{31} + \Delta m^2_{21} - a\right)^2 - 4\Delta m^2_{21}\Delta m^2_{31} + 4a\Delta m^2_{21}|U_{e2}|^2 + \\ + 4a\Delta m^2_{31}|U_{e3}|^2 .$$

Even though it is clear from this definition that $\Delta\tilde{m}^2_+ > \Delta m^2_-$, notice that $\left|\Delta\tilde{m}^2_+\right| > \left|\Delta\tilde{m}^2_-\right|$ for Normal Hierarchy, whereas $\left|\Delta\tilde{m}^2_-\right| > \left|\Delta\tilde{m}^2_+\right|$ for Inverted Hierarchy. This expression for $\Delta\tilde{m}^2_\pm$ is a good starting point from which one can easily derive approximate formulae in the physical region $\tilde{m}^2_0 \leq \Delta m^2_{21} \ll \left|\Delta m^2_{31}\right|$. In order to write $\Delta\tilde{m}^2_\pm$ as functions of vacuum parameters only, this same limit can be used directly in Eq. (3.5) to find $\tilde{m}^2_0$ perturbatively, as we will do in the following Subsection.

We finish this Subsection writing explicitly the exact eigenstates of $\Delta H'_{ij}$ in the canonical basis of mass eigenstates in vacuum,

$$|\tilde{\nu}_i\rangle = \frac{1}{N_i}\begin{bmatrix} a\left[\left(\lambda_i - \Delta m^2_{31}\right)|U_{e2}|^2 + \left(\lambda_i - \Delta m^2_{21}\right)|U_{e3}|^2\right] U^*_{e1} \\ \left[\lambda_i - a|U_{e1}|^2\right]\left[\lambda_i - \Delta m^2_{31}\right] U^*_{e2} \\ \left[\lambda_i - a|U_{e1}|^2\right]\left[\lambda_i - \Delta m^2_{21}\right] U^*_{e3} \end{bmatrix}, \qquad (3.10)$$

where the normalization factor N_i is needed to ensure $\langle\tilde{\nu}_i|\tilde{\nu}_i\rangle = 1$, and its phase must be chosen so that $\lim_{a\to 0}|\tilde{\nu}_i\rangle = |\nu_i\rangle$.

The eigenvalues λ_i, labeled according to $\lambda_1 < \lambda_2 < \lambda_3$ for the Normal Hierarchy and $\lambda_3 < \lambda_1 < \lambda_2$ for the Inverted Hierarchy,

Table 3.1: Relation between the eigenvalues λ_i, with the convention $\lambda_i \xrightarrow{a\to 0} \Delta m^2_{i1}$, and the quantities $\tilde{m}^2_0$ and $\Delta\tilde{m}^2_\pm$ as calculated from Eq. (3.9) with the corresponding sign of a for $\nu/\bar{\nu}$ and the sign and value of Δm^2_{31} for NH/IH. According to Hierarchy, the eigenvalues are ordered from larger to smaller. The observable $\Delta\tilde{m}^2_{ij} = \lambda_i - \lambda_j$ can be read from the table.

	Neutrinos ($a > 0$)	Antineutrinos ($a < 0$)
NH ($\Delta m^2_{31} > 0$)	$\lambda_3 = \tilde{m}^2_0 + \Delta\tilde{m}^2_+$ $\lambda_2 = \tilde{m}^2_0 + \Delta\tilde{m}^2_-$ $\lambda_1 = \tilde{m}^2_0$	$\bar{\lambda}_3 = \tilde{\bar{m}}^2_0 + \Delta\tilde{m}^2_+$ $\bar{\lambda}_2 = \tilde{\bar{m}}^2_0$ $\bar{\lambda}_1 = \tilde{\bar{m}}^2_0 + \Delta\tilde{m}^2_-$
IH ($\Delta m^2_{31} < 0$)	$\lambda_2 = \tilde{m}^2_0 + \Delta\tilde{m}^2_+$ $\lambda_1 = \tilde{m}^2_0$ $\lambda_3 = \tilde{m}^2_0 + \Delta\tilde{m}^2_-$	$\bar{\lambda}_2 = \tilde{\bar{m}}^2_0$ $\bar{\lambda}_1 = \tilde{\bar{m}}^2_0 + \Delta\tilde{m}^2_+$ $\bar{\lambda}_3 = \tilde{\bar{m}}^2_0 + \Delta\tilde{m}^2_-$

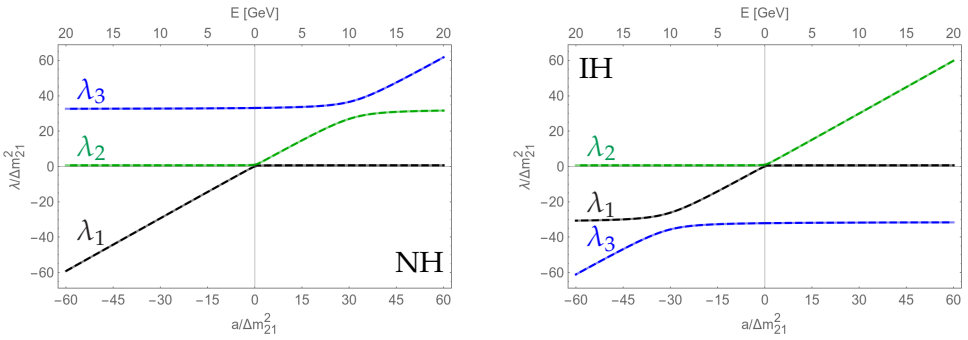

Figure 3.7: Eigenvalues λ_i of the mass matrix in matter in units of Δm^2_{21}, for both neutrinos ($a > 0$) and antineutrinos ($a < 0$). The horizontal axis shows both the evolution of the matter parameter a at fixed energy (lower labels), i.e. changing the matter density, and as function of the energy if the constant density is chosen as that of the Earth crust (upper labels). Both the exact (dashed) and the analytical (solid) results from Eqs. (3.11, 3.12) are shown to illustrate the excellence of the analytic approximation. Normal (Inverted) Hierarchy in the left (right) panel.

are given by $\tilde{m}_0^2$ and $\Delta\tilde{m}_\pm^2$ as shown in Table 3.1 for neutrinos and antineutrinos. The reason why $\lambda_1 = \tilde{m}_0^2$ whereas $\bar{\lambda}_2 = \tilde{\bar{m}}_0^2$ will be explained analytically when exploring the vacuum limit. This fact is also shown in Figure 3.7 by a numerical determination of the evolution of the eigenvalues of $\Delta H'$ with the matter parameter a, where one identifies $\tilde{m}_0^2$ ($\tilde{\bar{m}}_0^2$) as the (anti)neutrino eigenvalue bounded by Δm_{21}^2.

As seen, the eigenvalues that fulfill $0 \leq \tilde{m}_0^2 \leq \Delta m_{21}^2$ are λ_1 and $\bar{\lambda}_2$, independently of whether the Hierarchy is Normal or Inverted. In order to distinguish these two functions, we call them $\lambda_1 \equiv \tilde{m}_0^2$ and $\bar{\lambda}_2 \equiv \tilde{\bar{m}}_0^2$. Notice that, even if both $\tilde{m}_0^2$ and $\tilde{\bar{m}}_0^2$ are bounded by Δm_{21}^2, they are necessarily different functions, as seen by their different vacuum limits $\lim_{a\to 0} \tilde{m}_0^2 = 0$ and $\lim_{a\to 0} \tilde{\bar{m}}_0^2 = \Delta m_{21}^2$.

3.2.2 The way to the vacuum limit at fixed (E, L)

The perturbation theory used in the literature to make profit of the relation $\Delta m_{21}^2 \ll |\Delta m_{31}^2|$ also assumes $\Delta m_{21}^2 \ll |a|$. In order to ensure that all our expressions will reproduce the right vacuum limit, which is crucial to study the CPT-invariant limit of the three disentangled components, we expand $\Delta m_{21}^2 \ll |\Delta m_{31}^2|$ without any assumption between Δm_{21}^2 and a. Up to first order in this regime, the characteristic polynomial (3.5) —that fixes $\tilde{m}_0^2$— and the squared mass differences in matter (3.9) reduce to

$$\begin{aligned}(\tilde{m}_0^2)^2(\Delta m_{31}^2 + a) - \\ - \tilde{m}_0^2[\Delta m_{21}^2 \Delta m_{31}^2 + a\Delta m_{21}^2(1 - |U_{e2}|^2) + a\Delta m_{31}^2(1 - |U_{e3}|^2)] + \\ + a|U_{e1}|^2 \Delta m_{21}^2 \Delta m_{31}^2 = 0\,, \end{aligned} \tag{3.11}$$

and

$$\begin{aligned}\Delta\tilde{m}_\pm^2 = &\frac{1}{2}(\Delta m_{31}^2 + a + \Delta m_{21}^2 - 3\tilde{m}_0^2) \pm \\ &\pm \frac{1}{2}\sqrt{\begin{array}{l}(\Delta m_{31}^2 - a)^2 + 4|U_{e3}|^2 a\Delta m_{31}^2 - \\ \quad - 2(\Delta m_{21}^2 + \tilde{m}_0^2)(\Delta m_{31}^2 + a) + 4|U_{e2}|^2 a\Delta m_{21}^2\end{array}}\,. \end{aligned} \tag{3.12}$$

These analytical results are shown in Figure 3.7 for neutrinos ($a > 0$) and antineutrinos ($a < 0$), as well as both Normal ($\Delta m^2_{31} > 0$) and Inverted ($\Delta m^2_{31} < 0$) Hierarchies, and they match perfectly the exact numerical values. Notice that the two solutions of Eq. (3.11) in vacuum, $\tilde{m}^2_0(\tilde{m}^2_0 - \Delta m^2_{21}) = 0$, are $\tilde{m}^2_0 = 0, \Delta m^2_{21}$. From the discussion in the previous Subsection we know that the first one corresponds to $\tilde{m}^2_0$, which is bound by Δm^2_{21} when $a > 0$, whereas the second one, $\tilde{\bar{m}}^2_0$, is bound by Δm^2_{21} when $a < 0$.

As illustrated in Figure 3.8, the appropriate expansion up to first order for $\Delta\tilde{m}^2_\pm$ in both $\Delta m^2_{21} \ll |\Delta m^2_{31}|$ and $|a| \ll |\Delta m^2_{31}|$ is

$$\Delta\tilde{m}^2_{+\text{sign}(\Delta m^2_{31})} = \Delta m^2_{31} + a|U_{e3}|^2 - \tilde{m}^2_0\,, \tag{3.13a}$$

$$\Delta\tilde{m}^2_{-\text{sign}(\Delta m^2_{31})} = \Delta m^2_{21} + a(1 - |U_{e3}|^2) - 2\tilde{m}^2_0\,. \tag{3.13b}$$

The same expressions apply to antineutrinos changing $a \to -a$, $\tilde{m}^2_0 \to \tilde{\bar{m}}^2_0$, and the dependence on the Hierarchy is implicit in $\text{sign}(\Delta m^2_{31})$, that accounts for the interchange of the expressions $\Delta\tilde{m}^2_\pm|_{\text{NH}} \leftrightarrow \Delta\tilde{m}^2_\mp|_{\text{IH}}$.

The approximation of $\tilde{m}^2_0$ and $\tilde{\bar{m}}^2_0$, on the other hand, comes from neglecting Δm^2_{31}-independent terms in the characteristic equation (3.11),

$$\begin{aligned}\tilde{m}^2_0 = \frac{1}{2}\left[\Delta m^2_{21} + a(1 - |U_{e3}|^2)\right] \pm \\ \pm \frac{1}{2}\sqrt{\left[\Delta m^2_{21} + a(1 - |U_{e3}|^2)\right]^2 - 4|U_{e1}|^2 a\Delta m^2_{21}}\,,\end{aligned} \tag{3.14}$$

where the $-(+)$ sign corresponds to $\tilde{m}^2_0$ ($\tilde{\bar{m}}^2_0$), as shown by their $a \to 0$ limit. In order to compare their behavior above and below Δm^2_{21}, one can further expand Eq. (3.14) in the two regions $|a| \ll \Delta m^2_{21}$,

$$\tilde{m}^2_0 = a|U_{e1}|^2\left[1 - \frac{a|U_{e2}|^2}{\Delta m^2_{21}} + \cdots\right]\,, \tag{3.15a}$$

$$\tilde{\bar{m}}^2_0 = \Delta m^2_{21} - |a||U_{e2}|^2\left[1 - \frac{|a||U_{e1}|^2}{\Delta m^2_{21}} + \cdots\right]\,, \tag{3.15b}$$

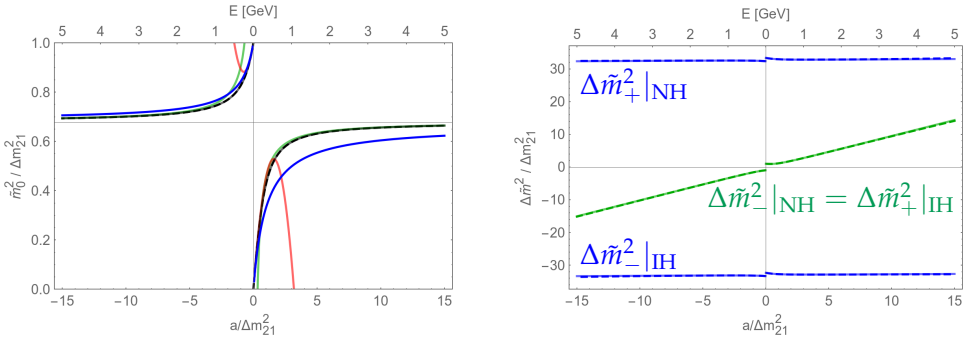

Figure 3.8: Dependence of the Hierarchy-independent $\tilde{m}_0^2$ (left), and the two $\Delta\tilde{m}_\pm^2$ (right) in units of Δm_{21}^2, for both Hierarchies and both neutrinos ($a > 0$) and antineutrinos ($a < 0$). The horizontal axis shows both the evolution of the matter parameter a at fixed energy (lower labels), i.e. changing the matter density, and as function of the energy if the constant density is chosen as that of the Earth crust (upper labels). Both the exact (dashed) and the analytical (solid) $1^{\rm st}$ order approximations for $\Delta\tilde{m}_\pm^2$ (3.13) and $\tilde{m}_0^2$ (3.14) are shown. Besides this excellent $\tilde{m}_0^2$ (black), also shown are the different approximations discussed: red for $|a| \ll \Delta m_{21}^2$ (3.15), green for $|a| \gg \Delta m_{21}^2$ (3.16), and blue for the interpolation (3.17).

and $\Delta m_{21}^2 \ll |a|$,

$$\tilde{m}_0^2 = \frac{\Delta m_{21}^2 |U_{e1}|^2}{1 - |U_{e3}|^2} \left[1 - \frac{\Delta m_{21}^2 |U_{e2}|^2}{a \left(1 - |U_{e3}|^2\right)^2} + \cdots \right], \tag{3.16a}$$

$$\tilde{\tilde{m}}_0^2 = \frac{\Delta m_{21}^2 |U_{e1}|^2}{1 - |U_{e3}|^2} \left[1 + \frac{\Delta m_{21}^2 |U_{e2}|^2}{|a| \left(1 - |U_{e3}|^2\right)^2} + \cdots \right], \tag{3.16b}$$

adequate when looking at the CPT-invariant (vacuum) limit or the T-invariant limit, respectively. Notice that both $\tilde{m}_0^2$ and $\tilde{\tilde{m}}_0^2$ converge to the same asymptotic limit in $|a|$ above Δm_{21}^2, as seen in Figure 3.8.

At the expense of losing precision, the evolution of these parameters between the two limits is illustrated by the approximate interpolations

$$\tilde{m}_0^2 \approx |U_{e1}|^2 \, \frac{a\,\Delta m^2_{21}}{a + \Delta m^2_{21}}\,, \quad \tilde{\tilde{m}}_0^2 \approx \Delta m^2_{21} - |U_{e2}|^2 \, \frac{|a|\,\Delta m^2_{21}}{|a| + \Delta m^2_{21}}\,, \tag{3.17}$$

with errors $\sim 20\%$, that roughly describe their behavior: their vacuum limits are $\tilde{m}_0^2 \to 0$ and $\tilde{\tilde{m}}_0^2 \to \Delta m^2_{21}$, both vanish when Δm^2_{21} goes to zero (since $\tilde{m}_0^2 \leq \Delta m^2_{21}$) and go to $\approx |U_{e1}|^2 \Delta m^2_{21}$ above Δm^2_{21}. Notice that first-order approximations in Eqs. (3.17) reproduce all four limits in Eqs. (3.15, 3.16) if one neglects $|U_{e3}|^2$ terms. Since these parameters are already $\mathcal{O}(\Delta m^2_{21})$, the effects of extra $\mathcal{O}(\Delta m^2_{21}|U_{e3}|^2)$ corrections are typically negligible higher-order terms.

The expansion of the exact eigenstates in Eq. (3.10) up to leading order, together with the eigenvalues in Eqs. (3.13), leads to the simple expressions

$$|\tilde{\nu}_1\rangle = \frac{1}{N_1}\begin{bmatrix} 1 \\ \frac{\tilde{m}_0^2 - a|U_{e1}|^2}{aU_{e1}^* U_{e2}} \\ 0 \end{bmatrix}, \quad |\tilde{\nu}_2\rangle = \frac{1}{N_2}\begin{bmatrix} \frac{aU_{e1}^* U_{e2}}{\Delta m^2_{21} - \tilde{m}_0^2 + a|U_{e2}|^2} \\ 1 \\ 0 \end{bmatrix}, \tag{3.18}$$

and $|\tilde{\nu}_3\rangle = |\nu_3\rangle$, valid for both Hierarchies. Analogously, antineutrino eigenstates are given by

$$|\tilde{\bar{\nu}}_1\rangle = \frac{1}{\bar{N}_1}\begin{bmatrix} 1 \\ -\frac{\Delta m^2_{21} - \tilde{\tilde{m}}_0^2 - a|U_{e2}|^2}{aU_{e1} U_{e2}^*} \\ 0 \end{bmatrix}, \quad |\tilde{\bar{\nu}}_2\rangle = \frac{1}{\bar{N}_2}\begin{bmatrix} -\frac{aU_{e1} U_{e2}^*}{\tilde{\tilde{m}}_0^2 + a|U_{e1}|^2} \\ 1 \\ 0 \end{bmatrix}, \tag{3.19}$$

and $|\tilde{\bar{\nu}}_3\rangle = |\bar{\nu}_3\rangle$.

These eigenstates determine the columns of the V mixing matrix between matter and vacuum mass eigenstates, which allows us to write $\tilde{U} = UV$ for both neutrinos,

$$\tilde{U}_{\alpha 1} = \frac{1}{N_1}\left[U_{\alpha 1} + \frac{\tilde{m}_0^2 - a|U_{e1}|^2}{aU_{e1}^* U_{e2}}\, U_{\alpha 2}\right], \tag{3.20a}$$

$$\tilde{U}_{\alpha 2} = \frac{1}{N_2}\left[U_{\alpha 2} + \frac{aU_{e1}^* U_{e2}}{\Delta m^2_{21} - \tilde{m}_0^2 + a|U_{e2}|^2}\, U_{\alpha 1}\right], \tag{3.20b}$$

$$\tilde{U}_{\alpha 3} = U_{\alpha 3}\,, \tag{3.20c}$$

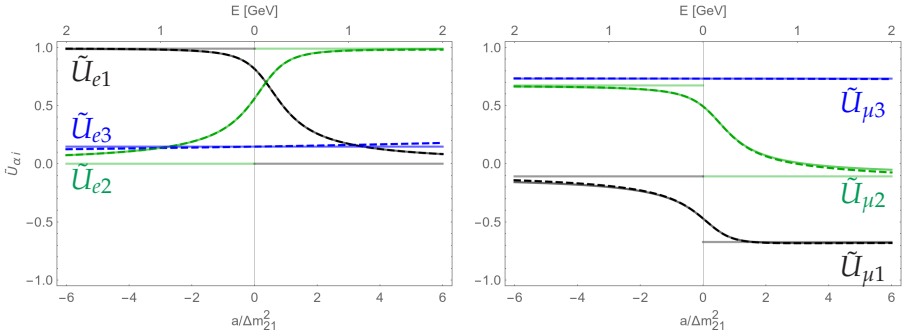

Figure 3.9: Mixing elements $\tilde{U}_{ei}$ (left) and $\tilde{U}_{\mu i}$ (right) in matter, for both neutrinos ($a > 0$) and antineutrinos ($a < 0$), assuming $\delta = 0$. The horizontal axis shows both the evolution of the matter parameter a at fixed energy (lower labels), i.e. changing the matter density, and as function of the energy if the constant density is chosen as that of the Earth crust (upper labels). Exact (dashed) and analytical (solid) results from Eqs. (3.20, 3.21) shown. The thin horizontal lines show the vacuum limit *after* setting $\Delta m^2_{21} \to 0$.

and antineutrinos,

$$\tilde{\bar{U}}_{\alpha 1} = \frac{1}{\bar{N}_1}\left[U^*_{\alpha 1} - \frac{\Delta m^2_{21} - \tilde{\bar{m}}^2_0 - |a||U_{e2}|^2}{|a|U_{e1}U^*_{e2}}\,U^*_{\alpha 2}\right], \tag{3.21a}$$

$$\tilde{\bar{U}}_{\alpha 2} = \frac{1}{\bar{N}_2}\left[U^*_{\alpha 2} - \frac{|a|U_{e1}U^*_{e2}}{\tilde{\bar{m}}^2_0 + |a||U_{e1}|^2}\,U^*_{\alpha 1}\right], \tag{3.21b}$$

$$\tilde{\bar{U}}_{\alpha 3} = U^*_{\alpha 3}\,. \tag{3.21c}$$

Figure 3.9 shows the excellent agreement of these expressions with the numerical results within the density/energy region $|a| \ll |\Delta m^2_{31}|$, corresponding in the Figure to $|a|/|\Delta m^2_{21}| \ll 33$.

Since matter effects do not depend on all elements of U_{PMNS} but only U_{ei}, the above expressions are simpler in the $\alpha = e$ case. In particular, notice that both

$$\tilde{U}_{e1} = \frac{U_{e1}}{N_1}\,\frac{\tilde{m}^2_0}{a|U_{e1}|^2}\,, \qquad \tilde{\bar{U}}_{e2} = \frac{U^*_{e2}}{\bar{N}_2}\,\frac{\tilde{\bar{m}}^2_0}{\tilde{\bar{m}}^2_0 + a|U_{e2}|^2}\,, \tag{3.22}$$

vanish if $\Delta m^2_{21} = 0$ for all a, due to $\tilde{m}^2_0 \leq \Delta m^2_{21}$. This fact originates in the transmutation [111] of masses in vacuum to mixings

in matter, leading to the absence of genuine CP violation in matter if $\Delta m^2_{21} = 0$, even though there are three non-degenerate neutrino masses.

These expressions reproduce the right vacuum limit, as seen by developing $|a| \ll \Delta m^2_{21}$ for both neutrinos,

$$\tilde{U}_{\alpha 1} = U_{\alpha 1} - \frac{a}{\Delta m^2_{21}} U_{e1} U^*_{e2} U_{\alpha 2}\,, \tag{3.23a}$$

$$\tilde{U}_{\alpha 2} = U_{\alpha 2} + \frac{a}{\Delta m^2_{21}} U_{e2} U^*_{e1} U_{\alpha 1}\,, \tag{3.23b}$$

and antineutrinos,

$$\tilde{\bar{U}}_{\alpha 1} = U^*_{\alpha 1} + \frac{|a|}{\Delta m^2_{21}} U^*_{e1} U_{e2} U^*_{\alpha 2}\,, \tag{3.24a}$$

$$\tilde{U}_{\alpha 2} = U^*_{\alpha 2} - \frac{|a|}{\Delta m^2_{21}} U^*_{e2} U_{e1} U^*_{\alpha 1}\,. \tag{3.24b}$$

When assuming $\Delta m^2_{21} \ll |a|$, however, a surprising result appears for both neutrinos

$$\tilde{U}_{\alpha 1} = \frac{|U_{e2}|}{\sqrt{1-|U_{e3}|^2}} \left[U_{\alpha 1} - \frac{U_{e1}}{U_{e2}} U_{\alpha 2} + \right. \\ \left. + \frac{\Delta m^2_{21}}{a} \frac{U_{e1}\,(U^*_{e1} U_{\alpha 1} + U^*_{e2} U_{\alpha 2})}{(1-|U_{e3}|^2)^2} \right]\,, \tag{3.25a}$$

$$\tilde{U}_{\alpha 2} = \frac{|U_{e2}|}{\sqrt{1-|U_{e3}|^2}} \left[U_{\alpha 2} + \frac{U^*_{e1}}{U^*_{e2}} U_{\alpha 1} - \right. \\ \left. - \frac{\Delta m^2_{21}}{a} \frac{U^*_{e1}\,(U_{e2} U_{\alpha 1} - U_{e1} U_{\alpha 2})}{(1-|U_{e3}|^2)^2} \right]\,, \tag{3.25b}$$

and antineutrinos,

$$\tilde{\bar{U}}_{\alpha 1} = \frac{|U_{e1}|}{\sqrt{1-|U_{e3}|^2}} \left[U^*_{\alpha 1} + \frac{U_{e2}}{U_{e1}} U^*_{\alpha 2} - \right. \\ \left. - \frac{\Delta m^2_{21}}{|a|} \frac{U_{e2}\,(U^*_{e2} U^*_{\alpha 1} - U^*_{e1} U^*_{\alpha 2})}{(1-|U_{e3}|^2)^2} \right]\,, \tag{3.26a}$$

$$\tilde{\tilde{U}}_{\alpha 2} = \frac{|U_{e1}|}{\sqrt{1-|U_{e3}|^2}} \left[U^*_{\alpha 2} - \frac{U^*_{e2}}{U^*_{e1}} U^*_{\alpha 1} + \right.$$
$$\left. + \frac{\Delta m^2_{21}}{|a|} \frac{U^*_{e2}\,(U_{e1}U^*_{\alpha 1} + U_{e2}U^*_{\alpha 2})}{(1-|U_{e3}|^2)^2} \right] , \quad (3.26b)$$

showing that $\lim\limits_{a\to 0}\lim\limits_{\Delta m^2_{21}\to 0} \tilde{U} \neq U_{\rm PMNS} = \lim\limits_{\Delta m^2_{21}\to 0}\lim\limits_{a\to 0} \tilde{U}$! This is strongly illustrated in the case $\lim\limits_{\Delta m^2_{21}\to 0} \tilde{U}_{e1} = \lim\limits_{\Delta m^2_{21}\to 0} \tilde{\tilde{U}}_{e2} = 0$ for all a. The subtlety behind this non-commutability of the $a \to 0$ and $\Delta m^2_{21} \to 0$ limits in the effective mixing matrix in matter is the following.

Setting $\Delta m^2_{21} = 0$ in vacuum means that ν_1 and ν_2 are degenerate. Therefore, any two independent linear combinations of them can be chosen as basis states, which in the language of the standard parametrization would mean that θ_{12} is nonphysical. Adding the matter potential to this system breaks the degeneracy: the arbitrariness in θ_{12} is lost in favor of the eigenstates of the perturbation. Since the matter term in the neutrino Hamiltonian adds $a > 0$ to the e-flavor component, this fact results $\tilde{\nu}_1$ and $\tilde{\nu}_2$ such that the heavier $\tilde{\nu}_2$ is mainly ν_e, forcing the $\tilde{U}_{e1} = 0$ we obtained. The change of sign in a for the antineutrino case forces analogously the lighter $\tilde{\bar{\nu}}_1$ to be mainly $\bar{\nu}_e$, explaining the (different) limit $\tilde{\tilde{U}}_{e2} = 0$.

This behavior shows that the vacuum connection should be analyzed in the regime where $|a| \ll \Delta m^2_{21} \ll \left|\Delta m^2_{31}\right|$. The definite a-parity of the disentangled components defined in the previous Chapter forces the leading-order term in $A^{\rm CP;T}_{\alpha\beta}$ to be independent of a, whereas both $A^{\rm CP;CPT}_{\alpha\beta}$ and $A^{\rm T;CPT}_{\alpha\beta}$ are linear. To provide a precise description in this region, we keep all linear terms in $a/\Delta m^2_{21}$ and $a/\Delta m^2_{31}$ in both the mass squared differences,

$$\Delta\tilde{m}^2_{21} \approx \Delta m^2_{21} - a(|U_{e1}|^2 - |U_{e2}|^2)\,, \quad (3.27a)$$
$$\Delta\tilde{m}^2_{31} \approx \Delta m^2_{31} - a|U_{e1}|^2\,, \quad (3.27b)$$
$$\Delta\tilde{m}^2_{32} \approx \Delta m^2_{32} - a|U_{e2}|^2\,, \quad (3.27c)$$

and the mixings,

$$\tilde{U}_{\alpha 1} \approx U_{\alpha 1} - \frac{a\,U_{e1}}{\Delta m^2_{21}}\,U^*_{e2}U_{\alpha 2} - \frac{a\,U_{e1}}{\Delta m^2_{31}}\,U^*_{e3}U_{\alpha 3}\,, \tag{3.28a}$$

$$\tilde{U}_{\alpha 2} \approx U_{\alpha 2} + \frac{a\,U_{e2}}{\Delta m^2_{21}}\,U^*_{e1}U_{\alpha 1} - \frac{a\,U_{e2}}{\Delta m^2_{31}}\,U^*_{e3}U_{\alpha 3}\,, \tag{3.28b}$$

$$\tilde{U}_{\alpha 3} \approx U_{\alpha 3} + \frac{a\,U_{e3}}{\Delta m^2_{31}}\,U^*_{e1}U_{\alpha 1} + \frac{a\,U_{e3}}{\Delta m^2_{31}}\,U^*_{e2}U_{\alpha 2}\,. \tag{3.28c}$$

Figure 3.10 shows computations of the CP asymmetry components $A_{\mu e}^{\mathrm{CP;CPT}}$ (green) and $A_{\mu e}^{\mathrm{CP;T}}$ (blue) from Eqs. (2.5), as well as the T asymmetry interference component $A_{\mu e}^{\mathrm{T;CPT}}$ (red) from Eq. (2.9b), using these expressions for the mixings in matter. They are compared with the exact results for both Hierarchies, at fixed E and L as functions of the matter potential, i.e. as function of the (constant) matter density. Since all three components depend on δ, we take the following convention. All components are represented by a band showing all their possible values if δ is arbitrarily changed in $(0, 2\pi)$. The comparison with the numerical results is done for the values of δ corresponding to the central and extremal curves of the bands: $\sin\delta = 0, \pm 1$ for the T-odd components, and $\cos\delta = 0, \pm 1$ for the T-invariant one.

These analytic approximations for constant $A_{\mu e}^{\mathrm{CP;T}}$ and linear $A_{\mu e}^{\mathrm{CP;CPT}}$ and $A_{\mu e}^{\mathrm{T;CPT}}$ work well at low matter densities, as they should, but their range of validity is much larger than expected. For the values used in the Figure, the point $a = \Delta m^2_{21}$ corresponds to $\rho = 0.44\rho_E$, so the previous expansions should only work for $\rho \ll 0.44\rho_E$. Their working reasonably well even above ρ_E hints that higher-order corrections are dominated by $(a/\Delta m^2_{31})^2$.

This surprising feature stems from the fact that corrections $(a/\Delta m^2_{21})^2$ are inoperative in the region $|a| \ll \Delta m^2_{21} \ll |\Delta m^2_{31}|$ for the $A_{\mu e}^{\mathrm{CP;CPT}}$ and $A_{\mu e}^{\mathrm{CP;T}}$ observables. This behavior is explained by the peculiar dependence on the mixings and masses of the oscillation probabilities, as can be understood from the matter-vacuum invariants we will exploit in the following Chapter for both $\mathrm{Im}\tilde{J}^{ij}_{\alpha\beta}$ (Section 4.1) and $\mathrm{Re}\tilde{J}^{ij}_{\alpha\beta}$ (Section 4.2). As will be discussed, they lead to dependencies in the oscillation probabilities in Eq. (2.3) on the phases associated to the small quantities a and

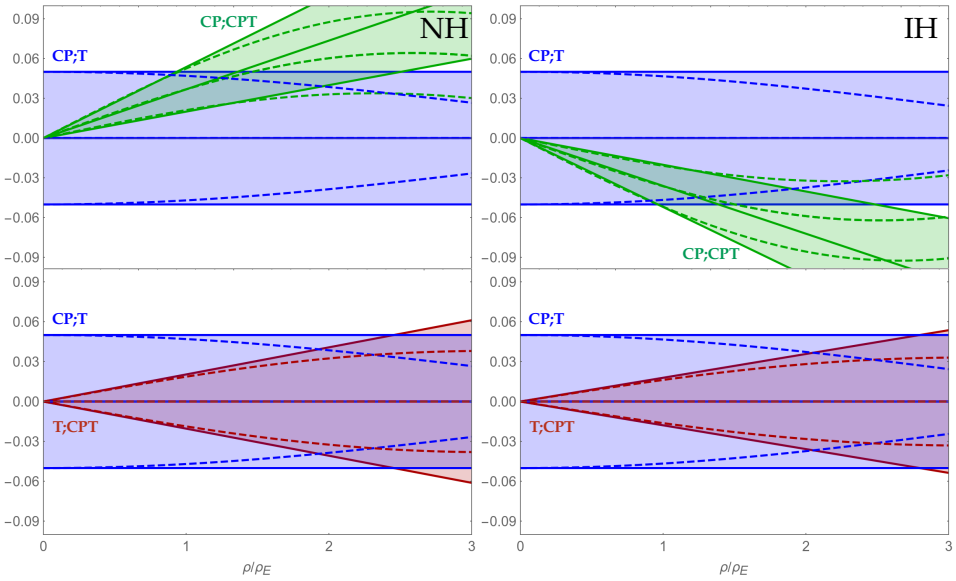

Figure 3.10: CPT-odd T-invariant (green) and T-odd CPT-invariant (blue) components of the CP asymmetry $\mathcal{A}_{\mu e}^{\mathrm{CP}}$ (top), and CPT-odd CP-invariant (red) and CP-odd CPT-invariant (blue) components of the T asymmetry $\mathcal{A}_{\mu e}^{\mathrm{T}}$ (bottom), as functions of the matter density ρ in units of that of the Earth crust, at fixed energy-baseline values of $(E, L) = (0.75\ \mathrm{GeV}, 1300\ \mathrm{km})$. Both exact (dashed) and analytical (solid) results from Eqs.(3.27, 3.28) shown. Normal (Inverted) Hierarchy in the left (right). The bands correspond to all possible values changing δ in $(0, 2\pi)$; the central lines for $A_{\mu e}^{\mathrm{CP;CPT}}$ ($A_{\mu e}^{\mathrm{CP;T}}$ and $A_{\mu e}^{\mathrm{T;CPT}}$) correspond to $\cos\delta(\sin\delta) = 0$; the upper/lower lines for $A_{\mu e}^{\mathrm{CP;CPT}}(A_{\mu e}^{\mathrm{CP;T}})$ correspond to $\cos\delta(\sin\delta) = \mp 1$, whereas those for $A_{\mu e}^{\mathrm{T;CPT}}$ correspond to $\sin\delta = \mp\mathrm{sign}(\Delta m_{31}^2)$.

Δm_{21}^2 of the form $\frac{1}{\Delta}\sin\Delta$, which cancel out if both of them are small, independently of whether $|a| \ll \Delta m_{21}^2$ or $\Delta m_{21}^2 \ll |a|$. This cancellation will happen as long as $\Delta_\epsilon \equiv \frac{\epsilon L}{4E} \ll 1$, for $\epsilon = a, \Delta m_{21}^2$. This peculiar dependence in the oscillation probabilities is responsible for the restoration of the commutability of the limits $a \to 0$ and $\Delta m_{21}^2 \to 0$ at this level, even though they do not commute at the mixings level.

3.3 ACTUAL EXPERIMENTS: E DEPENDENCE AT FIXED L IN THE EARTH CRUST

In the previous Subsection we discussed the way to obtain analytic approximated expressions for neutrino oscillations in matter that reproduce the right vacuum limit, i.e. the limit when the matter parameter $a \to 0$ at fixed energy due to the matter density going to zero.

In the following, we consider the constant value of the matter density in the Earth crust [112] $\rho_E \approx 3$ g/cm^3, and discuss dependencies in a as dependencies in the neutrino energy in $\nu_\mu \to \nu_e$ transitions. In fact, the actual best-fit value [9] for Δm^2_{21} shows that the relation between a and Δm^2_{21} is given by $|a| \approx 3(E/\text{GeV})\Delta m^2_{21}$, so we can use the mixings in Eqs. (3.20, 3.21) expanding up to second order in $\Delta m^2_{21}/a$, with errors only $\sim 3\%$ around 1 GeV.

As in the oscillation probabilities in Eq. (2.3), all observable quantities can be written in terms of the rephasing-invariant mixings $\tilde{J}^{ij}_{\alpha\beta}$ and the oscillation phases $\tilde{\Delta}_{ij}$. Since $\tilde{U}_{e1}$ in Eq. (3.22) is already a first order quantity, as we discussed, and expanding up to second order also in $|U_{e3}| \ll 1$, which is of the same size as $\Delta m^2_{21}/a$, we find that all $\tilde{J}^{ij}_{e\alpha}$ can be calculated at second order in these two quantities using our first-order $\tilde{U}_{\alpha i}$ in Eqs. (3.25),

$$\tilde{J}^{13}_{e\alpha} = \frac{\Delta m^2_{21}}{a}\left(|U_{e2}|^2 J^{13}_{e\alpha} - |U_{e1}|^2 J^{23}_{e\alpha}\right) , \tag{3.29a}$$

$$\tilde{J}^{23}_{e\alpha} = J^{23}_{e\alpha} + J^{13}_{e\alpha} - \frac{\Delta m^2_{21}}{a}\left(|U_{e2}|^2 J^{13}_{e\alpha} - |U_{e1}|^2 J^{23}_{e\alpha}\right) , \tag{3.29b}$$

$$\begin{aligned}\tilde{J}^{12}_{e\alpha} = {} & \frac{\Delta m^2_{21}}{a}\left[|U_{e2}|^2 J^{12}_{e\alpha} - |U_{e1}|^2 J^{21}_{e\alpha} + |U_{e1}|^2|U_{e2}|^2\left(|U_{\alpha 1}|^2 - |U_{\alpha 2}|^2\right)\right] \\ & - \left[\frac{\Delta m^2_{21}}{a}\right]^2 |U_{e1}|^2|U_{e2}|^2(1 - |U_{\alpha 3}|^2) .\end{aligned} \tag{3.29c}$$

However, as discussed in the previous Subsection, the definite odd a-parity of the two CPT-odd components implies that linear corrections in $a/\Delta m^2_{31}$ are relevant to accurately describe them, so we must keep these terms as well. These linear terms can

be easily calculated setting $\Delta m^2_{21} \to 0$ in the eigenstates in Eq. (3.10) and expanding for $|a| \ll |\Delta m^2_{31}|$. Analogously, we obtain linear corrections in $\Delta m^2_{21}/\Delta m^2_{31}$ to the previous $\tilde{J}^{ij}_{\alpha\beta}$ setting $a \to 0$ in the eigenstates and expanding in $\Delta m^2_{21} \ll |\Delta m^2_{31}|$. The resulting rephasing-invariant mixings, written in the standard parametrization for $\alpha = \mu$, which is the relevant transition for accelerator experiments, are

$$\tilde{J}^{13}_{e\mu} = -\left(\frac{\Delta m^2_{21}}{a} + \frac{\Delta m^2_{21}}{\Delta m^2_{31}}\right) J_r\, e^{i\delta}\,, \tag{3.30a}$$

$$\tilde{J}^{23}_{e\mu} = -S\left(1 + \frac{2a}{\Delta m^2_{31}}\right) + \left(\frac{\Delta m^2_{21}}{a} + \frac{\Delta m^2_{21}}{\Delta m^2_{31}}\right) J_r\, e^{i\delta}\,, \tag{3.30b}$$

$$\tilde{J}^{12}_{e\mu} = \left(\frac{\Delta m^2_{21}}{a} + \frac{\Delta m^2_{21}}{\Delta m^2_{31}}\right) J_r\, e^{i\delta} - \left[\frac{\Delta m^2_{21}}{a}\right]^2 T\,, \tag{3.30c}$$

in terms of the four observable reparametrization invariants $\mathcal{J} \equiv J_r \sin\delta = c_{12}c^2_{13}c_{23}s_{12}s_{13}s_{23}\sin\delta$, $R \equiv J_r \cos\delta$, $S \equiv c^2_{13}s^2_{13}s^2_{23}$ and $T \equiv c^2_{12}s^2_{12}c^2_{23}$. Notice that these are the same results found in Ref. [107] after further expanding in $|a| \ll |\Delta m^2_{31}|$, as expected. Since $|\Delta m^2_{31}| \approx 33\Delta m^2_{21}$, it turns out that the largest mass splitting $|\Delta m^2_{31}| \approx 11|a|/(E/\text{GeV})$, so expanding in $|a| \ll |\Delta m^2_{31}|$ around the $E \sim$ GeV region is as reasonable as expanding in $|U_{e3}| \ll 1$. All $\tilde{J}^{ij}_{\mu e}$ are already second order in Δm^2_{21} and $|U_{e3}|$, so we can neglect all non-leading terms in the oscillation arguments,

$$\Delta\tilde{m}^2_{21} \approx a\,, \qquad \Delta\tilde{m}^2_{31} \approx \Delta m^2_{31}\,, \qquad \Delta\tilde{m}^2_{32} \approx \Delta m^2_{31} - a\,, \tag{3.31a}$$

$$\Delta\tilde{\bar{m}}^2_{21} \approx |a|\,, \qquad \Delta\tilde{\bar{m}}^2_{31} \approx \Delta m^2_{31} + |a|\,, \qquad \Delta\tilde{\bar{m}}^2_{32} \approx \Delta m^2_{31}\,. \tag{3.31b}$$

In this regime, the only oscillation phases are the vacuum phase $\Delta_{31} \propto L/E$ and the constant (for a given baseline through the Earth crust)

$$\Delta_a \equiv \frac{aL}{4E} = 3.8\,\Delta m^2_{21}(\text{eV}^2)\,L(\text{km}) = 0.29\,\frac{L}{1000\text{ km}}\,. \tag{3.32}$$

This value is not particularly small at long baselines, but we again remind the reader that all three $A^{\text{CP;T}}_{\mu e}$, $A^{\text{CP;CPT}}_{\mu e}$ and $A^{\text{T;CPT}}_{\mu e}$ have definite parity in a, the first one being even, the second and third ones odd, as we proved in Chapter 2. This means

that corrections to the leading order in each component will be quadratic in a, and so we can also expand up to leading order in Δ_a with errors $\sim 8\%$ around 1000 km.

In summary, the expansion quantities used are the standard parameters

$$\frac{\Delta m^2_{21}}{\Delta m^2_{31}} \sim 0.030\,, \qquad |U_{e3}| \sim 0.15\,, \tag{3.33}$$

up to second order, and the quadratic (due to the definite parity of the disentangled components)

$$\left[\frac{\Delta m^2_{21}}{a}\right]^2 \sim \frac{0.12}{(E/\mathrm{GeV})^2}\,, \qquad \left[\frac{a}{\Delta m^2_{31}}\right]^2 \sim 0.008\,(E/\mathrm{GeV})^2\,,$$
$$[\Delta_a]^2 \sim 0.084\,(L/1000\mathrm{km})^2\,. \tag{3.34}$$

Taking into account Eqs. (3.30) for the rephasing-invariant mixings, with the symmetry property $\tilde{J}^{ij}_{\mu e} = \tilde{J}^{ji}_{e\mu}$, and Eqs. (3.31) for the mass differences in matter, we find the approximate expressions

$$A^{\mathrm{CP;T}}_{\mu e} \approx -16\,J_r \sin\delta\,\Delta_{21}\sin^2\Delta_{31}\,, \tag{3.35a}$$

$$A^{\mathrm{CP;CPT}}_{\mu e} \approx 16\Delta_a\left[\frac{\sin\Delta_{31}}{\Delta_{31}} - \cos\Delta_{31}\right](S\sin\Delta_{31} + J_r\cos\delta\,\Delta_{21}\cos\Delta_{31})\,, \tag{3.35b}$$

$$A^{\mathrm{T;CPT}}_{\mu e} \approx -16\Delta_a J_r \sin\delta\,\Delta_{21}\sin\Delta_{31}\left[\frac{\sin\Delta_{31}}{\Delta_{31}} - \cos\Delta_{31}\right]\,, \tag{3.35c}$$

where $S \equiv c^2_{13}s^2_{13}s^2_{23}$, $J_r \equiv c_{12}c^2_{13}c_{23}s_{12}s_{13}s_{23}$, $\Delta_a \equiv \frac{aL}{4E} \propto L$ and the two $\Delta_{ij} \equiv \frac{\Delta m^2_{ij}L}{4E} \propto L/E$. From these expressions, which are precise enough to provide understanding of the physics behind these observables, we find that $A^{\mathrm{CP;T}}_{\mu e}$ in matter is well described by its vacuum value. Since Δ_{21} is small, this means that this genuine component oscillates as $\frac{1}{E}\sin^2\Delta_{31}$. Conversely, the matter-induced $A^{\mathrm{CP;CPT}}_{\mu e}$ and interference $A^{\mathrm{T;CPT}}_{\mu e}$ components, which vanish when $a \to 0$, are well described by their first order in a.

The agreement of Eqs. (3.35) with the exact results is shown in Figure 3.11, which makes clear that, even if the value of the asymmetry components in the maxima is a bit off, their position and

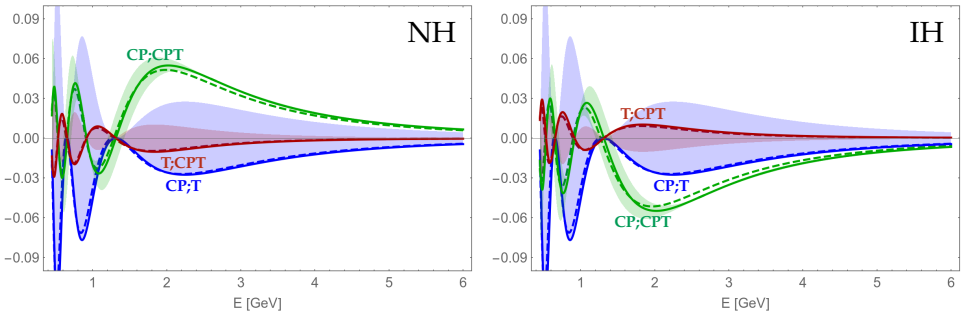

Figure 3.11: $A_{\mu e}^{\mathrm{CP;T}}$ (blue), $A_{\mu e}^{\mathrm{CP;CPT}}$ (green) and $A_{\mu e}^{\mathrm{T;CPT}}$ (red) components as functions of the neutrino energy E through the Earth crust (of constant density) and a baseline of $L = 1300$ km. Both exact (dashed) and analytical (solid) results from Eqs.(3.35) are shown. Normal (Inverted) Hierarchy in the left (right) panel. The bands correspond to all possible values changing δ in $(0, 2\pi)$; the lines correspond to $\delta = \pi/2$, the T-odd components proportional to $\sin\delta$, the T-even one extremal when $\cos\delta = \pm 1$.

the general behavior are well reproduced. Therefore, Eqs. (3.35) are the perfect tool to understand the energy dependencies of the disentangled components and search for their actual experimental separation. We will break down the insight they provide in the next Chapter, explaining all the properties and interesting behaviors found in Section 3.1.

4 SIGNATURES OF THE THREE SEPARATE COMPONENTS

In the previous two Chapters, we established a theorem to cleanly separate the effects of the different sources of CP, T and CPT violation, finding observables with definite parity under all three symmetries, and developed the appropriate tools to understand its implications.

In this Chapter, we will break down all the information provided by the precise enough analytical approximations for each of the three disentangled components in Eqs. (3.35). All the properties observed in the numerical scan in Section 3.1 will be explained, and in particular the nearly definite parity of the components under a change of Hierarchy, the particular dependencies on the CP phase δ, and the existence of a magic point where the experimental asymmetries are fully genuine.

4.1 A CLOSER LOOK AT THE GENUINE COMPONENT

According to its last term in Eq. (2.2), the Hamiltonian of our problem in the flavor basis is proportional to the hermitian mass matrix squared in matter $\tilde{M}_\nu$ as

$$2E\,H \equiv H' = \tilde{M}_\nu \tilde{M}_\nu^\dagger\,. \tag{4.1}$$

In such a basis, the necessary and sufficient condition for CP invariance is [113]

$$\mathrm{Im}[H'_{e\mu} H'_{\mu\tau} H'_{\tau e}] = 0\,. \tag{4.2}$$

For any flavor-diagonal interaction of neutrinos with matter, this condition is equal to that for neutrino mass matrices in vacuum. This invariance [114] of the left-hand side of the last

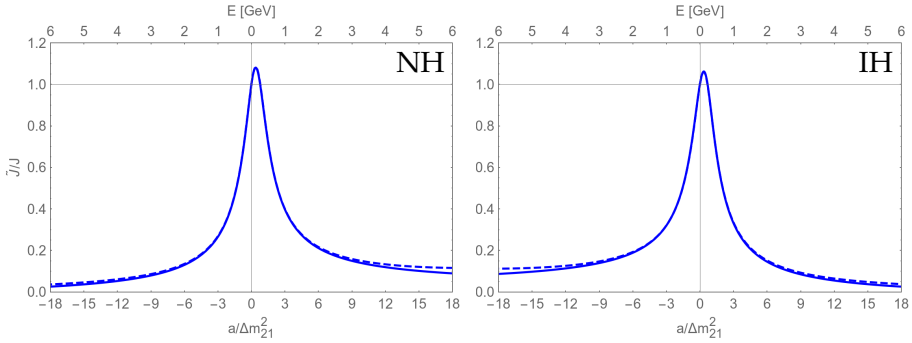

Figure 4.1: $\tilde{\mathcal{J}}/\mathcal{J}$ ratio for both neutrinos ($a > 0$) and antineutrinos ($a < 0$). The horizontal axis shows both the evolution of the matter parameter a at fixed energy (lower labels), i.e. changing the matter density, and as function of the energy if the constant density is chosen as that of the Earth crust (upper labels). Exact (dashed) and analytical (solid) results from Eqs. (4.4). Normal (Inverted) Hierarchy in the left (right) panel.

equation (4.2) between the CP behavior of neutrinos in vacuum and in matter has far-reaching consequences for the observable rephasing-invariant mixings of neutrinos $\tilde{J}^{ij}_{\alpha\beta}$ and antineutrinos $\tilde{\bar{J}}^{ij}_{\alpha\beta}$ in matter.

The explicit calculation of the matter-vacuum invariant genuine CP violation expression for neutrinos, antineutrinos and in vacuum leads to

$$\Delta\tilde{m}^2_{12}\Delta\tilde{m}^2_{23}\Delta\tilde{m}^2_{31}\tilde{\mathcal{J}} = \Delta\tilde{\bar{m}}^2_{12}\Delta\tilde{\bar{m}}^2_{23}\Delta\tilde{\bar{m}}^2_{31}\tilde{\bar{\mathcal{J}}} = \Delta m^2_{12}\Delta m^2_{23}\Delta m^2_{31}\mathcal{J}\,, \quad (4.3)$$

where $\mathcal{J}$ is the rephasing-invariant CP-violating quantity in vacuum [115], $\mathcal{J} = c_{12}c^2_{13}c_{23}s_{12}s_{13}s_{23}\sin\delta$. The proportionality of $\tilde{\mathcal{J}}$ and $\tilde{\bar{\mathcal{J}}}$ to the vacuum Δm^2_{21} explains the absence of genuine CP violation in matter in the limit of vanishing Δm^2_{21}, even in the presence of three non-degenerate neutrinos and antineutrinos in matter. The vanishing of $\tilde{\mathcal{J}}$ and $\tilde{\bar{\mathcal{J}}}$ in this limit comes from the transmutation of masses in vacuum to mixings in matter calculated in Section 3.2.2, leading to $\tilde{U}_{e1} = 0$ and $\tilde{\bar{U}}_{e2} = 0$. To leading order in Δm^2_{21}, the non-vanishing $\tilde{\mathcal{J}}$ and $\tilde{\bar{\mathcal{J}}}$ differ by

linear terms in the matter potential a present in the neutrino masses in matter.

Using the analytic perturbation expansion of Section 3.2 for the connection between quantities in matter and in vacuum, we can write

$$\tilde{\mathcal{J}} = \frac{\Delta m^2_{21}\left[\Delta m^2_{31} + a\right]}{\Delta m^2_{31}\left[\Delta m^2_{21} - 2\tilde{m}^2_0 + a(1 - |U_{e3}|^2)\right]}\,\mathcal{J}\,, \tag{4.4a}$$

$$\tilde{\bar{\mathcal{J}}} = \frac{\Delta m^2_{21}\left[\Delta m^2_{31} - |a|\right]}{\Delta m^2_{31}\left[2\tilde{\bar{m}}^2_0 - \Delta m^2_{21} + |a|(1 - |U_{e3}|^2)\right]}\,\mathcal{J}\,. \tag{4.4b}$$

Notice that the proportionality factors in Eqs. (4.4) are energy dependent through a, as shown in Figure 4.1.

The behavior at low/high energies can be easily understood using the expansions at leading order of $\tilde{m}^2_0$ and $\tilde{\bar{m}}^2_0$ in Eqs. (3.15) and (3.16). Indeed, at low energies

$$\tilde{\mathcal{J}} \approx \mathcal{J}\left[1 + \frac{a(|U_{e1}|^2 - |U_{e2}|^2)}{\Delta m^2_{21}} + \frac{a}{\Delta m^2_{31}}\right] > \mathcal{J}\,, \tag{4.5a}$$

$$\tilde{\bar{\mathcal{J}}} \approx \mathcal{J}\left[1 - \frac{|a|(1 - |U_{e2}|^2)}{\Delta m^2_{21}} - \frac{|a|}{\Delta m^2_{31}}\right] < \mathcal{J}\,, \tag{4.5b}$$

the ratio increases (decreases) with respect to 1 for (anti)neutrinos independently of $\text{sign}(\Delta m^2_{31})$ due to both $\Delta m^2_{21} \ll |\Delta m^2_{31}|$ and $|U_{e1}| > |U_{e2}|$, whereas at high energies

$$\tilde{\mathcal{J}} \approx \mathcal{J}\,\frac{\Delta m^2_{21}(\Delta m^2_{31} + a)}{a\,\Delta m^2_{31}}\,, \tag{4.6a}$$

$$\tilde{\bar{\mathcal{J}}} \approx \mathcal{J}\,\frac{\Delta m^2_{21}(\Delta m^2_{31} - |a|)}{|a|\,\Delta m^2_{31}}\,, \tag{4.6b}$$

both of them decrease roughly as $1/a$, and changing the $\text{sign}(a)$ is equivalent to changing the $\text{sign}(\Delta m^2_{31})$. This degeneracy between NHν and IH$\bar{\nu}$ explains why the two plots in Figure 4.1 seem to be symmetrical.

The decreasing value of the $\tilde{\mathcal{J}}/\mathcal{J}$ ratio at higher energies described by Eqs. (4.6), i.e. when $|a| \gg \Delta m^2_{21}$, is a consequence of the absence of genuine CP violation in matter in the limit

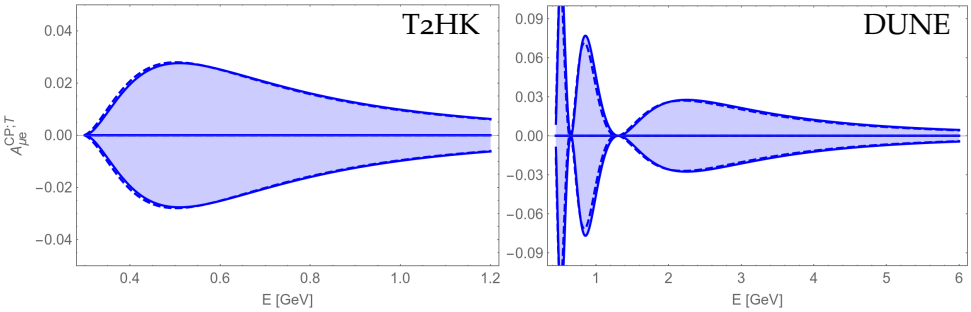

Figure 4.2: Energy distribution of the genuine component $A_{\mu e}^{\mathrm{CP;T}}$ at T2HK baseline $L = 295$ km (left) and DUNE $L = 1300$ km (right), which is Hierarchy independent. Exact (dashed) and analytical (solid) results from Eq. (3.35a). The bands correspond to all possible values changing δ in $(0, 2\pi)$; the upper/central/lower lines correspond to $\sin\delta = -1, 0, 1$.

$\Delta m^2_{21} = 0$ even if there are three non-vanishing neutrino masses in matter. The transmutation of masses in vacuum to mixings in matter forces the smallness of the imaginary part of the rephasing-invariant mixing in matter at high energies. However, this fact does not necessarily mean that genuine CP violation is unobservable at these energies, since the genuine T-odd component of the CP asymmetry contains this energy-dependent factor together with the matter-dependent oscillation function —odd in L— that depends on both energy and baseline.

The effects of the baseline are shown in Figure 4.2, comparing the whole genuine component $A_{\mu e}^{\mathrm{CP;T}}$ as function of the energy for T2HK $L = 295$ km and DUNE $L = 1300$ km. The Figure shows that the oscillation amplitude of the genuine component at each experiment (fixed baseline L) decreases as $1/E$, as expected, whereas a higher baseline (at fixed E; look e.g. at 1 GeV) enhances the values of $A_{\mu e}^{\mathrm{CP;T}}$.

This behavior is understood with the perturbation expansion in $|U_{e3}|^2 \ll 1$ in the energy regime $\Delta m^2_{21} \ll |a| \ll |\Delta m^2_{31}|$, between the two MSW resonances, that we performed in the previous Chapter. The $1/E$ dependence in $\tilde{\mathcal{J}}$ is changed by the approximated oscillating functions into L/E, producing genuine CPV components of the same size at the spectrum peak for both exper-

iments. In fact, the matter effects in $\tilde{\mathcal{J}}$ and oscillating phases just compensate to generate in this approximation a genuine component equal to that in vacuum, i.e. Eq. (3.35a). As such, it is odd in L/E, independent of a and the Hierarchy, and proportional to $\sin\delta$.

4.2 NEUTRINO MASS ORDERING DISCRIMINATION

Last Section has demonstrated that the genuine component $A_{\mu e}^{\mathrm{CP;T}}$ in matter is, to a good approximation for energies between the two resonances $\Delta m^2_{21} \ll |a| \ll |\Delta m^2_{31}|$, as planned in accelerator facilities, given by the vacuum CP (and T) asymmetry. Its information content is then crucial to identify experimental signatures of genuine CP violation. On the other hand, it has nothing to say about the neutrino mass ordering: it is invariant under the change of sign in Δm^2_{31}. This simple change of sign, without changing the absolute value $|\Delta m^2_{31}|$, is in fact the only effect of changing the Hierarchy under the approximations leading to Eqs. (3.35).

Even though we found in Section 3.1 that the interference component $A_{\mu e}^{\mathrm{T;CPT}}$ changes its sign under a change of Hierarchy, its proportionality to $\sin\delta$ makes it impossible to extract information on the Hierarchy from its measurement unless the CP phase δ is already known. Under these conditions, a direct determination of the neutrino mass ordering must come from the matter-induced component $A_{\mu e}^{\mathrm{CP;CPT}}$, even in L and $\sin\delta$ and odd in a. We thus discuss in this Section the information on the neutrino mass ordering that the matter-induced component introduces in the experimental CP asymmetry $\mathcal{A}_{\mu e}^{\mathrm{CP}}$. Propagation in matter is needed to generate effects of the change of Hierarchy and our $A_{\mu e}^{\mathrm{CP;CPT}}$ is able to separate out this information, going beyond studies of its influence on transition probabilities [116].

Contrary to the $\tilde{\mathcal{J}}$ discussed in the previous Section, there is no simple matter-vacuum relation such as Eq. (4.3) to easily write

$\mathrm{Re}\tilde{J}^{ij}_{\alpha\beta}$ as function of the vacuum $\mathrm{Re}J^{ij}_{\alpha\beta}$ —the most compact result following this idea is [117, 118]

$$\Delta\tilde{m}^2_{12}\Delta\tilde{m}^2_{23}\Delta\tilde{m}^2_{31}\Delta\tilde{m}^2_{ij}\,\mathrm{Re}\tilde{J}^{ij}_{\alpha\beta} = K^{ij}_{\alpha\beta} + \Delta m^2_{12}\Delta m^2_{23}\Delta m^2_{31}\Delta m^2_{ij}\,\mathrm{Re}J^{ij}_{\alpha\beta}\,, \tag{4.7}$$

where all $K^{ij}_{\alpha\beta}$ vanish in vacuum [no ij sum implied in Eq. (4.7)]. This relation explains the dependence of all L-even terms in the oscillation probabilities in each of the $\tilde{\Delta}_{ij}$ phases as $\frac{1}{\tilde{\Delta}^2_{ij}}\sin^2\tilde{\Delta}_{ij}$, which is the reason why the vacuum limit $a \to 0$ is restored in these observables even after taking $\Delta m^2_{21} \ll |a|$, as discussed in Section 3.2.2. However, the $K^{ij}_{\alpha\beta}$ are complicated functions of the vacuum quantities, and do not provide a clear insight into the behavior of $A^{\mathrm{CP;CPT}}_{\alpha\beta}$, so we will use Eq. (3.35b) instead,

$$A^{\mathrm{CP;CPT}}_{\mu e} \approx 16\Delta_a\left[\frac{\sin\Delta_{31}}{\Delta_{31}} - \cos\Delta_{31}\right](S\sin\Delta_{31} + J_r\cos\delta\,\Delta_{21}\cos\Delta_{31})\,.$$

In general, this matter-induced component of the CP asymmetry has no definite transformation properties under the change of sign in Δm^2_{31}. Under the approximations made in Section 3.3, there are two distinct terms in $A^{\mathrm{CP;CPT}}_{\mu e}$, a first one A^{H}_{-} which is an odd function of Δm^2_{31} and a second one A^{H}_{+} which is an even function of Δm^2_{31}, so that $A^{\mathrm{CP;CPT}}_{\mu e} = A^{\mathrm{H}}_{-} + A^{\mathrm{H}}_{+} + \mathcal{O}(\Delta^3_a)$,

$$A^{\mathrm{H}}_{-} = 16\,\Delta_a\left[\frac{\sin\Delta_{31}}{\Delta_{31}} - \cos\Delta_{31}\right]S\sin\Delta_{31}\,, \tag{4.8a}$$

$$A^{\mathrm{H}}_{+} = 16\,\Delta_a\left[\frac{\sin\Delta_{31}}{\Delta_{31}} - \cos\Delta_{31}\right]J_r\cos\delta\,\Delta_{21}\cos\Delta_{31}\,. \tag{4.8b}$$

Notice that both terms, as well as the whole $A^{\mathrm{CP;CPT}}_{\mu e}$, vanish simultaneously when the δ-independent common prefactor vanishes. Alternatively, the matter-induced component vanishes δ-dependently when these A^{H}_{-} and A^{H}_{+} terms compensate each other.

As seen, the information content in $A^{\mathrm{CP;CPT}}_{\mu e}$ on the neutrino mass Hierarchy is due to A^{H}_{-} only, its dominant zeroth-order term in Δm^2_{21} independent of the phase δ. Consistently with the energy-dependence of the neutrino masses in matter computed

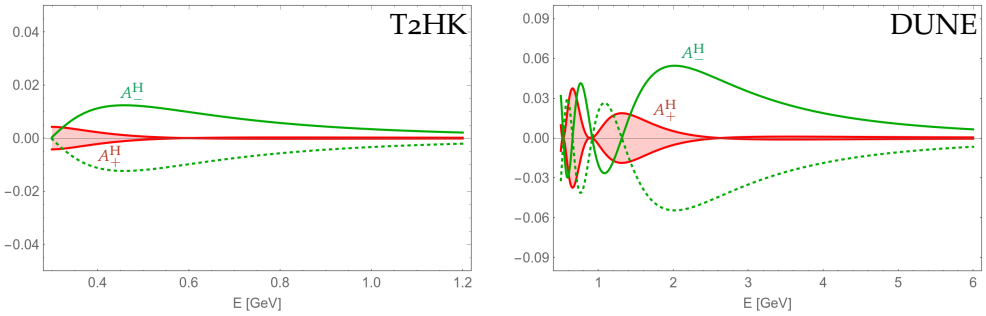

Figure 4.3: Energy distribution of the two distinct terms of $A_{\mu e}^{\text{CP;CPT}}$ as defined in Eqs. (4.8), A_-^H (green, δ-independent, Hierarchy-odd) and A_+^H (red, $\cos\delta$-odd, Hierarchy-invariant), at T2HK $L = 295$ km (left) and DUNE $L = 1300$ km (right). Both Normal Hierarchy (solid) and Inverted Hierarchy (dashed) shown for the Hierarchy-dependent term. The bands correspond to all possible values changing δ in $(0, 2\pi)$.

numerically in Section 3.1, our results for $\Delta\tilde{m}^2_{ij}$ from Eq. (3.31) show that, in the limit $\Delta m^2_{21} \to 0$, the mass spectrum in matter changes under a change of Hierarchy from neutrinos to antineutrinos as

$$\Delta\tilde{m}^2_{21} \leftrightarrow \Delta\tilde{\bar{m}}^2_{21}\,, \qquad \Delta\tilde{m}^2_{31} \leftrightarrow -\Delta\tilde{\bar{m}}^2_{32}\,, \qquad \Delta\tilde{m}^2_{32} \leftrightarrow -\Delta\tilde{\bar{m}}^2_{31}\,, \tag{4.9}$$

whereas the $\tilde{J}^{ij}_{\alpha\beta}$ do not change sign, since Δm^2_{31} effects are subleading corrections to Eqs. (3.29). Therefore, all L-even terms in the oscillation probabilities —which are blind to the sign change in Eq. (4.9)— are simply interchanged between neutrinos and antineutrinos. As the CP asymmetry is a difference between neutrino and antineutrino oscillation probabilities, the matter-induced component $A_{\mu e}^{\text{CP;CPT}}$ is only changing its sign under a change of Hierarchy in the vanishing limit of Δm^2_{21}, explaining why only A_-^H is non-vanishing in this case.

A non-vanishing Δm^2_{21} affects the matter-induced component generating the A_+^H term in Eq. (4.8b). It is thus only appreciable at low energies, and sensitive to the δ phase as a CP-conserving $\cos\delta$ factor. In Figure 4.3 we represent these two terms of the matter-induced component $A_{\mu e}^{\text{CP;CPT}}$ as function of the energy for

the baselines of T2HK and DUNE, and for both Normal and Inverted Hierarchies.

To test the neutrino mass ordering from $A_{\mu e}^{\mathrm{CP;CPT}}$, we find that imposing the condition $\left|A_{-}^{\mathrm{H}}\right| > \left|A_{+}^{\mathrm{H}}\right|$ in the non-oscillating (high energy) region leads to $E > 1.1\, E_{1^{\mathrm{st}}\,\mathrm{node}}$. For these energies above the first node of the vacuum oscillation probability, the whole effect of the change of sign in Δm_{31}^2 is an almost odd $A_{\mu e}^{\mathrm{CP;CPT}}$. At long enough baselines such that the matter-induced component dominates the CP asymmetry over the genuine one, as happens at DUNE (see Figure 3.11), we find that the A_{-}^{H} term in $A_{\mu e}^{\mathrm{CP;CPT}}$ dominates the whole CP asymmetry for any value of δ, so the measurement of the sign of the experimental $\mathcal{A}_{\mu e}^{\mathrm{CP}}$ at these energies fixes the Hierarchy.

4.3 THE GENUINE–MATTER INTERFERENCE COMPONENT

The genuine component $A_{\mu e}^{\mathrm{CP;T}}$ analyzed in Section 4.1 is non-zero, even in matter, only if there is genuine CP violation in the lepton sector, which is why it is a trustworthy observable to test CP violation in neutrino oscillations. Conversely, the matter-induced component $A_{\mu e}^{\mathrm{CP;CPT}}$ analyzed in Section 4.2 is non-zero due to the CPT-violating matter effects, even if there is no genuine CP violation, and we found it carries precious information on the neutrino mass ordering.

After looking into these two components of the CP asymmetry, a question could immediately arise: are these $A_{\alpha\beta}^{\mathrm{CP;T}}$ and $A_{\alpha\beta}^{\mathrm{CP;CPT}}$ components coincident with the T and CPT asymmetries, respectively? As the genuine T-odd $A_{\alpha\beta}^{\mathrm{CP;T}}$ component is CPT-invariant and thus CP-odd, a positive answer to this question would be equivalent to claim the absence of fake matter-induced terms in the T asymmetries, and hence a vanishing value for the interference component $A_{\alpha\beta}^{\mathrm{T;CPT}}$. In this case, the usual factorization of *fake* matter effects in the CP asymmetry, namely

$$\mathcal{A}_{\alpha\beta}^{\mathrm{CP}} = \mathcal{A}_{\alpha\beta}^{\mathrm{T}} + \mathcal{A}_{\alpha\beta}^{\mathrm{F}}\,, \tag{4.10}$$

would be equivalent to our Disentanglement Theorem, with $\mathcal{A}^{\mathrm{F}}_{\alpha\beta}$ identified as the CPT asymmetry. For a non-vanishing interference component, however, this separation is not conceptually possible in the sense that the two asymmetries in which the CP asymmetry is separated include CP-even terms.

In the literature on neutrino oscillations T asymmetries [92, 105, 106, 114, 119–127], however, one does not find definite claims on this question, even for a T-symmetric matter between the source and the detector (and, a fortiori, for uniform matter) neither in one nor the other sense of the response. Contrary to the matter-induced component of the CP asymmetry, which exists even in the absence of true CP violation, if the medium is T-symmetric it *by itself* cannot generate a T asymmetry in neutrino oscillations. However, in the presence of genuine CP violation this last reasoning does not lead to a definite conclusion whether the entire T asymmetry is also CP-odd and CPT-invariant. In this last case, the genuine component in the disentangled CP asymmetry could be separately measured by the T asymmetry. On the contrary, a non-vanishing value of the interference component $A^{\mathrm{T;CPT}}_{\alpha\beta}$ would mean that the medium generates an additional term in the T asymmetry which is CP-even by the combined effect of genuine *and* matter amplitudes. This CPT-odd component would then be a fake effect even for a T-symmetric medium.

We focus in this Section on this open question and break down the case of the interference component $A^{\mathrm{T;CPT}}_{\mu e}$, which is thus unique, for it needs both genuine CP violation and matter effects to be non-zero. In the region between the two MSW resonances $\Delta m^2_{21} \ll a \ll \left|\Delta m^2_{31}\right|$ leading to its approximate expression in Eq. (3.35c),

$$A^{\mathrm{T;CPT}}_{\mu e} = -16\Delta_a J_r \sin\delta\, \Delta_{21} \sin\Delta_{31} \left[\frac{\sin\Delta_{31}}{\Delta_{31}} - \cos\Delta_{31}\right] + \mathcal{O}(\Delta_a^3)\,,$$

these two requirements for its non-vanishing value translate into the proportionality of the interference component to the T-odd $\Delta m^2_{21}\sin\delta$ factor and the CPT-odd Δ_a factor.

Further implications can be understood from this fact. As happens with the CP-odd genuine component $A^{\mathrm{CP;T}}_{\mu e}$, their T-odd parity together with the matter-vacuum invariance in Eq. (4.3)

ensure that a non-vanishing value of any of these two components is a proof of genuine CP violation. Information on the CP phase δ in the standard parametrization, however, is not clearly extracted from $A_{\mu e}^{\mathrm{T;CPT}}$ due to its CPT-odd parity: as happens with the matter-induced $A_{\mu e}^{\mathrm{CP;CPT}}$, their CPT-odd parity is related to Hierarchy-dependent terms in these two components —the difference in nature between them explaining why the Hierarchy-odd term in $A_{\mu e}^{\mathrm{CP;CPT}}$ is independent of Δm^2_{21}, whereas $A_{\mu e}^{\mathrm{T;CPT}}$ is fully Hierarchy-odd and proportional to Δm^2_{21}.

Notice that the non-vanishing value for this interference component claims, indeed, that T-symmetric matter effects are able to change the value of the experimental T-odd asymmetry $\mathcal{A}^{\mathrm{T}}_{\alpha\beta}$. Although this change does not affect the genuine character of the T asymmetry as a test of genuine CP violation, it means that, strangely enough, its non-vanishing value does not prove that CP violation has actually been observed in the T asymmetry.

Such a proof would need the experimental measurement of both neutrino and antineutrino T asymmetries in Eq. (2.13b),

$$\mathcal{A}^{\mathrm{T}}_{\alpha\beta} = A^{\mathrm{T;CPT}}_{\alpha\beta} + A^{\mathrm{T;CP}}_{\alpha\beta}\,, \qquad \bar{\mathcal{A}}^{\mathrm{T}}_{\alpha\beta} = A^{\mathrm{T;CPT}}_{\alpha\beta} - A^{\mathrm{T;CP}}_{\alpha\beta}\,,$$

under the same conditions of baseline and energy, from which one could separate the two components as

$$A^{\mathrm{T;CP}}_{\alpha\beta} = \frac{1}{2}(\mathcal{A}^{\mathrm{T}}_{\alpha\beta} - \bar{\mathcal{A}}^{\mathrm{T}}_{\alpha\beta})\,, \quad A^{\mathrm{T;CPT}}_{\alpha\beta} = \frac{1}{2}(\mathcal{A}^{\mathrm{T}}_{\alpha\beta} + \bar{\mathcal{A}}^{\mathrm{T}}_{\alpha\beta})\,. \quad (4.11)$$

The first component, blind to Hierarchy effects, would provide information on the CP phase δ, which could then be used to extract the Hierarchy from the second one.

4.4 SIGNATURES OF THE COMPONENTS' PECULIAR ENERGY DISTRIBUTIONS

Having analyzed in detail the information accessible by each of the three components, and thinking especially in accelerator experiments, in this Section we identify those aspects of the energy distribution of the CP asymmetry $\mathcal{A}^{\mathrm{CP}}_{\mu e}$ that can offer an

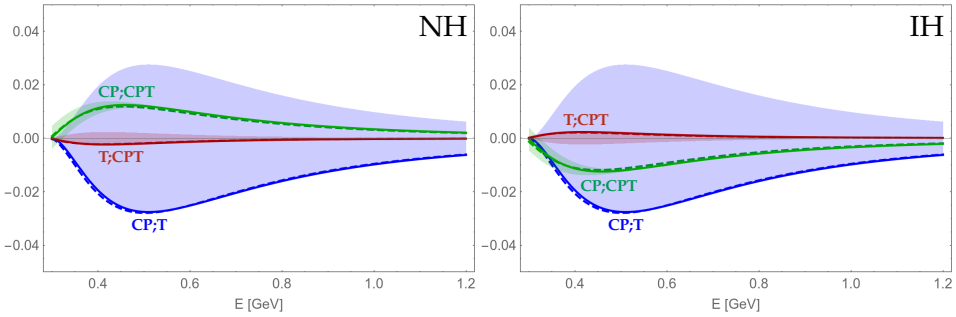

Figure 4.4: CPT-odd T-invariant (green) and T-odd CPT-invariant (blue) components of the CP asymmetry $\mathcal{A}^{\mathrm{CP}}_{\mu e}$, together with the CPT-odd CP-invariant (red) component of the T asymmetry $\mathcal{A}^{\mathrm{T}}_{\mu e}$, as functions of the neutrino energy E through the Earth crust (of constant density) at T2HK baseline $L = 295$ km. Exact (dashed) and analytical (solid) results from Eqs.(3.35) shown. Normal (Inverted) Hierarchy in the left (right) panel. The bands correspond to all possible values changing δ in $(0, 2\pi)$; the lines correspond to $\delta = \pi/2$, the T-odd components proportional to $\sin\delta$, the T-even one extremal when $\cos\delta = \pm 1$.

experimental signature for the separation of its genuine and matter-induced components. We will, nevertheless, also include the interference component in the analysis, for the sake of completeness.

With experiments in which the fingerprint of the baseline dependence, L-odd and L-even functions, cannot be used, the peculiar patterns of the energy distribution provide precious information. The general trend of this dependence for $L = 1300$ km is given in Figure 3.11, showing the appearance of oscillations in the low and medium energy regions of the spectrum. The genuine $A^{\mathrm{CP;T}}_{\mu e}$ behaves differently from the two CPT-odd $A^{\mathrm{CP;CPT}}_{\mu e}$ and $A^{\mathrm{T;CPT}}_{\mu e}$, with nodes and extremal values at different energies.

However, this rich structure is lost when the baseline is decreased to a medium baseline $L = 295$ km and a threshold energy of 300 MeV is imposed. The emerging picture under these conditions is given in Figure 4.4 and the main conclusion is the relative suppression of $A^{\mathrm{CP;CPT}}_{\mu e}$ and $A^{\mathrm{T;CPT}}_{\mu e}$ with respect to $A^{\mathrm{CP;T}}_{\mu e}$, due to

their proportionality to $\Delta_a \propto L$. In addition, this small matter-induced $A_{\mu e}^{\mathrm{CP;CPT}}$ is mainly the δ-independent A_{-}^{H} in Eq. (4.8a) and so it can be subtracted away from the experimental $\mathcal{A}_{\mu e}^{\mathrm{CP}}$, if the neutrino mass Hierarchy is previously known, as a theoretical background. This would allow to separate the genuine $A_{\mu e}^{\mathrm{CP;T}}$.

Using the analytical approximate expressions of the observable components given in Eqs. (3.35), we perform a detailed study of the position of extremal values and zeros of each of them, as well as their behavior around the zeros. The energy dependence is controlled by the phase $\Delta_{31} \propto 1/E$ and we will take as reference the functional form of the CP-conserving transition probability $f(\Delta) = \sin^2 \Delta$.

For the genuine component $A_{\mu e}^{\mathrm{CP;T}}$ in Eq. (3.35a),

$$A_{\mu e}^{\mathrm{CP;T}} = -16\, J_r \sin\delta\, \Delta_{21} \sin^2 \Delta_{31} + \mathcal{O}(\Delta_a^2)\,,$$

the energy distribution is

$$f_{\mathrm{gen}}(\Delta) = \Delta \sin^2 \Delta\,. \tag{4.12}$$

Contrary to $f(\Delta)$, the amplitude of the oscillations of $f_{\mathrm{gen}}(\Delta)$ decreases as $1/E$, but the zeros are the same $\Delta_0 = 0,\ \pi,\ 2\pi \ldots$ as for $f(\Delta)$. There are, however, two series of extremal values given by

$$f'_{\mathrm{gen}}(\Delta) = \sin\Delta(\sin\Delta + 2\Delta\cos\Delta) = 0\,. \tag{4.13}$$

The first kind, those corresponding to solutions of $\sin\Delta = 0$ as for the zeros, are double zeros, which indicates that $A_{\mu e}^{\mathrm{CP;T}}$ keeps the same sign around the zeros, and so in the whole energy spectrum. From Eq. (3.35a) for the analytical approximation of the genuine component, it is clear that the sign is given by $\mathrm{sign}(A_{\mu e}^{\mathrm{CP;T}}) = -\mathrm{sign}(\sin\delta)$.

The additional extremal values appear for

$$\tan\Delta = -2\Delta\,. \tag{4.14}$$

In Figure 4.5 we identify graphically (in blue) the solutions to Eq. (4.14), which appear slightly above the oscillation maxima $\Delta_{\mathrm{max}}^{\mathrm{osc}} = (2n+1)\frac{\pi}{2}$. This is a first fortunate fact, implying that the

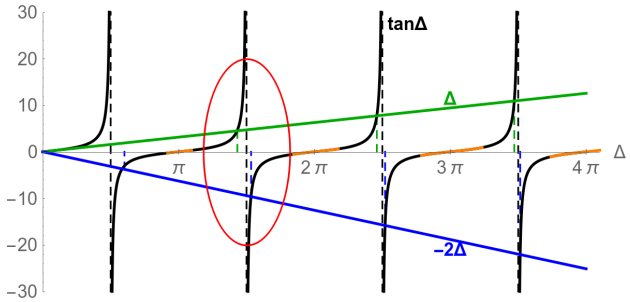

Figure 4.5: Illustration of the position of the relevant zeros of the two CPT-odd components, given by $\tan\Delta_{31} = \Delta_{31}$, and the maxima of $|A_{\mu e}^{\mathrm{CP;T}}|$, given by $\tan\Delta_{31} = -2\Delta_{31}$. The vertical dashed lines are the asymptotes of $\tan\Delta$ (black), corresponding to oscillation maxima, and the perturbative solutions of the previous equations given, respectively, by $\Delta_0^{\mathrm{CPT}} = (2n+1)\frac{\pi}{2} - \left[(2n+1)\frac{\pi}{2}\right]^{-1}$ (green) and $\Delta_{\mathrm{max}}^{\mathrm{T}} = (2n+1)\frac{\pi}{2} + \frac{1}{2}\left[(2n+1)\frac{\pi}{2}\right]^{-1}$ (blue). As calculated in Eq. (4.17), the δ-dependent zeros of $A_{\mu e}^{\mathrm{CP;CPT}}$ around $\Delta_0 = n\pi$ are bounded within the orange regions of $\tan\Delta$. The highest-energy point, i.e. smallest Δ, where $A_{\mu e}^{\mathrm{CP;CPT}}$ vanishes δ-independently is emphasized by the red ellipse.

experimental configurations with maximal $|A_{\mu e}^{\mathrm{CP;T}}|$ are close to those with highest statistics. A perturbative expansion of $\cot\Delta$ around $\Delta_{\mathrm{max}}^{\mathrm{osc}}$ leads to the approximate solutions

$$\begin{aligned}\Delta_{\mathrm{max}}^{\mathrm{T}} &= (2n+1)\frac{\pi}{2} + \frac{1}{2}\left[(2n+1)\frac{\pi}{2}\right]^{-1} + \cdots, \qquad n \geq 0 \\ &\approx \frac{\pi}{2} + \frac{1}{\pi}, \frac{3\pi}{2} + \frac{1}{3\pi}, \frac{5\pi}{2} + \frac{1}{5\pi} \cdots, \end{aligned} \tag{4.15}$$

which show that the interesting (see below) second and higher maxima in $|A_{\mu e}^{\mathrm{CP;T}}|$ are within a 3% interval above the oscillation maxima.

In the case of the matter-induced component $A_{\mu e}^{\mathrm{CP;CPT}}$ of the CP asymmetry, the energy distribution in Eq. (3.35b) is

$$f_{\mathrm{mat}}(\Delta) = \left(\frac{\sin\Delta}{\Delta} - \cos\Delta\right)\left(S\sin\Delta + J_r\,\frac{\Delta m_{21}^2}{\Delta m_{31}^2}\cos\delta\,\Delta\cos\Delta\right), \tag{4.16}$$

which has two kinds of zeros with distinct implications. The vanishing points for the second factor are the δ-dependent solutions of

$$\tan\Delta = -\frac{J_r}{S}\frac{\Delta m^2_{21}}{\Delta m^2_{31}}\cos\delta\ \Delta = -0.09\cos\delta\ \Delta\,, \tag{4.17}$$

that reduce to the vacuum nodes $\sin\Delta = 0$ if $\cos\delta = 0$, where the genuine $A^{\mathrm{CP;T}}_{\mu e}$ also vanishes. The actual position of these zeros is strongly dependent on $\cos\delta$, and the set of solutions is illustrated in Figure 4.5 by the region around $\Delta_0 = n\pi$ where $\tan\Delta$ is orange.

The second kind of zeros in Eq. (4.16) are solutions of the equation

$$\tan\Delta = \Delta\,, \tag{4.18}$$

and are graphically depicted in Figure 4.5 too (in green). As seen, they appear slightly below the oscillation maxima in the vacuum $f(\Delta)$ starting from the second one, with approximate values given by

$$\begin{aligned}\Delta^{\mathrm{CPT}}_0 &= (2n+1)\frac{\pi}{2} - \left[(2n+1)\frac{\pi}{2}\right]^{-1} + \cdots\,, \qquad n \geq 1\\ &\approx \frac{3\pi}{2} - \frac{2}{3\pi},\ \frac{5\pi}{2} - \frac{2}{5\pi}\cdots\,,\end{aligned} \tag{4.19}$$

which almost coincide with the values of the maxima $\Delta^{\mathrm{T}}_{\mathrm{max}}$ of $|A^{\mathrm{CP;T}}_{\mu e}|$ in Eq. (4.15). Not only that: these zeros Δ^{CPT}_0 of $A^{\mathrm{CP;CPT}}_{\mu e}$ are again near the oscillation maxima $\Delta^{\mathrm{osc}}_{\mathrm{max}} = (2n+1)\frac{\pi}{2}$, so we conclude that there are "magic energies" at these phase values (4.19), within a 5% interval below the corresponding oscillation maximum, in which $A^{\mathrm{CP;CPT}}_{\mu e}$ vanishes and $|A^{\mathrm{CP;T}}_{\mu e}|$ is close to a maximum. These magic points for the measurement of the experimental CP asymmetry have additional bonuses:

- The zero of the matter-induced component $A^{\mathrm{CP;CPT}}_{\mu e}$ is independent of $\cos\delta$ and the Hierarchy, providing no ambiguity in its position. This Hierarchy independence is consistent with the below 1% effect observed numerically in Figure 3.4, which could be calculated with higher-order corrections.

- These Δ_0^{CPT} are simple zeros, in such a way that the sign of $A_{\mu e}^{\text{CP;CPT}}$ is changing around them, and so its average value around the zero remains small.

- Although the genuine component $|A_{\mu e}^{\text{CP;T}}|$ is not exactly at its maximum value when $A_{\mu e}^{\text{CP;CPT}} = 0$, the leading-order deviations from $\Delta_{\text{max}}^{\text{osc}}$ we calculated show that its value is above 90%$|A_{\mu e}^{\text{CP;T}}|_{\text{max}}$

A look into the derivative of $f_{\text{mat}}(\Delta)$ shows that the sign-change of $A_{\mu e}^{\text{CP;CPT}}$ around these zeros is such that $A_{\mu e}^{\text{CP;CPT}}$ is always decreasing (increasing) around the relevant δ-independent zeros for Normal (Inverted) Hierarchy, and opposite around δ-dependent zeros, explaining the behavior observed in Figure 3.11.

Even though the analysis so far would be enough to break down the signatures of the CP asymmetry components, we also study the zeros of the interference component, in which the T asymmetries for both neutrinos and antineutrinos are genuine. From the analytical approximation (3.35c), one reads the energy spectrum to be

$$f_{\text{int}}(\Delta) = \Delta \sin\Delta \left(\frac{\sin\Delta}{\Delta} - \cos\Delta \right) . \tag{4.20}$$

We find that $A_{\mu e}^{\text{T;CPT}}$ vanishes in two families of zeros, the first one the vacuum nodes Δ_0 as for $A_{\mu e}^{\text{T;CP}}$, the second one the solutions Δ_0^{CPT} to Eq. (4.18) as for $A_{\mu e}^{\text{CP;CPT}}$. The two kind of solutions are both Hierarchy- and δ-independent, so there is no ambiguity in their position.

Notice that both CPT-odd components vanish in the same set of "magic energies" associated to Δ_0^{CPT} in (4.19) near the maximal values of the genuine $|A_{\mu e}^{\text{CP;T}}|$, which means that all three experimental asymmetries ($\mathcal{A}_{\mu e}^{\text{CP}}$, $\mathcal{A}_{\mu e}^{\text{T}}$ and $\mathcal{A}_{\mu e}^{\text{CPT}}$) are blind to CPT-violating matter-effects in these configurations. In the same sense that the CP and T asymmetries could thus be used to test genuine CP violation, each of the CPT-odd components could be used in these magic points Δ_0^{CPT} to test genuine CPT violation in the lepton sector, as had been suggested for the whole CPT asymmetry at its zeros [104].

Taking into account the dependence in L/E of these remarkable values of the phases, we give in Table 4.1 the relevant energies around the second oscillation maximum for both the baselines of the T2HK and DUNE experiments. In consistency with our numerical results in Section 3.1, the precise position of this energy —slightly above the second oscillation maximum— is proportional to $L\left|\Delta m^2_{31}\right|$ as

$$E = 0.92 \text{ GeV} \, \frac{L}{1300 \text{ km}} \, \frac{\left|\Delta m^2_{31}\right|}{2.5 \times 10^{-3} \text{ eV}^2} \,, \tag{4.21}$$

which explains the absence of this rich oscillatory structure in Figure 4.4: at the short baseline of T2HK, all of these interesting points lie below the threshold energy of 300 MeV. The highest-energy one, corresponding to $L/E = 1420$ km/GeV, would appear at $E = 210$ MeV.

Table 4.1: Specific position of the first zero Δ_0^{CPT} in Eq. (4.19), corresponding to the highest-energy zero of the two CPT-odd components independent of δ and the Hierarchy, the second vacuum oscillation maximum, and the second maximum $\Delta^{\text{T}}_{\text{max}}$ in Eq. (4.15). For each of these three points, we show the value of the oscillation phase, which is independent of any experimental parameter; the L/E, whose value depends linearly on the inverse of $\left|\Delta m^2_{31}\right|$; and the particular energy associated to this L/E for T2HK $L = 295$ km and DUNE $L = 1300$ km. Uncertainties show the variability of each quantity within the 1σ ranges in the best fit (1.20). Notice that these three values of the phase Δ_{31} correspond to the position of the green/black/blue dashed lines within the red ellipse in Figure 4.5.

	Δ_{31}	$\frac{L}{E}\left(\frac{\text{km}}{\text{GeV}}\right)$	E (GeV)	
			T2HK	DUNE
Vanishing $A_{\mu e}^{\text{CP;CPT}}$ & $A_{\mu e}^{\text{T;CPT}}$	4.50	1417 (17)	0.208 (2)	0.917 (11)
2nd Oscillation Maximum	4.71	1484 (18)	0.199 (2)	0.876 (11)
Maximum $\left\|A_{\mu e}^{\text{CP;T}}\right\|$	4.82	1518 (18)	0.194 (2)	0.857 (10)

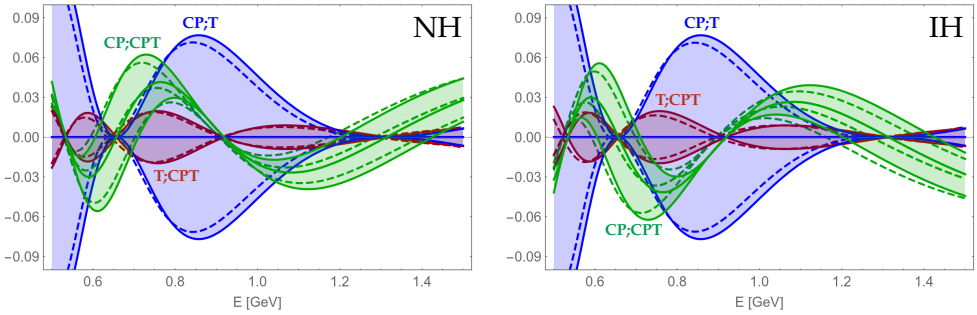

Figure 4.6: Zooming Figure 3.11 at low energy, showing the CPT-odd T-invariant (green) and T-odd CPT-invariant (blue) components of the CP asymmetry $\mathcal{A}_{\mu e}^{\mathrm{CP}}$, together with the CPT-odd CP-invariant (red) component of the T asymmetry $\mathcal{A}_{\mu e}^{\mathrm{T}}$, at DUNE $L = 1300$ km. Normal (Inverted) Hierarchy in the left (right) panel. The bands correspond to all possible values changing δ in $(0, 2\pi)$; the lines correspond to $\delta = \pi/2$, the T-odd components proportional to $\sin\delta$, the T-even one extremal when $\cos\delta = \pm 1$.

This magic configuration around the second oscillation maximum is well apparent in the results presented in Figure 4.6 for[1] $L = 1300$ km. One can observe that the uninteresting (increasing/decreasing for NH/IH) zeros in $A_{\mu e}^{\mathrm{CP;CPT}}$ are strongly dependent on $\cos\delta$, as seen in Eq. (4.17), and their position when $\cos\delta = 0$ is that of the δ-independent zeros Δ_0 of the two T-odd components. As understood from the previous discussion, we have identified the most relevant δ-independent zeros (4.19) of $A_{\mu e}^{\mathrm{CP;CPT}}$, decreasing/increasing for NH/IH, correlated to zeros for $A_{\mu e}^{\mathrm{T;CPT}}$ and near maximal $|A_{\mu e}^{\mathrm{CP;T}}|$ proportional to $\sin\delta$. Due to the first-order character of this δ-independent (and nearly Hierarchy-independent too) zeros, $A_{\mu e}^{\mathrm{CP;CPT}}$ is changing sign around them, whereas the genuine $A_{\mu e}^{\mathrm{CP;T}}$ keeps the same sign —given by $\mathrm{sign}(\sin\delta)$— in the whole energy spectrum.

Integrating statistics in an energy bin around this point would still result in a vanishing matter-induced CP-violating term in

1 An equivalent Figure could be obtained at $L = 295$ km for energies between 100 and 350 MeV, with the same energy dependence for all components, but relatively smaller $A_{\mu e}^{\mathrm{CP;CPT}}$ and $A_{\mu e}^{\mathrm{T;CPT}}$ due to their proportionality to $\Delta_a \propto L$.

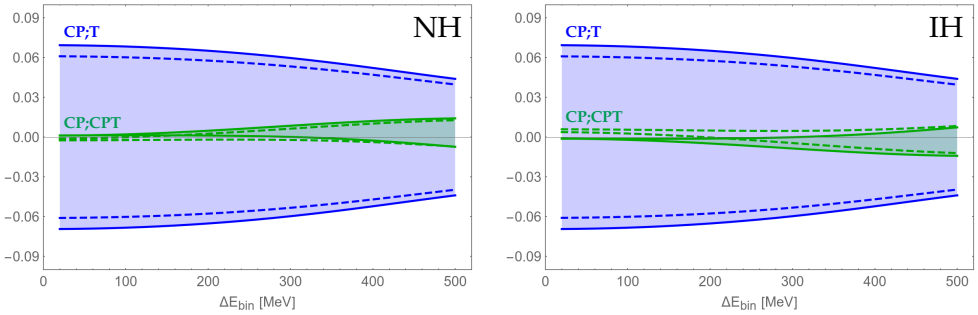

Figure 4.7: Average value of the CPT-odd T-invariant (green) and T-odd CPT-invariant (blue) components of the CP asymmetry $\mathcal{A}_{\mu e}^{\mathrm{CP}}$, at DUNE baseline $L = 1300$ km, in an energy bin width ΔE_{bin} centered on the magic energy (4.21). Both the exact (dashed) and the analytical (solid) results computed using Eqs.(3.35) are shown. Normal (Inverted) Hierarchy in the left (right) panel. The bands correspond to all possible values changing δ in $(0, 2\pi)$; the upper/lower lines for $A_{\mu e}^{\mathrm{CP;CPT}}(A_{\mu e}^{\mathrm{CP;T}})$ correspond to $\cos\delta(\sin\delta) = -1, 1$.

the experimental CP asymmetry, providing a direct test of CP violation in the lepton sector as clean as in vacuum. As shown in Figure 4.7, we have checked that this is the case for an energy bin width up to $0.15 - 0.20$ GeV, which keeps an almost vanishing $A_{\mu e}^{\mathrm{CP;CPT}}$ for all δ and an almost maximal $A_{\mu e}^{\mathrm{CP;T}} \propto \sin\delta$. Such an energy resolution appears to be feasible at DUNE [103] around the second oscillation maximum, and the accumulated events would provide enough statistical significance to the transition probability distribution.

The whole discussion in this Section, which stems from the analytical expressions (3.35), allows the reader to understand the peculiar energy distributions of the three disentangled components observed in the numerical results in Section 3.1. In particular, the value of the magic energy (4.21), as well as its (in)dependence on the different oscillation parameters, is explained. This result in the energy distribution of the experimental CP asymmetry provides a positive response to our search of observable signatures able to separate out the genuine and matter-induced components.

4.5 EXPLOITATION OF THE COMPONENTS DISENTANGLEMENT

This Section culminates the study of the separate physics involved in the genuine and fake matter-induced effects for all observable CP, T and CPT asymmetries in neutrino oscillations, stemmed from the key concept of the 3-dimensional basis (2.13) of components with definite transformation properties under all three symmetries

$$\begin{aligned}
\mathcal{A}^{\rm CP}_{\alpha\beta} &= A^{\rm CP;T}_{\alpha\beta} + A^{\rm CP;CPT}_{\alpha\beta}\,, \\
\mathcal{A}^{\rm T}_{\alpha\beta} &= A^{\rm T;CPT}_{\alpha\beta} + A^{\rm T;CP}_{\alpha\beta}\,, \qquad & \bar{\mathcal{A}}^{\rm T}_{\alpha\beta} &= A^{\rm T;CPT}_{\alpha\beta} - A^{\rm T;CP}_{\alpha\beta}\,, \\
\mathcal{A}^{\rm CPT}_{\alpha\beta} &= A^{\rm CPT;T}_{\alpha\beta} + A^{\rm CPT;CP}_{\alpha\beta}\,, \qquad & \bar{\mathcal{A}}^{\rm CPT}_{\alpha\beta} &= A^{\rm CPT;T}_{\alpha\beta} - A^{\rm CPT;CP}_{\alpha\beta}\,.
\end{aligned}$$

The genuine component in the CP and T asymmetries is given by $A^{\rm CP;T}_{\alpha\beta}$, which is CPT invariant as in vacuum; the other two independent components, $A^{\rm CP;CPT}_{\alpha\beta}$ and $A^{\rm T;CPT}_{\alpha\beta}$, are induced by matter in the neutrino propagation and thus they are odd in the matter potential. However, there is a very interesting distinction between these two fake components: whereas $A^{\rm CP;CPT}_{\alpha\beta}$ can be induced by matter alone without any fundamental CP violation for neutrinos, we found that the genuine-matter interference component $A^{\rm T;CPT}_{\alpha\beta}$, which requires both genuine CP violation and matter effects, can be non-vanishing even for T-symmetric matter.

All in all, the conditions for a direct evidence of genuine CP and T violation for neutrino oscillations in matter by means of the measurement of an observable component odd under the symmetry are now met. From the detailed analysis in this Chapter, we find that —excluding the possibility of scanning the asymmetries as a function of the baseline— one may follow two complementary procedures: the exploitation of the unique properties of the magic energy (4.21), and a thorough determination of all three independent components.

4.5.1 Signatures of the magic $L/E = 1420$ km/GeV

Since accelerator neutrino experiments produce beams of ν_μ and $\bar{\nu}_\mu$, the only observable they could possibly access is the CP asymmetry (2.1)

$$\mathcal{A}_{\mu e}^{\rm CP} = P(\nu_\mu \to \nu_e) - P(\bar{\nu}_\mu \to \bar{\nu}_e)\,,$$

so the separation of the genuine and the matter-induced components must come from their different energy spectrum. As discussed, from these two components one can extract separate information on the neutrino mass ordering and genuine CP violation.

Since $A_{\mu e}^{\rm CP;T}$ is blind to $\text{sign}(\Delta m^2_{31})$, a determination of the neutrino mass ordering must come from regions where the Hierarchy-odd (and δ-independent) term $A_-^{\rm H}$ in $A_{\mu e}^{\rm CP;CPT}$ dominates the whole CP asymmetry. Due to the proportionality of $A_{\mu e}^{\rm CP;CPT}$ to $\Delta_a \propto L$, this can only happen at long baselines, and only at energies $E > 1.1\, E_{1^{\rm st}\,\rm node}$, so that $\left|A_-^{\rm H}\right| > \left|A_+^{\rm H}\right|$. Consistent with our analysis, the spectrum at DUNE baseline $L = 1300$ km in Figure 3.11 shows that, for energies above the first node of the vacuum oscillation, the sign of the experimental $\mathcal{A}_{\mu e}^{\rm CP}$ determines the Hierarchy.

The strategy towards the measurement of genuine CP violation depends on the baseline. At medium baselines such as T2HK $L = 295$ km in Figure 4.4, the CPT-odd component $A_{\mu e}^{\rm CP;CPT}$ is small and, for energies above the first oscillation node, dominated by its δ-independent term. Therefore, it can be theoretically subtracted from the experimental $\mathcal{A}_{\mu e}^{\rm CP}$, if the Hierarchy is previously known, in order to obtain the genuine component $A_{\mu e}^{\rm CP;T}$.

At long baselines, both $A_{\mu e}^{\rm CP;CPT}$ and $A_{\mu e}^{\rm CP;T}$ are of the same order, so $\mathcal{A}_{\mu e}^{\rm CP}$ will directly test genuine CP violation only when the CPT-odd component vanishes. We found a family of simple zeros (4.19) of $A_{\mu e}^{\rm CP;CPT}$, with decreasing/increasing slope for Normal/Inverted Hierarchy, corresponding to the solutions of $\tan\Delta_{31} = \Delta_{31}$. These zeros are close to the second and higher vacuum oscillation maxima $\sin^2\Delta_{31} = 1$, implying that their position is independent of δ and correspond to a nearly maximal $|A_{\mu e}^{\rm CP;T}|$ proportional to $\sin\delta$.

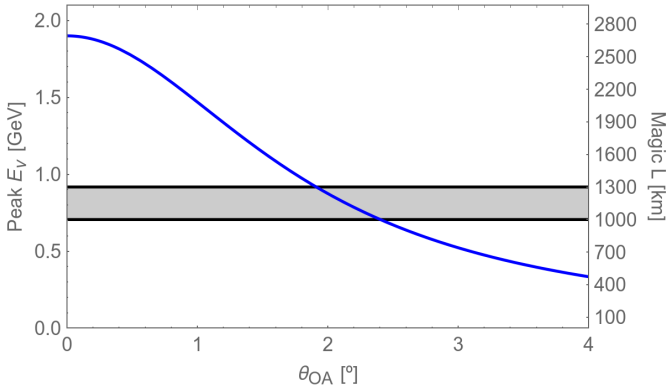

Figure 4.8: Peak energy E_ν of the T2K neutrino beam, as a function of the off-axis deviation θ_{OA} of the detector. On the right labels, we show the associated magic baseline to each energy value so that the detector is positioned at the magic $L/E = 1420$ km/GeV from Eq. (4.21). The gray band shows the possible baseline region for the T2HKK second detector.

The main conclusion is thus that the magic energy (4.21) around the second oscillation maximum,

$$E = 0.92 \text{ GeV} \frac{L}{1300 \text{ km}} \frac{\left|\Delta m^2_{31}\right|}{2.5 \times 10^{-3} \text{ eV}^2} ,$$

is the ideal choice to find a direct evidence of genuine CP violation in the lepton sector, since the matter-induced component $A_{\mu e}^{\text{CP;CPT}}$ vanishes and the experimental CP asymmetry is fully genuine.

Any experiment able to probe the $L/E = 1420$ km/GeV region would thus have access to this matter-independent configuration, and we have studied its possible exploitation at T2HKK, a possible second HK detector in Korea [128], measuring the same beam as T2HK with baseline within $1000-1300$ km. Whereas DUNE has a wide-band beam and we talked about reconstructing neutrino energy bins, the beams envisaged for T2HKK are off-axis beams with (almost) definite energy. From the configuration of the T2K beam [129–131], we looked into the beam peak energy for different off-axis angles θ_{OA}, as shown in Figure 4.8. For each of those peak energies E_ν, we compute its associated magic

baseline L yielding $L/E = 1420$ km, also shown in the Figure in the right lables, together with the possible baselines for T2HKK (gray band). These magic configurations range within the values

$$\begin{aligned} \theta_{\rm OA} &= 2.4^{\,o}\,, \quad E_\nu = 0.71\ {\rm GeV}\,, \quad L = 1000\ {\rm km}\,, \\ \theta_{\rm OA} &= 1.9^{\,o}\,, \quad E_\nu = 0.92\ {\rm GeV}\,, \quad L = 1300\ {\rm km}\,. \end{aligned} \tag{4.22}$$

Choosing a $(\theta_{\rm OA},\, L)$ setup corresponding to the blue points in the Figure would ensure that the beam is centered on the magic point at that specific baseline, allowing the experiment to probe a genuine CP asymmetry $\mathcal{A}^{\rm CP}_{\mu e}$.

4.5.2 Separate determination of all three components

In experiments with sources of electron neutrinos of the same energy as muon neutrinos, as would be natural for a neutrino factory but are also ingredients in atmospheric neutrino analyses, not only the CP asymmetry is available. There would also be the possibility to measure the neutrino and antineutrino T asymmetries (2.7) and (2.8),

$$\begin{aligned} \mathcal{A}^{\rm T}_{\alpha\beta} &\equiv P(\nu_\alpha \to \nu_\beta) - P(\nu_\beta \to \nu_\alpha)\,, \\ \bar{\mathcal{A}}^{\rm T}_{\alpha\beta} &\equiv P(\bar\nu_\alpha \to \bar\nu_\beta) - P(\bar\nu_\beta \to \bar\nu_\alpha)\,. \end{aligned}$$

Unlike the previous case, the two observable T asymmetries for neutrinos and antineutrinos allow the experimental separation (4.11) of genuine and fake effects under the same conditions of baseline and energy,

$$A^{\rm T;CP}_{\alpha\beta} = \frac{1}{2}(\mathcal{A}^{\rm T}_{\alpha\beta} - \bar{\mathcal{A}}^{\rm T}_{\alpha\beta})\,, \qquad A^{\rm T;CPT}_{\alpha\beta} = \frac{1}{2}(\mathcal{A}^{\rm T}_{\alpha\beta} + \bar{\mathcal{A}}^{\rm T}_{\alpha\beta})\,.$$

The first component is the genuine one —odd in L and $\sin\delta$, even in a and the Hierarchy— which directly test CP violation in the lepton sector. The second one is the interference component —odd in L, $\sin\delta$, a and the Hierarchy— which can be used to extract the mass ordering once $\sin\delta$ is known. Indeed, the relative signs of these genuine $A^{\rm T;CP}_{\mu e}$ and fake $A^{\rm T;CPT}_{\mu e}$ components are equal (opposite) for Normal (Inverted) Hierarchy, the last one being smaller in magnitude at all energies and baselines. This is in

contrast with the other fake component $A_{\mu e}^{\mathrm{CP;CPT}}$, which is larger in magnitude than the genuine $A_{\mu e}^{\mathrm{CP;T}}$ at large energies for long baselines, so its information on the Hierarchy can complement that of $A_{\mu e}^{\mathrm{T;CPT}}$.

This other independent fake component $A_{\mu e}^{\mathrm{CP;CPT}}$ can then be obtained, using these ingredients, from the CP asymmetry disentanglement (2.5) —or, equivalently, from the asymmetry sum rule (2.10)— as

$$A_{\alpha\beta}^{\mathrm{CP;CPT}} = \mathcal{A}_{\alpha\beta}^{\mathrm{CP}} - A_{\alpha\beta}^{\mathrm{CP;T}}\,, \tag{4.23}$$

being even in L and $\sin\delta$ and odd in a.

Equivalently, the three components can be obtained from the measurement of the three CP, T and CPT asymmetries as

$$A_{\alpha\beta}^{\mathrm{CP;T}} = \frac{1}{2}\left(\mathcal{A}_{\alpha\beta}^{\mathrm{CP}} + \mathcal{A}_{\alpha\beta}^{\mathrm{T}} - \mathcal{A}_{\alpha\beta}^{\mathrm{CPT}}\right)\,, \tag{4.24a}$$

$$A_{\alpha\beta}^{\mathrm{CP;CPT}} = \frac{1}{2}\left(\mathcal{A}_{\alpha\beta}^{\mathrm{CP}} - \mathcal{A}_{\alpha\beta}^{\mathrm{T}} + \mathcal{A}_{\alpha\beta}^{\mathrm{CPT}}\right)\,, \tag{4.24b}$$

$$A_{\alpha\beta}^{\mathrm{T;CPT}} = \frac{1}{2}\left(\mathcal{A}_{\alpha\beta}^{\mathrm{T}} - \mathcal{A}_{\alpha\beta}^{\mathrm{CP}} + \mathcal{A}_{\alpha\beta}^{\mathrm{CPT}}\right)\,. \tag{4.24c}$$

Even though this thorough approach is experimentally more demanding, it provides a general roadmap which one can follow at any $(E,\, L)$ configuration, for any flavor channel, in order to extract the whole basis of components (2.13) from the experimental asymmetries.

GLOBAL LEPTON NUMBER VIOLATION BY MAJORANA NEUTRINOS

5 RESONANT ATOM MAJORANA MIXING

The experimental evidence of neutrino oscillations is one of the most important discoveries in particle physics, confirming that neutrinos are massive particles and that the three left-handed flavor neutrinos ν_e, ν_μ, ν_τ are mixtures of the neutrinos with definite masses ν_k.

Knowing that neutrinos are massive, we focus in the following on possible signatures to answer the most fundamental open problem: whether neutrinos are Dirac or Majorana particles. The key distinction between the two cases is that Majorana mass terms violate total lepton number via $\Delta L = 2$ operators. As a consequence, no charge can be assigned to definite mass neutrinos being a coherent superposition of interacting neutrinos and antineutrinos. Majorana neutrinos are truly neutral fermions.

In this Chapter, we look into neutrino-mediated $\Delta L = 2$ processes. Since these transitions are forbidden in the Standard Model, their observation would be a proof that neutrinos are Majorana particles.

5.1 NEUTRINOLESS DOUBLE BETA DECAY

There is a consensus that the highest known sensitivity to small Majorana neutrino masses can be reached in experiments searching for the L-violating neutrinoless double-β decay process ($0\nu\beta\beta$)

$$ {}^{A}\mathrm{Z} \to {}^{A}(\mathrm{Z}+2) + 2e^{-} \,, \tag{5.1} $$

where ${}^{A}\mathrm{Z}$ is a nucleus with atomic number Z and mass number A. The two-neutrino double-β decay process ($2\nu\beta\beta$)

$$ {}^{A}\mathrm{Z} \to {}^{A}(\mathrm{Z}+2) + 2e^{-} + 2\bar{\nu}_e \tag{5.2} $$

is allowed by the Standard Model for some even-even nuclei for which the single-β decay or electron capture is forbidden. The process (5.2) represents an irreducible background in the search of (5.1), which needs an excellent energy resolution in order to separate the definite peak in (5.1) from the high-energy tail of the $2e^-$ spectrum in (5.2).

Dozens of experiments [132–152] around the world are seeking out a positive signal of $o\nu\beta\beta$. The most favorable decays for the experimental search are those with high mass difference between the ground state neutral atoms. The most sensitive limits at present are from GERDA-Phase II [151], located at the Laboratori Nazionali del Gran Sasso (LNGS), which bounded the ^{76}Ge half-life $T^{0\nu}_{1/2} > 8.0 \times 10^{25}$ yr at 90% confidence level; and from KAMLAND-Zen [147], located at the Kamioka Observatory, which bounded the ^{136}Xe half-life $T^{0\nu}_{1/2} > 1.07 \times 10^{26}$ yr.

If the decay process is mediated by the exchange of light Majorana neutrinos, the mismatch between the e-flavor neutrino and the definite mass neutrinos ν_k in the Majorana propagator generates a decay amplitude proportional to the effective Majorana neutrino mass

$$m_{\beta\beta} \equiv \sum_k U^2_{ek}\, m_{\nu_k}\,, \tag{5.3}$$

which is a coherent combination of the three neutrino masses. Its determination would thus provide a measure of the absolute neutrino mass scale, unobservable at flavor oscillation experiments. In the standard parametrization with the PMNS matrix (1.25), this effective mass

$$m_{\beta\beta} = c^2_{12}c^2_{13}m_1 + s^2_{12}c^2_{13}e^{i\alpha}m_2 + s^2_{13}e^{i(\beta-2\delta)}m_3 \tag{5.4}$$

depends on the three mixing angles and two relative CP phases.

Assuming that neutrinos are Majorana particles, the present knowledge of mixing angles and neutrino mass differences in the best-fit values in Eq. (1.20), from neutrino flavor oscillations, produces the information [153, 154] condensed in Figure 5.1 for the fundamental quantity $m_{\beta\beta}$. Present experimental limits are approaching the interval of $m_{\beta\beta}$ values predicted for the Inverse Hierarchy in the neutrino mass spectrum. The lightest case

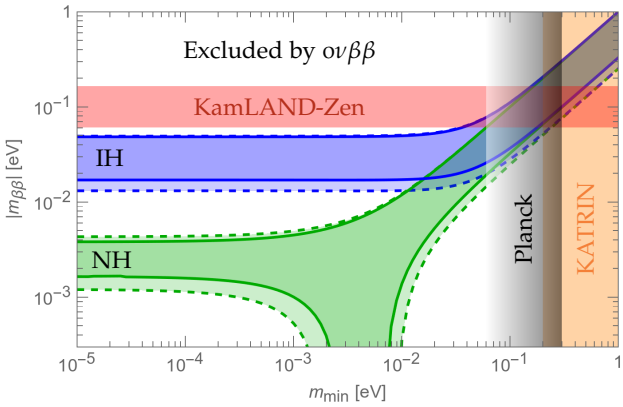

Figure 5.1: Allowed parameter space for $0\nu\beta\beta$, as a function of the smallest neutrino mass, for both Normal (green) and Inverted (blue) Hierarchies. Solid lines show the limits for the best-fit configuration (1.20), dashed lines show the limits changing the parameters in their 2σ ranges. Current experimental bounds are also shown for the $0\nu\beta\beta$ KamLAND-Zen bound [147] (red), β-decay KATRIN sensitivity [155] (orange), and cosmological Planck results [156] (gray).

$m_3 = 0$ corresponds to $\sum m_\nu = 0.10$ eV, whereas the Normal Hierarchy lightest case $m_1 = 0$ produces $\sum m_\nu = 0.06$ eV.

A possibly vanishing $m_{\beta\beta}$ would make this decay process unobservable, even if neutrinos are Majorana particles, and the experiments looking for this signal would remain inconclusive. Imposing $m_{\beta\beta} = 0$ leads to the consistency condition

$$|\cos\alpha| = \left| \frac{c_{12}^4 c_{13}^4 m_1^2 + s_{12}^4 c_{13}^4 m_2^2 - s_{13}^4 m_3^2}{2 c_{12}^2 s_{12}^2 c_{13}^4 m_1 m_2} \right| \leq 1\,, \tag{5.5}$$

which for the best-fit configuration in Eq. (1.20) becomes

$$\frac{1}{m_1 m_2}(1.059\, m_1^2 + 0.236\, m_2^2 - 0.001\, m_3^2) \leq 1\,. \tag{5.6}$$

The absence of the vanishing $m_{\beta\beta}$ for the Inverted Hierarchy is now clear: only if m_3 is larger than the other two masses can it (partially) compensate their terms for the bound to hold. In the case of the Normal Hierarchy, and taking into account the

dependence in m_1 of $m_2 = \sqrt{m_1^2 + \Delta m_{21}^2}$ and $m_3 = \sqrt{m_1^2 + \Delta m_{31}^2}$, the consistency condition for vanishing $m_{\beta\beta}$ leads to the range of values $m_1 \in (2.7, 6.9) \times 10^{-3}$ eV, as shown by the solid lines in the Figure.

5.2 NEUTRINOLESS DOUBLE ELECTRON CAPTURE

There is an alternative to $0\nu\beta\beta$ by means of the mechanism of neutrinoless double electron capture ($0\nu\epsilon\epsilon$),

$$ {}^{A}\mathrm{Z} + 2e^- \rightarrow {}^{A}(\mathrm{Z}-2)^* . \tag{5.7} $$

This is actually a mixing, differing in the total lepton number L by two units, between two states of two different neutral atoms with the same baryonic number A, and not a process conserving energy and momentum in general. The daughter atom is in an excited state with two electron holes, and its decay provides the signal for (5.7).

When the mass of the daughter $(\mathrm{Z}-2)^*$ atom is below the parent atomic mass, the standard 2ν decay channel

$$ {}^{A}\mathrm{Z} + 2e^- \rightarrow {}^{A}(\mathrm{Z}-2)^* + 2\nu_e \tag{5.8} $$

becomes allowed. This $2\nu\epsilon\epsilon$ process has been observed recently in ^{124}Xe with a half-life of 10^{22} yr [157].

Ref. [158] first pointed out that the monumental coincidence of the initial energy of the parent atom and that of the intermediate excited atom would give rise to a large enhancement of the decay probability. The concept of resonant enhancement of $0\nu\epsilon\epsilon$ was further developed [159, 160] for the exceptional circumstance of almost degeneracy between the parent and daughter atomic states in (5.7). The *almost* matching condition is fulfilled when the 2X-ray decay occurs through the tail of the width of the atomic state, as shown schematically in Figure 5.2. These works stimulated many experimental searches [161–171] of candidates when the remarkable trap technique [172] for precision measurements of atomic masses became available.

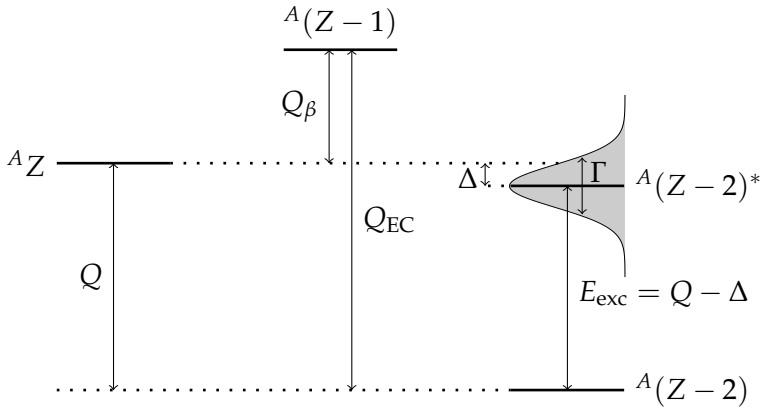

Figure 5.2: Schematic representation of the $^{A}Z \leftrightarrow {}^{A}(Z-2)^*$ mixed atomic system.

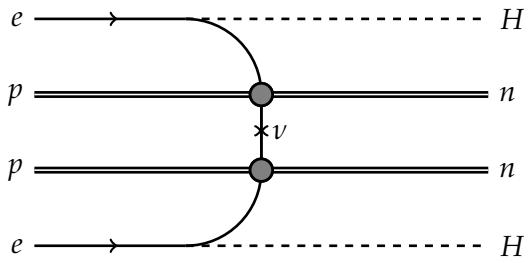

Figure 5.3: Feynman diagram for the Majorana mixing amplitude of the ^{A}Z atom ground state and the 2-hole $^{A}(Z-2)^*$ state.

The mixing amplitude was calculated in Ref. [160] from the diagram in Figure 5.3 and, in a good approximation, it can be factorized leading to

$$M_{21} = m^*_{\beta\beta} \left(\frac{G_F \cos\theta_C}{\sqrt{2}} \right)^2 \langle F_{21} \rangle \, \frac{g_A^2}{2\pi} \, M_{0\nu} \,, \tag{5.9}$$

where G_F is the Fermi coupling constant, θ_C is the Cabibbo angle, $\langle F_{21} \rangle$ gives the probability amplitude of finding the two electrons in the nucleus, $M_{0\nu}$ is the nuclear matrix element, which is of the order of the inverse nuclear radius, g_A is the axial-vector nucleon coupling, and the effective Majorana neutrino mass $m_{\beta\beta}$ appears as the complex conjugate of the expression (5.3) for neutrinoless double beta decay.

The experimental activity in recent years has in turn stimulated the calculation [173–180] of the nuclear matrix elements for the cases of interest. A list of likely resonant transitions was provided in Ref. [176], excluding some of those previously suggested in Ref. [160]. After the improvements in measurements of atomic masses, the remaining candidates include ${}^{152}_{64}\mathrm{Gd} \to {}^{152}_{62}\mathrm{Sm}$, ${}^{164}_{68}\mathrm{Er} \to {}^{164}_{66}\mathrm{Dy}$ and ${}^{180}_{74}\mathrm{W} \to {}^{180}_{72}\mathrm{Hf}$, for the atomic mixing to the daughter atom with the nucleus in the ground state, and having two holes in the inner atomic shells. More recent detailed analyses, using the state of the art in nuclear QRPA and IBM models, agree in the results, showing that the most promising known candidates are ${}^{152}\mathrm{Gd}$ and ${}^{180}\mathrm{W}$.

The case of ${}^{152}\mathrm{Gd} \to {}^{152}\mathrm{Sm}$ mixing and decay is particularly attractive. The values of the relevant parameters are the experimental $\Delta = M_1 - M_2 = (0.91 \pm 0.18)$ keV [167] for the masses of the parent "1" and daughter "2" atoms, $\Gamma = 0.023$ keV [161] for the two-hole atomic width, and the Q-value of the ground state to ground state transition $Q = (55.70 \pm 0.18)$ keV [167]. The theoretical mixing is [177, 180]

$$|M_{21}| = 10^{-24} \left[\frac{|m_{\beta\beta}|}{0.1\ \mathrm{eV}}\right] \mathrm{eV}\,. \tag{5.10}$$

As seen, the optimal resonant enhancement condition is still off by at least a factor $\Delta/\Gamma \sim 40$, implying a loss of 3 orders of magnitude in the expected X-ray rate from the parent atom. We will use the values for this transition as a benchmark configuration for all the calculations in this Chapter, exploring the phenomenology of $0\nu\epsilon\epsilon$ and the possibility to enhance the transition rate.

5.3 THE EVOLUTION HAMILTONIAN

In the basis of the $\left|{}^{A}Z\right\rangle$ and $\left|{}^{A}(Z-2)^{*}\right\rangle$ states, which we label as "1" and "2", the dynamics of this two-state system of interest is governed by the Hamiltonian

$$H = M - \frac{i}{2}\Gamma = \begin{bmatrix} M_1 & M_{21}^{*} \\ M_{21} & M_2 \end{bmatrix} - \frac{i}{2}\begin{bmatrix} 0 & 0 \\ 0 & \Gamma \end{bmatrix}, \tag{5.11}$$

with a Majorana $\Delta L = 2$ mass mixing M_{21} as given by Eq. (5.9). The anti-Hermitian part of this Hamiltonian is due to the instability of $\left|{}^{A}(Z-2)^{*}\right\rangle$, which de-excites into the ground state $\left|{}^{A}(Z-2)_{\text{g.s.}}\right\rangle$ —external to the two-body system in Eq. (5.11)— emitting its two-hole characteristic X-ray spectrum. The appropriate non-Hermitian Hamiltonian formalism for describing the mixing of an unstable two-state system is known since Weisskopf-Wigner [181], and has been used in many instances. It has been employed [174, 176] with the objective of reproducing the rate, induced by atom mixing, as previously given in Ref. [160].

Besides being non-Hermitian, the Hamiltonian (5.11) is not a normal operator, i.e. M and Γ are not compatible, $[M,\Gamma] \neq 0$. The states of definite time evolution, eigenstates of H, have complex eigenvalues and are given in non-degenerate perturbation theory [182] by

$$|\lambda_L\rangle = \left|{}^{A}\mathrm{Z}\right\rangle + \alpha \left|{}^{A}(\mathrm{Z}-2)^{*}\right\rangle ,$$
$$\lambda_L \equiv E_L - \frac{i}{2}\Gamma_L = M_1 + |\alpha|^2 \left[\Delta - \frac{i}{2}\Gamma\right] , \tag{5.12a}$$
$$|\lambda_S\rangle = \left|{}^{A}(\mathrm{Z}-2)^{*}\right\rangle - \beta^{*} \left|{}^{A}\mathrm{Z}\right\rangle ,$$
$$\lambda_S \equiv E_S - \frac{i}{2}\Gamma_S = M_2 - \frac{i}{2}\Gamma - |\alpha|^2 \left[\Delta - \frac{i}{2}\Gamma\right] , \tag{5.12b}$$

with $\Delta = M_1 - M_2$. Thus the eigenstates lifetimes $\Gamma_{L,S}$ are *not* the eigenvalues of the Γ matrix. The eigenstates are modified at first order in M_{21} via

$$\alpha = \frac{M_{21}}{\Delta + \frac{i}{2}\Gamma} , \qquad \beta = \frac{M_{21}}{\Delta - \frac{i}{2}\Gamma} , \tag{5.13}$$

so the "stationary" states of the system do not have well-defined atomic properties: both the number of electrons and their atomic properties are a superposition of Z and $Z-2$. Also, these states are *not* orthogonal —their overlap is given by

$$\langle \lambda_S | \lambda_L \rangle = \alpha - \beta = -i \frac{M_{21}\Gamma}{\Delta^2 + \frac{1}{4}\Gamma^2} , \tag{5.14}$$

with its non-vanishing value due to the joint presence of the mass mixing M_{21} and the decay width Γ. Notice that $\mathrm{Im}(M_{21})$ originates a real overlap.

As seen in Eqs. (5.12), the modifications in the corresponding eigenvalues appear at second order in $|M_{21}|$ and they are equidistant with opposite sign. Since these corrections are small, we will use the leading-order values

$$\begin{aligned} E_L &\approx M_1\,, & E_S &\approx M_2\,, \\ \Gamma_L &\approx |\alpha|^2\,\Gamma\,, & \Gamma_S &\approx \Gamma\,. \end{aligned} \tag{5.15}$$

The only relevant correction at order $|\alpha|^2$ is the one to Γ_L, since the parent $\left|{}^{A}\mathrm{Z}\right\rangle$ was a stable state —even if small, the mixing produces a non-zero decay width.

This result shows that, at leading order, the Majorana mixing becomes observable through $\Gamma_L \propto |\alpha|^2$. The key parameter α in Eq. (5.13), which for the ^{152}Gd case has the value

$$|\alpha|^2 = 10^{-54}\left[\frac{|m_{\beta\beta}|}{0.1\ \mathrm{eV}}\right]^2\,, \tag{5.16}$$

emphasizes the relevance of the condition $\Delta \sim \Gamma$, which produces a resonant enhancement [160] of the effect of the $\Delta L = 2$ mass mixing M_{21}.

5.4 NATURAL TIME HISTORY FOR INITIAL $^{A}\mathrm{Z}$

The diagonalization (5.12) of the Hamiltonian (5.11) shows that the states $\left|{}^{A}\mathrm{Z}\right\rangle$ and $\left|{}^{A}(\mathrm{Z}-2)^{*}\right\rangle$ are not the stationary states of the system. For an initially prepared $\left|{}^{A}\mathrm{Z}\right\rangle$, the time history is far from trivial and the appropriate language to describe the system short times after is that of *atom oscillations* [174] between $\left|{}^{A}\mathrm{Z}\right\rangle$ and $\left|{}^{A}(\mathrm{Z}-2)^{*}\right\rangle$, due to the interference of their amplitudes through $|\lambda_S\rangle$ and $|\lambda_L\rangle$ in the time evolution. The time-evolved $\left|{}^{A}\mathrm{Z}\right\rangle$ state becomes

$$\left|{}^{A}\mathrm{Z}(t)\right\rangle = e^{-i\lambda_L t}\,|\lambda_L\rangle - \alpha\, e^{-i\lambda_S t}\,|\lambda_S\rangle\,, \tag{5.17}$$

and the appearance probability at $t \ll \tau_L$ is then given by

$$\left|\left\langle {}^{A}(\mathrm{Z}-2)^{*}\middle|{}^{A}\mathrm{Z}(t)\right\rangle\right|^2 = |\alpha|^2\left\{1 + e^{-\Gamma t} - 2e^{-\frac{1}{2}\Gamma t}\cos(\Delta\cdot t)\right\}\,, \tag{5.18}$$

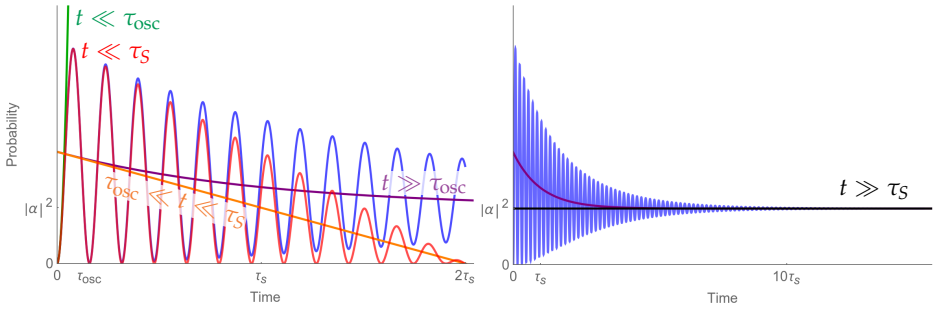

Figure 5.4: Probability of the $\left|{}^{A}Z\right\rangle \to \left|{}^{A}(Z-2)^*\right\rangle$ transition in Eq. (5.18) as a function of time (blue), for time regions below (left) and above (right) τ_S. Also shown the approximations for $t \ll \tau_{osc}$ (green) and $t \ll \tau_S$ (red), together with the three averaged-out cases $t \gg \tau_{osc}$ (purple), $\tau_S \gg t \gg \tau_{osc}$ (orange), and $t \gg \tau_S \gg \tau_{osc}$ (black).

as shown in Figure 5.4 (in blue). We also show in the Figure the approximate expressions for the different time regions in the following discussion. The smallness of the mixing $|\alpha|$, as in Eq. (5.16), simplifies the derivation of Eq. (5.18) by assuming $\Gamma_L t \ll 1$ in the state (5.17), which ensures that the long-lived state will effectively behave as stable throughout the time evolution of $\left|{}^{A}Z\right\rangle$. In fact, we find that ^{152}Gd has $\tau_L \equiv \Gamma_L^{-1} \sim 10^{29}$ yr, so this assumption is valid even for cosmological times.

Eq. (5.18) indicates that the transition probability is controlled by an oscillation angular frequency $|\Delta|$ and a decay width $\Gamma_S = \Gamma$. The characteristic oscillation time $\tau_{osc} = 2\pi\,|\Delta|^{-1}$ is the shortest time scale in systems with $|\Delta|$ significantly larger than Γ, as happens even for ^{152}Gd, whose $\Delta \sim 40\Gamma$. For $t \ll \tau_{osc}$, one has

$$\left|\left\langle {}^{A}(Z-2)^*\middle|{}^{A}Z(t)\right\rangle\right|^2 \approx |M_{21}|^2\, t^2 \tag{5.19}$$

induced by the mass mixing, whereas for $t \gg \tau_{osc}$ the only change with respect to Eq. (5.18) is that the interference region disappears. The two slits $|\lambda_L\rangle$ and $|\lambda_S\rangle$ in (5.17) would thus contribute incoherently, averaging the oscillations out and yielding

$$\left|\left\langle {}^{A}(Z-2)^*\middle|{}^{A}Z(t)\right\rangle\right|^2 \approx |\alpha|^2 \left\{1 + e^{-\Gamma t}\right\} . \tag{5.20}$$

The next shortest characteristic time in this system is the decay time $\tau_S = \Gamma^{-1}$, associated to the $|\lambda_S\rangle$ state. For $t \ll \tau_S$, the short-lived state $|\lambda_S\rangle$ has not fully decayed and the transition probability (5.18) reduces to the nearly-stable oscillation

$$\left|\left\langle {}^A(Z-2)^* \middle| {}^AZ(t)\right\rangle\right|^2 \approx |\alpha|^2\ (2-\Gamma t)\ \{1-\cos(\Delta\cdot t)\}\ . \tag{5.21}$$

At intermediate times $\tau_{\rm osc} \ll t \ll \tau_S$, these oscillations are averaged out and the transition is governed by the slow $|\lambda_S\rangle$ decay,

$$\left|\left\langle {}^A(Z-2)^* \middle| {}^AZ(t)\right\rangle\right|^2 \approx |\alpha|^2\ (2-\Gamma t)\ . \tag{5.22}$$

For $t \gg \tau_S \gg \tau_{\rm osc}$, conversely, the contribution of $|\lambda_S\rangle$ disappears and the appearance probability simply becomes

$$\left|\left\langle {}^A(Z-2)^* \middle| {}^AZ(t)\right\rangle\right|^2 = |\alpha|^2 . \tag{5.23}$$

In other words, the initially prepared $\left|{}^AZ\right\rangle$ state evolves towards the stationary metastable state $|\lambda_L\rangle$,

$$\left|{}^AZ(t)\right\rangle \to e^{-i\lambda_L t}\,|\lambda_L\rangle\ , \tag{5.24}$$

with the long lifetime $\tau_L = \Gamma_L^{-1}$ in Eqs. (5.15).

For a realistic time resolution δt in an actual experiment, this regime is the interesting one, with the behavior in Eq. (5.24). As shown in Figure 5.5, the different time scales involved in this problem are thus

$$\tau_{\rm osc} \ll \tau_S \ll \delta t \ll t \ll \tau_L\,, \tag{5.25}$$

where t refers to the elapsed time since the production of ${}^AZ$, either by Nature or in the lab —given the smallness of the mixing, the metastability of the state (5.24) is valid even for cosmological times. Therefore, for any time between the two scales τ_S and τ_L, the oscillatory behavior is averaged out and the populations of the three states involved are given by the probabilities

$$\tau_S \ll t \ll \tau_L \qquad \Longrightarrow \qquad \begin{aligned} P_L(t) &= 1-\Gamma_L\, t && \text{(5.26a)}\\ P_S(t) &= 0 && \text{(5.26b)}\\ P_{\rm g.s.}(t) &= |\alpha|^2\,\Gamma\, t && \text{(5.26c)}\end{aligned}$$

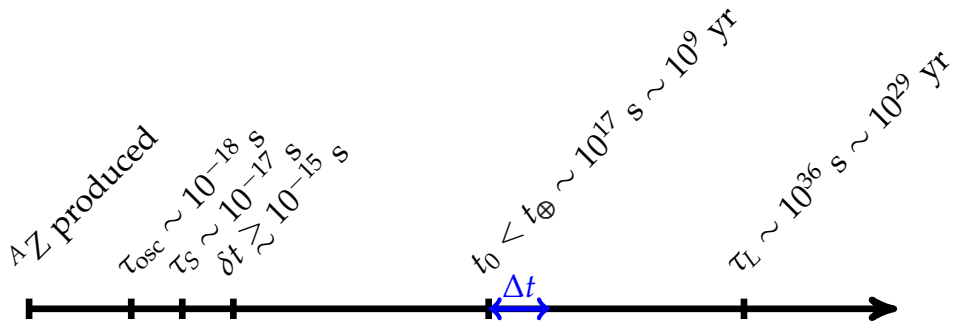

Figure 5.5: Timeline of the mixed atomic system. The τ_{osc}, τ_S and τ_L values are for ^{152}Gd$\rightarrow^{152}$Sm, whereas δt is a typical time resolution, t_0 is the age of the sample ore, $t_\oplus$ is the age of the Earth and Δt is the observation time in an actual experiment.

where $P_{\text{g.s.}}(t)$ refers to the population of the ground state of the $^{A}(Z-2)$ atom after the decay of the unstable "stationary" state $|\lambda_S\rangle$ in (5.17), with rate Γ. No matter whether t refers to laboratory or cosmological times, the linear approximation in t is excellent.

With this spontaneous evolution of the system, an experiment beginning its measurements a time t_0 after the ^{A}Z was produced will probe the three-level system with relative populations $P_L \approx 100\%$, $P_S \approx 0$, $P_{\text{g.s.}} \approx |\alpha|^2 \Gamma\, t_0$. One discovers two methods, involving the third state beyond the two mixed states, to be sensitive to the resonant Majorana mixing of atoms:

1. **Spontaneous emission from the metastable state to the daughter atom ground state.** The population in the upper level $|\lambda_L\rangle$, as shown in Eq. (5.26a), decreases with time as $P_L(\Delta t) \approx 1 - \Gamma_L\, \Delta t$, where $\Delta t = t - t_0$, due to the decay of the metastable "stationary" state $|\lambda_L\rangle$ to $\left|^{A}(Z-2)_{\text{g.s.}}\right\rangle$. This process is associated to the spontaneous emission of X-rays with a rate Γ_L, considered in the literature after the concept of resonant mixing was introduced in Ref. [160]. For one mole of ^{152}Gd, the X-ray emission rate would be of the order of 10^{-12} s$^{-1} \sim 10^{-5}$ yr^{-1}. The initial state in the transition at observable times, being $|\lambda_L\rangle$, tells us that the total energy

of the two-hole X-ray radiation is displaced by Δ with respect to the characteristic $\left|{}^{A}(Z-2)^{*}\right\rangle \to \left|{}^{A}(Z-2)_{\text{g.s.}}\right\rangle$ X-ray spectrum, i.e. its energy release is the Q-value between the two atoms in their ground states (as seen in Figure 5.2).

2. **Daughter atom population.** The presence of the daughter atom in the parent ores, expected from Eq. 5.26c, can be probed e.g. by geochemical methods. For one mole of the nominally stable ^{152}Gd isotope produced at the time of the Earth formation, the values in Figure 5.5 would predict an accumulated number of the order of 10^4 ^{152}Sm atoms. This observable could be of interest for cosmological times t_0 since, contrary to $\beta\beta$-decay, in the $o\nu\epsilon\epsilon$ case there is no irreducible background from a 2ν channel for a resonant atom mixing.

We would like to emphasize that, even though $\Gamma_L = |\alpha|^2\Gamma$ ensures the probability conservation, an interpretation of Eqs. (5.26a) and (5.26c) in different terms is of interest. On the one hand, Γ_L is the rate for the decay of $|\lambda_L\rangle$ at any time t, which accounts for the observable **1**. On the other hand, the population of the daughter atom in the ground state is obtained from the mixing probability leading to $|\lambda_S\rangle$ in Eq. (5.17) at all times, given by $|\alpha|^2$ [Eq. (5.23)], times its decay rate to the ground state, $\Gamma_S = \Gamma$ [Eqs. (5.15)]. This mixing$\times$decay temporal evolution explains the non-zero population of ${}^{A}(Z-2)_{\text{g.s.}}$, producing the second observable.

One may wonder whether there is, for $\Delta > 0$, a spontaneous emission of lower energy X-rays from $|\lambda_L\rangle$ to $|\lambda_S\rangle$ leading to a regeneration of the short-lived mixed state, and providing a third observable. From the mixing parameters of these states in Eq. (5.12), the dynamics of this process would be that of the Compton amplitudes for the Z and $(Z-2)^*$ atoms, whereas the kinematics correspond to two-photon emission instead of scattering. At these intermediate energies between atomic and nuclear physics, the Compton amplitude $T_{2\gamma}$ can be taken to be an incoherent sum of the electron contributions [183, 184],

$$T_{2\gamma} = \alpha\, T_{2\gamma}^{Z-2} - \beta\, T_{2\gamma}^{Z}\,, \tag{5.27}$$

where

$$T^{Z}_{2\gamma} = \frac{Z\,e^2}{m}\,(\boldsymbol{\epsilon}'^{*}\cdot\boldsymbol{\epsilon}^{*})\,, \tag{5.28}$$

m is the electron mass and $\boldsymbol{\epsilon}$ the polarization vectors of the photons. A straightforward calculation of the rate for this electromagnetic $|\lambda_L\rangle \to |\lambda_S\rangle$ transition, when compared to the transition to the daughter atom ground state, gives a branching ratio of the order 10^{-7}, showing that this process is negligible for resonant atoms.

5.5 STIMULATED TRANSITIONS

The observable **1** is analogous to $0\nu\beta\beta$ in that both of them require no external factor to happen: their observation is a matter of detector sensitivity and exposure. Observable **2** is unique to $0\nu\epsilon\epsilon$ thanks to the absence of a 2ν background mode, which ensures that, if the atom is otherwise stable, the Majorana mixing is the only mechanism that can produce the daughter traces in the parent ore.

Further advantages can be taken into account in the $0\nu\epsilon\epsilon$ case by exploiting the understood description of the atomic system in terms of the $|\lambda_L\rangle$ and $|\lambda_S\rangle$ eigenstates (5.12), instead of using the "flavor" states $\left|{}^{A}\mathrm{Z}\right\rangle$ and $\left|{}^{A}(\mathrm{Z}-2)\right\rangle$. This description in terms of the energy levels E_L, E_S with widths Γ_L, Γ_S in Eqs. (5.15) opens the door to study the possible stimulation of their atomic transitions by means of an adequately-tuned electromagnetic radiation. We explore the different possibilities for the typical transition energies of these mixed atomic systems.

5.5.1 Emission from $|\lambda_L\rangle$

A careful reading of Eqs. (5.26) shows that, for any parent ore under consideration, the metastable state $|\lambda_L\rangle$ and the ground state $\left|{}^{A}(\mathrm{Z}-2)_{\mathrm{g.s.}}\right\rangle$ have a *natural population inversion*, with an overwhelming abundance of the long-lifetime upper level of the system. This result suggests the exploitation of the bosonic

properties of the X-radiation, used as a signal of the Majorana mixing in this problem, and considering the external action of an X-ray beam to stimulate the emission from the metastable level to the ground state of this atomic system.

Stimulating radiation for the emission from $|\lambda_L\rangle$ to the ground state $\left|{}^{A}(Z-2)_{\text{g.s.}}\right\rangle$ could thus enhance the rate, and we present an estimate of the gain which could be envisaged in future facilities of X-ray beams. A setup with an incident pulsed beam allows the observation of low rate events in directions outside the beam direction and the control of background conditions in the absence of the beam. Therefore, we discover a third observable:

3. **Stimulated emission from $|\lambda_L\rangle$ to $\left|{}^{A}(Z-2)_{\text{g.s.}}\right\rangle$.** The natural population inversion between the ground state and the metastable "stationary" state $|\lambda_L\rangle$ gives raise to the possibility of stimulating the decay $|\lambda_L\rangle \to \left|{}^{A}(Z-2)_{\text{g.s.}}\right\rangle$. The experimental signature of this process would be the emission of X-rays with total energy equal to the Q-value of the process, just like in observable **1** of spontaneous emission.

For the emission between the two levels $|\lambda_L\rangle \to \left|{}^{A}(Z-2)_{\text{g.s.}}\right\rangle$ of radiation with angular frequency ω, the stimulated rate of the transition is described in terms of the Einstein coefficients [185] as[1]

$$\frac{\mathrm{d}N_L}{\mathrm{d}t} = -\frac{\pi^2 c^3}{\hbar\omega^3}\,\rho_\omega\,\Gamma_L N_L\,, \tag{5.29}$$

where N_L is the population of the upper metastable $|\lambda_L\rangle$ level, Γ_L its width and ρ_ω is the energy density of the beam per unit of angular frequency, i.e.

$$\rho_\omega = \frac{\mathrm{d}E}{c\,\mathrm{d}t\,\mathrm{d}S\,\mathrm{d}\omega}\,. \tag{5.30}$$

Therefore, this observable is enhanced with respect to the first one by a gain factor

$$G = \frac{\pi^2\,c^3}{\hbar\,\omega^3}\,\rho_\omega\,, \tag{5.31}$$

1 For the sake of clarity, throughout this discussion we keep all $\hbar$ and c factors.

which is the ratio between the stimulated and spontaneous emission rates.

In order to produce a sizable gain, one should devise a setup with as large a ρ_ω as possible. The transition energy of this system is of the order of tens of keV, so a high-luminosity X-ray beam is mandatory. Such high-energy beams are produced at free-electron laser (FEL) facilities, through a kind of laser consisting of very-high-speed electrons moving freely through a magnetic structure. Free-electron lasers are tunable and have the widest frequency range of any laser type, currently ranging in wavelength from microwaves, through terahertz radiation and infrared, to the visible spectrum, ultraviolet, and X-ray. The highest frequencies are obtained in XFEL facilities like the running SLAC Linac Coherent Light Source (LCLS) [19, 20] and the commissioned European XFEL (EXFEL) at DESY [18].

The determination of the gain factor one could achieve in these facilities is clearer after rewriting the spectral energy density (5.30) in terms of beam parameters,

$$\rho_\omega = \frac{\hbar}{c}\frac{\mathrm{d}N}{\mathrm{d}t\,\mathrm{d}S}\left[\frac{\mathrm{d}\omega}{\omega}\right]^{-1}. \tag{5.32}$$

Taking $\mathrm{d}N/\mathrm{d}t$ as the number of photons per pulse duration, $\mathrm{d}S$ as the beam section and $\mathrm{d}\omega/\omega$ as the full width half maximum (FWHM) spectrum width, one finds the gain factor

$$G = \hbar\,(\hbar c)^2\,\frac{\pi^2}{(\hbar\omega)^3}\,\frac{\mathrm{d}N}{\mathrm{d}t\,\mathrm{d}S}\left[\frac{\mathrm{d}\omega}{\omega}\right]^{-1} \tag{5.33}$$

to be written in terms of clearly defined beam properties, where $\mathrm{d}N/\mathrm{d}t\mathrm{d}S$ is the luminosity $\mathcal{L}$ of the beam.

At EXFEL, a sound simulation of the conditions of the machine [186] gives, for typical energies of tens of keV, the expected number of photons per pulse duration $dN/dt = 10^{10}$ fs^{-1} and the spectral width $\mathrm{d}\omega/\omega = 1.12 \times 10^{-3}$. Nanofocusing of this X-ray FELs has been contemplated [187]; using a beam spot of the order of 100 nm would lead to a gain factor from Eq. (5.33) of $G \sim 100$. The continuous interaction of these X-rays with a mole of ^{152}Gd atoms would provide a stimulated rate of the order of 10^{-10} s^{-1} $\sim 10^{-3}$ yr^{-1}, as shown in Figure 5.6

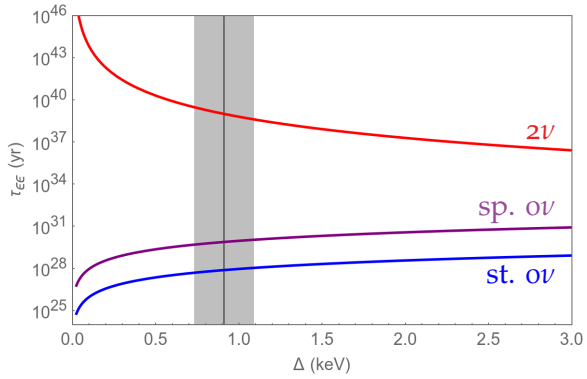

Figure 5.6: Lifetime of the ^{152}Gd $\rightarrow$ ^{152}Sm double electron capture transition, as a function of the mass difference Δ between the two states —the black line and gray band show the measured value $\Delta = (0.91 \pm 0.18)$ keV [167]. The longer lived $2\nu\epsilon\epsilon$ (red) is shown together with the spontaneous $0\nu\epsilon\epsilon$ (purple) and a gain (5.33) $G = 100$ stimulated $0\nu\epsilon\epsilon$ (blue). Notice that, at the resonant $\Delta \sim \Gamma = 0.023$ keV [161], the 2ν mode is suppressed and the 0ν mode is enhanced.

One should notice that this rate of events assumes a constant irradiation of the whole target. The straightforward setup of a cylindrical target alongside the pulsating X-ray beam presents different issues. Most notoriously, pulsed beams limit the enhancing time to a fraction of the running time. EXFEL manages to produce 2.7×10^4 pulses per second, so that the fraction of effective time is of the order of 10^{-9}; LCLS-II expects to produce pulses at 1 MHz, increasing this number by two orders of magnitude, but still far away from a promising factor. Furthermore, radiation of these energies has an attenuation length in Gd of tens of microns, limiting the amount of material one could use to a fraction of a mole. This setup has the general drawback that the high energy density effect associated with the small beam spot size is lost when considering the small interaction volume.

The attenuation of the beam is associated to its interaction with the sample, which is dominated by the photoelectric effect and, to a lesser extent, inelastic Compton scattering, leading to ionization. Successive interactions of the secondary electrons

will heat the material. A recent simulation [188] of this effect under realistic experimental conditions on a cylindrical target, assuming the extreme limit that the whole absorption power is converted into heating power, shows that a temperature of about 700 ^{o}C is reached for an incoming beam of spot size 100 nm and an average of 10^{14} X-ray photons/s. Since this temperature is proportional to the flux, in all high-flux experiments like the one contemplated in this work, the small interaction-volume target is actually destroyed. The design of a macroscopic sample with a very large number of thermally isolated micro-targets, built on a plane in transversal motion synchronized with the pulse frequency of the beam, is a subject of current interest [189].

The use of this approach in order to stimulate the $\Delta L = 2$ emission rate should be explored after a suitable candidate is found. The limiting factors in the expected integrated rate of events also suggest an alternative ingenuity program more in the line of micro-particles inserted into a dreamed X-ray resonant cavity.

5.5.2 Absorption from $\left|{}^{A}(Z-2)_{\text{g.s.}}\right\rangle$

A different observable may also be considered. The existing population of the daughter atom in its ground state is, by itself, a signal of the atom Majorana mixing, as discussed in the previous Section as a relic of the previous history with an initial parent atom. Analogous to the stimulation of $|\lambda_L\rangle \rightarrow \left|{}^{A}(Z-2)_{\text{g.s.}}\right\rangle$ benefiting from their natural population inversion, the absence of atoms in the $|\lambda_S\rangle$ state of this three-level system opens the door to stimulate the absorption from $\left|{}^{A}(Z-2)_{\text{g.s.}}\right\rangle$ to $|\lambda_S\rangle$.

In fact, there is no reason to limit the daughter atom detection via absorption to this particular energy level: its population can be identified by using an intense photon beam, leading to the characteristic absorption spectrum of the daughter atom and its subsequent decay to the ground state. This fourth observable is thus:

4. **Stimulated absorption spectrum of the daughter atom.** In the presence of a light beam, the daughter atom population

would absorb the characteristic frequencies corresponding to its energy levels, which would then de-excite emitting light of the same frequency. In the case of the one mole ^{152}Gd ore that we mentioned in the previous Section, all 10^4 Sm atoms could be easily excited to any of its ~ 1 eV levels using a standard pulsed laser of the order of 100 fs pulse duration, with a mean power of 5 W and a pulse rate of 100 MHz.

Notice that these numbers imply, for a laser with FWHM spot size ~ 40 μm, an absorption rate

$$\left.\frac{\mathrm{d}N_{\mathrm{g.s.}}}{\mathrm{d}t}\right|_{\mathrm{abs}} = -60\%\, N_{\mathrm{g.s.}} \left[\frac{100\ \mathrm{ns}}{\tau}\right] \mathrm{fs}^{-1}\,. \tag{5.34}$$

Since Sm levels have lifetimes between $10 - 1000$ ns [190], one expects to excite them all during the 100 fs pulse. Disentangling the parent and daughter lines should not be difficult —the relatively small number of atomic absorption lines (compared to atomic emission lines) and their narrow width (a few pm) make spectral overlap rare, not being expected between Z and $(Z-2)$ atoms.

5.6 LOOKING FOR A BETTER RESONANT CANDIDATE

Neutrinoless double electron capture in atoms, a quantum mixing mechanism between the neutral atoms ${}^{A}Z$ and ${}^{A}(Z-2)^{*}$ with two electron holes, is allowed by the Majorana neutrino mediation responsible for this $\Delta L = 2$ transition. This Majorana mixing leads to the X-ray de-excitation of the $\left|{}^{A}(Z-2)^{*}\right\rangle$ daughter atomic state, which under the resonance condition has no Standard Model background from the two-neutrino decay.

The intense experimental activity looking for atomic candidates satisfying the resonance condition $\Delta \sim \Gamma$, by means of precise measurements of atomic masses, has already led to a few cases of remarkable enhancement effects and there is still room for additional adjustments of the resonance condition. With this

situation, it has proved relevant to understand the complete time evolution of an atomic state since its inception, and whether one can find, from this information, different signals of the Majorana mixing.

As is worth noting, the results of the last Section show that the bosonic nature of the atomic radiation is a property that can help in getting observable rates of the atom Majorana mixing, including the stimulated X-ray emission from the parent atom as well as the detection of the presence of the daughter atoms by means of its characteristic absorption lines. These two stimulated observables, together with the spontaneous ones from Section 5.4, are schematically represented in Figure 5.7.

The actual numerical values presented in this Chapter correspond to the specific case of ^{152}Gd $\rightarrow$ ^{152}Sm, which is still off the resonance condition by a factor 40, implying a missing factor 10^3

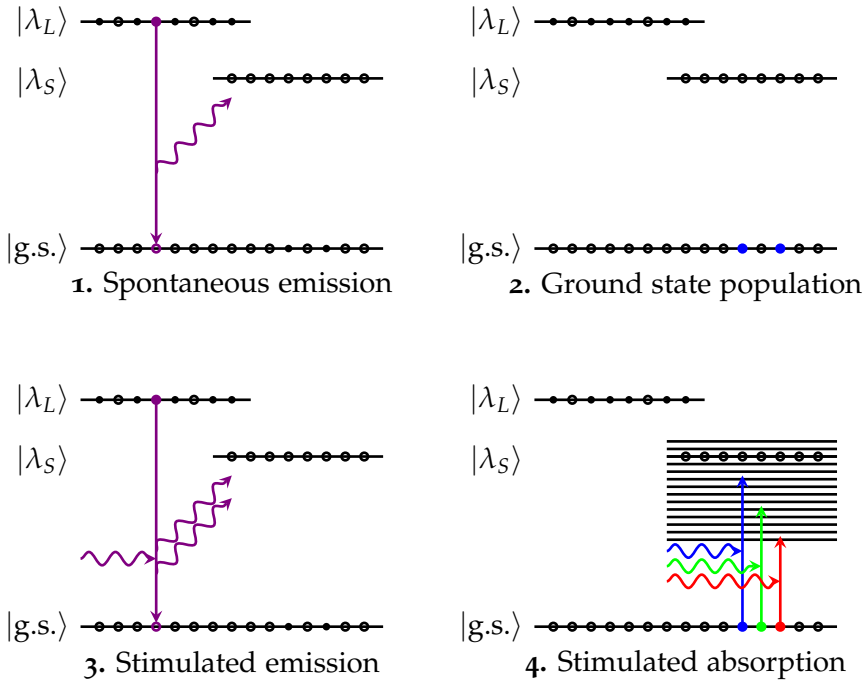

Figure 5.7: Schematic representation of the four observables discussed in this Chapter.

in the rates. Taking into account the ongoing searches for new isotope candidates with a better fulfillment of the resonance condition, there is room for finding a system with $0\nu\epsilon\epsilon$ spontaneous rates competitive with the best-known $0\nu\beta\beta$ isotopes.

Depending on the results of these searches, it remains to be seen whether these processes, with the ideas on stimulating the transitions, could become actual alternatives in the quest for the Dirac/Majorana nature of neutrinos.

6 NEUTRINO-MEDIATED LONG RANGE FORCES

Global lepton number is conserved in the Standard Model. Contrary to charged leptons and quarks, neutrinos may have a $\Delta L = 2$ Majorana mass term which has to be generated by beyond the Standard Model physics. For relativistic neutrinos, the corresponding "confusion theorem" explains the very long lifetimes of $\Delta L = 2$ processes such as neutrinoless double beta decay or neutrinoless double electron capture analyzed in the previous Chapter: even though the neutrinos are virtually exchanged, the energies involved in these processes are MeV's or keV's. In this Chapter, we follow an alternative approach in the search for global lepton number violation: explore the effects of $\Delta L = 2$ contributions to a $\Delta L = 0$ process allowed in the Standard Model.

For a $\Delta L = 0$ process involving neutrinos that can be eventually observed, the possible change in the measured observable due to these $\Delta L = 2$ terms will prove whether neutrinos are either Dirac or Majorana particles. Thus the answer to this fundamental question is a matter of experimental resolution between the two distinct mass terms. This is unlike $\Delta L = 2$ processes, where there would be no signal —and thus no experimental answer— if neutrinos are Dirac. Another benefit of measuring such an observable is its expected dependence on neutrino masses, which could give information on the absolute mass scale even with a still unknown neutrino character. Indeed, this is another fundamental question still unanswered, since the expected small value of neutrino masses ($m_\nu < 1$ eV) makes it hard to observe.

In any case, the fact that their masses are very low stands, and we discuss here another property of neutrinos as mediators of a new force. As is well known, the processes represented in Quantum Field Theory by the exchange of a massless particle give raise to long-range interactions. A clear example is the

scattering of two particles mediated by a photon, which —at tree level— describes Coulomb scattering. Our objective in this Chapter is the application of these ideas to a process mediated by neutrinos. According to the electroweak Lagrangian, the lowest-order process is a neutrino-pair exchange, which —since neutrinos are nearly massless— describes an interaction of long range. For a typical neutrino mass of $m_\nu \sim 0.1$ eV, the range of such an interaction would be $R \sim 1\ \mu$m, well above the atomic scale. At these distances, the force will probe mass terms. Since this interaction is expected to be much weaker than Coulomb's, we will focus on obtaining the coherent 2ν-mediated potential between electrically neutral atoms. We will prove that neutral atoms do have a non-vanishing weak charge, and the coherent character of the interaction vertex makes it easy to extend this result to larger aggregates of ordinary matter.

6.1 INTERACTION POTENTIAL FROM A QUANTUM FIELD THEORY

When discussing the effects of different forces on particles, the usual language is that of an interaction potential between them. This picture of an interaction in position space allows for an easy understanding of its implications in terms of forces. In particle physics, however, we are used to calculate interaction processes using the Feynman approach in momentum space.

We thus begin this Chapter with a consistent map between the two representations, and clearly set the ingredients that will be needed from the Feynman amplitude in the calculation of the interaction potential.

6.1.1 Single particle exchange

The interaction between two electrically charged particles, say A and B, is described by the Coulomb potential,

$$V_C(r) = \frac{e^2}{4\pi}\,\frac{Q_A Q_B}{r}\,, \tag{6.1}$$

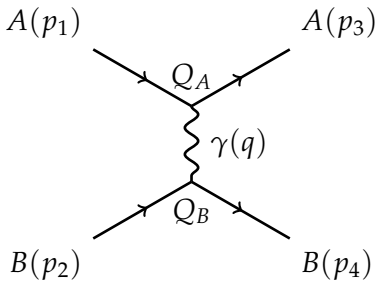

Figure 6.1: Lowest-order Feynman diagram for $AB \to AB$ elastic scattering mediated by a photon, where A and B are particles of electric charge Q_A and Q_B.

where e is the charge of the positron, Q_i is the charge of the particle $i = A, B$ in units of e, and r is the distance between the two particles.

We are interested in deriving this potential from the QED amplitude in Figure 6.1, which is described by the interaction Lagrangian

$$\mathscr{L}_{\text{QED}} \supset -eQ_i\,\bar{\psi}_i\gamma^\mu\psi_i\,A_\mu\,. \tag{6.2}$$

Using the QED Feynman rules [191], the amplitude of the process is

$$i\mathcal{M} = \left[\bar{u}^A_{p_3}(-ieQ_A\gamma^\mu)u^A_{p_1}\right]\,\frac{-ig_{\mu\nu}}{q^2}\,\left[\bar{u}^B_{p_4}(-ieQ_B\gamma^\nu)u^B_{p_2}\right]\,, \tag{6.3}$$

written in such a way that the phase conventions for the amplitude, vertex factors and propagator are clear.

The terms leading to Coulomb scattering are only the coherent ones, so we can consider

$$\mathcal{M} \approx e^2Q_AQ_B\left[\bar{u}^A_{p_3}\,\gamma^0\,u^A_{p_1}\right]\,\frac{1}{q^2}\,\left[\bar{u}^B_{p_4}\,\gamma_0\,u^B_{p_2}\right]\,, \tag{6.4}$$

taking into account the fact that γ^0 is related to the electric charge, which is coherent, whereas $\boldsymbol{\gamma}$ is related to the electromagnetic current, an incoherent quantity.

Using $(\gamma^0)^2 = 1$ and dropping external-line factors, we get the reduced amplitude

$$M(q^2) = e^2Q_AQ_B\,\frac{1}{q^2} \tag{6.5}$$

from its definition as

$$\mathcal{M}(q^2) \equiv \bar{u}^A_{p_3}\, \bar{u}^B_{p_4}\, M(q^2)\, u^B_{p_2}\, u^A_{p_1}\,. \tag{6.6}$$

We can study this scattering process in the Breit reference frame, defined by $q^0 = 0$. This choice is consistent with the low energy transfer in the non-relativistic limit, leading to

$$M(q^2) = -e^2 Q_A Q_B \,\frac{1}{\mathbf{q}^2}\,. \tag{6.7}$$

Since this $M(q^2)$ is the reduced amplitude describing the process in the low-energy coherent limit, it must be the ingredient from which the potential can be calculated. In order to transform the amplitude in momentum space into the potential in position space, we calculate its 3-dimensional Fourier Transform

$$\mathcal{F}\left\{M\right\}(r) \equiv \int \frac{\mathrm{d}^3 q}{(2\pi)^3}\, e^{i\mathbf{q}\,\mathbf{r}}\, M(q^2) = -\frac{e^2}{4\pi}\,\frac{Q_A Q_B}{r}\,. \tag{6.8}$$

Comparing this Fourier transform with the Coulomb potential in Eq. (6.1) yields the relation between the Feynman amplitude and the interaction potential used in a potential description of the system dynamics,

$$V(r) = -\mathcal{F}\left\{M\right\}(r)\,, \tag{6.9}$$

without any numerical factor between them beyond the sign due to our phase convention for the Feynman amplitude.

6.1.2 Particle-pair exchange

As we have just seen, the interaction potential between particles A and B is the Fourier Transform

$$V(r) = -\int \frac{\mathrm{d}^3 q}{(2\pi)^3}\, e^{i\mathbf{q}\,\mathbf{r}}\, M(q^2)\,, \tag{6.10}$$

where M is the lowest order Feynman amplitude for the process $AB \to AB$, with both A and B on-shell but without external-leg factors, as is discussed in Ref. [192]. In the case of a pair exchange, this process will be the one represented in Figure 6.2.

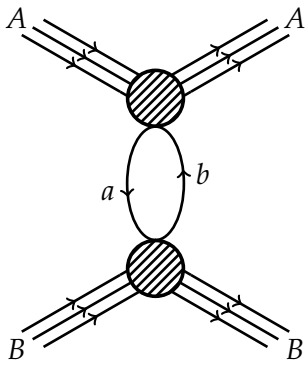

Figure 6.2: Feynman diagram for $AB \to AB$ elastic scattering mediated by a, b exchange.

The dispersion theory for long-range forces was developed in Ref. [193] for its application to two-photon exchange, giving origin to Van der Waals interaction between neutral objects. The generalization to charge-neutral electromagnetic potentials was performed in Ref. [194], as well as its extension for a low momentum transfer theorem [195] in lepton-hadron scattering. The case of the two-neutrino exchange force was first announced [196] in 1968 by Gerald Feinberg and Joseph Sucher for electron-electron interactions due to charged currents. Its formulation in the dispersion approach, including weak neutral current interactions, was given for massless neutrinos in Refs. [197–199].

With the discovery of neutrino masses and mixings, the interaction potential will be modified near its finite range. In Ref. [200] the Dirac neutrino exchange case has been calculated for charged leptons and nucleon interactions using old-fashioned perturbation theory. In the dispersion approach, this Thesis develops for the first time the physical case of 3 neutrino species with masses and mixings, with the appropriate treatment of Dirac and Majorana masses. For aggregate matter, there will be coherent weak charges associated to each pair of intermediate massive neutrinos. This study is needed for the exploration of the effective interaction mediated by two-neutrino exchange at distances of the order of the Compton wavelength of neutrinos.

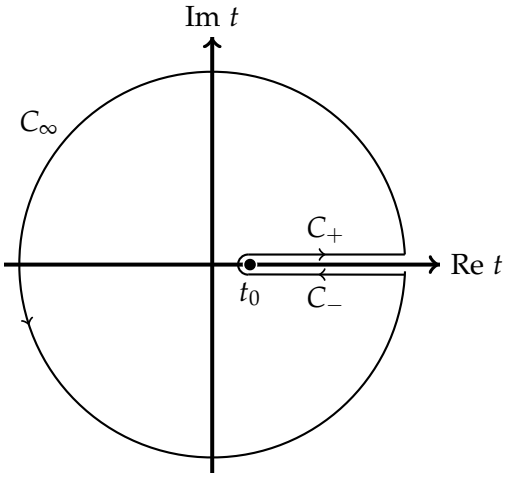

Figure 6.3: Integration path $C = C_\infty + C_- + C_+$ in the complex plane of the Mandelstam t variable, used in the dispersion relation decomposition of the Feynman amplitude of the process, as discussed in the text.

In order to compute the integral (6.10), we rewrite the amplitude as a dispersion relation: we extend $t \equiv q^2$ to the complex plane and expand the amplitude using Cauchy's Formula,

$$f(z) = \frac{1}{2\pi i} \int_C \mathrm{d}z' \, \frac{f(z')}{z' - z} \,, \tag{6.11}$$

which is valid whenever $f(z)$ is analytic inside C.

The physical region of the t variable of elastic scattering processes has $t < 0$, so we want the $\mathbb{R}^-$ axis inside C. Furthermore, the t-channel amplitude will have a branching point at $t_0 \equiv (m_a + m_b)^2 \geq 0$, so we can use Cauchy's Formula with the integration path shown in Figure 6.3. If the amplitude vanishes along the C_∞ circumference, i.e. as $|t| \to \infty$, the only contribution is the one coming from the integral on both sides of the cut along the real t axis,

$$M(t) = \frac{1}{2\pi i} \lim_{\epsilon \to 0} \int_{t_0}^{\infty} \mathrm{d}t' \, \frac{M(t' + i\epsilon) - M(t' - i\epsilon)}{t' - t} \,. \tag{6.12}$$

If not vanishing at C_∞, we would have to either rewrite the dispersion relation for the subtracted amplitude or include the

contribution of C_∞. We continue with the formulation without subtractions, because the contribution along C_∞ is of short range. We thus understand Eq. (6.12) for the long-range amplitude.

In order to calculate the analytically extended amplitude both above and below the unitarity cut, we can relate them using the Schwarz Reflexion Principle,

$$M(t - i\epsilon) = M^*(t + i\epsilon)\,. \tag{6.13}$$

Using this relation, one finds

$$M(t) = \frac{1}{\pi}\int_{t_0}^{\infty} \mathrm{d}t'\,\frac{\mathrm{Im}\ M(t')}{t' - t}\,, \tag{6.14}$$

which is the so-called $t-$channel dispersion relation of the Feynman amplitude.

Taking into account the Fourier transform of a spherical wave,

$$\frac{1}{t' - t} = \frac{1}{4\pi}\int \mathrm{d}^3 r\, e^{-i\mathbf{q}\,\mathbf{r}}\,\frac{e^{-\sqrt{t'}r}}{r}\,, \tag{6.15}$$

the integral (6.10) shows that the non-relativistic potential is

$$V(r) = \frac{-1}{4\pi^2 r}\int_{t_0}^{\infty} \mathrm{d}t'\, e^{-\sqrt{t'}r}\,\mathrm{Im}\ M(t')\,, \tag{6.16}$$

determined by the absorptive part of the Feynman amplitude only. As seen, for the determination of the long-range potential we will not be interested in the whole 1-loop $M(t)$, but only in its $\mathrm{Im}\, M(t)$, so we can make a profit from the unitarity of the S matrix to simplify our calculations.

6.2 UNITARITY: AMPLITUDE ABSORPTIVE PART

Physical processes are determined by matrix elements of the scattering matrix S. The S matrix relates the orthonormal bases of initial and final states, so it has to be a unitary operator,

$$S^\dagger S = 1\,. \tag{6.17}$$

We define the reduced scattering matrix T as $S \equiv 1 + i\,T$, which describes processes where there really is an interaction —initial and final states are not the same ones. In terms of this operator, the unitarity relation (6.17) becomes

$$T^\dagger T = -i(T - T^\dagger)\,. \tag{6.18}$$

In order to describe a physical process, we have to consider the matrix element

$$\langle f|\,T\,|i\rangle \equiv (2\pi)^4\delta^{(4)}(p_f - p_i)\mathcal{M}(i \to f)\,, \tag{6.19}$$

where $|i\rangle$ is the initial state and $|f\rangle$ is the final one. Therefore, we need to sandwich the previous relation between those states.

Assuming that Time Reversal is a good symmetry, i.e.

$$T(i \to f) - T(f \to i)^* = 2\,\mathrm{Im}\;T(i \to f)\,, \tag{6.20}$$

the right-hand side of Eq. (6.18) is

$$\langle f|\,\mathrm{RHS}\,|i\rangle = 2\,\mathrm{Im}\;\langle f|\,T\,|i\rangle\;. \tag{6.21}$$

On the other hand, an identity relation

$$1 = \sum_n \int \prod_{j=1}^{n} \frac{\mathrm{d}^3 q_j}{(2\pi)^3 2E_{q_j}}\,|q_n\rangle\,\langle q_n| \tag{6.22}$$

can be inserted into the left-hand side to find

$$\langle f|\,\mathrm{LHS}\,|i\rangle = \sum_n \int \prod_{j=1}^{n} \frac{\mathrm{d}^3 q_j}{(2\pi)^3 2E_{q_j}}\,\langle f|\,T^\dagger\,|q_n\rangle\,\langle q_n|\,T\,|i\rangle\;, \tag{6.23}$$

with $|q_n\rangle$ representing a state of n particles with 4-momenta $q_1, q_2 \ldots q_n$. Under these conditions, the unitarity relation for physical processes is

$$\mathrm{Im}\;\langle f|\,T\,|i\rangle = \frac{1}{2}\sum_n \int \mathrm{d}Q_n\,\langle q_n|\,T\,|f\rangle^*\,\langle q_n|\,T\,|i\rangle\;, \tag{6.24}$$

stating that the absorptive part of the $|i\rangle \to |f\rangle$ amplitude is determined by the scattering amplitudes of $|i\rangle$ and $|f\rangle$ going to all possible intermediate states $|q_n\rangle$.

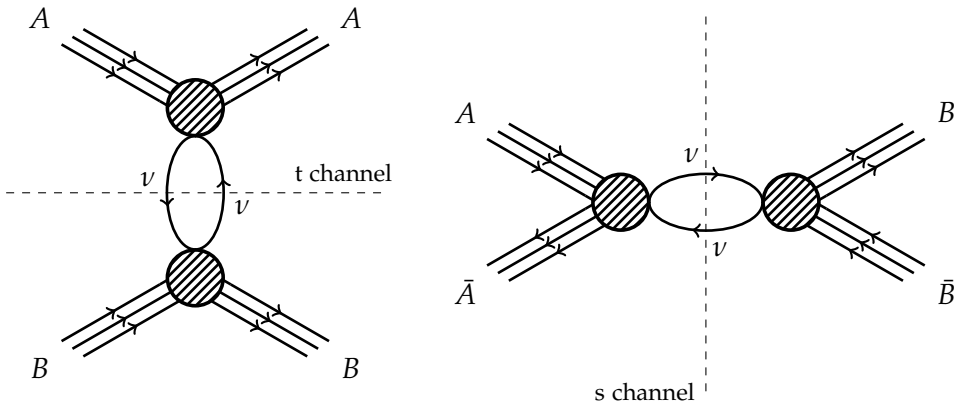

Figure 6.4: Leading-order Feynman diagrams for the neutrino-pair mediated t-channel $AB \to AB$ scattering (left) and s-channel $A\bar{A} \to B\bar{B}$ scattering (right).

This relation applies to our process. We are interested in calculating the absorptive part of the $AB \to AB$ amplitude mediated by a neutrino pair, so we need to do a t-channel unitarity cut of the diagram in Figure 6.4. Therefore, we apply Eq. (6.24) to the crossed process $A\bar{A} \to B\bar{B}$, corresponding to the s channel in Figure 6.4, with a 2ν intermediate state,

$$\begin{aligned}\text{Im}\,\mathcal{M}(A\bar{A} \to B\bar{B}) = \frac{1}{2}\int \frac{\mathrm{d}^3k_1}{(2\pi)^3 2E_{k_1}} \frac{\mathrm{d}^3k_2}{(2\pi)^3 2E_{k_2}} \times \\ \times (2\pi)^4\delta^{(4)}(k_1 + k_2 - p_i)\mathcal{M}(B\bar{B} \to \nu\bar{\nu})^*\mathcal{M}(A\bar{A} \to \nu\bar{\nu})\,.\end{aligned} \tag{6.25}$$

This expression, written in an explicitly Lorentz-invariant manner as

$$\begin{aligned}\text{Im}\,\mathcal{M}(A\bar{A} \to B\bar{B}) = \frac{1}{2}\int \frac{\mathrm{d}^4k_1}{(2\pi)^3}\,\delta(k_1^2 - m_\nu^2) \frac{\mathrm{d}^4k_2}{(2\pi)^3}\,\delta(k_2^2 - m_\nu^2) \times \\ \times (2\pi)^4\delta^{(4)}(k_1 + k_2 - p_i)\mathcal{M}(B\bar{B} \to \nu\bar{\nu})^*\mathcal{M}(A\bar{A} \to \nu\bar{\nu})\end{aligned} \tag{6.26}$$

provides a clear insight into the ingredients needed to determine the interaction potential: there is no need to calculate the 1-loop

amplitude in Figure 6.4, for its absorptive part is completely determined by the tree-level scattering amplitudes $A\bar{A} \to \nu\bar{\nu}$ and $B\bar{B} \to \nu\bar{\nu}$.

6.3 LOW-ENERGY EFFECTIVE COUPLINGS

As is well known, the interactions of neutrinos with the other fundamental particles are described by the electroweak charged-current (CC) and neutral-current (NC) Lagrangians,

$$\mathscr{L}_{\rm CC} = -\frac{e}{\sqrt{2}\sin\theta_W} W^\dagger_\mu \left[\bar{u}_i \gamma^\mu P_L V_{ij}\, d_j + \bar{\nu}_i \gamma^\mu P_L e_i\right] + \text{h.c.} \quad (6.27a)$$

$$\mathscr{L}_{\rm NC} = -eA_\mu\, Q_j \bar{\psi}_j\, \gamma^\mu\, \psi_j - \\ - \frac{e}{4\sin\theta_W \cos\theta_W} Z_\mu\, \bar{\psi}_j\, \gamma^\mu \left(g_{V_j} - g_{A_j}\gamma_5\right) \psi_j\,, \quad (6.27b)$$

where θ_W is the weak mixing angle, e is the electric coupling and g_V (g_A) are the weak neutral vector (axial) couplings.

For any elementary particle, the weak neutral couplings are given by

$$g_V = 2T_3 - 4Q\sin^2\theta_W, \qquad g_A = 2T_3\,, \quad (6.28)$$

where T_3 is the third component of weak isospin and Q is the electric charge. The electroweak charges of the SM fermions are written in Table 6.1.

The electroweak Lagrangians in Eqs. (6.27) provide the Feynman rules needed to compute the scattering amplitude $A\bar{A} \to \nu\bar{\nu}$.

Table 6.1: Electroweak charges of the Standard Model fermions: electric Q, neutral weak vector g_V and axial g_A.

Particle	Q	g_V	g_A
u_i	$2/3$	$1 - \frac{8}{3}\sin^2\theta_W$	1
d_i	$-1/3$	$-1 + \frac{4}{3}\sin^2\theta_W$	-1
ν_i	0	1	1
e_i	-1	$-1 + 4\sin^2\theta_W$	-1

Our focus, however, is to determine the long-range interaction potential mediated by a neutrino pair. Its long-range nature is connected with its blindness to the high-energy details of the theory, for this potential is given by the low momentum transfer terms in the amplitude. Therefore, the relevant terms for the potential are the leading terms in the limit $|q^2| \ll M_W^2, M_Z^2$, and we can simplify our calculations by obtaining low-energy effective interactions from the above Lagrangians.

6.3.1 Effective Lagrangian for neutrino-matter interactions

In the scattering process $A\nu \to A\nu$ at low energy, the neutrino can interact with the three "elementary" particles which the aggregate of matter A is formed with —electrons, protons and neutrons.

We can consider that nucleons are point-like Dirac particles because the scattering happens at low energy: the neutrino is a large scale probe that cannot resolve the structure of nucleons. The vector current is conserved, so both the electric charge Q and the weak vector charge g_V of the nucleons are the sum of their valence quarks' charges,

$$\begin{aligned} Q_p &= 1\,, & g_V^p &= 1 - 4\sin^2\theta_W\,, \\ Q_n &= 0\,, & g_V^n &= -1\,. \end{aligned} \tag{6.29}$$

On the other hand, the axial current is not conserved, so this argument does not apply to the weak axial charge of the nucleon. In fact, Eq. (6.28) shows that the axial coupling is independent of the electric charge —it only depends on the weak isospin coupled to the W_μ^3 boson. Therefore, it can be expected due to weak isospin symmetry, if it coincides with strong isospin for the (p, n) doublet, that the weak neutral axial coupling at low momentum transfer, $q^2 \to 0$, is related to the coupling to the $W_\mu^\pm$-mediated charged current responsible of the $n \to p$ process, $g_A = 1.2723(23)$ [201]. In general, we may distinguish g_A^N for $N = p, n$.

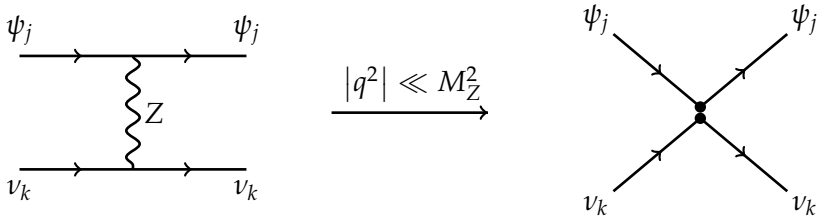

Figure 6.5: Tree-level Feynman diagrams for the $\psi\nu \to \psi\nu$ scattering corresponding to the Standard Model NC Lagrangian (left) and the effective low-energy Lagrangian obtained integrating out the Z degrees of freedom (right).

Taking all of this into account, the Lagrangian describing the $A\nu \to A\nu$ interaction has three terms, related to the processes

$$\nu_e + e \longrightarrow \nu_e + e\,, \tag{6.30a}$$

$$\nu_i + e \longrightarrow \nu_i + e\,, \qquad (i = \mu, \tau) \tag{6.30b}$$

$$\nu_j + N \longrightarrow \nu_j + N\,. \qquad (j = e, \mu, \tau) \tag{6.30c}$$

There are contributions to all of these processes from Z-mediated NC interactions, via the Feynman diagram in Figure 6.5. As discussed, the long-range potential will be blind to $|q^2| \gtrsim M_Z^2$ effects, so we work with a low-energy effective Lagrangian obtained from (6.27b) after integrating out the Z boson degrees of freedom. This procedure is done by setting the field Z^μ in the full Lagrangian to the solution of its equation of motion,

$$0 = \frac{\partial \mathscr{L}_{\text{NC}}}{\partial Z_\mu} = M_Z^2 Z^\mu - \frac{e}{4 \sin\theta_W \cos\theta_W}\, \bar{\psi}_j\, \gamma^\mu \left(g_{V_j} - g_{A_j}\gamma_5\right) \psi_j\,. \tag{6.31}$$

The resulting effective Lagrangian,

$$\mathscr{L}_{\text{NC}}^{\text{eff}} = -\frac{G_F}{2\sqrt{2}} \left[\bar{\nu}_k\, \gamma^\mu\, (1 - \gamma_5)\, \nu_k\right] \left[\bar{\psi}_j\, \gamma_\mu\, \left(g_{V_j} - g_{A_j}\gamma_5\right) \psi_j\right]\,, \tag{6.32}$$

describes the contact interaction represented in Figure 6.5.

On the other hand, the only contribution from CC interactions to the long-range potential will come from the scattering of

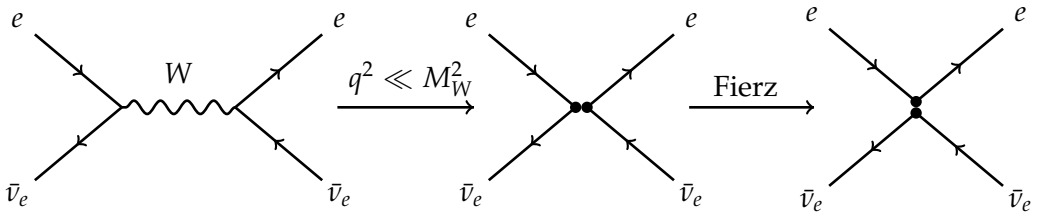

Figure 6.6: Tree-level Feynman diagrams for the $\bar{\nu}_e e \to \bar{\nu}_e e$ scattering corresponding to the Standard Model CC Lagrangian (left), the effective low-energy Lagrangian obtained integrating out the W degrees of freedom (middle) and this last Lagrangian after Fierz reordering the fields and writing the currents as flavor diagonal (right).

electron neutrinos with electrons in process (6.30a). Integrating out the W from Lagrangian (6.27a) leads to

$$\mathscr{L}_{\text{CC}}^{\text{eff}} = -\frac{G_F}{\sqrt{2}} \left[\bar{\nu}_e \gamma^\mu (1-\gamma_5) e\right] \left[\bar{e} \gamma_\mu (1-\gamma_5) \nu_e\right] , \tag{6.33}$$

where the Fermi constant is given by $\frac{G_F}{\sqrt{2}} = \frac{e^2}{8 M_W^2 \sin^2\theta_W}$.

As shown in Figure 6.6, it is convenient to rewrite this Lagrangian as flavor diagonal, so that both NC and CC Lagrangians explicitly contribute to the same interaction vertices, and we can obtain their effective coupling adding them up. This simplification can be achieved using the Fierz identity

$$[\bar{\psi}_1 \Gamma P_L \psi_2] \, [\bar{\psi}_3 P_R \Phi \psi_4] = -\frac{1}{2} [\bar{\psi}_1 \Gamma \gamma_\mu P_R \Phi \psi_4] [\bar{\psi}_3 \gamma^\mu P_L \psi_2] , \tag{6.34}$$

valid for any pair of gamma matrices Γ, Φ. This reordering of the fields in the current-current interaction leads to the flavor-diagonal CC effective Lagrangian

$$\mathscr{L}_{\text{CC}}^{\text{eff}} = -\frac{G_F}{\sqrt{2}} \left[\bar{\nu}_e \gamma^\mu (1-\gamma_5) \nu_e\right] \left[\bar{e} \gamma_\mu (1-\gamma_5) e\right] . \tag{6.35}$$

Unlike the NC effective Lagrangian, which is diagonal in both neutrino flavor and mass basis, this CC effective Lagrangian couples only electron neutrinos. Written explicitly in terms of definite-mass fields,

$$\mathscr{L}_{\text{CC}}^{\text{eff}} = -\frac{G_F}{\sqrt{2}} U_{ei} U_{ej}^* \left[\bar{\nu}_j \gamma^\mu (1-\gamma_5) \nu_i\right] \left[\bar{e} \gamma_\mu (1-\gamma_5) e\right] , \tag{6.36}$$

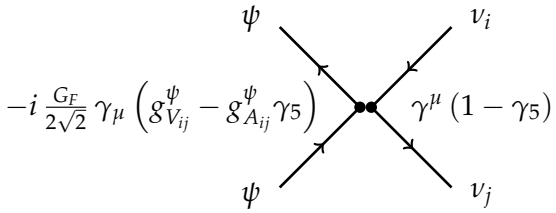

Figure 6.7: Fundamental vertex of the effective low-energy Lagrangian (6.39). The effective couplings $g^{\psi}_{V_{ij}}$, $g^{\psi}_{A_{ij}}$ in Eqs. (6.38) and (6.40) depend on both the neutrino masses and which is the fermion ψ, as discussed in the text.

the Lagrangian shows that propagation of two neutrinos with different masses is allowed if mixing is taken into account.

From these two low-energy weak Lagrangians, the complete effective Lagrangian describing the relevant interactions for the long-range potential is

$$\mathscr{L}_{\text{eff}} = -\frac{G_F}{2\sqrt{2}}\left\{\left[\bar{\nu}_j\,\gamma^\mu\,(1-\gamma_5)\,\nu_i\right]\left[\bar{e}\,\gamma_\mu\,\left(g^{e}_{V_{ij}}-g^{e}_{A_{ij}}\gamma_5\right)e\right]+\right.$$
$$\left.+\left[\bar{\nu}_k\,\gamma^\mu\,(1-\gamma_5)\,\nu_k\right]\left[\bar{N}\,\gamma_\mu\,\left(g^{N}_{V}-g^{N}_{A}\gamma_5\right)N\right]\right\} \quad (6.37)$$

where $N = p, n$, and the effective electron couplings $g^{\psi}_{V_{ij}}$, $g^{\psi}_{A_{ij}}$ include both e-flavor CC and diagonal NC interactions,

$$g^{e}_{V_{ij}} = 2U_{ei}U^*_{ej} + g^{e}_{V}\delta_{ij}\,, \quad (6.38a)$$
$$g^{e}_{A_{ij}} = 2U_{ei}U^*_{ej} + g^{e}_{A}\delta_{ij}\,. \quad (6.38b)$$

Notice that the neutrino current can be factored out if a Kronecker δ_{ij} is added in the nucleon current, so all fundamental vertices of this Lagrangian have the same structure,

$$\mathscr{L}_{\text{eff}} = -\frac{G_F}{2\sqrt{2}}\,\left[\bar{\nu}_j\,\gamma^\mu\,(1-\gamma_5)\,\nu_i\right]\left[\bar{\psi}\,\gamma_\mu\,(g^{\psi}_{V_{ij}}-g^{\psi}_{A_{ij}}\gamma_5)\,\psi\right]\,, \quad (6.39)$$

as represented in Figure 6.7. This fact reduces the calculation of the required amplitudes to a single one followed by adequate substitutions, taking into account the effective $ee\nu_i\nu_j$ couplings in Eqs. (6.38), the fundamental $e\nu_i$ NC couplings in Table (6.1),

and the nucleon couplings in Eq. (6.29), which enter the effective Lagrangian (6.39) as

$$g^N_{V_{ij}} = g^N_V \delta_{ij}\,, \tag{6.40a}$$

$$g^N_{A_{ij}} = g^N_A \delta_{ij}\,. \tag{6.40b}$$

6.4 ν–MATTER SCATTERING AMPLITUDE

All ingredients for the calculation of the 2ν-mediated long-range potential between two aggregates of matter A and B are now clear. With the two electrically neutral aggregates parametrized by their number of protons and electrons Z, and their number of neutrons N, the procedure is as follows:

1. Calculate the ${}^A_N\mathrm{Z}\,\nu \to {}^A_N\mathrm{Z}\,\nu$ scattering amplitude using the low-energy effective Lagrangian (6.39).

2. Combine the two amplitudes for A and B as in Eq. (6.26) to obtain the absorptive part of the 2ν-mediated $A\bar{A} \to B\bar{B}$ scattering amplitude.

3. Crossing this absorptive part from the s channel to the t channel yields $\mathrm{Im}(AB \to AB)$, the last ingredient needed to calculate the long-range potential as in the integral transform in Eq. (6.16).

We focus in this Section on the first two steps, analyzing their implications for the cases of massless neutrinos, Dirac neutrinos and Majorana neutrinos, with special emphasis on the distinction of the Dirac/Majorana neutrino character. The discussion of their effects on the long-range potentials will be broken down in the next Section 6.5.

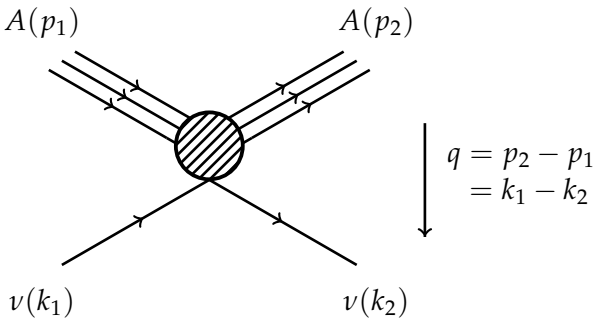

Figure 6.8: Lowest order Feynman diagram for the $A\nu \to A\nu$ scattering in the low-energy effective weak theory.

6.4.1 Massless neutrinos

In the simpler case of massless neutrinos, flavor and mass states are equivalent, leading to $U_{\rm PMNS} = \mathbf{1}$. In terms of flavor fields, Lagrangian (6.39) is simplified to the flavor-diagonal

$$\mathscr{L}_{\rm eff} = -\frac{G_F}{2\sqrt{2}} \left[\bar{\nu}_\alpha \, \gamma^\mu \, (1-\gamma_5) \, \nu_\alpha\right] \left[\bar{\psi} \, \gamma_\mu \, (g^\psi_{V_\alpha} - g^\psi_{A_\alpha} \gamma_5) \, \psi\right] \,, \quad (6.41)$$

written in terms of the flavor couplings

$$\begin{aligned} g^e_{V_\alpha} &= 2\delta_{\alpha e} + g^e_V \,, & g^N_{V_\alpha} &= g^N_V \,, \\ g^e_{A_\alpha} &= 2\delta_{\alpha e} + g^e_A \,, & g^N_{A_\alpha} &= g^N_A \,. \end{aligned} \quad (6.42)$$

The scattering of a matter aggregate A with Z protons, Z electrons and N neutrons is thus determined by this interaction with its constituent fields as the Feynman diagram in Figure 6.8. For the diagonal current of massless neutrinos, the possible channels are the three flavors $A(p_1)\,\nu_\alpha(k_1) \to A(p_2)\,\nu_\alpha(k_2)$.

We write the current-current amplitude as

$$T_{A_\alpha} = -\frac{G_F}{2\sqrt{2}} \int \mathrm{d}^4x \, j^\mu_{\nu_\alpha}(x) J^\alpha_{A,\mu}(x) \,, \quad (6.43)$$

with the usual current for the fundamental neutrino field

$$j^\mu_{\nu_\alpha}(x) = \left[\bar{u}(k_2) \, \gamma^\mu \, (1-\gamma_5) \, u(k_1)\right] \, e^{-i(k_1-k_2)x} \,, \quad (6.44)$$

and the aggregate current

$$J^{\alpha}_{A,\mu}(x) = e^{-i(p_1-p_2)x} \sum_{\psi} \langle A(p_2)|\, \bar{\psi}(0)\gamma_\mu \left(\tilde{g}^{\psi}_{V_\alpha} - \tilde{g}^{\psi}_{A_\alpha}\gamma_5\right) \psi(0)\, |A(p_1)\rangle \ , \tag{6.45}$$

summed for $\psi = e,\, p,\, n$. This matrix element will depend on the structure of the matter aggregate, but we do not need to consider this general case, since we are only interested in finding the relevant terms to the coherent long-range interaction. Looking separately at each component of the current, we find:

- γ^0 is a scalar quantity, related to the matrix element of $\psi^\dagger\psi$, which is the number operator, so its contribution is coherent.
- $\gamma^0\gamma_5$ is a pseudo-scalar quantity, so its matrix element is related to $\boldsymbol{\sigma}\mathbf{q}/M$, where $\boldsymbol{\sigma}$ is the spin of A, M its mass and $\mathbf{q} = \mathbf{p}_1 - \mathbf{p}_2$ the momentum transfer. Since this contribution depends on the spin $\boldsymbol{\sigma}$, it is not coherent. Also, any contribution of the form $\mathbf{q}/M$ gives a relativistic correction to the potential, negligible in the long-range regime.
- $\boldsymbol{\gamma}$ is a polar vector, so its matrix element must be proportional to $\mathbf{q}/M$. Again, this is a relativistic correction we will not consider.
- $\boldsymbol{\gamma}\gamma_5$ is an axial vector, directly related to the spin of the particle, so this contribution is also incoherent.

Therefore, the coherent contribution to the long-range amplitude is solely determined by the γ^0 term in the time-like $\mu = 0$ component of the aggregate current, given by the number operator of each species $\psi = e,\, p,\, n$ as

$$J^{\alpha}_{A,0}(x) \equiv \sum_{\psi} J^{\psi\alpha}_{A,0}(x) = \sum_{\psi} N_\psi\, g^{\psi}_{V_\alpha}\, e^{-i(p_1-p_2)x}\,. \tag{6.46}$$

In order to work in a Lorentz-covariant formalism, we write the scattering amplitude in momentum space as

$$\mathcal{M}_{A_\alpha} = -\frac{G_F}{2\sqrt{2}}\, J^{\alpha}_{A,\mu} \left[\bar{u}(k_2)\, \gamma^\mu\, (1-\gamma_5)\, u(k_1)\right] \ , \tag{6.47}$$

in terms of the full aggregate current $J^{\alpha}_{A,\mu} \equiv \sum_{\psi} J^{\psi\alpha}_{A,\mu}$, even though the only relevant component of $J^{\alpha}_{A,\mu}$ in the coherent long-range amplitude is, as seen from Eq. (6.46) and the couplings in Eq. (6.42),

$$J^{\alpha}_{A,0} = 2Z\delta_{\alpha e} - N\,. \tag{6.48}$$

This relation shows that NC interactions of neutrinos with protons and electrons cancel each other out due to the conservation of the vector current leading to $g^{p}_{V} = -g^{e}_{V}$. The remaining terms are the Z-dependent CC interaction of electron neutrinos with electrons and the N-dependent NC interaction of all three neutrinos with neutrons.

6.4.1.1 *The weak flavor charge of aggregate matter*

The behavior of the amplitude (6.47) in terms of the coherent $J^{0}_{A_\alpha}$ in Eq. (6.48) has conceptually significant consequences, worth analyzing in detail.

Notice that this amplitude is analogous to the QED scattering of a photon off a charged fermion. The amplitude of the $\gamma\psi\psi$ fundamental vertex is

$$\mathcal{M}_{\gamma} = -eQ\,\gamma^{\mu}\epsilon_{\mu}\,, \tag{6.49}$$

where Q is the electric charge of the fermion field. Due to vector current conservation, this vertex does also apply to non-fundamental particles, which have an electric charge equal to the sum of its constituents' charges —and the amplitude would be this charge times the coupling e.

In this sense of coherent interactions being described by coupling $\times$ charge $\times$ current, our non-relativistic coherent amplitude for neutrino-matter scattering

$$\mathcal{M}_{2\nu_\alpha} = -\frac{G_F}{2\sqrt{2}}\,J^{\alpha}_{A,0}\left[\bar{u}(k_2)\,\gamma^{0}(1-\gamma_5)\,u(k_1)\right] \tag{6.50}$$

shows that $Q^{\alpha}_{W,A} \equiv J^{\alpha}_{A,0} = 2Z\delta_{\alpha e} - N$ is the weak charge of the aggregate of matter A. It depends on the flavor of the neutrino,

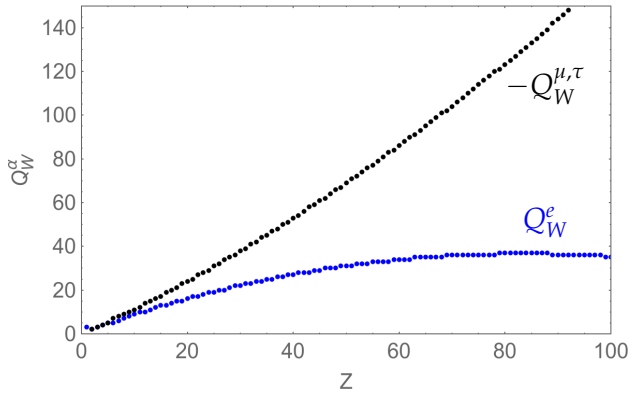

Figure 6.9: e (blue), μ and τ (black) weak flavor charges in Eqs. (6.51) of the elements with (Z, N) in the valley of stability, Eq. (6.52). Beware a minus sign in the μ, τ flavor charges.

so we can speak of three weak flavor charges of aggregate matter, which are given by

$$Q_{W,A}^e = 2Z_A - N_A\,, \tag{6.51a}$$

$$Q_{W,A}^\mu = Q_{W,A}^\tau = -N_A\,. \tag{6.51b}$$

Eqs. (6.51) state the fact that, whereas aggregate matter is neutral of electric charge, it is not neutral of weak charges!

It is interesting to analyze the value of those charges for "normal" matter. In order to do that, we look at stable nuclei. According to the semi-empirical mass formula [202], the (Z, N) values of stable nuclei are related by

$$Z \approx \frac{A}{2 + 0.0157 A^{2/3}}\,, \tag{6.52}$$

where $A \equiv Z + N$. Using those pairs of values, the weak charges of each element (neutral atom) are represented in Figure 6.9, where we see that the e flavor weak charge is always positive, whereas the μ and τ flavor charges are always negative. The weak charge of an aggregate of matter is obtained from the values in the Figure, multiplying by the number of the constituent atoms.

6.4.1.2 *Absorptive part of* $AB \to AB$ *at low* t

According to the discussion leading to Eq. (6.26), the absorptive part of the s-channel $A\bar{A} \to B\bar{B}$ scattering amplitude is obtained from crossing the t channel amplitude (6.47) into the s channel $A\bar{A} \to \nu_\alpha \bar{\nu}_\alpha$ amplitude

$$\mathcal{M}_{A_\alpha} = -\frac{G_F}{2\sqrt{2}} \tilde{J}^\alpha_{A,\mu} \left[\bar{u}(k_2)\, \gamma^\mu\, (1-\gamma_5)\, v(k_1)\right] , \tag{6.53}$$

where $\tilde{J}^\alpha_{A,\mu}$ are the components of the crossed aggregate current, still yielding $\tilde{J}^\alpha_{A,0} = Q^\alpha_{W,A}$ in the coherent non-relativistic limit.

The quantity that determines the absorptive part is the product of intermediate-state amplitudes

$$\mathcal{M}_{A_\alpha} \mathcal{M}^*_{B_\alpha} = G_F^2\, \tilde{Z}^\alpha_{\mu\nu} \left[k_1^\mu k_2^\nu + k_1^\nu k_2^\mu - \frac{1}{2} s g^{\mu\nu} + a^{\mu\nu}\right] , \tag{6.54}$$

where we defined $\tilde{Z}^\alpha_{\mu\nu} \equiv \tilde{J}^\alpha_{A,\mu}\, \tilde{J}^\alpha_{B,\nu}$ and $a^{\mu\nu}$ is some antisymmetric tensor which we will no longer consider because it vanishes in the non-relativistic limit, where the only relevant component is $\mu = \nu = 0$.

The phase-space integral (6.26) of the product of intermediate-state amplitudes in Eq. (6.54) is easily solved using Lorentz covariance[1], yielding

$$\mathrm{Im}\mathcal{M}(A\bar{A} \to B\bar{B}) = \frac{G_F^2}{48\pi} \sum_\alpha \tilde{Z}^\alpha_{\mu\nu} \left[\, q^\mu q^\nu - s g^{\mu\nu} \,\right] , \tag{6.55}$$

whose tensor structure is transverse, a requirement which any quantity built from conserved currents must satisfy. We can now uncross back to the t channel to obtain the $AB \to AB$ absorptive part

$$\mathrm{Im}\mathcal{M}(AB \to AB) = \frac{G_F^2}{48\pi} \sum_\alpha Z^\alpha_{\mu\nu} \left[\, q^\mu q^\nu - t g^{\mu\nu} \,\right] . \tag{6.56}$$

1 The relevant integrals in the massless neutrino case are

$$I \equiv \int \frac{\mathrm{d}^3 k_1}{2E_1} \frac{\mathrm{d}^3 k_2}{2E_2}\, \delta^{(4)}(k_1 + k_2 - q) = \frac{\pi}{2} ,$$

$$I^{\mu\nu} \equiv \int \frac{\mathrm{d}^3 k_1}{2E_1} \frac{\mathrm{d}^3 k_2}{2E_2}\, \delta^{(4)}(k_1 + k_2 - q)\, k_1^\mu k_2^\nu = \frac{\pi}{24} \left(s g^{\mu\nu} + 2 q^\mu q^\nu\right) .$$

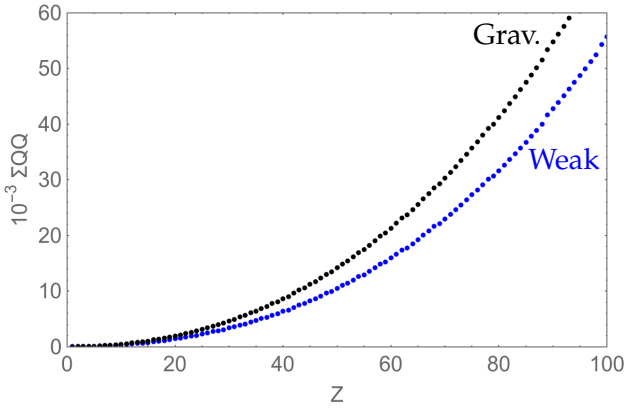

Figure 6.10: Weak coupling $\sum_\alpha Q_W^\alpha Q_W^\alpha$ (blue), which is written in Eq. (6.58), for the elements of the valley of stability as determined from Eq. (6.52), each one interacting with itself. The gravitational coupling $M^2/m_p^2 \approx (Z+N)^2$, neglecting binding energies, is also shown (black).

As discussed, the long-range potential is determined by the coherent non-relativistic contribution to the amplitude, which is given by the $\mu = \nu = 0$ component with $q^0 \approx 0$,

$$\mathrm{Im}\mathcal{M}(AB \to AB) = -\frac{G_F^2}{48\pi} \sum_\alpha Q_{W,A}^\alpha Q_{W,B}^\alpha \, t \,. \tag{6.57}$$

This result shows that, in the massless neutrino limit, all the flavor dependence of the absorptive part —and, therefore, of the long-range potential— is factorized in the weak charges. Since the sign of each flavor charge is the same for all stable elements, as shown in Figure 6.9, the negative sign of the absorptive part for all $t > 0$ ensures that the potential will be repulsive for *all* matter, independently of its composition.

The coherent character of the interaction is also determined by this flavor-to-flavor product of weak charges

$$\sum_\alpha Q_{W,A}^\alpha Q_{W,B}^\alpha = (2Z_A - N_A)(2Z_B - N_B) + 2N_A N_B \,. \tag{6.58}$$

For the list of stable nuclei considered in the analysis of the weak flavor charges, we show in Figure 6.10 the value of the coupling (6.58) if each atom is interacting with itself. We also show

the gravitational coupling for these pairs of atoms, approximated to $(Z+N)^2$, from which we find that gravitation grows more rapidly by enlarging the matter aggregate than the 2ν-mediated interaction does. Even though both of them increase with the number of particles composing the interacting systems, their different scale proves that our coherent weak interaction could introduce a deviation from the weak equivalence principle, as had been announced in Ref. [198].

6.4.2 Dirac neutrinos

Although the procedure in calculating the absorptive part of the scattering amplitude is the same for Dirac neutrinos as for the massless case, the addition of a mass term as in Eq. (1.21) in the Lagrangian introduces some significant differences. Most notoriously, the mismatch between flavor and mass eigenstates given by U_{PMNS} must be taken into account, which means that the full Lagrangian (6.39) must be used, with the PMNS-dependent couplings $g^e_{V_{ij}}$ and $g^e_{A_{ij}}$ in Eqs. (6.38) describing the different contributions from ν_e and $\nu_{\mu,\tau}$ to the $\nu_i\bar{\nu}_j$ intermediate state.

Analogous to the Feynman diagram in Figure 6.8, the relevant process in obtaining the scattering to the intermediate state will thus be $A\nu_i \to A\nu_j$. Its amplitude can be written in the same form as the massless amplitude (6.47),

$$\mathcal{M}_{A_{ij}} = -\frac{G_F}{2\sqrt{2}}\, J^{ij}_{A,\mu}\left[\bar{u}_j(k_2)\,\gamma^\mu\,(1-\gamma_5)\,u_i(k_1)\right]\,, \tag{6.59}$$

with the qualitatively different dynamics in the couplings in the matter current $J^{ij}_{A,\mu}$ leading to its coherent non-relativistic limit

$$J^{ij}_{A,0} = \sum_\psi N_\psi\, g^\psi_{V_{ij}} = 2ZU_{ei}U^*_{ej} - N\delta_{ij}\,. \tag{6.60}$$

One can easily check that the massless limit $U_{\alpha k} = \delta_{\alpha k}$ of these mixed charges $Q^{ij}_{W,A} \equiv 2ZU_{ei}U^*_{ej} - N\delta_{ij}$ correctly reproduces the weak flavor charges in Eqs. (6.51).

Besides this difference in dynamics, there is also the expected kinematical difference due to the involved particles being mas-

sive: treating the neutrino spinors u_i as solutions to the Dirac equation with mass m_i leads to the intermediate-state product

$$\mathcal{M}_{A_{ij}}\mathcal{M}^*_{B_{ij}} = G_F^2\,\tilde{Z}^{ij}_{\mu\nu}\left[k_1^\mu k_2^\nu + k_1^\nu k_2^\mu - \frac{1}{2}(s - m_i^2 - m_j^2)g^{\mu\nu} + a^{\mu\nu}\right] \tag{6.61}$$

and the absorptive part[2]

$$\mathrm{Im}\mathcal{M}(AB \to AB) = -\frac{G_F^2}{48\pi}\,t \times$$
$$\times \sum_{ij} Q^{ij}_{W,A}(Q^{ij}_{W,B})^* \left[1 - \frac{\overline{m_{ij}^2}}{t} - \frac{1}{2}\left[\frac{\Delta m_{ij}^2}{t}\right]^2\right]\sqrt{1 - \frac{4\overline{m_{ij}^2}}{t} + \left[\frac{\Delta m_{ij}^2}{t}\right]^2}\,, \tag{6.62}$$

written in terms of the mass-squared mean and difference values $\overline{m_{ij}^2} \equiv \frac{1}{2}(m_i^2 + m_j^2)$, $\Delta m_{ij}^2 \equiv m_i^2 - m_j^2$.

Several comments are in order. First of all, one would expect this result to reproduce the massless one at high-enough energies, $m_i^2 \ll |t|$. Neglecting all mass-dependent terms in the amplitude, we find that the unitarity of the PMNS matrix ensures that this results reproduces Eq. (6.57), since $\sum_i |U_{ei}|^2 = 1$ reduces

$$\sum_{ij} Q^{ij}_{W,A}(Q^{ij}_{W,B})^* = \sum_{ij} 4Z_A Z_B |U_{ei}|^2 |U_{ej}|^2 + N_A N_B \delta_{ij} - $$
$$- (Z_A N_B + Z_B N_A) U_{ei} U^*_{ej} \delta_{ij} \tag{6.63}$$

to $\sum_\alpha Q^\alpha_{W,A} Q^\alpha_{W,B}$ in Eq. (6.58). Furthermore, notice that even though the dependence of Q^{ij}_W on U_{ei} implies that they are complex quantities, the observable product $Q^{ij}_{W,A}(Q^{ij}_{W,B})^*$ depends only on $|U_{ei}|^2$, thus being real and CP-conserving, as it should.

2 The relevant integrals in the massive neutrino case are

$$I_{ij} \equiv \int \frac{\mathrm{d}^3k_1}{2E_1}\frac{\mathrm{d}^3k_2}{2E_2}\,\delta^{(4)}(k_1 + k_2 - q) = \frac{\pi}{2}\sqrt{1 - \frac{4\overline{m_{ij}^2}}{t} + \left[\frac{\Delta m_{ij}^2}{t}\right]^2}\,,$$
$$I^{\mu\nu}_{ij} \equiv \int \frac{\mathrm{d}^3k_1}{2E_1}\frac{\mathrm{d}^3k_2}{2E_2}\,\delta^{(4)}(k_1 + k_2 - q)\,k_1^\mu k_2^\nu = \frac{s}{12}\left[1 - \frac{\overline{m_{ij}^2}}{t} - \frac{1}{2}\left[\frac{\Delta m_{ij}^2}{t}\right]^2\right] I_{ij} g^{\mu\nu} + a q^\mu q^\nu\,,$$

with a an irrelevant constant due to the vanishing contribution of the $q^\mu q^\nu$ tensor to the long-range amplitude.

We also checked that our result reproduces the particular case considered in Ref. [203] in the context of neutron stars for the potential between neutrons due to 2ν-exchange of a single neutrino species, i.e. $Z_{A,B} = 0$, $N_{A,B} = 1$ and $i = j = 1$,

$$\mathrm{Im}\mathcal{M}(nn \to nn)_{11} = -\frac{G_F^2}{48\pi}\, t \left[1 - \frac{m^2}{t}\right] \sqrt{1 - \frac{4m^2}{t}}\,. \quad (6.64)$$

Our inclusion of mixing and different masses for the three neutrinos reveals particular behaviors. Even though the tree-level $A\bar{A} \to \nu_i \bar{\nu}_j$ amplitudes we calculated after the unitarity cut distinguish the mass indices i and j, since one corresponds to a neutrino and the other to an antineutrino, the non-relativistic coherent contribution to the absorptive part in Eq. (6.62) is symmetric under $i \leftrightarrow j$. This fact can be understood from different points of view. Regarding the whole 1-loop scattering amplitude before the unitarity cut, the distinction between particle and antiparticle in the propagators makes no sense: the interaction is mediated by the fields $\nu_i \nu_j$, symmetric under ij exchange, so the necessity of the ij symmetry in our absorptive part is clear. After the unitarity cut, on the other hand, we have discussed the determination of the absorptive part from the tree-level scattering amplitudes for the $A\nu_i \to A\nu_j$ processes. At this level, the invariance of these amplitudes under Time Reversal is the fundamental principle imposing ij symmetry.

There is one especially important difference of Eq. (6.62) with respect to the massless amplitude in Eq. (6.57). Whereas in the massless case the weak flavor charges are factored out from the energy dependence, the mass-dependent terms in the massive case entangle their energy-dependent terms with the corresponding Q_W^{ij}. This fact indicates that the massive-neutrino long-range potential will not be written as the product of a coupling times a function of the distance, but will be built up from the sum of six[3] such contributions.

3 Notice that, even though $\sum_{ij}$ is a 9-element sum for the case of three light active neutrinos, the ij symmetry discussed ensures that all ij-dependent quantities are necessarily 3×3 symmetric tensors, and thus determined by only 6 independent terms.

6.4.3 Majorana neutrinos

If a Majorana mass term as Eq. (1.23) is included in the Lagrangian instead of a Dirac one, the only difference is dynamical: all the kinematics we worked out in the previous Section still apply. The effect of the Majorana mass in the interaction dynamics, on the other hand, affects the structure of the neutrino vertex in Dirac space only, leaving the previous discussion on the effects of neutrino mixing also unchanged.

The change in the neutrino vertex originates from the fact that the exchanged neutrinos for the absorptive part are of definite masses (m_i, m_j), not of definite chirality. Whereas Dirac neutrinos interact as the V-A vertex in Lagrangian (6.39) due to the V+A part of the mass state being sterile, Majorana neutrinos present both contributions: the V-A interacting neutrino vertex *and* the conjugate V+A term with opposite sign. Thus their interaction is twice the axial one, and the Lagrangian can be written as

$$\mathscr{L}_{\text{eff}} = -\frac{G_F}{\sqrt{2}} \left[\bar{\nu}_j \gamma^\mu \gamma_5 \nu_i\right] \left[\bar{\psi} \gamma_\mu \left(g^{\psi}_{V_{ij}} - g^{\psi}_{A_{ij}} \gamma_5\right) \psi\right] , \qquad (6.65)$$

with a different Dirac structure than for Dirac neutrinos given by $\gamma^\mu(1-\gamma_5) \mapsto 2\gamma^\mu\gamma_5$.

Even though there is no kinematical difference between the two massive cases, this change in dynamics ensures that the dependence of our process on neutrino masses will differ. Indeed, the product of Majorana intermediate amplitudes reads

$$\mathcal{M}_{A_{ij}} \mathcal{M}^*_{B_{ij}} = 2G_F^2 \tilde{Z}^{ij}_{\mu\nu} \left[k_1^\mu k_2^\nu + k_1^\nu k_2^\mu - \frac{1}{2}(s - m_i^2 - m_j^2 - 2m_i m_j) g^{\mu\nu} + a^{\mu\nu}\right] . \qquad (6.66)$$

The factor 2 with respect to the Dirac one in Eq. (6.61) is compensated in the phase space integration: the Majorana condition leads to $\nu_i\bar{\nu}_j$ and $\nu_j\bar{\nu}_i$ being identical final states, so the phase space integration in the unitarity cut will include an identical-particles factor 1/2 compensating this 2. Thus the only difference between Dirac and Majorana neutrinos is the extra interference term $2m_i m_j$ present in the Majorana case, which we emphasize in

Eq. (6.66) in blue. Removing this term would take us back to the Dirac-neutrino result. We realize that the Dirac/Majorana distinction is apparent in the quantum undistinguishibility associated to identical Majoranas with no global lepton charge for definite mass eigenstates. For Dirac, the two neutrinos are distinguished by the global lepton charge.

This subtle change between the Dirac and Majorana cases propagates itself to the absorptive part of the amplitude,

$$\mathrm{Im}\mathcal{M}(AB \to AB) = -\frac{G_F^2}{48\pi}\, t \times$$
$$\times \sum_{ij} Q^{ij}_{W,A}(Q^{ij}_{W,B})^* \left[1 - \frac{\overline{m^2_{ij}} + 3m_i m_j}{t} - \frac{1}{2}\left[\frac{\Delta m^2_{ij}}{t}\right]^2\right] \sqrt{1 - \frac{4\overline{m^2_{ij}}}{t} + \left[\frac{\Delta m^2_{ij}}{t}\right]^2}\,, \tag{6.67}$$

whose only difference with respect to the Dirac case is the $3m_i m_j$ interference term in blue, present only for Majorana neutrino exchange. The properties and behavior of the mixed charges Q^{ij}_W, however, remain the same for Majorana neutrino exchange as they were for Dirac neutrinos.

As expected, this result reproduces the massless case in Eq. (6.57) in the limit $m_i \to 0$, as happened in the Dirac case, thanks to the identity

$$\sum_{ij} Q^{ij}_{W,A}(Q^{ij}_{W,B})^* = \sum_{\alpha} Q^{\alpha}_{W,A} Q^{\alpha}_{W,B}\,, \tag{6.68}$$

ensured by the PMNS matrix unitarity.

We also checked that our result reproduces the single-neutrino neutron-neutron amplitude in Ref. [203],

$$\mathrm{Im}\mathcal{M}(nn \to nn)_{11} = -\frac{G_F^2}{48\pi}\, t \left[1 - \frac{4m^2}{t}\right] \sqrt{1 - \frac{4m^2}{t}}\,. \tag{6.69}$$

The difference between Dirac and Majorana neutrino exchange at this level is now clear. The exclusion (Dirac) or inclusion (Majorana) of the blue term in Eq. (6.67) will affect the value of the long-range potential calculated in the next Section, leading to a definite answer to the Dirac/Majorana character if it is eventually observed.

6.5 2ν-MEDIATED LONG-RANGE POTENTIAL

With all the ingredients ready to calculate the long-range potential $V(r)$ as in Eq. (6.16), we can compare its r dependence for Dirac and Majorana neutrinos, both of whom must reproduce the same (massless) limit when $m_i\, r \ll 1$.

For the simple case of massless neutrinos, the branching point for all channels appears at $t_0 = 0$, leading to the calculation of the potential as

$$V_{2\nu_0}(r) = \frac{-1}{4\pi^2 r} \int_0^\infty \mathrm{d}t\, e^{-\sqrt{t}\, r}\, \mathrm{Im}\; M_0(t)\,, \tag{6.70}$$

determined by the absorptive part in Eq. (6.57). This integration yields the long-range potential

$$V_{2\nu_0}(r) = \frac{G_F^2}{16\pi^3} \sum_\alpha Q^\alpha_{W,A} Q^\alpha_{W,B}\, \frac{1}{r^5}\,, \tag{6.71}$$

in terms of the weak flavor charges $Q^\alpha_W = 2Z\delta_{\alpha e} - N$ in Eqs. (6.51). The analysis in Section 6.4.1 of the weak charges of aggregate matter showed that each Q^α_W has the same sign for all atoms. Thus $\sum_\alpha Q^\alpha_{W,A} Q^\alpha_{W,B}$ is always positive and, as seen, the r^{-5} potential is always repulsive for aggregate matter. For atomic and nuclear spectroscopy [204], however, it is not necessarily so.

The interesting cases with exchange of massive neutrinos have a different branching point $t_{ij} = (m_i + m_j)^2$ for each channel, so the integral transform has to be calculated for each of them separately,

$$V_{2\nu}(r) = \frac{-1}{4\pi^2 r} \sum_{ij} \int_{t_{ij}}^\infty \mathrm{d}t\, e^{-\sqrt{t}\, r}\, \mathrm{Im}\; M_{ij}(t)\,, \tag{6.72}$$

where Im M_{ij} is the $\nu_i \bar{\nu}_j$-channel contribution to the absorptive parts in Eqs. (6.62) and (6.67) for Dirac and Majorana neutrinos, respectively.

We perform these integrals numerically, and show the resulting Dirac and Majorana 2ν-exchange long-range potentials, $V_{2\nu_D}(r)$ and $V_{2\nu_M}(r)$, in Figure 6.11. The computation requires two sets of parameters to be chosen: the number of constituent particles

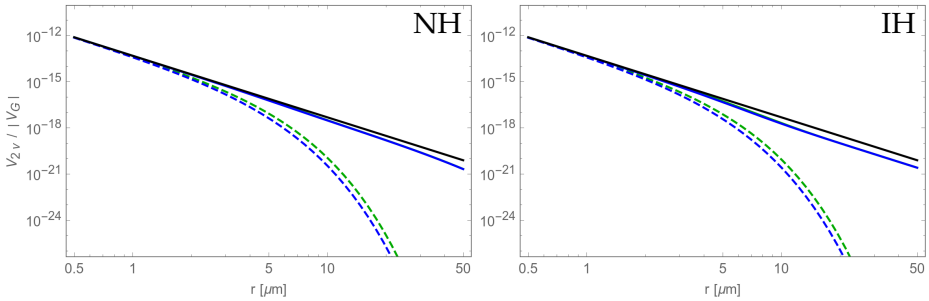

Figure 6.11: Coherent long-range potential between two $^{39}_{19}$K atoms, for massless (black), Dirac (green) and Majorana (blue) two-neutrino exchange $V_{2\nu}(r)$, normalized to the absolute value of the gravitational potential, $|V_G(r)| = -V_G(r)$. Normal (Inverted) Hierarchy on the left (right) panel. Solid lines for a massless lightest neutrino, $m_{\rm min} = 0$, dashed lines for $m_{\rm min} = 0.1$ eV.

of the interacting aggregates, and the values of the exchanged neutrino absolute masses.

We show the potential describing the interaction between two $^{39}_{19}$K atoms, which is an isotope usually employed in tests of the weak equivalence principle, and thus interesting for the observation of this interaction. Regarding the choice of neutrino masses, we use the experimental values of the mass squared differences in Eq. (1.20), and a lower/higher bound pair of values for the lightest neutrino mass as in Figure 5.1, $m_{\rm min} = (0, 0.1)$ eV. We show these cases for both Neutrino Mass Orderings, which correspond to the mass values in Table 6.2.

Table 6.2: Absolute neutrino masses (in eV) used in this Section.

NH		
m_3	0.0500	0.1118
m_2	0.0087	0.1004
m_1	0	0.1

IH		
m_2	0.0500	0.1118
m_1	0.0492	0.1115
m_3	0	0.1

As seen in the Figure, both Dirac and Majorana potentials reproduce the massless case in Eq. (6.71) below 1 micron, i.e. in the region with $m_i r \ll 1$. Indeed, for the neutrino masses $m_i \lesssim 0.1$ eV in Table 6.2, their Compton wavelength is

$$\lambda_\nu = \frac{\hbar c}{m_\nu c^2} = 2\ \mu\text{m} \left[\frac{0.1\ \text{eV}}{m_\nu}\right] , \tag{6.73}$$

explaining the effectively massless behavior of the exchanged neutrinos below 1 micron. At any distance, nevertheless, they keep one of the key features of the massless potential: their sign ensures that the interaction is *always* repulsive.

This λ_ν value is also a good approximation for the range of the interaction: once mass effects become relevant, a Yukawa-like suppression makes the potential decrease rapidly. For the heavier $m_{\text{min}} = 0.1$ eV, this fact is already apparent at few microns, as expected from its $\lambda_\nu = 2\ \mu$m. For the lightest case $m_{\text{min}} = 0$, however, there is a qualitative difference: the contributions involving the two massive neutrino states will indeed be Yukawa suppressed at ranges above several microns, but the channel due to the exchange of two massless neutrinos will behave as the r^{-5} potential without cut-off. Thus the solid lines in the Figure show that, at long ranges, the massive potentials have the same r-dependence as the massless one, albeit being smaller due to the Yukawa suppression of two of the three neutrinos.

This fact also explains why the Dirac/Majorana cases are so similar with $m_{\text{min}} = 0$. Both below the micron scale, where all neutrinos are effectively massless, and above the micron scale, where the massless state is the dominant one, the potential is determined by massless behavior for the neutrinos. The confusion theorem thus ensures that there is no distinguishing the neutrino character in those cases.

If the lightest state is not massless, however, that behavior above the micron scale does no longer apply. Indeed, the curves for $m_{\text{min}} = 0.1$ eV show that, in the region above λ_ν where the Yukawa suppression starts to kill the interaction, the Dirac and Majorana potentials are no longer degenerate. Therefore, a measurement of this interaction providing information on the neutrino character should be made at distances of the order

of the neutrino Compton wavelength, i.e. around the micron, finding a compromise between the two potentials no longer being degenerate and the Yukawa suppression still not having made the interaction too weak.

As a final remark, notice that Hierarchy effects are not significant in these interactions. The potentials differ slightly between the two possible mass orderings, but their overall behavior is the same. This fact can be understood taking into account that, regardless of the absolute mass scale m_{min}, the masses of the lightest and heaviest neutrino states have the same values in both Hierarchies —our two particular cases with the values in Table 6.2 illustrate this relation. Therefore, the range at which (a) the massive potentials start to differ from the massless one, given by the Compton wavelength of the heaviest neutrino, and (b) the full potential is Yukawa-suppressed, given by the Compton wavelength of the lightest neutrino, are the same for both Hierarchies.

After this discussion on the overall behavior of the potential for both Dirac and Majorana neutrinos, we look in higher detail into the differences between the two cases, which had arisen from the blue term in the absorptive part in Eq. (6.67). We show in Figure 6.12 two comparisons of $V_{2\nu_D}$ and $V_{2\nu_M}$.

On the top panels, we show the ratio $V_{2\nu_D}(r)/V_{2\nu_M}(r)$ for the same two values of m_{min}. As mentioned in the previous discussion, this comparison clearly shows that the Dirac/Majorana distinction is negligible at ranges below 1 micron. As expected, these differences are more significant the more important mass effects are, which in this case is at ranges above the neutrino Compton wavelength. For a massless lightest neutrino, the Dirac/Majorana ratio remains close to 1 at all ranges due to the potential being dominated by the massless state both below and above λ_ν, whereas for three massive neutrinos the ratio increases at longer ranges even up to a factor ~ 10.

This larger effect, however, is compensated by the Yukawa suppression of the potential. In order to show the region most

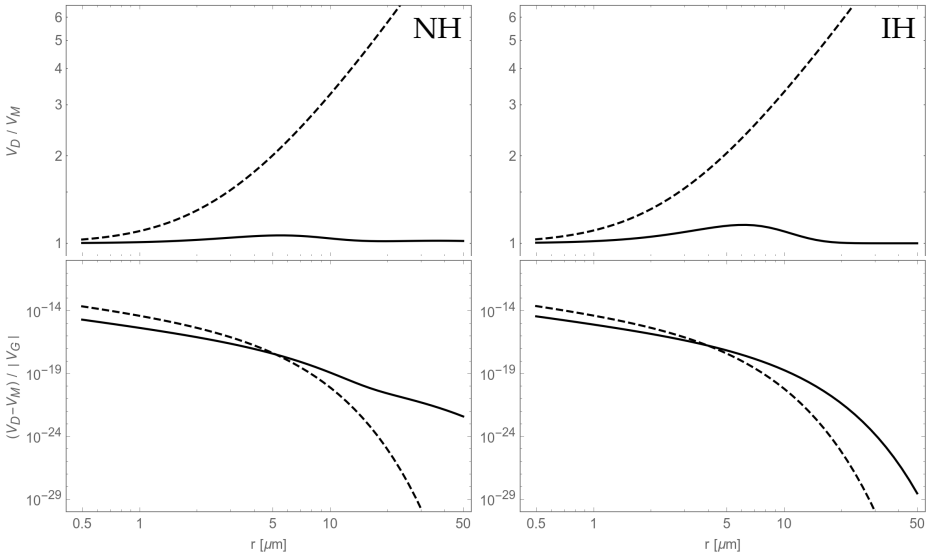

Figure 6.12: Comparison of the 2ν-exchange potential between two $^{39}_{19}$K atoms for Dirac and Majorana neutrinos. The ratio Dirac/Majorana is shown in the top panels, the difference Dirac - Majorana, normalized to the gravitational potential, in the bottom ones. Normal (Inverted) Hierarchy on the left (right) panels. Solid lines for a massless lightest neutrino, $m_{\rm min} = 0$, dashed lines for $m_{\rm min} = 0.1$ eV.

promising for the Dirac/Majorana distinction, we also computed the ratio

$$\rho(r) \equiv \frac{V_{2\nu_D}(r) - V_{2\nu_M}(r)}{V_G(r)}\,, \tag{6.74}$$

normalizing the difference between the Dirac and Majorana potentials to the value of gravitation at that distance —this quantity is shown in the lower panels. Again, notice that the neutrino mass ordering plays a minor role in this discussion: the quantities analyzed change slightly in their value, but their overall behavior remains the same.

The behavior in the Figure is the expected one: an easier Dirac/Majorana distinction for larger neutrino masses, and thus the dashed line ($m_{\rm min} = 0.1$ eV) above the solid one ($m_{\rm min} = 0$). However, the larger the neutrino mass the shorter its Compton

wavelength, and so the interaction is suppressed at shorter distances, ensuring the lighter case is more relevant at long distances. Indeed, the heavier (dashed) ratio is above the lighter (solid) one at distances of 1-10 microns, whereas the lighter case is larger above 10 microns.

Since this interaction competes with gravitation in its observation, this Figure shows that the optimal region for the Dirac/Majorana distinction is around 1 micron, where a heavier absolute mass scale for neutrinos would provide an easier discrimination of the neutrino character.

7 CONCLUSIONS

Neutrino Physics changed its history in 1998 with the discovery of neutrino oscillations in atmospheric neutrinos, and later in solar, reactor and accelerator experiments. Neutrinos do have mass and flavor mixing among the three families of light active left-handed neutrinos. The present state of the art still has a number of fundamental open pending questions in this field. Related to symmetry principles, this Thesis has addressed:

1. Genuine CP violation in the lepton sector, under the historical problem of fake CP Violation induced by the neutrino propagation in matter —and its spin-off of allowing the discrimination of the hierarchy in the neutrino mass ordering. There are two ideas/questions around this problem that deserve attention, and this Thesis has provided affirmative answers:
   i) Is it theoretically possible to disentangle the observable CP asymmetry into two well defined components, genuine and fake?
   ii) Are these two components experimentally separable in planned neutrino oscillations with terrestrial accelerators?

2. Global lepton number violation, with alternative concepts to the well known activity in neutrinoless double beta decay. The question on whether neutrinos are either Dirac or Majorana particles is of fundamental importance, including its implications for beyond-the-Standard-Model physics and leptogenesis. Besides the nuclear decay process, we have contemplated two additional paths in the quest of discovering the possible presence of $\Delta L = 2$ neutrino mass terms:

i) Neutrinoless double electron capture corresponding to $\Delta L = 2$ atom mixing, becoming visible by different observables mediated by the mixed daughter atom and enhanced by a resonance condition and stimulated X-ray emission.

ii) Neutrino-mass-dependent terms, different for Dirac or Majorana nature, in the $\Delta L = 0$ long range interaction of aggregate matter mediated by two-neutrino exchange, at distances around the micron —the Compton wavelength of neutrinos.

Regarding subject **1.i**,

- We have considered the problem of the CP-violating asymmetry together with the T- and CPT-violating asymmetries for neutrino oscillations in matter. Our results represent the culmination of the solution for this historical problem of the contamination by matter effects in the discrete CP, T, CPT asymmetries for neutrino propagation. Using that vacuum is CPT-symmetric and matter is T-symmetric, the goal is accomplished in terms of **a basis of three independent components: genuine CPT-even, matter-induced T-even, interference CP-even**.

- Independent of the theoretical framework for the dynamics of the active neutrino flavors, we prove the **Disentanglement Theorem**

$$\mathcal{A}^{\rm CP}_{\alpha\beta} = A^{\rm CP;T}_{\alpha\beta} + A^{\rm CP;CPT}_{\alpha\beta}\,, \tag{2.13a}$$

$$\mathcal{A}^{\rm T}_{\alpha\beta} = A^{\rm T;CPT}_{\alpha\beta} + A^{\rm T;CP}_{\alpha\beta}\,, \qquad \bar{\mathcal{A}}^{\rm T}_{\alpha\beta} = A^{\rm T;CPT}_{\alpha\beta} - A^{\rm T;CP}_{\alpha\beta}\,, \tag{2.13b}$$

$$\mathcal{A}^{\rm CPT}_{\alpha\beta} = A^{\rm CPT;T}_{\alpha\beta} + A^{\rm CPT;CP}_{\alpha\beta}\,, \quad \bar{\mathcal{A}}^{\rm CPT}_{\alpha\beta} = A^{\rm CPT;T}_{\alpha\beta} - A^{\rm CPT;CP}_{\alpha\beta}\,, \tag{2.13c}$$

  for the three independent experimental asymmetries in terms of the three components. For even a T-symmetric matter, $\mathcal{A}^{\rm T}_{\alpha\beta}$ has a fake component due to quantum interference.

- The asymmetry sum rule $\mathcal{A}^{\rm CPT}_{\alpha\beta} = \mathcal{A}^{\rm CP}_{\alpha\beta} + \bar{\mathcal{A}}^{\rm T}_{\alpha\beta}$ (2.10), when expressed in terms of the components for each term, ensures that $A^{\rm S_1;S_2}_{\alpha\beta} = A^{\rm S_2;S_1}_{\alpha\beta}$.

- For the effective Hamiltonian written as the sum of free mass propagation plus the matter potential for electron neutrinos, **the three components have definite parities** under the baseline L, the matter potential a, the imaginary part $\sin\delta$ of the PMNS mixing matrix, and the hierarchy $h = \pm 1$ in the neutrino mass ordering: $A^{\mathrm{CP;T}}_{\alpha\beta}$ is odd in L and $\sin\delta$ plus even in a and h, $A^{\mathrm{CP;CPT}}_{\alpha\beta}$ is even in L and $\sin\delta$ plus odd in a and h, $A^{\mathrm{T;CPT}}_{\alpha\beta}$ is odd in all L, $\sin\delta$, a and h. The last interference component thus contains the factor $a\sin\delta$.

- At a fixed baseline L and energy E, we have checked the Disentanglement Theorems studying the components as a function of the matter potential V in $a = 2EV$ and the CPV parameter $\sin\delta$. The genuine and interference components vanish at $\sin\delta = 0$ for all a, whereas the two fake components vanish at $a = 0$ for all δ.

- Fixing V for the Earth crust potential, we consider the energy region $\Delta m^2_{21} \ll |a| \ll |\Delta m^2_{31}|$ between the two MSW resonances, relevant to present and planned accelerator neutrino facilities. We have been able to solve the problem of eigenvalues and eigenvectors of the Hamiltonian H in matter and express all components of the asymmetries to first order in Δm^2_{21} and a. They are given by

  Genuine Component

$$A^{\mathrm{CP;T}}_{\mu e} \approx -16\, J_r \sin\delta\, \Delta_{21} \sin^2\Delta_{31}\,, \tag{3.35a}$$

  Matter-Induced Component

$$A^{\mathrm{CP;CPT}}_{\mu e} \approx 16\Delta_a \left[\frac{\sin\Delta_{31}}{\Delta_{31}} - \cos\Delta_{31}\right] \left(S\sin\Delta_{31} + J_r\cos\delta\,\Delta_{21}\cos\Delta_{31}\right)\,, \tag{3.35b}$$

  Interference Component

$$A^{\mathrm{T;CPT}}_{\mu e} \approx -16\Delta_a J_r \sin\delta\,\Delta_{21}\sin\Delta_{31}\left[\frac{\sin\Delta_{31}}{\Delta_{31}} - \cos\Delta_{31}\right]\,. \tag{3.35c}$$

  These analytic expressions give precise results when compared to exact numerical results. This is well explained thanks to the definite parity of the components under a.

- The analytic results demonstrate that **the genuine $A_{\mu e}^{\mathrm{CP;T}}$ component is blind to the Hierarchy** in the neutrino mass spectrum. On the contrary, **the sign of the fake $A_{\mu e}^{\mathrm{CP;CPT}}$ and $A_{\mu e}^{\mathrm{T;CPT}}$ components discriminates** between the Normal and Inverted mass orderings.

Regarding subject **1**.ii,

- The independent measurement of all components could only be made in neutrino factories and atmospheric neutrinos. In these cases, the three components can be extracted from either $\mathcal{A}_{\mu e}^{\mathrm{T}}$, $\bar{\mathcal{A}}_{\mu e}^{\mathrm{T}}$, $\mathcal{A}_{\mu e}^{\mathrm{CP}}$ or $\mathcal{A}_{\mu e}^{\mathrm{CP}}$, $\mathcal{A}_{\mu e}^{\mathrm{T}}$, $\mathcal{A}_{\mu e}^{\mathrm{CPT}}$.
- For present terrestrial accelerator sources of muon neutrinos and antineutrinos, the two components of the appearance **CP asymmetry** $\mathcal{A}_{\mu e}^{\mathrm{CP}}$ can be **disentangled by either baseline dependence** (T2HKK), with detectors at Kamioka and Korea, **or energy dependence** (DUNE). With a single detector in the first oscillation maximum, T2HK has a dominant genuine effect, and the fake component can be subtracted out if the Hierarchy of neutrino masses is previously known.
- At the DUNE baseline , the higher energy region above the first oscillation node provides a dominant matter-induced $A_{\mu e}^{\mathrm{CP;CPT}}$ component, and **the sign of the experimental asymmetry $\mathcal{A}_{\mu e}^{\mathrm{CP}}$ fixes the Hierarchy** in the neutrino mass ordering.
- Conversely, there is a **magic energy at $L/E = 1420$ km/GeV around the second oscillation maximum**, in which the fake $A_{\mu e}^{\mathrm{CP;CPT}}$ component has a first-rank zero whereas the genuine $A_{\mu e}^{\mathrm{CP;T}}$ component is maximal (proportional to $\sin\delta$).
- The magic L/E relation is given by

$$E = 0.92\ \mathrm{GeV}\ \frac{L}{1300\ \mathrm{km}}\ \frac{\left|\Delta m_{31}^2\right|}{2.5\times 10^{-3}\ \mathrm{eV}^2}\,, \tag{4.21}$$

  which corresponds to $E = 0.92$ GeV for the DUNE baseline. With a modest energy resolution $\Delta E \sim 200$ MeV, an effective zero remains in the matter-induced $A_{\mu e}^{\mathrm{CP;CPT}}$ component.

Regarding subject 2.i,

- Neutrinoless double electron capture is a virtual mixing between a parent ${}^{A}\mathrm{Z}$ atom and a daughter ${}^{A}(\mathrm{Z}-2)^{*}$ excited atom with two electron holes. The observable signal is the emission of two-hole X-rays, and the strategy, experimental signature and background are different from neutrinoless double beta decay.

- The mixing is resonantly enhanced for almost degeneracy and, under these conditions, there is no irreducible background from the standard two-neutrino channel.

- We reconstruct the **natural time history of a nominally stable parent atom** since its production either by nature or in the laboratory. After the time periods of atom oscillations and the decay of the short-lived daughter atom, the relevant "stationary" states at observable times are the mixed metastable long-lived state and the non-orthogonal short-lived excited state, as well as the ground state of the daughter atom. We find that they have **a natural population inversion** which is most appropriate for exploiting the bosonic nature of the observed atomic transitions radiation.

- Among different observables of the atom Majorana mixing, we include the enhanced rate of **stimulated X-ray emission** from the long-lived metastable state by a high-intensity X-ray beam: a **gain factor of** ~ 100 can be envisaged at current XFEL facilities.

- Conversely, the historical population of the daughter atom ground state can be probed by exciting it with a current pulsed optical laser, showing the characteristic absorption lines.

- These results are contingent to finding a candidate isotope with a better fulfillment of the resonance condition $\Delta \sim \Gamma$, with a still possible improvement of a factor up to ~ 1000 in the observable rates.

Regarding subject **2.ii**,

- A calculation of the realistic long-range interaction between aggregate matter, mediated by 2ν exchange, is presented for the first time near its range. We have included all ingredients known today in neutrino physics relevant to the coherent interaction with matter, including all vector charges for electrons, protons and neutrons, the neutrino mass terms relevant to distances of the order of their Compton wavelenght and the mixing distinguishing the flavor neutrinos in the $\nu_e\, e$ charged current interaction vertex from the mass eigenstate neutrinos relevant to the absorptive part of the amplitude. A detailed analysis of the implications of each of these ingredients, as a function of the distance, is still lacking. However, one result emerges as a key point: this interaction, if detected **at micron distances**, could provide a completely **novel methodology for solving the Dirc/Majorana neutrino confusion.** Instead of searching for a $\Delta L = 2$ process allowed for Majorana neutrinos only, search for mass effects distinguishing Dirac and Majorana, both cases being allowed.

- The Compton wavelength of massive neutrinos is of order 1 micron. Although the absolute scale of neutrino masses is still unknown, the present upper limit and the known $\left|\Delta m^2_{31}\right|$ and Δm^2_{21} values tell us that $m_\nu \sim 0.1$ eV is expected. Our dispersion theory of the 2ν-mediated force includes the region of distances near this value. In fact, our results demonstrate the extreme **sensitivity of the potential to the lightest neutrino mass for distances between 1 and 10 microns.**

- Such a range for the two-neutrino mediated force is well above the atomic scale, so it will be operative for atoms and **aggregates of matter** if they **have a weak charge**, being neutral in electric charge. Indeed a coherent weak charge is built from NC interactions of electrons, protons and neutrons, and CC interactions of electron neutrinos with electrons. These weak charges for the interaction with ν_e and $\nu_{\mu,\tau}$ are proportional to the number operator and thus they **violate the weak equivalence principle**. Since its tests already reached lev-

els better than 10^{-14}, a deep exploration of the experimental implications of our atom-atom potential is in demand.

- For the neutral current interactions, flavor mixing is unoperative and the intermediate neutrino propagation with definite mass directly appears. For the charged current interaction, the mixing U_{ei} of electron neutrinos to all neutrinos of definite mass will be needed. This ingredient is also well known from neutrino oscillation experiments.

- The dispersion theory of long-range forces leads to the effective potential in terms of the absorptive part of the low t, i.e. the energy of the neutrino-pair in the t-channel, amplitude. Hence the physics involved, by unitarity, is that of a **pair of non-relativistic neutrinos with definite mass**.

- For Dirac neutrinos with definite lepton charge, the interaction vertex is the chiral charge distinguishing neutrinos from antineutrinos. For Majorana neutrinos with no conserved charge, the interaction vertex is the axial charge and so, contrary to the Dirac case, the pair is in P-wave. **The absorptive parts for Dirac and Majorana neutrinos differ in the mass-dependent terms.**

- **For massive neutrinos**, independently of their nature, **the three weak flavor charges** Q_W^α found in the massless case **become mixed**, giving raise to a 3×3 symmetric tensor Q_W^{ij}. It depends on the neutrino mixings U_{ei}, with each element the vertex of $\nu_i \bar{\nu}_j$ exchange. The unitarity of the PMNS matrix ensures the consistency of the two descriptions in the effectively massless neutrino region $m_\nu r \ll 1$.

- The obtained interaction potentials for Dirac and Majorana neutrinos reproduce the massless r^{-5} case at distances below 1 micron. Above the micron scale, the potentials are Yukawa suppressed, with a behavior nearly **independent of the mass ordering**. The region **around the micron** where mass effects become significant and the potentials are still not too small is the **optimal range for the distinction of the Dirac/Majorana neutrino character.**

PROSPECTS

This Thesis has a number of open implications and relevant aspects which need further thinking and developments. To mention a few of them,

1.i The theoretical disentanglement of matter effects from vacuum neutrino propagation has been emphasized here with a view to extract the genuine symmetry breakings. However, the fake components are due to the presence of a uniform potential which is not associated to any force anywhere. The effect of this component has probably a formulation à la Aharonov-Bohm leading to selected flavor interferometric observables. The reader should remember that the Aharonov-Bohm effect has not been performed for an electric scalar potential, and that the experimental result for the magnetic spatial interferometry is interpreted either as the vector potential being a physical entity or as non-local effects of the existing magnetic field outside the interferometric arms.

1.ii The urgent studies on this topic after this Thesis are evident. Once we have demonstrated that a direct evidence of genuine CP violation in neutrino oscillations is now experimentally reachable by either baseline dependence or energy dependence, the selection of the best strategy for the two planned T2HK and DUNE experiments is mandatory. We are going to start a collaboration for a detailed simulation of the physics reach at T2HKK, with an off-axis beam, and at DUNE, with energy reconstruction using a wide-band beam.

2.i The idea of exploiting the virtues of a $\Delta L = 2$ quantum mixing between two atoms, with the associated "forbidden" X-ray emission as a signal of Majorana neutrino mass, needs the resonant enhancement. The present accuracy in the measurement of atomic masses, thanks to the trapping techniques, allows the search of better candidates in order to get closer to the $\Delta \sim \Gamma$ condition. In this case, the 2ν double electron capture channel, as recently observed, becomes nonexistent as a background. Several atomic physics groups in the world are looking for new candidates. If nature is kind enough, an additional gain can be envisaged by stimulated transitions in the XLaser facilities.

2.ii At present there appears to exist a lucky coincidence at distances of the order of 1 micron. They set the scale for the Compton wavelength of the neutrino and, independently, they are in the frontier of gravity experiments testing with fantastic precision the Weak Equivalence Principle (WEP), which is indeed violated by our interaction with internal gauge charges. The earlier tests of WEP using torsion balance methods have evolved to optical levitated microsphere techniques and, even more promising, atom interferometry. Precision limits for the Eotvos coefficient $\eta = \Delta a/a$, with a the acceleration, of 10^{-14} are already available at distances of 10 microns. One expects a brilliant experimental future in this field by some orders of magnitude, and going to the distance of microns.

As the WEP test is the best devisable one, our next objective will be the comparison between gravity and weak forces at distances around microns, and study the different values and behaviors of the last force for Dirac and Majorana neutrinos. A rough estimate tells us that gravity and weak forces become comparable at distances of 1 nm, where they are both unobservable and hidden by the Van der Waals forces. We have obtained in our study that, in the region 1–10 μm, the ratio between weak and gravity forces for micro-particles is around 10^{-13}–10^{-17}, as was expected. It remains to be seen whether this level of precision could be achievable for a test of WEP in this case. A novel methodology to extract the absolute neutrino mass scale and to solve the Dirac/Majorana neutrino confusion by a detailed study of this WEP-violating effects seems promising.

BIBLIOGRAPHY

[1] Y. Fukuda *et al.* [Super-Kamiokande Collaboration], «Evidence for oscillation of atmospheric neutrinos,» *Phys. Rev. Lett.* **81** (1998) 1562–1567.
doi: 10.1103/PhysRevLett.81.1562.
arXiv: hep-ex/9807003.

[2] Q. R. Ahmad *et al.* [SNO Collaboration], «Direct evidence for neutrino flavor transformation from neutral current interactions in the Sudbury Neutrino Observatory,» *Phys. Rev. Lett.* **89** (2002) 011301.
doi: 10.1103/PhysRevLett.89.011301.
arXiv: nucl-ex/0204008.

[3] T. Araki *et al.* [KamLAND Collaboration], «Measurement of neutrino oscillation with KamLAND: Evidence of spectral distortion,» *Phys. Rev. Lett.* **94** (2005) 081801.
doi: 10.1103/PhysRevLett.94.081801.
arXiv: hep-ex/0406035.

[4] M. H. Ahn *et al.* [K2K Collaboration], «Measurement of Neutrino Oscillation by the K2K Experiment,» *Phys. Rev.* **D74** (2006) 072003.
doi: 10.1103/PhysRevD.74.072003.
arXiv: hep-ex/0606032.

[5] B. Pontecorvo, «Mesonium and anti-mesonium,» *Sov. Phys. JETP* **6** (1957) 429, [Zh. Eksp. Teor. Fiz. **33** (1957) 549].

[6] Z. Maki, M. Nakagawa, and S. Sakata, «Remarks on the unified model of elementary particles,» *Prog. Theor. Phys.* **28** (1962) 870–880.
doi: 10.1143/PTP.28.870.

[7] F. Capozzi, G. L. Fogli, E. Lisi, A. Marrone, D. Montanino, and A. Palazzo, «Status of three-neutrino oscillation parameters, circa 2013,» *Phys. Rev.* **D89** (2014) 093018. doi: 10.1103/PhysRevD.89.093018. arXiv: 1312.2878 [hep-ph].

[8] I. Esteban, M. C. Gonzalez-Garcia, M. Maltoni, I. Martinez-Soler, and T. Schwetz, «Updated fit to three neutrino mixing: exploring the accelerator-reactor complementarity,» *JHEP* **01** (2017) 087. doi: 10.1007/JHEP01(2017)087. arXiv: 1611.01514 [hep-ph].

[9] P. F. de Salas, D. V. Forero, C. A. Ternes, M. Tortola, and J. W. F. Valle, «Status of neutrino oscillations 2018: 3σ hint for normal mass ordering and improved CP sensitivity,» *Phys. Lett.* **B782** (2018) 633–640. doi: 10.1016/j.physletb.2018.06.019. arXiv: 1708.01186 [hep-ph].

[10] K. Abe *et al.* [Hyper-Kamiokande Collaboration], «Hyper-Kamiokande Design Report» (2018) . arXiv: 1805.04163 [physics.ins-det].

[11] R. Acciarri *et al.* [DUNE Collaboration], «Long-Baseline Neutrino Facility (LBNF) and Deep Underground Neutrino Experiment (DUNE)» (2015) . arXiv: 1512.06148 [physics.ins-det].

[12] K. Abe *et al.* [T2K Collaboration], «Indication of Electron Neutrino Appearance from an Accelerator-produced Off-axis Muon Neutrino Beam,» *Phys. Rev. Lett.* **107** (2011) 041801. doi: 10.1103/PhysRevLett.107.041801. arXiv: 1106.2822 [hep-ex].

[13] Y. Abe *et al.* [Double Chooz Collaboration], «Indication of Reactor $\bar{\nu}_e$ Disappearance in the Double Chooz Experiment,» *Phys. Rev. Lett.* **108** (2012) 131801. doi: 10.1103/PhysRevLett.108.131801. arXiv: 1112.6353 [hep-ex].

[14] J. K. Ahn *et al.* [RENO Collaboration], «Observation of Reactor Electron Antineutrino Disappearance in the RENO Experiment,» *Phys. Rev. Lett.* **108** (2012) 191802.
DOI: 10.1103/PhysRevLett.108.191802.
arXiv: 1204.0626 [hep-ex].

[15] M. Fukugita and T. Yanagida, «Baryogenesis Without Grand Unification,» *Phys. Lett.* **B174** (1986) 45–47.
DOI: 10.1016/0370-2693(86)91126-3.

[16] L. Wolfenstein, «Neutrino Oscillations in Matter,» *Phys. Rev.* **D17** (1978) 2369–2374.
DOI: 10.1103/PhysRevD.17.2369.

[17] S. P. Mikheyev and A. Yu. Smirnov, «Resonance Amplification of Oscillations in Matter and Spectroscopy of Solar Neutrinos,» *Sov. J. Nucl. Phys.* **42** (1985) 913–917.

[18] M. Altarelli, R. Brinkmann, M. Chergui, *et al.*, Eds., *XFEL: The European X-Ray Free-Electron Laser. Technical design report*,
ISBN: 9783935702171.
DOI: 10.3204/DESY_06-097.

[19] R. Tatchyn, J. Arthur, M. Baltay, K. Bane, R. Boyce, M. Cornacchia, T. Cremer, A. Fisher, S.-J. Hahn, M. Hernandez, *et al.*, «Research and development toward a 4.5-1.5 Å linac coherent light source (LCLS) at SLAC,» *Nuclear Instruments and Methods in Physics Research Section A: Accelerators, Spectrometers, Detectors and Associated Equipment* **375**, no. 1-3 (1996) 274–283.

[20] J. Galayda [LCLS-II Collaboration], «The Linac Coherent Light Source-II Project,» in *Proceedings, 5th International Particle Accelerator Conference (IPAC 2014): Dresden, Germany, June 15-20, 2014*, 935–937.
DOI: 10.18429/JACoW-IPAC2014-TUOCA01.
URL: http://jacow.org/IPAC2014/papers/tuoca01.pdf.

[21] J. J. Thomson, «XL. Cathode rays,» *The London, Edinburgh, and Dublin Philosophical Magazine and Journal of Science* **44**, no. 269 (1897) 293–316.
DOI: 10.1080/14786449708621070.

[22] E. Rutherford, «LIV. Collision of α particles with light atoms. IV. An anomalous effect in nitrogen,» *The London, Edinburgh, and Dublin Philosophical Magazine and Journal of Science* **37**, no. 222 (1919) 581–587.
DOI: 10.1080/14786440608635919.

[23] E. Rutherford, «LXXIX. The scattering of α and β particles by matter and the structure of the atom,» *The London, Edinburgh, and Dublin Philosophical Magazine and Journal of Science* **21**, no. 125 (1911) 669–688.
DOI: 10.1080/14786440508637080.

[24] E. Rutherford, «VIII. Uranium radiation and the electrical conduction produced by it,» *The London, Edinburgh, and Dublin Philosophical Magazine and Journal of Science* **47**, no. 284 (1899) 109–163.
DOI: 10.1080/14786449908621245.

[25] H. Becquerel, «Influence d'un champ magnétique sur le rayonnement des corps radio-actifs,» *Journal de Physique Théorique et Appliquée* **9**, no. 1 (1900) 71–78.
DOI: 10.1051/jphystap:01900009007100.

[26] O. von Baeyer, O. Hahn, and L. Meitner, «Uber die β-Strahlen des aktiven Niederschlags des Thoriums,» *Physikalische Zeitschrift* **12** (1911) 273–279.

[27] J. Danysz and W. Duane, «Sur les charges électriques des rayons α et β,» *Le Radium* **9**, no. 12 (1912) 417–421.
DOI: 10.1051/radium:01912009012041700.

[28] J. Chadwick, «Intensitätsverteilung im magnetischen Spectrum der β-Strahlen von radium B + C,» *Verhandl. Dtsc. Phys. Ges.* **16** (1914) 383–391.
URL: http://cds.cern.ch/record/262756.

[29] L. Ornstein and W. Van Wijk, «Untersuchungen über das negative Stickstoff bandenspektrum,» *Zeitschrift für Physik* **49**, no. 5-6 (1928) 315–322.
DOI: 10.1007/BF01337921.

[30] J. Chadwick and C. D. Ellis, «A Preliminary Investigation of the Intensity Distribution in the β-Ray Spectra of Radium B and C,» in *Proceedings of the Cambridge Philosophical Society*, vol. 21, 274–280.

[31] C. D. Ellis and W. Wooster, «The β-ray Type of Disintegration,» in *Mathematical Proceedings of the Cambridge Philosophical Society*, Cambridge University Press, vol. 22, 849–860.
DOI: 10.1017/S030500410001447X.

[32] C. D. Ellis and W. A. Wooster, «The average energy of disintegration of radium E,» *Proceedings of the Royal Society of London. Series A, Containing Papers of a Mathematical and Physical Character* **117**, no. 776 (1927) 109–123.
DOI: 10.1098/rspa.1927.0168.

[33] N. Bohr, «Atomic stability and conservation laws,» *Reale Accademia d'Italia* (1932) 119–130.

[34] J. Chadwick, «Possible existence of a neutron,» *Nature* **129**, no. 3252 (1932) 312.
DOI: 10.1038/129312a0.

[35] C. D. Anderson, «The Positive Electron,» *Phys. Rev.* **43** (1933) 491–494.
DOI: 10.1103/PhysRev.43.491.

[36] E. Fermi, «Tentativo di una teoria dei raggi β,» *Il Nuovo Cimento (1924-1942)* **11**, no. 1 (1934) 1.
DOI: 10.1007/BF02959820.

[37] H. Bethe and R. Peierls, «The 'neutrino',» *Nature* **133** (1934) 532.
DOI: 10.1038/133532a0.

[38] C. L. Cowan, F. Reines, F. B. Harrison, H. W. Kruse, and A. D. McGuire, «Detection of the free neutrino: A Confirmation,» *Science* **124** (1956) 103–104.
DOI: 10.1126/science.124.3212.103.

[39] C. D. Anderson and S. H. Neddermeyer, «Cloud Chamber Observations of Cosmic Rays at 4300 Meters Elevation and Near Sea-Level,» *Phys. Rev.* **50** (1936) 263–271. DOI: 10.1103/PhysRev.50.263.

[40] C. M. G. Lattes, H. Muirhead, G. P. S. Occhialini, and C. F. Powell, «PROCESSES INVOLVING CHARGED MESONS,» *Nature* **159** (1947) 694–697, [,42(1947)]. DOI: 10.1038/159694a0.

[41] R. P. Feynman and M. Gell-Mann, «Theory of Fermi interaction,» *Phys. Rev.* **109** (1958) 193–198, [,417(1958)]. DOI: 10.1103/PhysRev.109.193.

[42] B. Pontecorvo, «Nuclear capture of mesons and the meson decay,» *Phys. Rev.* **72** (1947) 246. DOI: 10.1103/PhysRev.72.246.

[43] G. Puppi, «Sui mesoni dei raggi cosmici,» *Nuovo Cim.* **5** (1948) 587–588, [,590(1948)]. DOI: 10.1007/BF02780913.

[44] B. Pontecorvo, «Electron and Muon Neutrinos,» *J. Phys.* **43** (1959) C8–221.

[45] B. Pontecorvo, «Electron and Muon Neutrinos,» *Sov. Phys. JETP* **10** (1960) 1236–1240, [Zh. Eksp. Teor. Fiz. **37** (1959) 1751].

[46] G. Feinberg, «Decays of the mu Meson in the Intermediate-Meson Theory,» *Phys. Rev.* **110** (1958) 1482–1483. DOI: 10.1103/PhysRev.110.1482.

[47] D. Bartlett, S. Devons, and A. M. Sachs, «Search for the decay mode: mu –> e + gamma,» *Phys. Rev. Lett.* **8** (1962) 120–123. DOI: 10.1103/PhysRevLett.8.120.

[48] G. Danby, J. M. Gaillard, K. A. Goulianos, L. M. Lederman, N. B. Mistry, M. Schwartz, and J. Steinberger, «Observation of High-Energy Neutrino Reactions and the Existence of Two Kinds of Neutrinos,» *Phys. Rev. Lett.* **9** (1962) 36–44. DOI: 10.1103/PhysRevLett.9.36.

[49] M. L. Perl *et al.*, «Evidence for Anomalous Lepton Production in e+ - e- Annihilation,» *Phys. Rev. Lett.* **35** (1975) 1489–1492, [,193(1975)].
DOI: 10.1103/PhysRevLett.35.1489.

[50] K. Kodama *et al.* [DONUT Collaboration], «Observation of tau neutrino interactions,» *Phys. Lett.* **B504** (2001) 218–224.
DOI: 10.1016/S0370-2693(01)00307-0.
arXiv: hep-ex/0012035 [hep-ex].

[51] J. Bernstein, L. S. Brown, and G. Feinberg, «COSMOLOGICAL HELIUM PRODUCTION SIMPLIFIED,» *Rev. Mod. Phys.* **61** (1989) 25.
DOI: 10.1103/RevModPhys.61.25.

[52] M. Peimbert, «The Primordial Helium Abundance,» *Curr. Sci.* **95** (2008) 1165–1176.
arXiv: 0811.2980 [astro-ph].

[53] S. Schael *et al.* [ALEPH, DELPHI, L3, OPAL, SLD, LEP Electroweak Working Group, SLD Electroweak Group, SLD Heavy Flavour Group Collaboration], «Precision electroweak measurements on the Z resonance,» *Phys. Rept.* **427** (2006) 257–454.
DOI: 10.1016/j.physrep.2005.12.006.
arXiv: hep-ex/0509008 [hep-ex].

[54] H. Weyl, «Electron and Gravitation. 1. (In German),» *Z. Phys.* **56** (1929) 330–352, [,121(1929)].
DOI: 10.1007/BF01339504.

[55] C. S. Wu, E. Ambler, R. W. Hayward, D. D. Hoppes, and R. P. Hudson, «Experimental Test of Parity Conservation in Beta Decay,» *Phys. Rev.* **105** (1957) 1413–1414.
DOI: 10.1103/PhysRev.105.1413.

[56] M. Goldhaber, L. Grodzins, and A. W. Sunyar, «Helicity of Neutrinos,» *Phys. Rev.* **109** (1958) 1015–1017.
DOI: 10.1103/PhysRev.109.1015.

[57] B. Pontecorvo, «Chalk River Report,» *PD-205* (1946) .

[58] R. Davis Jr. and D. S. Harmer, «Attempt to observe the $Cl^{37}(\bar{\nu}e^{-})Ar^{37}$ reaction induced by reactor antineutrinos,» *Bull. Am. Phys. Soc.* **4** (1959) 217.

[59] E. Majorana, «Teoria simmetrica dell'elettrone e del positrone,» *Nuovo Cim.* **14** (1937) 171–184.
DOI: 10.1007/BF02961314.
URL: http://inspirehep.net/record/8251/.

[60] B. Pontecorvo, «Inverse beta processes and nonconservation of lepton charge,» *Sov. Phys. JETP* **7** (1958) 172–173, [Zh. Eksp. Teor. Fiz.34,247(1957)].

[61] K. Eguchi *et al.* [KamLAND Collaboration], «First results from KamLAND: Evidence for reactor anti-neutrino disappearance,» *Phys. Rev. Lett.* **90** (2003) 021802.
DOI: 10.1103/PhysRevLett.90.021802.
arXiv: hep-ex/0212021 [hep-ex].

[62] N. Cabibbo, «Unitary Symmetry and Leptonic Decays,» *Phys. Rev. Lett.* **10** (1963) 531–533, [,648(1963)].
DOI: 10.1103/PhysRevLett.10.531.

[63] B. Pontecorvo, «Neutrino Experiments and the Problem of Conservation of Leptonic Charge,» *Sov. Phys. JETP* **26** (1968) 984–988, [Zh. Eksp. Teor. Fiz. **53** (1967) 1717].

[64] R. Davis Jr., D. S. Harmer, and K. C. Hoffman, «Search for neutrinos from the sun,» *Phys. Rev. Lett.* **20** (1968) 1205–1209.
DOI: 10.1103/PhysRevLett.20.1205.

[65] K. S. Hirata *et al.* [Kamiokande-II Collaboration], «Experimental Study of the Atmospheric Neutrino Flux,» *Phys. Lett.* **B205** (1988) 416, [,447(1988)].
DOI: 10.1016/0370-2693(88)91690-5.

[66] J. Bernabeu, «On the history of the PMNS Matrix... with today's perspective,» *Nuovo Cim.* **C037**, no. 03 (2014) 145–154.
DOI: 10.1393/ncc/i2014-11774-6.
arXiv: 1312.7451 [hep-ph].

[67] D. Casper *et al.*, «Measurement of atmospheric neutrino composition with IMB-3,» *Phys. Rev. Lett.* **66** (1991) 2561–2564.
DOI: 10.1103/PhysRevLett.66.2561.

[68] P. Anselmann *et al.* [GALLEX Collaboration], «Solar neutrinos observed by GALLEX at Gran Sasso.,» *Phys. Lett.* **B285** (1992) 376–389.
DOI: 10.1016/0370-2693(92)91521-A.

[69] K. Daum *et al.* [Frejus Collaboration], «Determination of the atmospheric neutrino spectra with the Frejus detector,» *Z. Phys.* **C66** (1995) 417–428.
DOI: 10.1007/BF01556368.

[70] W. Hampel *et al.* [GALLEX Collaboration], «GALLEX solar neutrino observations: Results for GALLEX IV,» *Phys. Lett.* **B447** (1999) 127–133.
DOI: 10.1016/S0370-2693(98)01579-2.

[71] F. Boehm *et al.*, «Final results from the Palo Verde neutrino oscillation experiment,» *Phys. Rev.* **D64** (2001) 112001.
DOI: 10.1103/PhysRevD.64.112001.
arXiv: hep-ex/0107009 [hep-ex].

[72] M. Ambrosio *et al.* [MACRO Collaboration], «Atmospheric neutrino oscillations from upward through going muon multiple scattering in MACRO,» *Phys. Lett.* **B566** (2003) 35–44.
DOI: 10.1016/S0370-2693(03)00806-2.
arXiv: hep-ex/0304037 [hep-ex].

[73] M. Altmann *et al.* [GNO Collaboration], «Complete results for five years of GNO solar neutrino observations,» *Phys. Lett.* **B616** (2005) 174–190.
DOI: 10.1016/j.physletb.2005.04.068.
arXiv: hep-ex/0504037 [hep-ex].

[74] W. W. M. Allison *et al.* [Soudan-2 Collaboration], «Neutrino oscillation effects in Soudan-2 upward-stopping muons,» *Phys. Rev.* **D72** (2005) 052005.
DOI: 10.1103/PhysRevD.72.052005.
arXiv: hep-ex/0507068 [hep-ex].

[75] J. N. Abdurashitov *et al.* [SAGE Collaboration], «Measurement of the solar neutrino capture rate with gallium metal. III: Results for the 2002–2007 data-taking period,» *Phys. Rev.* **C80** (2009) 015807.
DOI: 10.1103/PhysRevC.80.015807.
arXiv: 0901.2200 [nucl-ex].

[76] P. Adamson *et al.* [MINOS Collaboration], «Measurement of the Neutrino Mass Splitting and Flavor Mixing by MINOS,» *Phys. Rev. Lett.* **106** (2011) 181801.
DOI: 10.1103/PhysRevLett.106.181801.
arXiv: 1103.0340 [hep-ex].

[77] S. Adrian-Martinez *et al.* [ANTARES Collaboration], «Measurement of Atmospheric Neutrino Oscillations with the ANTARES Neutrino Telescope,» *Phys. Lett.* **B714** (2012) 224–230.
DOI: 10.1016/j.physletb.2012.07.002.
arXiv: 1206.0645 [hep-ex].

[78] P. Adamson *et al.* [MINOS Collaboration], «Measurements of atmospheric neutrinos and antineutrinos in the MINOS Far Detector,» *Phys. Rev.* **D86** (2012) 052007.
DOI: 10.1103/PhysRevD.86.052007.
arXiv: 1208.2915 [hep-ex].

[79] B. Aharmim *et al.* [SNO Collaboration], «Measurement of the ν_e and Total ^{8}B Solar Neutrino Fluxes with the Sudbury Neutrino Observatory Phase-III Data Set,» *Phys. Rev.* **C87**, no. 1 (2013) 015502.
DOI: 10.1103/PhysRevC.87.015502.
arXiv: 1107.2901 [nucl-ex].

[80] M. Antonello *et al.* [ICARUS Collaboration], «Search for anomalies in the ν_e appearance from a ν_μ beam,» *Eur. Phys. J.* **C73** (2013) 2599.
DOI: 10.1140/epjc/s10052-013-2599-z.
arXiv: 1307.4699 [hep-ex].

[81] K. Abe *et al.* [T2K Collaboration], «Measurement of Neutrino Oscillation Parameters from Muon Neutrino Dis-

appearance with an Off-axis Beam,» *Phys. Rev. Lett.* **111**, no. 21 (2013) 211803.
DOI: 10.1103/PhysRevLett.111.211803.
arXiv: 1308.0465 [hep-ex].

[82] N. Agafonova *et al.* [OPERA Collaboration], «New results on $\nu_\mu \to \nu_\tau$ appearance with the OPERA experiment in the CNGS beam,» *JHEP* **11** (2013) 036, [Erratum: JHEP **04** (2014) 014].
DOI: 10.1007/JHEP11(2013)036.
arXiv: 1308.2553 [hep-ex].

[83] A. Gando *et al.* [KamLAND Collaboration], «^{7}Be Solar Neutrino Measurement with KamLAND,» *Phys. Rev.* **C92**, no. 5 (2015) 055808.
DOI: 10.1103/PhysRevC.92.055808.
arXiv: 1405.6190 [hep-ex].

[84] L. H. Whitehead [MINOS Collaboration], «Neutrino Oscillations with MINOS and MINOS+,» *Nucl. Phys.* **B908** (2016) 130–150.
DOI: 10.1016/j.nuclphysb.2016.03.004.
arXiv: 1601.05233 [hep-ex].

[85] K. Abe *et al.* [Super-Kamiokande Collaboration], «Solar Neutrino Measurements in Super-Kamiokande-IV,» *Phys. Rev.* **D94**, no. 5 (2016) 052010.
DOI: 10.1103/PhysRevD.94.052010.
arXiv: 1606.07538 [hep-ex].

[86] P. Adamson *et al.* [NOvA Collaboration], «Measurement of the neutrino mixing angle θ_{23} in NOvA,» *Phys. Rev. Lett.* **118**, no. 15 (2017) 151802.
DOI: 10.1103/PhysRevLett.118.151802.
arXiv: 1701.05891 [hep-ex].

[87] M. Agostini *et al.* [Borexino Collaboration], «Improved measurement of 8B solar neutrinos with 1.5 kt y of Borexino exposure» (2017) .
arXiv: 1709.00756 [hep-ex].

[88] M. G. Aartsen *et al.* [IceCube Collaboration], «Measurement of Atmospheric Neutrino Oscillations at 6–56 GeV with IceCube DeepCore,» *Phys. Rev. Lett.* **120**, no. 7 (2018) 071801.
DOI: 10.1103/PhysRevLett.120.071801.
arXiv: 1707.07081 [hep-ex].

[89] S. Adrian-Martinez *et al.* [KM3Net Collaboration], «Letter of intent for KM3NeT 2.0,» *J. Phys.* **G43**, no. 8 (2016) 084001.
DOI: 10.1088/0954-3899/43/8/084001.
arXiv: 1601.07459 [astro-ph.IM].

[90] M. G. Aartsen *et al.* [IceCube PINGU Collaboration], «Letter of Intent: The Precision IceCube Next Generation Upgrade (PINGU)» (2014) .
arXiv: 1401.2046 [physics.ins-det].

[91] J. H. Christenson, J. W. Cronin, V. L. Fitch, and R. Turlay, «Evidence for the 2π Decay of the K_2^0 Meson,» *Phys. Rev. Lett.* **13** (1964) 138–140.
DOI: 10.1103/PhysRevLett.13.138.

[92] S. M. Bilenky, J. Hosek, and S. T. Petcov, «On Oscillations of Neutrinos with Dirac and Majorana Masses,» *Phys. Lett.* **94B** (1980) 495–498.
DOI: 10.1016/0370-2693(80)90927-2.

[93] M. Doi, T. Kotani, H. Nishiura, K. Okuda, and E. Takasugi, «CP Violation in Majorana Neutrinos,» *Phys. Lett.* **102B** (1981) 323–326.
DOI: 10.1016/0370-2693(81)90627-4.

[94] J. Bernabeu and P. Pascual, «CP Properties of the Leptonic Sector for Majorana Neutrinos,» *Nucl. Phys.* **B228** (1983) 21–30.
DOI: 10.1016/0550-3213(83)90393-0.

[95] K. M. Case, «Reformulation of the Majorana Theory of the Neutrino,» *Phys. Rev.* **107** (1957) 307–316.
DOI: 10.1103/PhysRev.107.307.

[96] C. Ryan and S. Okubo, «On the equivalence of the Majorana and two-component theories of the neutrino,» *Nuovo Cim. Suppl.* **2** (1964) 234.

[97] V. D. Barger, K. Whisnant, S. Pakvasa, and R. J. N. Phillips, «Matter Effects on Three-Neutrino Oscillations,» *Phys. Rev.* **D22** (1980) 2718.
DOI: 10.1103/PhysRevD.22.2718.

[98] T.-K. Kuo and J. T. Pantaleone, «Neutrino Oscillations in Matter,» *Rev. Mod. Phys.* **61** (1989) 937.
DOI: 10.1103/RevModPhys.61.937.

[99] H. W. Zaglauer and K. H. Schwarzer, «The Mixing Angles in Matter for Three Generations of Neutrinos and the Msw Mechanism,» *Z. Phys.* **C40** (1988) 273.
DOI: 10.1007/BF01555889.

[100] P. I. Krastev, «Searching for the MSW effect with neutrino beams from next generation accelerators,» *Nuovo Cim.* **A103** (1990) 361–374.
DOI: 10.1007/BF02790019.

[101] R. H. Bernstein and S. J. Parke, «Terrestrial long baseline neutrino oscillation experiments,» *Phys. Rev.* **D44** (1991) 2069–2078.
DOI: 10.1103/PhysRevD.44.2069.

[102] S. Choubey *et al.* [IDS-NF Collaboration], «International Design Study for the Neutrino Factory, Interim Design Report» (2011) .
arXiv: 1112.2853 [hep-ex].

[103] V. De Romeri, E. Fernandez-Martinez, and M. Sorel, «Neutrino oscillations at DUNE with improved energy reconstruction,» *JHEP* **09** (2016) 030.
DOI: 10.1007/JHEP09(2016)030.
arXiv: 1607.00293 [hep-ph].

[104] T. Ohlsson and S. Zhou, «Extrinsic and Intrinsic CPT Asymmetries in Neutrino Oscillations,» *Nucl. Phys.* **B893** (2015) 482–500.
DOI: 10.1016/j.nuclphysb.2015.02.015.
arXiv: 1408.4722 [hep-ph].

[105] S. T. Petcov and Y.-L. Zhou, «On Neutrino Mixing in Matter and CP and T Violation Effects in Neutrino Oscillations,» *Phys. Lett.* **B785** (2018) 95–104.
DOI: 10.1016/j.physletb.2018.08.025.
arXiv: 1806.09112 [hep-ph].

[106] Z.-z. Xing, «New formulation of matter effects on neutrino mixing and CP violation,» *Phys. Lett.* **B487** (2000) 327–333.
DOI: 10.1016/S0370-2693(00)00832-7.
arXiv: hep-ph/0002246 [hep-ph].

[107] A. Cervera, A. Donini, M. B. Gavela, J. J. Gomez Cadenas, P. Hernandez, O. Mena, and S. Rigolin, «Golden measurements at a neutrino factory,» *Nucl. Phys.* **B579** (2000) 17–55, [Erratum: *Nucl. Phys.* **B593** (2001) 731].
DOI: 10.1016/S0550-3213(00)00221-2.
arXiv: hep-ph/0002108.

[108] P. B. Denton, H. Minakata, and S. J. Parke, «Compact Perturbative Expressions For Neutrino Oscillations in Matter,» *JHEP* **06** (2016) 051.
DOI: 10.1007/JHEP06(2016)051.
arXiv: 1604.08167 [hep-ph].

[109] A. Ioannisian and S. Pokorski, «Three Neutrino Oscillations in Matter,» *Phys. Lett.* **B782** (2018) 641–645.
DOI: 10.1016/j.physletb.2018.06.001.
arXiv: 1801.10488 [hep-ph].

[110] Z.-z. Xing and J.-y. Zhu, «Analytical approximations for matter effects on CP violation in the accelerator-based neutrino oscillations with E $\lesssim$ 1 GeV,» *JHEP* **07** (2016) 011.
DOI: 10.1007/JHEP07(2016)011.
arXiv: 1603.02002 [hep-ph].

[111] M. C. Banuls, G. Barenboim, and J. Bernabeu, «Medium effects for terrestrial and atmospheric neutrino oscillations,» *Phys. Lett.* **B513** (2001) 391–400.
DOI: 10.1016/S0370-2693(01)00723-7.
arXiv: hep-ph/0102184.

[112] I. Mocioiu and R. Shrock, «Matter effects on neutrino oscillations in long baseline experiments,» *Phys. Rev.* **D62** (2000) 053017.
DOI: 10.1103/PhysRevD.62.053017.
arXiv: hep-ph/0002149.

[113] J. Bernabeu, G. C. Branco, and M. Gronau, «CP Restrictions on Quark Mass Matrices,» *Phys. Lett.* **169B** (1986) 243–247.
DOI: 10.1016/0370-2693(86)90659-3.

[114] P. F. Harrison and W. G. Scott, «CP and T violation in neutrino oscillations and invariance of Jarlskog's determinant to matter effects,» *Phys. Lett.* **B476** (2000) 349–355.
DOI: 10.1016/S0370-2693(00)00153-2.
arXiv: hep-ph/9912435.

[115] C. Jarlskog, «A Basis Independent Formulation of the Connection Between Quark Mass Matrices, CP Violation and Experiment,» *Z. Phys.* **C29** (1985) 491–497.
DOI: 10.1007/BF01565198.

[116] S.-F. Ge, K. Hagiwara, and C. Rott, «A Novel Approach to Study Atmospheric Neutrino Oscillation,» *JHEP* **06** (2014) 150.
DOI: 10.1007/JHEP06(2014)150.
arXiv: 1309.3176 [hep-ph].

[117] K. Kimura, A. Takamura, and H. Yokomakura, «Exact formula of probability and CP violation for neutrino oscillations in matter,» *Phys. Lett.* **B537** (2002) 86–94.
DOI: 10.1016/S0370-2693(02)01907-X.
arXiv: hep-ph/0203099.

[118] P. F. Harrison, W. G. Scott, and T. J. Weiler, «Exact matter covariant formulation of neutrino oscillation probabilities,» *Phys. Lett.* **B565** (2003) 159–168.
DOI: 10.1016/S0370-2693(03)00749-4.
arXiv: hep-ph/0305175.

[119] N. Cabibbo, «Time Reversal Violation in Neutrino Oscillation,» *Phys. Lett.* **72B** (1978) 333–335.
DOI: 10.1016/0370-2693(78)90132-6.

[120] J. Arafune and J. Sato, «CP and T violation test in neutrino oscillation,» *Phys. Rev.* **D55** (1997) 1653–1658.
DOI: 10.1103/PhysRevD.55.1653.
arXiv: hep-ph/9607437.

[121] S. M. Bilenky, C. Giunti, and W. Grimus, «Long baseline neutrino oscillation experiments and CP violation in the lepton sector,» *Phys. Rev.* **D58** (1998) 033001.
DOI: 10.1103/PhysRevD.58.033001.
arXiv: hep-ph/9712537.

[122] J. Bernabeu, «CP, T violation in neutrino oscillations,» in *Neutrino mixing. Festschrift in honour of Samoil Bilenky's 70th birthday. Proceedings, International Meeting, Turin, Italy, March 25-27, 1999*, 41–49.
arXiv: hep-ph/9904474.

[123] J. Bernabeu and M. C. Banuls, «CP and T violation in neutrino oscillations,» *Nucl. Phys. Proc. Suppl.* **87** (2000) 315–317.
DOI: 10.1016/S0920-5632(00)00690-3.
arXiv: hep-ph/0003299.

[124] M. Freund, «Analytic approximations for three neutrino oscillation parameters and probabilities in matter,» *Phys. Rev.* **D64** (2001) 053003.
DOI: 10.1103/PhysRevD.64.053003.
arXiv: hep-ph/0103300.

[125] E. K. Akhmedov, P. Huber, M. Lindner, and T. Ohlsson, «T violation in neutrino oscillations in matter,» *Nucl. Phys.* **B608** (2001) 394–422.
DOI: 10.1016/S0550-3213(01)00261-9.
arXiv: hep-ph/0105029.

[126] H. Minakata, H. Nunokawa, and S. J. Parke, «CP and T violation in neutrino oscillations,» *AIP Conf. Proc.* **670**, no. 1 (2003) 132–139.
DOI: 10.1063/1.1594326.
arXiv: hep-ph/0306221.

[127] E. M. Henley, M. B. Johnson, and L. S. Kisslinger, «Time Reversal in Neutrino Oscillations,» *Int. J. Mod. Phys.* **E20** (2011) 2463–2473, [Erratum: *Int. J. Mod. Phys.* **E21** (2012) 1292001].
DOI: 10.1142/S0218301311020472.
arXiv: 1205.6430 [hep-ph].

[128] K. Abe *et al.* [Hyper-Kamiokande Collaboration], «Physics potentials with the second Hyper-Kamiokande detector in Korea,» *PTEP* **2018**, no. 6 (2018) 063C01.
DOI: 10.1093/ptep/pty044.
arXiv: 1611.06118 [hep-ex].

[129] Y. Itow *et al.* [T2K Collaboration], «The JHF-Kamioka neutrino project,» in *Neutrino oscillations and their origin. Proceedings, 3rd International Workshop, NOON 2001, Kashiwa, Tokyo, Japan, December*, 239–248.
arXiv: hep-ex/0106019.

[130] K. Abe *et al.* [T2K Collaboration], «The T2K Experiment,» *Nucl. Instrum. Meth.* **A659** (2011) 106–135.
DOI: 10.1016/j.nima.2011.06.067.
arXiv: 1106.1238 [physics.ins-det].

[131] K. Ieki, «Observation of $\nu_\mu \to \nu_e$ oscillation in the T2K experiment,» PhD thesis, Kyoto U. (main).
DOI: 10.1007/978-4-431-55837-8.
URL: http://www.t2k.org/docs/thesis/040.

[132] C. E. Aalseth *et al.* [IGEX Collaboration], «Neutrinoless double-beta decay of Ge-76: First results from the International Germanium Experiment (IGEX) with six isotopically enriched detectors,» *Phys. Rev.* **C59** (1999) 2108–2113.
DOI: 10.1103/PhysRevC.59.2108.

[133] H. V. Klapdor-Kleingrothaus *et al.*, «Latest results from the Heidelberg-Moscow double beta decay experiment,» *Eur. Phys. J.* **A12** (2001) 147–154.
DOI: 10.1007/s100500170022.
arXiv: hep-ph/0103062 [hep-ph].

[134] C. E. Aalseth *et al.* [IGEX Collaboration], «The IGEX Ge-76 neutrinoless double beta decay experiment: Prospects for next generation experiments,» *Phys. Rev.* **D65** (2002) 092007.
DOI: 10.1103/PhysRevD.65.092007.
arXiv: hep-ex/0202026 [hep-ex].

[135] R. Arnold *et al.* [SuperNEMO Collaboration], «Probing New Physics Models of Neutrinoless Double Beta Decay with SuperNEMO,» *Eur. Phys. J.* **C70** (2010) 927–943.
DOI: 10.1140/epjc/s10052-010-1481-5.
arXiv: 1005.1241 [hep-ex].

[136] E. Andreotti *et al.*, «130Te Neutrinoless Double-Beta Decay with CUORICINO,» *Astropart. Phys.* **34** (2011) 822–831.
DOI: 10.1016/j.astropartphys.2011.02.002.
arXiv: 1012.3266 [nucl-ex].

[137] K. H. Ackermann *et al.* [GERDA Collaboration], «The GERDA experiment for the search of $0\nu\beta\beta$ decay in ^{76}Ge,» *Eur. Phys. J.* **C73**, no. 3 (2013) 2330.
DOI: 10.1140/epjc/s10052-013-2330-0.
arXiv: 1212.4067 [physics.ins-det].

[138] J. J. Gomez-Cadenas *et al.* [NEXT Collaboration], «Present status and future perspectives of the NEXT experiment,» *Adv. High Energy Phys.* **2014** (2014) 907067.
DOI: 10.1155/2014/907067.
arXiv: 1307.3914 [physics.ins-det].

[139] N. Abgrall *et al.* [Majorana Collaboration], «The Majorana Demonstrator Neutrinoless Double-Beta Decay Experiment,» *Adv. High Energy Phys.* **2014** (2014) 365432.
DOI: 10.1155/2014/365432.
arXiv: 1308.1633 [physics.ins-det].

[140] R. Arnold *et al.* [NEMO-3 Collaboration], «Search for neutrinoless double-beta decay of ^{100}Mo with the NEMO-3 detector,» *Phys. Rev.* **D89**, no. 11 (2014) 111101.
DOI: 10.1103/PhysRevD.89.111101.
arXiv: 1311.5695 [hep-ex].

[141] D. R. Artusa *et al.* [CUORE Collaboration], «Searching for neutrinoless double-beta decay of ^{130}Te with CUORE,» *Adv. High Energy Phys.* **2015** (2015) 879871.
DOI: 10.1155/2015/879871.
arXiv: 1402.6072 [physics.ins-det].

[142] J. B. Albert *et al.* [EXO-200 Collaboration], «Search for Majorana neutrinos with the first two years of EXO-200 data,» *Nature* **510** (2014) 229–234.
DOI: 10.1038/nature13432.
arXiv: 1402.6956 [nucl-ex].

[143] K. Alfonso *et al.* [CUORE Collaboration], «Search for Neutrinoless Double-Beta Decay of ^{130}Te with CUORE-0,» *Phys. Rev. Lett.* **115**, no. 10 (2015) 102502.
DOI: 10.1103/PhysRevLett.115.102502.
arXiv: 1504.02454 [nucl-ex].

[144] J. W. Beeman *et al.* [LUCIFER Collaboration], «Double-beta decay investigation with highly pure enriched ^{82}Se for the LUCIFER experiment,» *Eur. Phys. J.* **C75**, no. 12 (2015) 591.
DOI: 10.1140/epjc/s10052-015-3822-x.
arXiv: 1508.01709 [physics.ins-det].

[145] S. Andringa *et al.* [SNO+ Collaboration], «Current Status and Future Prospects of the SNO+ Experiment,» *Adv. High Energy Phys.* **2016** (2016) 6194250.
DOI: 10.1155/2016/6194250.
arXiv: 1508.05759 [physics.ins-det].

[146] J. Martín-Albo *et al.* [NEXT Collaboration], «Sensitivity of NEXT-100 to Neutrinoless Double Beta Decay,» *JHEP* **05** (2016) 159.
DOI: 10.1007/JHEP05(2016)159.
arXiv: 1511.09246 [physics.ins-det].

[147] A. Gando *et al.* [KamLAND-Zen Collaboration], «Search for Majorana Neutrinos near the Inverted Mass Hierarchy Region with KamLAND-Zen,» *Phys. Rev. Lett.* **117**, no. 8 (2016) 082503, [Addendum: *Phys. Rev. Lett.* **117**, no. 10 (2016) 109903].
DOI: 10.1103/PhysRevLett.117.082503.
arXiv: 1605.02889 [hep-ex].

[148] X. Chen *et al.*, «PandaX-III: Searching for neutrinoless double beta decay with high pressure ^{136}Xe gas time projection chambers,» *Sci. China Phys. Mech. Astron.* **60**, no. 6 (2017) 061011.
DOI: 10.1007/s11433-017-9028-0.
arXiv: 1610.08883 [physics.ins-det].

[149] L. Wang *et al.* [CDEX Collaboration], «First results on ^{76}Ge neutrinoless double beta decay from CDEX-1 experiment,» *Sci. China Phys. Mech. Astron.* **60**, no. 7 (2017) 071011.
DOI: 10.1007/s11433-017-9038-4.
arXiv: 1703.01877 [hep-ex].

[150] J. B. Albert *et al.* [nEXO Collaboration], «Sensitivity and Discovery Potential of nEXO to Neutrinoless Double Beta Decay,» *Phys. Rev.* **C97**, no. 6 (2018) 065503.
DOI: 10.1103/PhysRevC.97.065503.
arXiv: 1710.05075 [nucl-ex].

[151] M. Agostini *et al.* [GERDA Collaboration], «Improved Limit on Neutrinoless Double-β Decay of ^{76}Ge from GERDA Phase II,» *Phys. Rev. Lett.* **120**, no. 13 (2018) 132503.
DOI: 10.1103/PhysRevLett.120.132503.
arXiv: 1803.11100 [nucl-ex].

[152] V. Alenkov *et al.*, «First Results from the AMoRE-Pilot neutrinoless double beta decay experiment» (2019) .
arXiv: 1903.09483 [hep-ex].

[153] F. Vissani, «Signal of neutrinoless double beta decay, neutrino spectrum and oscillation scenarios,» *JHEP* **06** (1999) 022.
DOI: 10.1088/1126-6708/1999/06/022.
arXiv: hep-ph/9906525.

[154] F. Feruglio, A. Strumia, and F. Vissani, «Neutrino oscillations and signals in beta and onu2beta experiments,» *Nucl. Phys.* **B637** (2002) 345–377, [Addendum: *Nucl. Phys.* **B659** (2003) 359].
DOI: 10.1016/S0550-3213(02)00345-0,10.1016/S0550-3213(03)00228-1.
arXiv: hep-ph/0201291.

[155] J. Angrik *et al.* [KATRIN Collaboration], «KATRIN design report 2004» (2005) .
URL: http://inspirehep.net/record/680949.

[156] N. Aghanim *et al.* [Planck Collaboration], «Planck 2018 results. VI. Cosmological parameters» (2018) .
arXiv: 1807.06209 [astro-ph.CO].

[157] E. Aprile *et al.* [XENON Collaboration], «Observation of two-neutrino double electron capture in ^{124}Xe with XENON1T,» *Nature* **568**, no. 7753 (2019) 532–535.
DOI: 10.1038/s41586-019-1124-4.
arXiv: 1904.11002 [nucl-ex].

[158] R. G. Winter, «Double K Capture and Single K Capture with Positron Emission,» *Phys. Rev.* **100** (1955) 142–144.
DOI: 10.1103/PhysRev.100.142.

[159] R. A. Eramzhian, G. Mitselmakher, and M. B. Voloshin, «Conversion of an Atomic Electron Into a Positron and Double Beta+ Decay,» *JETP Lett.* **35** (1982) 656.

[160] J. Bernabeu, A. De Rujula, and C. Jarlskog, «Neutrinoless Double Electron Capture as a Tool to Measure the ν_e Mass,» *Nucl. Phys.* **B223** (1983) 15–28.
DOI: 10.1016/0550-3213(83)90089-5.

[161] J. L. Campbell and T. Papp, «Widths of the Atomic K- n7 Levels,» *Atomic Data and Nuclear Data Tables* **77** (2001) 1–56.
DOI: 10.1006/adnd.2000.0848.

[162] A. S. Barabash, P. Hubert, A. Nachab, and V. Umatov, «Search for beta+ EC and ECEC processes in Se-74,» *Nucl. Phys.* **A785** (2007) 371–380.
DOI: 10.1016/j.nuclphysa.2007.01.002.
arXiv: hep-ex/0610046.

[163] A. S. Barabash, P. Hubert, A. Nachab, S. I. Konovalov, I. A. Vanyushin, and V. I. Umatov, «Search for beta+ EC and ECEC processes in Sn-112 and beta- beta- decay of Sn-124 to the excited states of Te-124,» *Nucl. Phys.* **A807** (2008) 269–281.
DOI: 10.1016/j.nuclphysa.2008.04.009.
arXiv: 0804.3849 [nucl-ex].

[164] M. F. Kidd, J. H. Esterline, and W. Tornow, «Double-electron capture on Sn-112 to the excited 1871 keV state in Cd-112: A possible alternative to double-beta decay,» *Phys. Rev.* **C78** (2008) 035504.
DOI: 10.1103/PhysRevC.78.035504.

[165] A. S. Barabash, P. Hubert, A. Nachab, S. I. Konovalov, and V. Umatov, «Search for beta+EC and ECEC processes in Sn-112,» *Phys. Rev.* **C80** (2009) 035501.
DOI: 10.1103/PhysRevC.80.035501.
arXiv: 0909.1177 [nucl-ex].

[166] V. S. Kolhinen, V. V. Elomaa, T. Eronen, J. Hakala, A. Jokinen, M. Kortelainen, J. Suhonen, and J. Aysto, «Accurate Q value for the Se-74 double-electron-capture decay,» *Phys. Lett.* **B684** (2010) 17–21.
DOI: 10.1016/j.physletb.2009.12.052.

[167] S. Eliseev *et al.*, «Resonant Enhancement of Neutrinoless Double-Electron Capture in Gd-152,» *Phys. Rev. Lett.* **106** (2011) 052504.
DOI: 10.1103/PhysRevLett.106.052504.

[168] V. S. Kolhinen, T. Eronen, D. Gorelov, J. Hakala, A. Jokinen, A. Kankainen, J. Rissanen, J. Suhonen, and J. Aysto, «On the resonant neutrinoless double-electron-

capture decay of Ce-136,» *Phys. Lett.* **B697** (2011) 116–120.
DOI: 10.1016/j.physletb.2011.01.050.

[169] S. Eliseev, D. Nesterenko, K. Blaum, M. Block, C. Droese, F. Herfurth, E. Minaya Ramirez, Yu. N. Novikov, L. Schweikhard, and K. Zuber, «Q values for neutrinoless double-electron capture in Ru-96, Er-162, and Yb-168,» *Phys. Rev.* **C83** (2011) 038501.
DOI: 10.1103/PhysRevC.83.038501.

[170] M. Goncharov, K. Blaum, M. Block, C. Droese, S. Eliseev, F. Herfurth, E. Minaya Ramirez, Yu. N. Novikov, L. Schweikhard, and K. Zuber, «Probing the nuclides Pd-102, Cd-106, and Sm-144 for resonant neutrinoless double-electron capture,» *Phys. Rev.* **C84** (2011) 028501.
DOI: 10.1103/PhysRevC.84.028501.

[171] C. Droese *et al.*, «Probing the nuclide 180W for neutrinoless double-electron capture exploration,» *Nucl. Phys.* **A875** (2012) 1–7.
DOI: 10.1016/j.nuclphysa.2011.11.008.
arXiv: 1111.6377 [nucl-ex].

[172] K. Blaum, Y. N. Novikov, and G. Werth, «Penning traps as a versatile tool for precise experiments in fundamental physics,» *Contemporary Physics* **51**, no. 2 (2010) 149–175.

[173] Z. Sujkowski and S. Wycech, «Neutrinoless double electron capture: A Tool to search for Majorana neutrinos,» *Phys. Rev.* **C70** (2004) 052501.
DOI: 10.1103/PhysRevC.70.052501.
arXiv: hep-ph/0312040.

[174] F. Simkovic and M. Krivoruchenko, «Mixing of neutral atoms and lepton number oscillations,» *Phys. Part. Nuclei Lett.* **6** (2009) 298.
DOI: 10.1134/S1547477109040037.

[175] J. Suhonen and M. T. Mustonen, «Nuclear matrix elements for rare decays,» *Prog. Part. Nucl. Phys.* **64** (2010) 235–237.
DOI: 10.1016/j.ppnp.2009.12.018.

[176] M. I. Krivoruchenko, F. Simkovic, D. Frekers, and A. Faessler, «Resonance enhancement of neutrinoless double electron capture,» *Nucl. Phys.* **A859** (2011) 140–171.
DOI: 10.1016/j.nuclphysa.2011.04.009.
arXiv: 1012.1204 [hep-ph].

[177] D.-L. Fang, K. Blaum, S. Eliseev, A. Faessler, M. I. Krivoruchenko, V. Rodin, and F. Simkovic, «Evaluation of the resonance enhancement effect in neutrinoless double-electron capture in 152Gd, 164Er and 180W atoms,» *Phys. Rev.* **C85** (2012) 035503.
DOI: 10.1103/PhysRevC.85.035503.
arXiv: 1111.6862 [hep-ph].

[178] T. R. Rodriguez and G. Martinez-Pinedo, «Calculation of nuclear matrix elements in neutrinoless double electron capture,» *Phys. Rev.* **C85** (2012) 044310.
DOI: 10.1103/PhysRevC.85.044310.
arXiv: 1203.0989 [nucl-th].

[179] J. Suhonen, «Nuclear matrix elements for the resonant neutrinoless double electron capture,» *Eur. Phys. J.* **A48** (2012) 51.
DOI: 10.1140/epja/i2012-12051-4.

[180] J. Kotila, J. Barea, and F. Iachello, «Neutrinoless double-electron capture,» *Phys. Rev.* **C89**, no. 6 (2014) 064319.
DOI: 10.1103/PhysRevC.89.064319.
arXiv: 1509.01927 [nucl-th].

[181] V. Weisskopf and E. Wigner, «Over the natural line width in the radiation of the harmonius oscillator,» *Z. Phys.* **65** (1930) 18–29.
DOI: 10.1007/BF01397406.

[182] A. Galindo and P. Pascual, *Quantum mechanics II*. Springer-Verlag,
ISBN: 3642841295.

[183] J. Bernabeu and M. Rosa-Clot, «Dispersive approach to the nuclear Compton amplitude and exchange effects,» *Nuovo Cim.* **A65** (1981) 87–98.
DOI: 10.1007/BF02804882.

[184] M. Ericson and M. Rosa-Clot, «Compton Scattering and Pion Number in Nuclei,» *Phys. Lett.* **B188** (1987) 11–16.
DOI: 10.1016/0370-2693(87)90696-4.

[185] R. C. Hilborn, «Einstein coefficients, cross sections, f values, dipole moments, and all that,» *American Journal of Physics* **50**, no. 11 (1982) 982–986.
arXiv: physics/0202029.

[186] E. Schneidmiller and M. Yurkov, *DESY note* (2017), private communication from M. Altarelli.

[187] K. Yamauchi, M. Yabashi, H. Ohashi, T. Koyama, and T. Ishikawa, «Nanofocusing of X-ray free-electron lasers by grazing-incidence reflective optics,» *Journal of Synchrotron Radiation* **22**, no. 3 (2015) 592–598.
DOI: 10.1107/S1600577515005093.

[188] H. Wallander and J. Wallentin, «Simulated sample heating from a nanofocused X-ray beam,» *Journal of Synchrotron Radiation* **24**, no. 5 (2017) 925–933.
DOI: 10.1107/S1600577517008712.

[189] P. Roedig *et al.*, «High-speed fixed-target serial virus crystallography,» *Nature Methods* **14** (2017) 805–810.
DOI: 10.1038/nmeth.4335.

[190] E. A. D. Hartog and J. E. Lawler, «Radiative lifetimes of neutral samarium,» *Journal of Physics B: Atomic, Molecular and Optical Physics* **46**, no. 18 (2013) 185001.
DOI: 10.1088/0953-4075/46/18/185001.

[191] F. Mandl and G. Shaw, *Quantum field theory*. John Wiley & Sons,
ISBN: 978-0471496847.

[192] G. Feinberg and J. Sucher, «Long-Range Electromagnetic Forces on Neutral Particles,» *Phys. Rev.* **139** (1965) B1619–1633.
DOI: 10.1103/PhysRev.139.B1619.

[193] G. Feinberg and J. Sucher, «General Theory of the van der Waals Interaction: A Model-Independent Approach,» *Phys. Rev.* **A2** (1970) 2395–2415.
DOI: 10.1103/PhysRevA.2.2395.

[194] J. Bernabeu and R. Tarrach, «Long Range Potentials and the Electromagnetic Polarizabilities,» *Annals Phys.* **102** (1976) 323.
DOI: 10.1016/0003-4916(76)90265-7.

[195] J. A. Penarrocha and J. Bernabeu, «Low Momentum Transfer Theorem in Lepton Hadron Scattering,» *Annals Phys.* **135** (1981) 321.
DOI: 10.1016/0003-4916(81)90157-3.

[196] G. Feinberg and J. Sucher, «Long-Range Forces from Neutrino-Pair Exchange,» *Phys. Rev.* **166** (1968) 1638–1644.
DOI: 10.1103/PhysRev.166.1638.

[197] G. Feinberg, J. Sucher, and C. K. Au, «The Dispersion Theory of Dispersion Forces,» *Phys. Rept.* **180** (1989) 83.
DOI: 10.1016/0370-1573(89)90111-7.

[198] J. Bernabeu, «Neutrino properties,» *Nucl. Phys. Proc. Suppl.* **28A** (1992) 0500–514.

[199] S. D. H. Hsu and P. Sikivie, «Long range forces from two neutrino exchange revisited,» *Phys. Rev.* **D49** (1994) 4951–4953.
DOI: 10.1103/PhysRevD.49.4951.
arXiv: hep-ph/9211301 [hep-ph].

[200] Q. Le Thien and D. E. Krause, «Spin-Independent Two-Neutrino Exchange Potential with Mixing and CP-Violation,» *Phys. Rev.* **D99**, no. 11 (2019) 116006.
DOI: 10.1103/PhysRevD.99.116006.
arXiv: 1901.05345 [hep-ph].

[201] M. Tanabashi *et al.* [Particle Data Group Collaboration], «Review of Particle Physics,» *Phys. Rev.* **D98**, no. 3 (2018) 030001.
DOI: 10.1103/PhysRevD.98.030001.

[202] K. S. Krane, *Introductory nuclear physics*. John Wiley & Sons,
ISBN: 047180553X.

[203] J. A. Grifols, E. Masso, and R. Toldra, «Majorana neutrinos and long range forces,» *Phys. Lett.* **B389** (1996) 563–565.
DOI: 10.1016/S0370-2693(96)01304-4.
arXiv: hep-ph/9606377 [hep-ph].

[204] Y. V. Stadnik, «Probing Long-Range Neutrino-Mediated Forces with Atomic and Nuclear Spectroscopy,» *Phys. Rev. Lett.* **120**, no. 22 (2018) 223202.
DOI: 10.1103/PhysRevLett.120.223202.
arXiv: 1711.03700 [physics.atom-ph].